

Interrogation of Rab8 as a therapeutic target  
for Huntington's disease in  
*Drosophila melanogaster*

Thesis submitted for the degree of

Doctor of Philosophy

at the University of Leicester

by

Laura Delfino

Department of Genetics

University of Leicester

June 2017

*“Above all, don’t fear difficult moments.  
The best comes from them.”*

Rita Levi Montalcini

## Abstract

Interrogation of Rab8 as a therapeutic target for Huntington's disease in

*Drosophila melanogaster*

Laura Delfino

Huntington's disease (HD) is a familial neurodegenerative disorder largely caused by atrophy in the striatal and cortical regions of the brain. At the molecular level HD is triggered by a trinucleotide CAG repeat expansion in the *Huntingtin* gene (*HTT*), which encodes a poly glutamine (polyQ) stretch, and ultimately leads to the production of the toxic, aggregation-prone protein mutant HTT (mHTT). Upon expression of mHTT, several cellular pathways are either disrupted or impaired, including the vesicle trafficking directed by the Rab GTPase family. Here, I focused on Rab8, a protein involved in the secretory traffic from the trans-Golgi network to the plasma membrane, whose down-regulation has been shown to worsen HD-related phenotypes in mammalian cells. My results show that pan-neuronal expression of *Drosophila* Rab8 (dRAB8) provides neuroprotection against HD-relevant phenotypes in *Drosophila* by reducing degeneration of the eye photoreceptors, ameliorating the rate of fly emergence from the pupal case and increasing average lifespan of adult flies. Notably, this rescue depends on the nucleotide-binding state of the GTPase. The protective role of dRAB8 was also validated in a subset of circadian clock cells, the Pigment Dispersing Factor (PDF) neurons. mHTT triggered arrhythmic locomotor behaviour in constant darkness and progressive death of a cluster of PDF neurons, the small lateral neurons ventral (s-LNvs), phenotypes which were partially or completely rescued by dRAB8 overexpression. The levels of aggregated mHTT are increased upon dRAB8 co-expression in flies and experiments performed in HEK293T cells suggest that the interaction dynamics between mHTT and dRAB8 increase in a polyQ dependent manner. Aggregation has been shown to be neuroprotective against toxic soluble mHTT species in several HD model organisms and might underlie the mechanism of dRAB8 rescue. In summary, this study validates Rab8 as a modifier of HD in *Drosophila*, provides insight into its mechanism of action, and may ultimately inform novel therapeutic approaches for HD.

## Acknowledgments

First and foremost, I wish to express my gratitude to my supervisors, Ezio Rosato, whose contagious enthusiasm for research and unrivalled knowledge of techniques have seen me grow a lot as a scientist, and Flaviano Giorgini, for ambitiously pushing this project, sharing his great expertise and for making me laugh. They have patiently guided me throughout these years, making sure I was constantly happy. No matter what, I have never found their doors closed, not even for the last-minute issues. Without their comments and encouragement this thesis would be just a pale shadow of its final version.

I am extremely thankful to Bambos Kyriacou for his invaluable guidance and advices, for his scientific comments and for reviewing all the stats. I can't wait to start the next project and I'll always owe him a huge debt of gratitude for this opportunity.

I am very grateful to everyone who has helped me to find my feet whenever I need it. Thanks to Ozge Ozkaya, Susanna Campesan and Carlo Breda, for introducing me to the wet/fly labs, for sharing handy fly stocks and showing me smart crosses shortcuts. I am thankful to Rob Mason for his help with PC12 cells and for always being ready to offer advice on anything really. I am thankful to Mariaelena Repici and Aisha Swaih, the "queens of BiFC" whose expertise has made the work with HEK293T cells almost too easy! Many thanks to Celia Hansen for sharing "the art of dissecting a perfect brain". Her ability to make anything work has rescued me many times from sure disasters over these years. I'll always be in debt with Kees Straattman, for teaching me everything I know about imaging and for enduring the several microscopy sessions without losing it! Without his help, I would not be even close to the final result.

Many thanks to all the members of labs 124, 104 and 106. I was lucky to find splendid colleagues who created a wonderful working atmosphere. Everyone has aided me in one way or another and I will never forget it. Special thanks go to John, for all the jokes, the protocols (I still treasure them all), for dealing with my "italianess", and for being the best bench-mate one could wish for!

This last year has not always been easy, but the LCFC and NPB colleagues have surely made everything less painful. I will be forever fearless! I am especially grateful to Carl – thanks for having taken me under your wings, ensuring that all my outfits were locust-free, for keeping the mood in 329 high and for making the best coffee around!

My friends have been my second family and my primary source of happiness. Their presence has made this city an exceptional place to live in. Five years ago, I'd have never said

it, but Leicester is and will always be special. I am grateful to Valeria, the first person in this foreigner country who I have considered a friend. Thanks for your ear always keen on listening (you know you made the difference) and for the long conversations about the different shades of nail polishes (for the joy of Enrico!). I could not imagine my life without the “people living downstairs”, thank you Chiara, for being such an open-minded and creative friend, Pier, for your witty jokes, Barbara, for never forgetting an opened-bottle of wine, Pille, for being anything but boring and Razan, for your contagious smile! Many thanks to Elisa – despite the undone homework and the endless texts, it did not take you long to gain a special place in my heart. Thanks for everything, the “merende”, the interesting stories, the hugs... #thankyouverdu and tante cose, tante cose, tante cose! Peppe and Irene – I still can’t believe you are leaving, it will be the end of an era! You have quickly become irreplaceable and trustworthy friends. Thank you Peppe for being up for anything, for cheering me up when I needed it, and for your carbonara, you are the best! Thanks Irene, you are surely the most “imboressata” of all the “imboressate” and quite possibly the only person who truly understands my OCDs! How shall I do without you? Thanks for the dinners, the time spent together and for keeping it together on the cab to Coron’s airport! I’ll deeply miss you! Thanks to my soul match and good friend Amir. The list with you could go on forever, from butterflies to nature-tennis-table, but I guess progressive indynamism says everything... and wait... of course thank you Alessandro!

Thanks to my family, who supported me throughout my education, encouraging me to pursue anything I believed in. Despite the distance, I never felt alone, especially during rough times.

Finally, to Giorgio, my true Love and best friend – no words will ever express my gratitude for your support and encouragement. You have been my rock. I’d never got this far without you.

Grazie

# Table of Contents

<b>Abstract</b>	i
<b>Acknowledgements</b>	ii
<b>Table of Contents</b>	iv
<b>List of Figures</b>	viii
<b>List of Tables</b>	x
<b>Abbreviations</b>	xi
<b>Chapter 1 Introduction</b>	1
1.1 Huntington's disease (HD)	1
1.1.1 Overview	1
1.1.2 Symptoms and neuropathology	1
1.1.3 The genetic mutation causing HD	6
1.1.4 Huntingtin	8
1.1.5 The molecular mechanisms leading to HD pathogenesis	10
1.1.5.1 mHTT misfolding and aggregation	10
1.1.5.2 Transcriptional dysregulation and its role in the loss of function of <i>brain-derived neurotropic factor (BDNF)</i>	14
1.1.5.3 Axonal and synaptic activity impairment	14
1.1.5.4 Mitochondrial dysfunction and oxidative stress	16
1.1.6 Autophagy in HD	16
1.2 Rab proteins	17
1.3 Rab8	22
1.3.1 Rab8 and HTT	23
1.4 Modeling HD in <i>Drosophila</i>	35
1.4.1 Rab8 as a putative modifier for HD	29
1.7 Aims and objectives	30
<b>Chapter 2 Materials and methods</b>	31
2.1 Materials	31
2.1.1 Oligonucleotides	31
2.1.2 Plasmids	32
2.1.3 Antibodies	33
2.1.4 Fly stocks	34
2.1.5 Cell lines	35

<b>2.2 Methods</b>	<b>36</b>
2.2.1 <i>Drosophila</i> husbandry	36
2.2.2 Cell culture	36
2.2.3 Molecular methods	36
2.2.3.1 Diagnostic genotyping	36
2.2.3.2 Cloning	36
2.2.4 Biochemical methods	37
2.2.4.1 Protein extraction from <i>Drosophila</i> heads	37
2.2.4.2 Protein extraction from cells	37
2.2.4.3 SDS-Polyacrilamyde gel electrophoresis (SDS-PAGE) and transfer	38
2.2.4.4 Immunoblotting	39
<b>2.3 Statistical analyses</b>	<b>39</b>
<b>Chapter 3 dRAB8 rescues HD-relevant phenotypes in <i>Drosophila melanogaster</i></b>	<b>40</b>
3.1 Introduction	40
3.2 Materials and methods	43
3.2.1 <i>Drosophila</i> crosses	43
3.2.2 Diagnostic genotyping	43
3.2.3 Eclosion assay	43
3.2.4 Pseudopupil analysis	44
3.2.5 Longevity assay	44
3.3 Results	44
3.3.1 Overexpression of dRAB8 ameliorates impaired eclosion in HD <i>Drosophila</i> model	44
3.3.2 dRAB8 overexpression ameliorates neurodegeneration in the eyes	47
3.3.3 dRAB8 overexpression improves shortened lifespan in HD flies	49
3.4 Discussion	55
<b>Chapter 4 Exploring Rab8-HTT interaction dynamics</b>	<b>58</b>
4.1 Introduction	58
4.2 Materials and Methods	62
4.2.1 Immunoblotting	62
4.2.2 Generation of constructs	62
4.2.3 Stable transfection of HTT103Q model PC12 cells	64
4.2.4 Caspase assay	64
4.2.5 ICC on cells	65
4.2.6 BIFC assay	67

4.3 Results	69
4.3.1 mHTT induced cellular toxicity is affected by rRAB8 expression levels	69
4.3.2 ICC on HEK293T cells suggests co-localisation between hRAB8 and mHTT aggregates	77
4.3.3 BiFC assay reveals interaction between mHTT and dRAB8 in HEK293T cells	83
4.4 Discussion	89
<b>Chapter 5 Investigating dRAB8 rescue mechanism in a fly model of HD</b>	<b>94</b>
5.1 Introduction	94
5.2 Materials and Methods	98
5.2.1 Autophagy assay	98
5.2.2 Filter retardation assay	98
5.2.3 AGERA	99
5.2.4 Fly co-Immunoprecipitation (Co-IP)	99
5.3 Results	100
5.3.1 dRAB8 overexpression does not up-regulate basal autophagy	100
5.3.2 dRAB8 likely promotes mHTT aggregation	102
5.3.3 dRAB8 likely promotes the formation of larger mHTT aggregates	104
5.3.4 Co-Immunoprecipitation in flies revealed no interaction between soluble mHTT and dRAB8	106
5.4 Discussion	108
<b>Chapter 6 Investigating neuronal dysfunction in PDF-expressing cells of <i>Drosophila melanogaster</i></b>	<b>111</b>
6.1 Introduction	111
6.1.1 <i>Drosophila</i> circadian rhythms	111
6.1.2 Pigment Dispersing Factors (PDF) neurons and their properties	114
6.1.3 Dual oscillator model and clock cells communication	116
6.1.4 Locomotor activity in <i>Drosophila</i>	116
6.2 Materials and methods	119
6.2.1 <i>Drosophila</i> crosses	119
6.2.2 Behavioural assays	119
6.2.3 Behavioural analysis	119
6.2.4 Immunofluorescence and confocal microscopy	120
6.3 Results	120
6.3.1 Expression of mHTT in LNvs neurons leads to arrhythmia and period	

shortening in total darkness.	120
6.3.1 mHTT-expressing flies exhibit loss of s-LNvs and accumulation of α-HTT signal in IB-like structures	129
6.4 Discussion	133
<b>Chapter 7 Discussion</b>	<b>134</b>
7.1 dRAB8 delays the onset of HD-phenotypes in <i>Drosophila</i>	135
7.2 The molecular mechanisms underlying dRAB8 rescue	138
7.3 Effects of Rab8 overexpression in HD model PC12 cells	140
7.4 Future directions	141
7.5 Concluding remarks	147
<b>Chapter 8 Appendix</b>	<b>145</b>
<b>Chapter 9 References</b>	<b>147</b>

## List of Figures

Figure 1-1 The basal ganglia pathways are impaired in early and late stages in HD.	3
Figure 1-2 Neuronal loss in HD.	5
Figure 1-3 Variability in the age of onset of HD.	7
Figure 1-4 Representation of the wild type HTT primary structure zooming in on the first exon.	9
Figure 1-5 Schematic representation of mHTT aggregation process.	11
Figure 1-6 Summary of the main pathways disrupted by mHTT.	13
Figure 1-7 Schematic representation of Rabs location and function in the cell.	18
Figure 1-8 Overview of the Rab function and role in the cell.	20
Figure 1-9 Schematic overview of Rab8 cellular pathways.	24
Figure 1-10 Cartoon showing the relationship between Rab8 and HTT at the TGN as proposed by Sahlender <i>et al.</i> (2005).	26
Figure 1-11 GAL4/UAS system.	28
Figure 3-1 Secondary structure alignment of dRAB8 with dRAB8DN and dRAB8CA.	42
Figure 3-2 Overexpression of dRAB8 partially rescues adult emergencies failure of HD flies.	46
Figure 3-3 Overexpression of dRAB8 slows down HD neurodegeneration in the rhabdomeres.	48
Figure 3-4 Overexpression of dRAB8 extends the lifespan of HD flies.	50
Figure 3-5 PCR results confirming the genotype of flies tested.	52
Figure 3-6 HTT expression is not titrated by the presence of a second UAS-transgene.	54
Figure 4-1 Schematic representation of mHTT induction process in PC12 cells.	59
Figure 4-2 Sequence alignment between rRAB8A and rRAB8B.	61
Figure 4-3 Reconstitution of a fluorophore by BiFC.	63
Figure 4-4 Schematic representation of the caspase assay layout.	66
Figure 4-5 Example of ScanR software cell recognition output.	68
Figure 4-6 Expression of rRAB8A and rRAB8B in PC12 cells	70
Figure 4-7 rRAB8 overexpression does not confer protection against mHTT induced toxicity in PC12 cells.	72
Figure 4-8 Absolute caspase-3/7 activation levels of non-induced cells are not toxic.	74
Figure 4-9 Caspase-3/7 activation correlates with rRAB8 expression levels.	74
dRAB8.	76
Figure 4-11 Endogenous distribution of hRAB8.	78

Figure 4-12 Distribution of hRAB8 is affected in presence of HTT97Q.	80
Figure 4-13 Correlation between hRAB8 and HTT is polyQ dependent.	82
Figure 4-14 BiFC constructs used in this study.	84
Figure 4-15 BiFC signal in HEK293T cells.	86
Figure 4-16 BiFC/RFP ratio intensity.	88
Figure 5-1 Overview of autophagy and the canonical autophagic core machinery.	96
Figure 5-2 Autophagic levels of ATG8-II in HD flies are not enhanced by dRAB8 overexpression.	101
Figure 5-3 Filter-blot reveals that overexpression of dRAB8 enhances levels of aggregate form of mHTT.	103
Figure 5-4 AGERA reveals that overexpression of dRAB8 enhances levels of aggregate form of mHTT.	105
Figure 5-5 Co-IP in flies reveals no direct interaction between soluble HTT93Q and dRAB8.	107
Figure 6-1 Transcriptional/Translational feedback Loops.	113
Figure 6-2 Schematic representation of <i>Drosophila</i> 's neuronal pacemaker.	115
Figure 6-3 Representative actogram of a wild-type fly.	118
Figure 6-4 Percentage of AR HD flies in DD decreases after the 1 <sup>st</sup> week.	122
Figure 6-5 <i>Pdf&gt;HTT93Q</i> flies recover from behavioural arrhythmia.	124
Figure 6-6 <i>Pdf&gt;HTT93Q</i> flies shorten their period over time.	126
Figure 6-7 Visual summary the behavioural pattern <i>Pdf&gt;HTT93Q</i> and <i>Pdf&gt;HTT93Q, dRab8</i> flies throughout three weeks of DD.	128
Figure 6-8 The number of s-LNVs is significantly decreases in mHTT expressing flies at day 14.	130
Figure 6-9 dRAB8 overexpression induces the formation of α-HTT positive speckles in the s-LNVs of mHTT flies.	132
Figure 7-1 Hypothesis on how Rab8 functions in conferring protection against mHTT-induced toxicity.	144
Figure 8-1 Replicate of the life-span assay.	145
Figure 8-2 Replicate of the pseudopupil analysis.	146

## List of Tables

Table 1-1 List of Rab proteins involved in autophagy.	22
Table 2-1 Oligonucleotides used in this study.	31
Table 2-2 Plasmids used in this study.	32
Table 2-3 Antibodies used in this study.	33
Table 2-4 List of lines used in this study.	34
Table 2-5 List of lines generated in this study.	35
Table 2-6 List of cell lines used in this study.	35
Table 3-1 Parental crosses and their F1 progeny genotypes of experimental lines.	54
Table 3-2 Log-rank (Mantel-Cox) analysis for pairwise comparison of survival curves.	61
Table 4-1 Biological variation in the caspase assay.	72
Table 4-2 Percentages of overexposed cells co-transfected with VC-dRab8 in the BiFC experiment.	88
Table 6-1 Parental crosses and F1 progeny tested.	119

## Abbreviations

AGERA	Agarose gel electrophoresis resolving aggregates	GEFs	Guanine nucleotide exchange factors
AMPA	Alpha-amino-3-hydroxy-5-methyl-4-isoxazole propionic acid	GFP	Green fluorescent protein
Atg	Autophagy-related	GGT	Geranylgeranyl transferase
ATP	Adenine triphosphate	Glu	Glutamate
BDNF	Brain-derived neurotrophic factor	GLUT	Glucose Transporter
BECN1	Beclin1	GN	GFP N-terminal
BiFC	Bimolecular fluorescence complementation	GN	GFP N-terminal
CA	Constitutive active	GPCR	G-protein coupled receptor
Caspase	Cysteinyl aspartate-specific protease	GPe	Globus pallidus externus
CCV	Clathrin-coated vesicles	GPi	Globus pallidus internus
CKII	Casein Kinase II	GRE	Glucocorticoid responsive element
CLK	Clock	GTP	Guanosine triphosphate
CMV	Cytomegalovirus	HAP1	Huntingtin associated protein 1
CNS	Central nervous system	HD	Huntington's disease
Co-IP	Co-Immunoprecipitation	HEAT	Huntingtin, Elongation factor 3, protein phosphatase 2A and TOR1
CRY	Cryptochrome	HIP	Huntingtin interacting proteins
Ctrl	Control	hRAB	Human Rab
CYC	Cycle	HRP	Horseradish peroxidase
DAG	Diacetyl glycerol	HTT	Huntingtin
DAM	<i>Drosophila</i> Activity Monitor	IBs	Inclusion bodies
DBT	Doubletime	IC	Intermediate compartment
DD	Dark Dark	ICC	Immunocytochemistry
DJ-1	Parkinson disease protein 7 (PARK7)	IP <sub>3</sub>	Inositol 1,4,5-trisphosphate
DN	Dominant negative	IP <sub>3</sub> Rs	IP <sub>3</sub> Receptors
DNs	Dorsal Neurons	KAR	Kainate receptor
dRAB	<i>Drosophila</i> Rab	KMO	Kynureneine-3-monooxygenase
ENK	Enkephalin	I-LNVs	large-Lateral ventral neurons
ER	Endoplasmic reticulum	LC3	Light chain 3
ERES	Endoplasmic reticulum exit site	LD	Light Dark
ERK	Extracellular signal-regulated protein kinase	LN	Lateral Neurons
ESCRTs	Endosomal sorting complex required for transport	LNDs	Lateral dorsal neurons
FL	Full length	LPN	Lateral posterior neurons
FRET	Förster Resonance Energy Transfer	MAP	Mitogen-activated protein
GABA	γ-amino-butyric-acid	MAP	Mitogen-activated protein
GAPs	GTPase activating proteins	MAP4K2	Mitogen-activated protein kinase kinase kinase 2
GCK	Germinal central kinase	MEKK1	MAP/ERK kinase kinase 1
GDF	GDI displacement factor	mGluR	Metabotropic Glutamate receptor
GDI	GTP dissociation inhibitor	mHTT	Mutant Huntingtin
GDP	Guanosine diphosphate	MVBs	Multi-vesicular Bodies
		NaChBac	Na <sup>+</sup> Channel Bacterial
		NES	Nuclear export signal

NIIs	Neuronal intranuclear inclusions	ROS	Reactive oxygen species
NLS	Nuclear localisation signal	rRAB	rat Rab
NMDAR	N-methyl-D-aspartate receptors	RXR	retinoid X receptor
OPTN	Optineurin	s-LNVs	small-Lateral ventral neurons
PA	Ponasterone	SGG	Shaggy
PC	Pheochromocytoma cell line	SMERs	Small-molecule enhancers of rapamycin
PCK	Protein kinase C	SNAREs	Soluble NFS attachment protein receptors
PDF	Pigment Dispersing Factor	SNC	Substantia nigra pars compacta
PDFR	PDF receptor	SNr	Substantia nigra pars reticulata
PDH	Pigment Dispersing Hormone	SNT	Subthalamic nucleus
PDP1 $\epsilon$	Par domain Protein 1 $\epsilon$	SP	Substance P
PE	Phosphorylethanolamine	STN	Subthalamic nucleus
PER	Period	TBK-1	TANK-binding kinase
PGT	Post Golgi trafficking	TGN	Trans Golgi network
PI3K	Phosphatidylinositol-4,5-bisphosphate 3-kinase	TIM	Timeless
PIP <sub>2</sub>	Phosphatidylinositol-4,5-bisphosphate	Tor	Target of rapamycin
PLC	Phospholipase C	TTL	Transcriptional/translational feedback loop
PolyP	Poly proline	UAS	Upstream activating sequence
PolyQ	Poly glutamine	UPS	Ubiquitin Proteasome System
PP1	Protein phosphatase 1	VC	Venus C-terminal
PP2A	Protein phosphatase 2A	VgEcR	Ecdysone receptor
PSD95	Post-synaptic density 95	VN	Venus N-terminal
PtdIns	Phosphatidylinositol	Vps	Vacuolar protein sorting
PtdIns3K	Phosphatidylinositol 3-kinase	VRI	Vrille
PtdIns3P	Phosphatidylinositol 3-phosphate	WT	Wild type
Rab	Ras-related proteins in brain	wtHTT	Wild type Huntington
Ras	Rat sarcoma	ZT	<i>Zeitgeber</i>
RE	Recycling endosome		
REP	Rab escort protein		
RFP	Red fluorescent protein		

# Chapter 1

## Introduction

### 1.1 Huntington's disease (HD)

#### 1.1.1 Overview

Huntington's disease (HD) is an autosomal dominant, neurodegenerative disorder caused by a mutation in the *Huntingtin* gene (*HTT*). HD leads to the progressive atrophy in regions of the brain such as the striatum and the cortex. HD is a rare disease, with a prevalence estimated at 4-10 cases per 100,000 in Europe, but it is less common among individuals of some ethnic groups (Pringsheim *et al.*, 2012). Death typically occurs ~15-20 years after the clinical diagnosis, and no cure or treatment to slow progression is currently available (Bates *et al.*, 2014).

#### 1.1.2 Symptoms and neuropathology

HD has been known for centuries, and the hallmark dance-like involuntary body movements associated with the disease earned it the appellative of chorea (from the Greek word *choros*, meaning dance) (Bates *et al.*, 2014). However, it was in 1872 that George Huntington first comprehensively described this disorder. In his work entitled "On Chorea", he provided the first clinical observation of families of patients affected by this disease. Spanning three generations of clinical records, Huntington described the dominant inheritance of the pathology and the cardinal features of HD: motor symptoms, cognitive decline and behavioural disturbances (Huntington, 2003). In the 1980s the name of the condition was changed into "disease", acknowledging that HD is characterized by a plethora of symptoms that are not only motor-related (Bates *et al.*, 2014).

Clinical manifestation of HD varies from patient to patient, even in the same family; however, motor symptoms are classically associated with the disease and are the criterion for HD diagnosis (Reilmann *et al.*, 2014). The most characteristic form of motor impairment is represented by choreatic movements, which progressively worsens over time, whereas a less common form of motor impairment is represented by hypokinesia, which characterizes late stages and juvenile forms of HD (Di Maio *et al.*, 1993; Roos, 2010). Additionally, dystonia (*i.e.* spasm) and tics can manifest in patients (Andrew *et al.*, 1993; Kirkwood *et al.*, 2001). Psychological symptoms and signs can precede motor manifestation, yet can be more difficult to be recognised as HD symptoms, and can therefore be misdiagnosed. Initially, patients manifest slower thinking, leading to lack of concentration. Short-term memory lapses are also frequent, until the procedural memory of patients and their spatio-temporal orientation is progressively lost. In

late stages, patients experience impairment of executive function, a clinical picture that culminates in complete dementia with loss of the ability to speak (Di Maio *et al.*, 1993; Bylsma *et al.*, 1990; Heindel *et al.*, 1988; Rosenblatt *et al.*, 2012). Psychiatric symptoms include progressive emotional disturbance, where the patients experience changes of mood and personality, depression, anxiety, apathy and irritability, often leading to suicide compulsion (Bamford *et al.*, 1995; Di Maio *et al.*, 1993).

These symptoms are strictly linked to prominent atrophy of the basal ganglia, with selective loss of the striatum (comprising the caudate nucleus and the putamen) and the damage of its two main neuronal pathways, the direct and the indirect pathways (Waldvogel *et al.*, 2014 and Figure 1-1). The basal ganglia controls movement and is implicated in cognitive functions, learning and mood, being integrated in a cortico-striatal circuit that modulates the activity of the thalamus and feedbacks to the cortex (Graybiel, 2000). The striatum receives the major excitatory glutamatergic and dopaminergic inputs from the cortex and substantia nigra pars compacta (SNc), respectively. In the direct pathway the striatum projects to the globus pallidus internus (GPi) and the substantia nigra pars reticulata (SNr) *via* neurons containing  $\gamma$ -amino-butyric-acid (GABA) and Substance P (SP). This results in the inhibition of the GPe and excitation of the thalamus, with activation of the cortex, ultimately facilitating movement (Figure 1-1). Conversely, in the indirect pathway, the striatum projects and inhibits the globus pallidus externus (GPe), *via* neurons containing GABA and enkephalin (ENK). The GPe consequently loses its ability to inhibit the subthalamic nucleus (STN). As a result, the STN sends excitatory messages to the GPe, which then inhibits the thalamus and consequently the cerebral cortex, suppressing movements (Figure 1-1). In HD, the excitatory glutamatergic cortical projections to the striatum are disrupted with consequent development of motor dysfunction (Sepers & Raymond, 2014). In the early stages, the indirect pathway is affected, with preferential loss of neurons containing GABA/ENK, leading to excitation of the thalamus, over-activation of the cerebral cortex and hence involuntary movements (Figure 1-1). Conversely, in late stages the direct neurons containing GABA and SP are lost, causing an increased inhibition of the thalamus (and hence of the cerebral cortex) leading to rigidity (Figure 1-1).

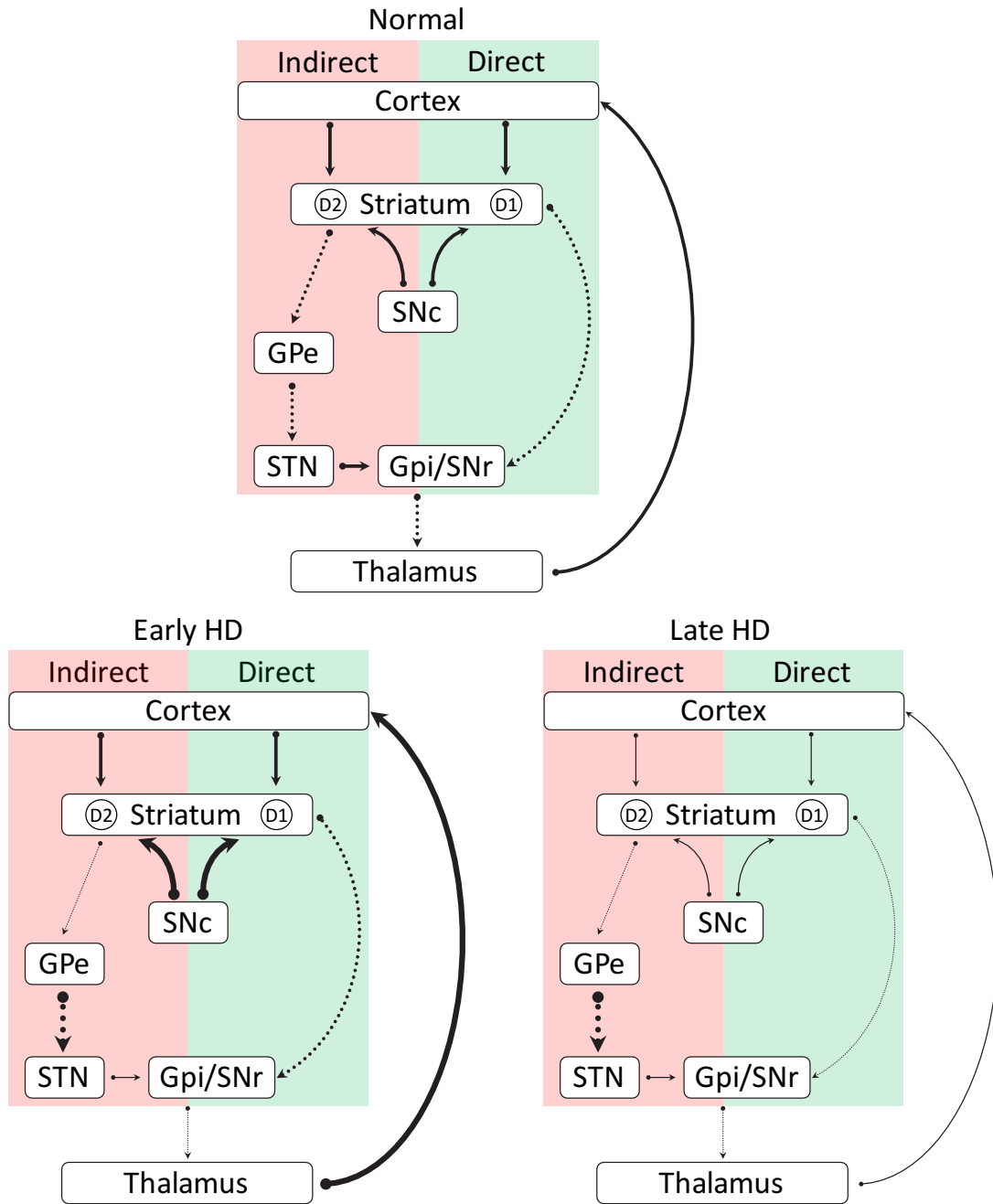


Figure 1-1 The basal ganglia pathways are impaired in early and late stages in HD.

Schematic representation of the direct (green background) and indirect (red background) pathways of the basal ganglia, with indication of the excitatory ( $\longrightarrow$ ) and inhibitory projections ( $\bullet\cdots\rightarrow$ ). Dopaminergic projections from the SNC are modulatory, depending upon the dopamine receptor (D1 or D2). In the normal brain the striatum receives glutamatergic projections from the cortex and dopaminergic projections from the SNC. In the direct way, the MSNs project to the GPi/SNr. In the indirect way, MSNs send their projections to the GPe, the latter influencing the output of the GPi/SNr via STN projections. Early stages are characterized by increased release of dopamine from the SNC, which lead to excitotoxicity of the MSNs in the indirect pathway, resulting in involuntary movement. Late stages of HD are characterized by reduced excitatory inputs from the thalamus and the cortex, reduced release of dopamine from the SNC and impairment of both pathways, resulting in rigidity and bradykinesia. D1, Dopamine receptor 1; D2, Dopamine receptor 2; GPe, globus pallidus externus; GPi, globus pallidus internus; MSNs, medium spiny neurons; SNC, substantia nigra pars compacta; SNr, substantia nigra pars reticulata; STN, subthalamic nucleus. Image redrawn from Sepers & Raymond, 2014.

In patients affected by HD, the striatum can shrink by more than 50% (de la Monte *et al.*, 1988; Niccolini & Politis, 2014 and Figure 1-2). The striatal volumetric reduction is due majorly to loss of the medium-sized spiny neurons (MSNs) that constitute ~95% of the striatal population, whereas the remaining neuronal cells, composed by a heterogeneous group of aspiny interneurons (fast-spiking, cholinergic and GABAergic interneurons) are differentially vulnerable to neuronal loss (Cicchetti *et al.*, 2000; Ferrante *et al.*, 1987). In addition, the globus pallidus and substantia nigra are severely affected by HD, with a globus pallidus volumetric loss that can reach ~50% (Albin *et al.*, 1992 and Figure 1-2). In patients affected by HD, the striatum can shrink by more than 50% (de la Monte *et al.*, 1988; Niccolini & Politis, 2014 and Figure 1-2).

Atrophy also severely affects the cerebral cortex especially in advanced stages and it is associated with motor impairment, dementia, psychological symptoms and visual deficiency (Rosas *et al.*, 2008). Several studies have found an overall cortical volume loss of ~30-50% (Halliday *et al.*, 1998; Hedreen *et al.*, 1991; Rosas *et al.*, 2002) and changes in neuron and glial cell size and density of ~9% (Rajkowska *et al.*, 1998). Reduction in size has been reported also for the other brain regions such as the STN, the thalamus, the hippocampus, the cerebellum, and the hypothalamus (Bates *et al.*, 2014).

In addition to chorea, psychological and psychiatric dysfunctions, which are referred to as “triad of symptoms”, there are other secondary manifestations that characterize the neuropathology. A hallmark of HD is unintentional weight loss, which occurs predominantly in late stages of the disease and contributes to higher mortality (Aziz *et al.*, 2008). Severe sleep and circadian rhythm disturbances affect HD patients, which are likely caused by dysfunction of the suprachiasmatic nucleus (Wulff *et al.*, 2010). Sleep impairment can increase irritability and anxiety, precipitating the mental decline of HD patients (Aziz *et al.*, 2010).

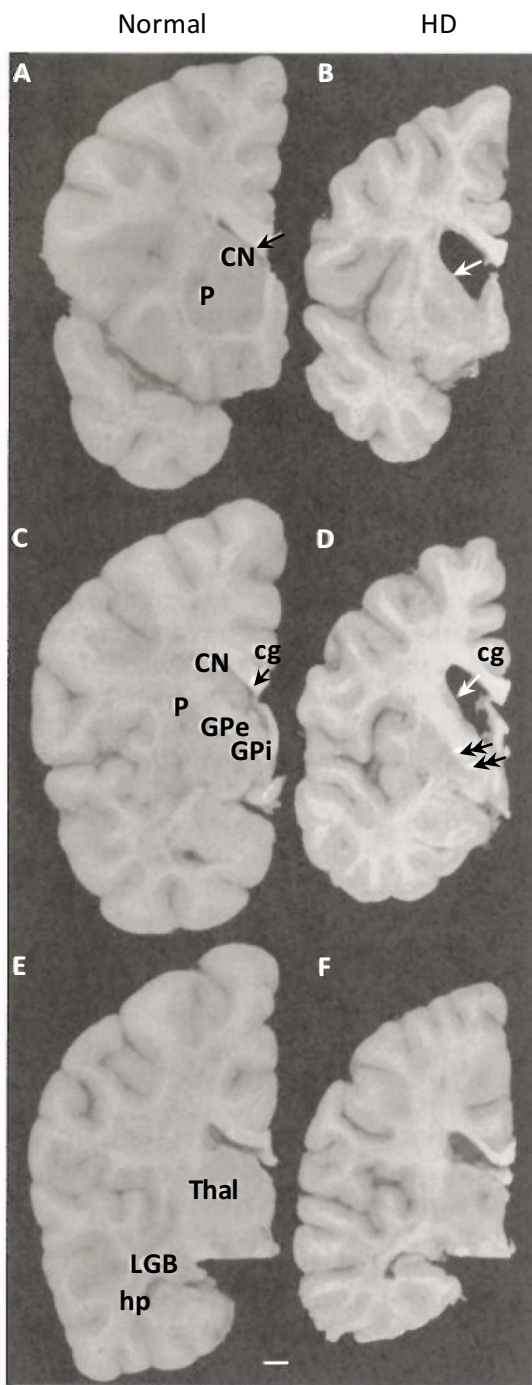


Figure 1-2 Neuronal loss in HD.

Coronal brain sections of three HD brains (B, D, F) compared to a control case (A, C, E). **B** Atrophy of the striatum (arrow) and cortex. **D** Atrophy of the globus pallidus (double arrows) and cortex. **F** Atrophy of the thalamus and cortex. Scale bar=1 cm. cg, cingulate gyrus; CN, caudate nucleus; GPe, globus pallidus externus; GPI, globus pallidus internus; hp, hippocampus; LGB, lateral geniculate body; P, putamen; Thal, thalamus. Modified from Bates *et al.*, 2014.

### 1.1.3 The genetic mutation causing HD

The work of MacDonald and colleagues (1993) localized the HD gene to the short arm of chromosome 4. This was later confirmed by the joint effort of “The HD Collaborative Research Group”. After studying the biggest HD kindred community in Venezuela, they identified the genetic locus as 4p16.3a, and named the HD gene *Huntingtin (HTT)* (Wexler, 2004). *HTT* contains 67 exons and encodes for a soluble, large protein of 348 kDa (Mangiarini *et al.*, 1996). *HTT* contains a *CAG* trinucleotide expansion lying in the first exon of the gene, which encodes an extended glutamine (polyQ) tract (Kremer *et al.*, 1994). In non-affected individuals the *CAG* region spans 9-35 *CAG* repeats. Individuals with the condition carry a mutated copy of *HTT* (*mHTT*) with a stretch of *CAG* that can reach 250 repeats. Clinical manifestations of HD emerge beyond a threshold of 35 repeats, with the disease being fully penetrant when *HTT* contains more than 40 *CAG* repeats. In individuals with 36-39 *CAG* repeats, HD is incompletely penetrant and the symptoms might not manifest (Brinkman *et al.*, 1997). The initial studies (Andrew *et al.*, 1993; Duyao *et al.*, 1993; Rubinsztein *et al.*, 1993; Snell *et al.*, 1993) identified an inverse correlation between the repeat length and the age of onset of the disease, *i.e.* a higher expansion leading to a faster progression of the pathology (Figure 1-3). In the majority of the cases the onset is in mid-life, however ~10% of HD cases are represented by the juvenile HD form, in which *CAGs* are above 70 and symptoms manifest before the age of 20 (Byers *et al.*, 1973). Clinical manifestations of juvenile cases are slightly different from those of adult onset; for instance, the motor symptoms are characterized by rigidity. Juvenile cases occur in patients with a positive family history of HD and are caused by anticipation. The *CAG* tract is unstable and shows a tendency to increasing its length if transmitted through the paternal line (Merritt *et al.*, 1969).

Interestingly, even among patients carrying the exact same number of repeats, there is a huge variability in terms of age of onset and disease manifestation (Wexler, 2004). In fact, the number of *CAG* repeats only accounts for ~47%-72% of the risk of developing disease, the rest depends upon environmental (up to ~62%) and genetic factors (up to ~38%) (Rosenblatt *et al.*, 2001). Natural variants of genes that modify the progression of the disease are called genetic modifiers. These can delay or accelerate the appearance of the first symptoms, especially in the low range of expanded *CAG* alleles, whereas when the *CAG* tract is very long, genetic modifiers have less of an effect (Gusella & MacDonald, 2009). The search for genetic modifiers has been the intense focus of the research in HD field, as identifying them could provide targets for therapeutic intervention, and deepen our knowledge about the molecular mechanisms relevant for HD.

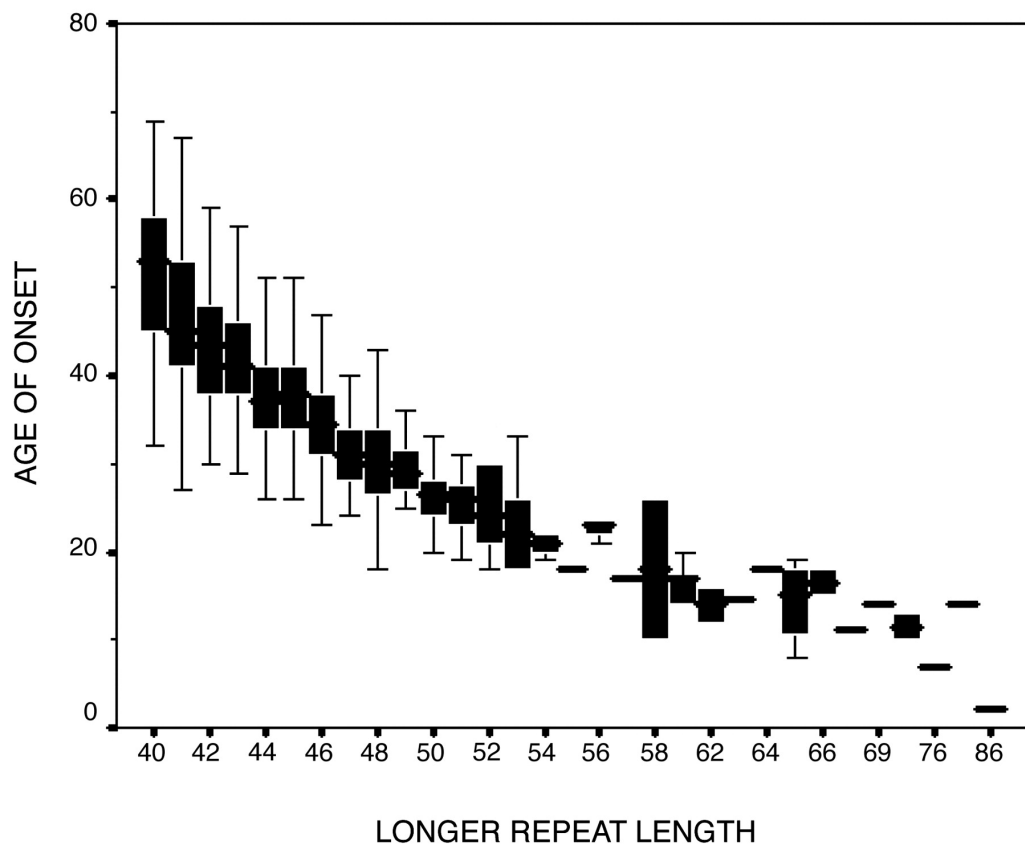


Figure 1-3 Variability in the age of onset of HD.

Age of onset and number of *CAG* repeats are inversely correlated in HD. Repeat length >70 leads to juvenile HD, with the age of manifestation of the first symptoms below 20 years. Importantly, the variability of the age of onset within patients carrying the same number of repeats inversely correlates the repeats. Image taken from Wexler, 2004.

#### 1.1.4 Huntington

HTT is a protein of 3,144 AA, with a molecular weight of 348 KDa, and a characteristic polyQ expansion at the N-terminus. By assuming different conformations, such as  $\alpha$ -helix, random coil, and extended loop, which are shown to improve the protein solubility, the polyQ tract is essential in mediating interactions with other proteins (Kim *et al.*, 2009). The conformation of the polyQ tract is influenced and stabilized by an adjacent poly proline (polyP) tract (Figure 1-4). The polyQ expansion in HD hampers the adoption of correct HTT secondary structures, stimulating aggregation of mHTT, which in turns affects the protein solubility and the protein interaction network, having profound consequences on its cellular functioning (Crick *et al.*, 2006). An important feature of HTT is represented by 16 HEAT domains. HEAT is an acronym that stands for 4 proteins in which this repeat structure is found: HTT, Elongator Factor 3, Protein Phosphatase2A and TOR1 (Figure 1-4). In HTT, these are organised in 4 clusters and postulated to serve as coordinators for protein-protein interactions (Andrade & Bork, 1995; Tartari *et al.*, 2008). HTT also possesses a C-terminus nuclear export signal (NES), a N-terminus nuclear localisation signal (NLS) and several post-translational sites (Bates *et al.*, 2014 and Figure 1-4). Post-translational modifications include ubiquitination, which targets HTT to the proteasome and therefore is essential for maintaining HTT homeostasis in the cells (Kalchman *et al.*, 1996); SUMOylation, which modulates HTT stability, function and subcellular localization (Steffan *et al.*, 2004); phosphorylation and acetylation, which are essential for HTT proteosomal and autophagy-lysosomal clearance (Aiken *et al.*, 2009; Jeong *et al.*, 2009); and palmitoylation, which plays an essential role in HTT vesicular trafficking (Yanai *et al.*, 2006). Post-translational modifications are impaired in HD, leading to proteosomal dysfunction, HTT aggregation and toxicity, axonal transport defects and impaired autophagy (Zuccato *et al.*, 2010). HTT possesses several cleavage sites, which enable the proteolytic cleavage of HTT. The best-known proteolytic events are catalysed by caspases (Bates *et al.*, 2014 and Figure 1-4). HTT proteolysis plays a major role in HD pathogenesis, as N-terminal mHTT fragments potentiate toxicity and are proposed to play a major role in HD pathogenesis (see below).

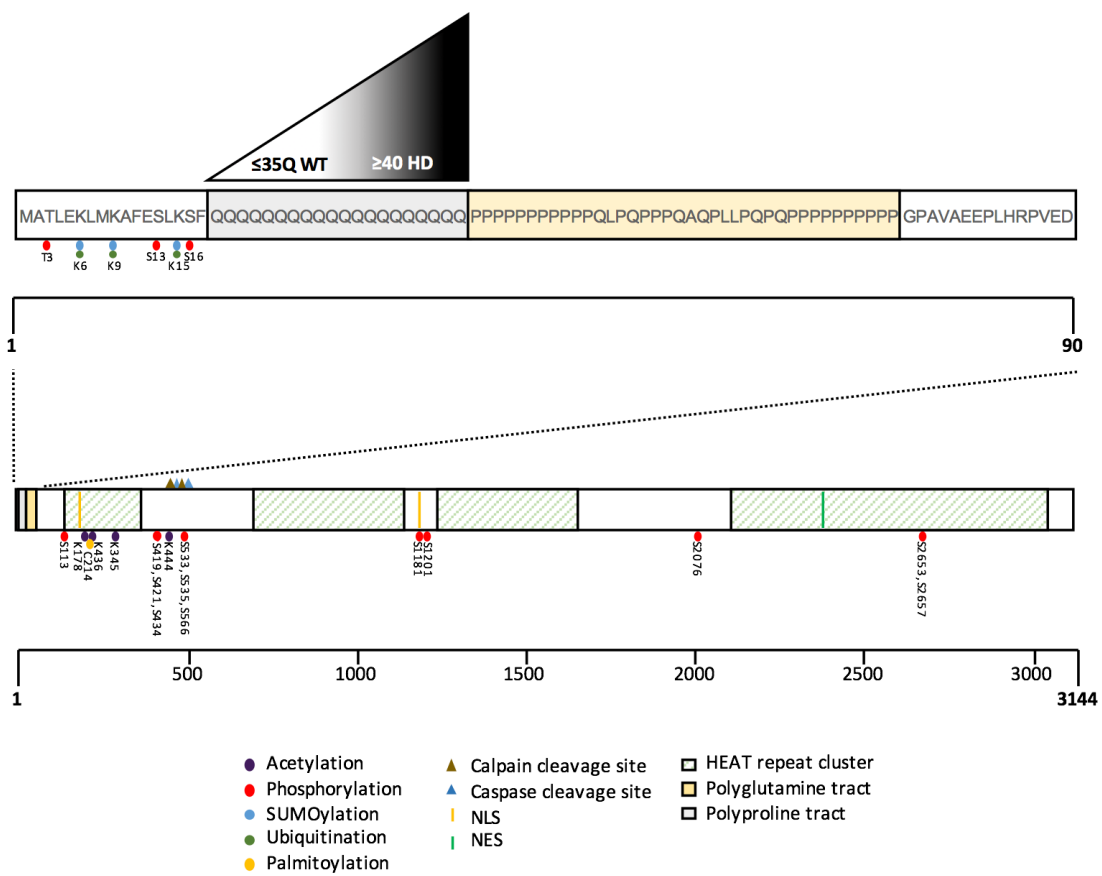


Figure 1-4 Representation of the wild type HTT primary structure zooming in on the first exon.

Post-translational modification, cleavage sites and the 4 HEAT domains are annotated. Threonine (T) and serine (S) are phosphorylated. Lysine (K) on the first exon are the target of either ubiquitination or SUMOylation, whereas in the rest of the protein are acetylated. HTT is palmitoylated at the cysteine (C) 214. The sequence of the first exon shows the polyQ tract (with annotation of the pathogenic threshold) and the adjacent polyP tract. NES, nuclear export signal; NLS, nuclear localisation signal. Image redrawn from Mort *et al.*, 2015.

HTT is ubiquitously expressed throughout the human body, with the highest levels being reported in the central nervous system (CNS) and the testes (Cattaneo *et al.*, 2005). Although found in the nucleus (Kegel *et al.*, 2002), HTT is expressed primarily in the cytoplasm, where it is associated with synaptic vesicles, the late endosomes, autophagic vesicles, the endoplasmic reticulum (ER), the Golgi complex, clathrin-coated vesicles (CCV), microtubules and mitochondria (Cattaneo *et al.*, 2005; DiFiglia *et al.*, 1995; Hoffner *et al.*, 2002; Velier *et al.*, 1998), highlighting essential functions in the cell.

HTT is required in early developmental stages, such as gastrulation. Early studies performed in mice reported embryonic lethality for homozygous HTT knockout mice (*Hdh*-/-) (Nasir *et al.*, 1995; Zeitlin *et al.*, 1995; Duyao *et al.*, 1995). Reduced levels of HTT led also to severe brain deficiency as demonstrated in heterozygous knockout mice (*Hdh*+/-) (Nasir *et al.*, 1995; O'Kusky *et al.*, 1999; White *et al.*, 1997). These findings have also been recapitulated in zebrafish, where morpholino-induced HTT knock-down led to neurodevelopmental defects (Henshall *et al.*, 2009). Recent studies, moreover, have elucidated the role of HTT in neurulation (Lo Sardo *et al.*, 2012), its involvement in cortical neurogenesis (Godin *et al.*, 2010), and brain development (Reiner *et al.*, 2003; Tong *et al.*, 2011). Both in humans and in mice, HTT exists in multiple forms: the full-length protein and truncated forms, the latter deriving from alternative splicing (Hughes *et al.*, 2014; Kegel *et al.*, 2002; Lin *et al.*, 1993; Lin *et al.*, 1994). In HD, mis-splicing of mHTT produces an exon 1 pathogenic variant, which, together with the small fragments derived from the proteolytic cleavage of full-length mHTT, is believed to trigger cellular and nuclear toxicity (Sathasivam *et al.*, 2013; Landles & Bates, 2004; Hughes *et al.*, 2014).

### 1.1.5 The molecular mechanisms leading to HD pathogenesis

#### 1.1.5.1 mHTT misfolding and aggregation

The propensity of mHTT to form intracellular aggregates is the pathological hallmark of HD. In post-mortem brains of both human and mice, early immunocytochemical analyses have highlighted the presence of cytoplasmic inclusion bodies (IBs) and neuronal intranuclear inclusions (NIIs), which were immunopositive for the N-terminus fragment of HTT (Davies *et al.*, 1997; DiFiglia *et al.*, 1997; Ordway *et al.*, 1997; Scherzinger *et al.*, 1999; Schilling *et al.*, 1999). mHTT is able to acquire a  $\beta$ -sheet conformation, which favours oligomerization and acts as a seed for the further fibrillation, a process that culminates in the formation of IBs and NIIs (Poirier *et al.*, 2005 and Figure 1-5). Misfolding and aggregation influence significantly the pathology, the onset, and

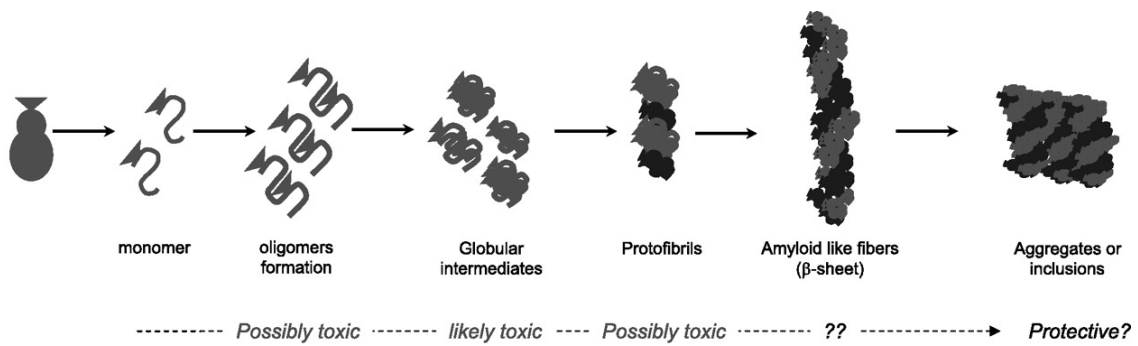


Figure 1-5 Schematic representation of mHTT aggregation process.

Aggregation is a multi-step process leading to IBs, which is believed to be neuroprotective. Misfolded mHTT assumes a  $\beta$ -sheet conformation, which favours the formation intermediate toxic species, before the assembly in amyloid like fibers. Inclusions are characterized by a diverse range of size, varying from very small aggregates in the range of 100 nm to large IBs of 5  $\mu\text{m}$  (Sahl *et al.*, 2012; DiFiglia *et al.*, 1997). Image taken from Zuccato *et al.*, 2010.

the progression of HD (Bates *et al.*, 2014). They lead to a *loss-of-function* state, where the misfolding creates a non-functional protein and consequent loss of the molecular activities fundamental for the survival and functioning of neurons, and to a *gain-of-function* state, where the misfolded protein becomes toxic for the cell (Cattaneo *et al.*, 2005). Most work suggests that the gain-of-function role is the predominant contribution to pathogenesis (Gusella & MacDonald, 2000). In the aggregation process, mHTT sequesters transcription factors and various proteins such as chaperones, synaptic constituents, proteins implicated in neurotransmission and in the ubiquitin-proteasome system, depleting the cell of functional components (Davies *et al.*, 1997).

Molecular chaperones assist in the folding of newly synthesized proteins into their native state, where they have a well-defined secondary and tertiary structure that confers solubility and stability. Correct protein folding ensures that the protein hydrophobic groups and a large portion of the polypeptide backbone are not exposed. When a globular protein partially or globally unfolds, it loses its native conformational state exposing those regions that would normally be hidden inside. Consequently, the protein gains high conformational flexibility, which enhances intramolecular interactions, leading to the formation of  $\beta$ -sheet-rich amyloid fibrils (Soto, 2003). Using Förster Resonance Energy Transfer (FRET), Caron and co-workers found that the N-terminal region of HTT can fold back onto its polyP region (Caron *et al.*, 2013). They also discovered that when the polyQ tract is more than 37Q, this conformation is altered due to a diminished intrinsic flexibility of the polyQ region itself, which loses the capacity to fold due to increased rigidity (Caron *et al.*, 2013). As a result, mHTT unfolds, a phenomenon that seems to underlie the structural changes favouring the assembly of mHTT in  $\beta$ -sheets, the first step in the formation of amyloid-like structures (Nagai *et al.*, 2007). Molecular chaperones and co-chaperones can assist in refolding (Morimoto, 2011), and when this process fails, the quality control system of the cell ensures that improperly folded proteins are targeted to the ubiquitin proteasome system (UPS) (Amm *et al.*, 2014). However, in HD this pathway is impaired (Figure 1-6). While initially IBs were proposed to physically “clog” the proteasome (Bence *et al.*, 2001), recent evidence suggest that non-aggregated mHTT is responsible for overwhelming the chaperone system, leading to an increased flux of ubiquinated proteins “queuing” to be degraded by the UPS (Hipp *et al.*, 2012). With a dysfunctional UPS, proteins can be alternatively degraded by macroautophagy (hereafter simply referred to as autophagy). In HD autophagy is impaired due to alteration in cargo recognition, which produces empty vesicles (Martinez-Vicente *et al.*, 2010 and Figure 1-6), hence, instead of being degraded, mHTT accumulates and aggregates.

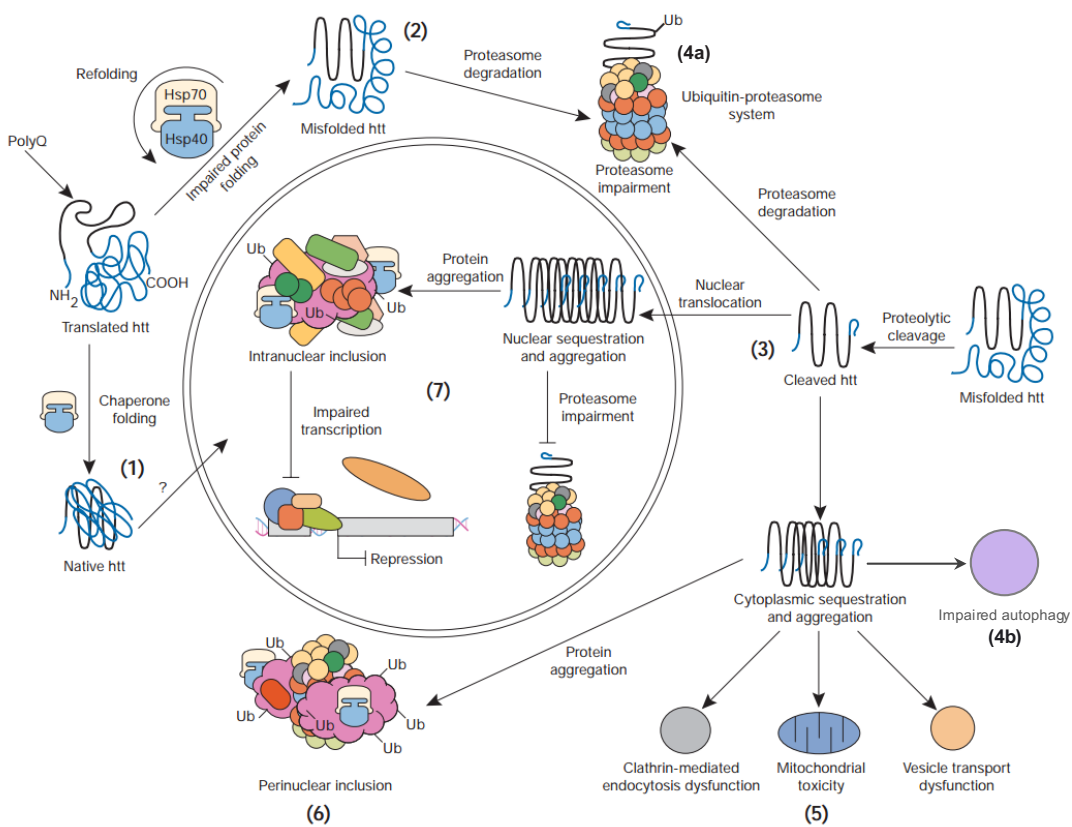


Figure 1-6 Summary of the main pathways disrupted by mHTT.

Chaperones activity ensures that newly synthesized proteins are correctly folded in their native state (1). However, in the presence of an expanded polyQ tract mHTT is misfolded (2). Misfolded mHTT undergoes proteolytic cleavage, which produces toxic N-terminal fragments, able to enter the nucleus (3). Proteins are triaged by the cellular quality control system, which would normally target misfolded proteins and cleaved fragments to the UPS for degradation; this is impaired in HD (4a). Deterioration of the lysosome-autophagy system prevents the clearance of misfolded and aggregated mHTT (4b). In the cytoplasm mHTT interacts and sequester a variety of proteins causing dysfunction of clathrin-mediated endocytosis, of vesicle transport and mitochondrial toxicity (5). Further aggregation results in cytoplasmic IBs and in NIIs (6). In the nucleus, mHTT sequester a variety of transcription factors leading to transcriptional dysregulation (7). Modified from Landles & Bates, 2004.

Similarly to other neurodegenerative disease, such as Alzheimer's disease, Parkinson's disease and amyothrophic lateral sclerosis, in HD aggregates can spread between neurons in a prion-like fashion, causing non-cell autonomous damage. This propagation occurs in neuronal networks and, although largely elusive, appears to be dependent upon the release of synaptic vesicles hence requiring both the exocytotic and endocytic machineries (Babcock & Ganetzky, 2016; Pecho-Vrieseling *et al.*, 2014).

Although IBs were initially associated with neuronal death (Davies *et al.*, 1997; DiFiglia *et al.*, 1997; Ordway *et al.*, 1997) other studies found evidence of a neuroprotective role (Cummings *et al.*, 1999; Saudou *et al.*, 1998; Taylor *et al.*, 2003), opening a long-term debate about the role of aggregates in HD pathogenesis. Inhibition of aggregation has been shown to be protective in a variety of HD models, equally, manipulation in the opposite direction produced positive effects (Sisodia, 1998). In a milestone study, Arrasate and colleagues used an automated microscopy system to examine a primary culture of rat striatal neurons transfected with N-terminal fragments of mHTT (Arrasate *et al.*, 2004). They measured IBs formed in relation to average neuronal survival, concluding that neuronal death was not associated with IBs formation and that neurons formed IBs earlier were also the most long-lived (Arrasate *et al.*, 2004). In their study the authors proposed that aggregation leading to IBs formation could be a mechanism for coping with ubiquitous toxic mHTT species. With the two main cellular degradative pathways impaired, IBs represent a neuroprotective process to confine toxic mHTT species into a compact structure reducing the toxic burden for the cell.

#### 1.1.5.2 Transcriptional dysregulation and its role in the loss of function of *brain-derived neurotropic factor (BDNF)*

Early microarray studies in R6/2 mice, which express the first exon of mHTT (Mangiarini *et al.*, 1996), have identified altered global transcription upon mHTT overexpression (Cha, 2000; Luthi-Carter *et al.*, 2000). As already mentioned, N-terminal fragments of mHTT are able to enter the nucleus where they interact and sequester a large number of transcription factors into aggregates, leading to transcriptional defects (Figure 1-6). Moreover, loss of functional wild type HTT contributes to transcriptional dysregulation in HD. One of the main roles of HTT is the transcriptional regulation of *brain-derived neurotropic factor (BDNF)*, a regulator of neuroplasticity, growth and survival of neurons (Zuccato *et al.*, 2001). As reported by Zuccato and colleagues, overexpression of HTT led to higher levels of *BDNF* mRNA, both in immortalized ST1A cells and in a mouse model of HD (Zuccato *et al.*, 2001). Conversely, constitutive or conditional *Hdh+/-* mice, showed decreased level of *BDNF* mRNA (Zuccato *et al.*, 2003; Zuccato & Cattaneo, 2007). Similarly, BDNF levels in patients affected by HD were 50% lower compared to a control sample,

demonstrating the inability to sustain normal BDNF production (Zuccato *et al.*, 2008). As BDNF is essential for neurons, *BDNF* transcriptional dysregulation is considered central in HD pathogenesis.

#### 1.1.5.3 Axonal and synaptic activity impairment

In HD, morphological abnormalities in the most vulnerable neurons of the brain can manifest even 20 years before the actual neuronal death and are responsible for the neuronal defects associated with the symptoms of the disease (Bates *et al.*, 2014). Several studies have implicated HTT in microtubule-based axonal transport. Reduction in endogenous HTT leads to vesicle and mitochondrial trafficking impairment in *Drosophila* (Gunawardena *et al.*, 2003). Moreover, knocking down HTT in mice and in the giant axon of squid compromises axonal transport (Szebenyi *et al.*, 2003; Trushina *et al.*, 2004). Wild type HTT participates in the assembly of motor complex on microtubules. It interacts with dynein (an essential component of the axonal transport) *via* HTT-associated protein 1 (HAP1), regulating vesicular trafficking, including that of BDNF (Saudou & Humbert, 2016). In HD, this interaction is altered due to HAP1 binding preferentially to mHTT, leading to a reduced anterograde and retrograde axonal transport rate, as observed in a variety of HD models (Gunawardena *et al.*, 2003; Trushina *et al.*, 2004). Moreover, phosphorylation of HTT at serine 421 is crucial in promoting the anterograde transport of vesicles along microtubules. Lack of mHTT phosphorylation further impairs vesicle trafficking (Colin *et al.*, 2008; Zala *et al.*, 2008).

Defects in synaptic components have been linked with HD. They have been attributed to various factors such as decreased expression or mislocalisation of several proteins regulating vesicle traffic to the membranes (Smith *et al.*, 2005). HTT is itself involved in clathrin-mediated endocytosis *via* interaction with HTT-interacting protein 1 (HIP1) (Li & Li, 2004). This association is decreased upon polyQ expansion and underlies impairment in vesicular transport (Kalchman *et al.*, 1997). The expanded polyQ protein has also been associated with a key molecule involved in synaptic transmission, namely post-synaptic density 95 (PSD95). mHTT has been shown to have lower affinity for PSD95 compared to wild type HTT. As a consequence, PSD95 binds more strongly with the glutamate receptor N-methyl-D-aspartate (NMDAR), an ionotropic receptor for glutamate, increasing its presence at the membrane (Sun *et al.*, 2001). This results in excitotoxicity, namely a toxic effect due to excessive glutamatergic transmission. In fact, when neurons are over-activated, they are also more permeable to  $\text{Ca}^{2+}$  influx in the cytoplasm, which in turn impairs the function of mitochondria and leads to neuronal death (Fan & Raymond, 2007).

#### 1.1.5.4 Mitochondrial dysfunction and oxidative stress

The pathological susceptibility of cortico-striatal neurons in HD is influenced by mitochondrial dysfunction (Lin & Beal, 2006). Much evidence has shown that morphological and electrophysiological defects of mitochondria, resulting in reduced activity of the mitochondrial respiratory complexes in the most vulnerable regions of the brain and in body muscles (Lin & Beal, 2006 and Figure 1-6). On the one hand, mHTT is responsible for mitochondrial transcriptional dysregulation. This affects the biogenesis of the mitochondria as well as the expression levels of mitochondrial components, with consequent reduction in the number of organelles in the cell (Bossy-Wetzel *et al.*, 2008). On the other side, there is evidence that mHTT N-terminal fragments can cause defects in healthy mitochondria, which are similar to those observed in HD (Panov *et al.*, 2002). In HD dysfunctional mitochondria cause alteration in  $\text{Ca}^{2+}$  buffering, a drop in ATP production and an overproduction of reactive oxygen species (ROS), which generate oxidative stress (Bossy-Wetzel *et al.*, 2008). Moreover, mHTT has been found at the mitochondrial membrane, where it is believed to stimulate the release of cytochrome c, with the consequent activation of the apoptotic pathway (Orr *et al.*, 2008).

#### 1.1.6 Autophagy in HD

Autophagy is a catabolic process that is of fundamental importance in the clearance of toxic misfolded mHTT. Through the formation of a double-membrane vesicle (autophagosomes) a small portion of cytoplasm is isolated from the rest of the cell. The subsequent fusion of the autophagosome with a lysosome produces an autophagolysosome, where proteases degrade the engulfed material. The canonical autophagic core machinery is composed of the Atg (Autophagy-related) proteins, which coordinate the cargo recognition and sequestration into the phagophore, direct the maturation of the phagosomes into autophagosomes and their fusion with the lysosomes (Jung *et al.*, 2010; Kroemer *et al.*, 2010; Klionsky & Emr, 2000). The importance of autophagy in HD was greatly emphasised by a series of early investigations conducted by DiFiglia and colleagues over two decades ago. Analysis of post-mortem brains of human patients revealed that mHTT accumulates in endosomal-like structures in cortical and striatal neurons (Sapp *et al.*, 1997). mHTT has also been found associated with endosomes in patient primary fibroblasts (Velier *et al.*, 1998) and the expression of full-length HTT carrying 100Q in clonal mouse striatal cells stimulates the production of autophagic vacuoles, lysosome-like bodies and tubulation of endosomal membranes (Kegel *et al.*, 2000). Similarly, an early report by Li and co-workers in 2001 demonstrated accumulation of autolysosomes in the lateral globus pallidus striatal projections of R6/2 HD model mouse brains. Since then, many lines of investigation have demonstrated that autophagy is impaired in HD. Expression levels of the autophagic core proteins are altered in HD (Hodges *et al.*, 2006; Martin *et al.*, 2015). Moreover, a prominent

effect of defective autophagy is represented by mHTT-triggered apoptosis. In this process, caspases, such as caspase-3 are activated, resulting in the targeting and destruction of autophagic factors such as Beclin1 (BECN1), Atg4D and Atg5, enhancing mHTT toxicity (Wirawan *et al.*, 2010). In fact, the defective degradative pathway impacts not only on the clearance of toxic mHTT species, but also on the degradation of damaged organelles, *e.g.* mitochondria, ultimately exacerbating cellular dysfunction. Thus, one strategy of intervention for HD has been largely centred on modulation of autophagy, in the attempt to improve the cellular degradative pathway and enhance cellular clearance. Induction of autophagy, *via* administration of rapamycin and subsequent inhibition of the Tor (Target of rapamycin) signalling pathway, has been shown to reduce mHTT accumulation and to ameliorate HD symptoms in *Drosophila* and in mouse model of HD (Ravikumar *et al.*, 2002; Ravikumar *et al.*, 2004). However, the human side effects of rapamycin paved the road for the search of compounds, which more selectively enhance cellular autophagic levels. Tor-independent induction of autophagy was identified through a screen conducted in yeast, which led to the discovery of a class of molecules called small-molecule enhancers of rapamycin (SMERs) which are able to stimulate autophagy and the consequent clearance of mHTT in HD model cells (Sarkar & Rubinsztein, 2008). In recent years, the Rab GTPase family has been the focus of intense attention, as a variety of its members have also been identified as modulators of autophagy (Szatmári & Sass, 2014). Rabs are coordinators of vesicle trafficking and their role in up-regulating the degradative clearance of mHTT has just begun to emerge as therapeutically relevant for HD (Agola *et al.*, 2011).

## 1.2 Rab proteins

Rab proteins belong to the Rat sarcoma (Ras) small GTPase superfamily, a group of proteins involved in a variety of cellular signal transduction cascades, comprising about 150 members belonging to 5 major subfamilies: Ras, Rab, Rac, Rho, and Arf. Rabs are highly related to the yeast Ypt1 and Sec4 proteins (Zhen & Stenmark, 2015) and they were first isolated from a rat brain cDNA library (Rab stands indeed for Ras-related proteins in brain) by means of oligonucleotide probes (Touchot *et al.*, 1987).

Rabs are a family of monomeric G proteins that play key roles in eukaryotic cells as major regulators of intracellular communication. They coordinate all the events in vesicle trafficking, from vesicle budding and motility, to its fusion and its target compartment (Figure 1-7). Rabs show a high degree of conservation sharing an identity of ~55-75% across species. With over 70 Rabs being identified in humans, 33 in flies and 11 in yeast, the members of this family show an extremely specific compartmentalization within the cell and an increasing complexity along the

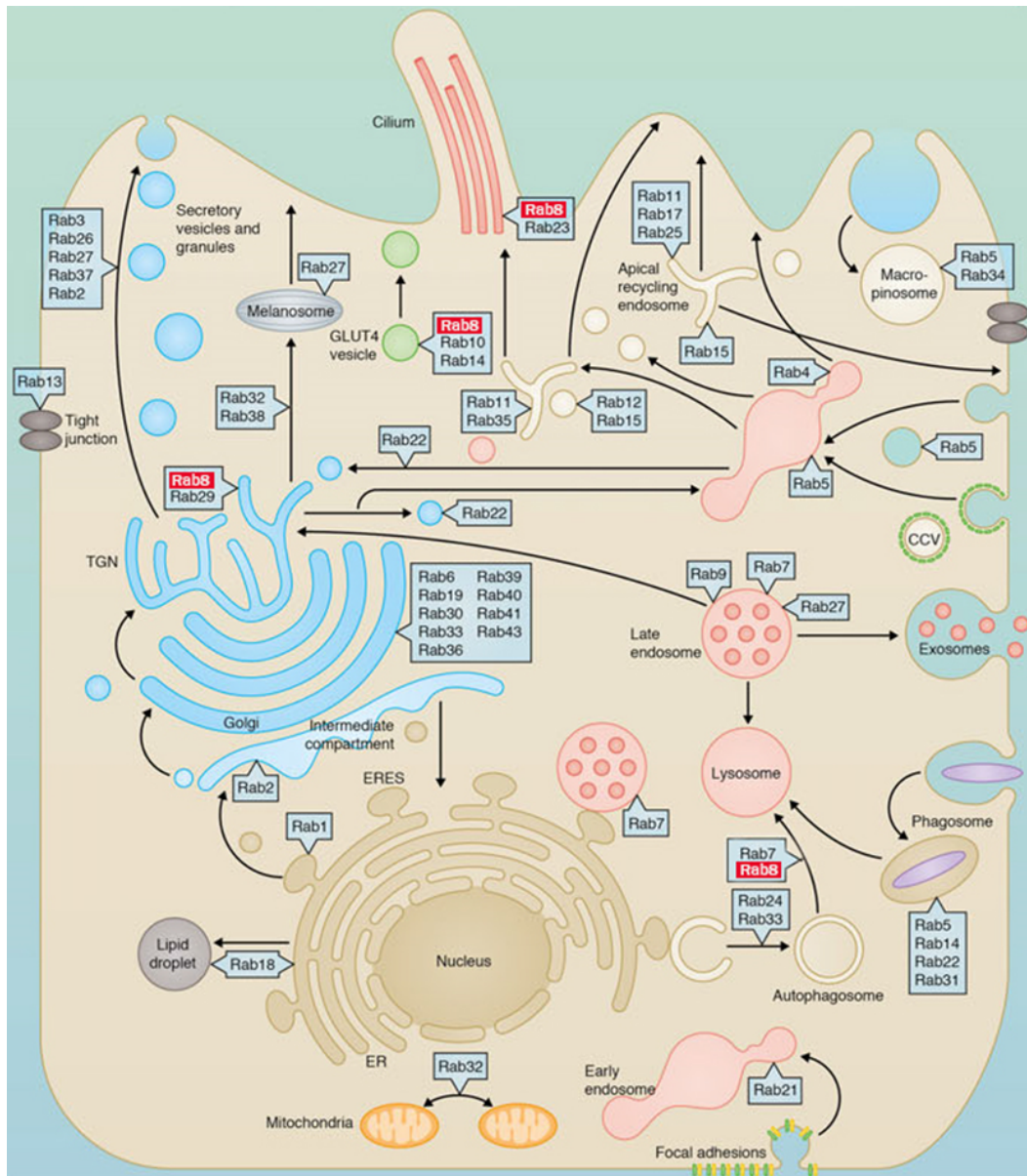


Figure 1-7 Schematic representation of Rabs location and function in the cell.

Rabs are involved in the coordination of vesicular trafficking in specific compartments of the cell. Trafficking at the endoplasmic reticulum exit site (ERES) and at the Golgi intermediate compartment (IC) is mediated by Rab1. Rab2 localizes at IC and mediates the trafficking to the Golgi. A number of Rabs, namely, Rab6, Rab19, Rab30, Rab33, Rab36, Rab39, Rab40, Rab41 and Rab43 are involved in the intra-Golgi trafficking. The secretory trafficking from the trans-Golgi network (TGN) to the membrane surface is regulated by Rab8, which, together with Rab10 and Rab14, coordinates also the glucose transporter type 4 (GLUT4) vesicle trafficking. Moreover Rab8 and Rab23 participate in ciliogenesis. Rab2, Rab3, Rab7, Rab26, Rab27, Rab37 direct secretory vesicles and granules to the plasma membrane. Rab27 is also involved in the apical translocation of melanosomes, whose biogenesis is mediated by Rab32 and Rab38. Rab13 mediates the regulation of tight junctions. Lipid droplets formation is controlled by Rab18. The TGN-early endosome bidirectional trafficking is mediated by Rab22. Rab5 is found at the early endosome, where it regulates endocytosis and clathrin-coated vesicles (CCVs) fusion. With Rab34, it participates to macropinocytosis, and with Rab14, Rab21, Rab22 and Rab31, it mediates phagocytosis. Another Rab localizing at the early endosome is Rab4, which mediates the fast endocytic recycling at the recycling endosomes. Rab15 and Rab12 mediate vesicle delivery to the recycling endosomes. At the apical recycling endosomes Rab15 regulates the trafficking to the basolateral membrane, whereas with Rab17 and Rab25, it mediates the trafficking to the apical membrane. The slow endocytic recycling is mediated by Rab11 and Rab35. Rab24 and Rab33 are involved in the autophagosomes formation, whereas Rab7 mediates the fusion of the autophagosomes with the lysosomes. Rab9, which localises at the late endosome, directs the vesicle trafficking to the TGN, and with Rab7 and Rab27, it directs vesicles to the lysosomes. Rab21 regulates endosomal trafficking of integrin. Mitochondrial fission is mediated by Rab32. Image modified from Zhen & Stenmark, 2015.

evolutionary scale (Colicelli, 2004; Zhang *et al.*, 2007; Chan *et al.*, 2011). By localising each one in a different compartment, Rab GTPases control the specificity and directionality of their cargos, according to the transport route that they control. Figure 1-7 illustrates the complexity and the specificity of the Rab vesicular trafficking in the cell.

The mechanisms of action of the Rab GTPases lie in their ability to switch between active GTP- and the inactive GDP-bound forms. These conformation changes are facilitated by guanine nucleotide exchange factors (GEFs) and GTPase-activating proteins (GAPs), two effectors that, acting in opposite directions, catalyse GDP dissociation and trigger GTP hydrolysis respectively (Zhen & Stenmark, 2015 and Figure 1-8). In addition, the Rab nucleotide cycling is further tuned by their reversible interaction with membranes, which is coordinated by two further effectors: GTP dissociation inhibitor (GDI) and GDI displacement factor (GDF). In their inactive form, Rabs bind to Rab Escort Protein (REP) and are geranylgeranylated by a geranylgeranyl transferase (GGT). This modification is possible thanks to the carboxy-terminal cysteine residues, typically being *xxCC*, *xCCx* or *CCxx* (where C represents the cysteine and the x any aminoacid) (Shen & Seabra, 1996). Once prenylated, Rabs recruit GDI, which, by preventing the release of GDP, favour the Rabs disassociation from membrane and their recycle back to the cytosol. On the other hand, the membrane association is favoured by GDF, which by recognizing the Rab-GDI complexes, promotes the release of GDI and allows the Rab to accumulate on the target membrane (Zhen & Stenmark, 2015). The fine tuning of Rab activity ensures the efficient spatio-temporal delivery of the membrane-bound cargos to their correct destinations (Figure 1-8).

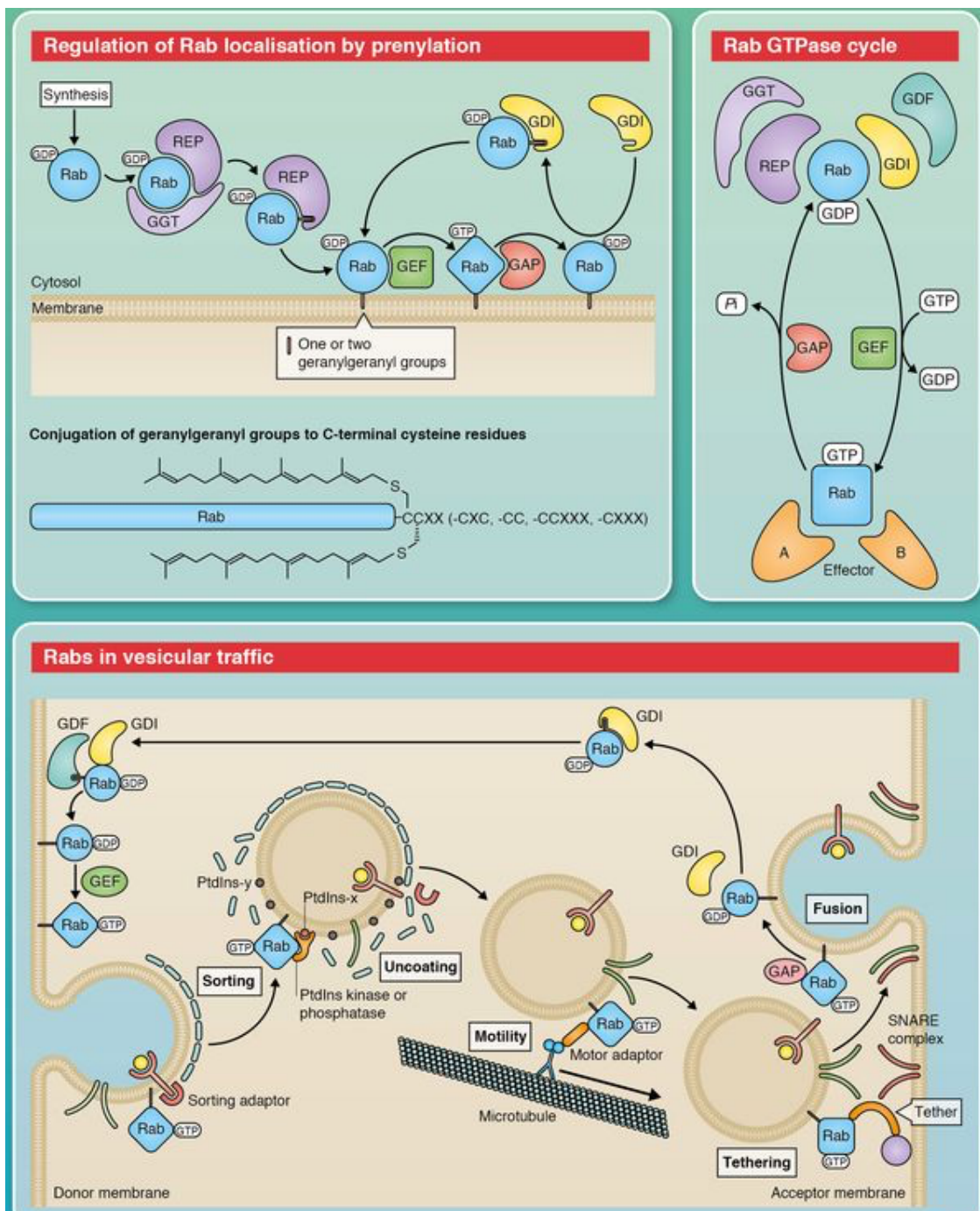


Figure 1-8 Overview of the Rab function and role in the cell.

Top panels: Schematic representation the two Rab activating mechanisms: regulation of Rab localisation by prenylation, and Rab GTPase cycle. For details, see text. Bottom panel: Schematic representation of Rab involvement in vesicular traffic. In the multi-step process that goes from the budding of a newly synthesized vesicle to its fusion with its acceptor membrane, Rab GTPases mediates the cargo sorting, the vesicle uncoating, the motility along microtubules, the tethering and the finally the fusion of the vesicle with the target membrane. Image taken from Zhen & Stenmark, 2015.

Intracellular communication is fundamental for neurons. Neuronal polarization, release of neurotransmitters, receptor uptake and recycling, and axonal transport are all events mediated by the Rab GTPases, and mutations of Rabs or of their effectors has been linked with neuropathologies that might manifest as mental retardation, peripheral neuropathy or neurological abnormalities (Ng & Tang, 2008; Szatmári & Sass, 2014). Moreover, impaired vesicle trafficking has been implicated in the pathogenesis of several neurodegenerative diseases (Agola *et al.*, 2011). In HD, the activity and/or the localisation of Rab5, Rab8 and Rab11 have been reported to be defective, possibly contributing to the progression of the neuropathology (del Toro *et al.*, 2009; Li *et al.*, 2009b; Li *et al.*, 2009a; Li *et al.*, 2012; Ravikumar *et al.*, 2008). Overexpression of Rab5 and Rab11 has been shown to ameliorate HD-induced phenotype in both flies and cell models (Li *et al.*, 2009b; Li *et al.*, 2010; Ravikumar *et al.*, 2008; Richards *et al.*, 2011; Steinert *et al.*, 2012). Conversely, manipulation in the opposite direction, *i.e.* knock down of Rab5, was shown to synergistically exacerbate mHTT toxicity. The ability of Rab5 to rescue HD-relevant phenotypes has been explained by up-regulation of autophagy (Ravikumar *et al.*, 2008). Given their role in vesicular trafficking, it is not surprising that Rabs are also involved in several steps of the autophagic-lysosomal pathway. A list of the Rabs that so far have been found to be involved in autophagy is provided in Table 1-1. Among these, Rab8, the focus of this work, has also been shown to be involved in autophagy.

Table 1-1 List of Rab proteins involved in autophagy.

Atg, Autophagy-related; PIK3, Phosphatidylinositol-4,5-bisphosphate 3-kinase; BECN1, Beclin 1; LC3, Light chain; TORC1, Target of Rapamycin Complex. Adapted from Szatmári & Sass, 2014.

Rab	Localization/role	Role in autophagy
Rab1	ER-Golgi transport	Phagophore assembly by regulating Atg9 localization Regulation of TORC1 activity
Rab4	Early endosomes, cargo recycling	Autophagosome formation
Rab5	Early endosomes	Regulation of PIK3-BECN1 complex Regulation of TORC1 activity
Rab7	Transport of secretory and recycling vesicles toward plasma membrane	Microtubular transport of autophagosomes Autophagosome maturation Autophagic lysosome reformation Autophagosome formation Regulation of TORC1 activity
Rab8	Recycling from late endosomes to TGN	Autophagy-based secretion Autophagosome maturation during antimicrobial autophagy
Rab9	Secretory pathway (yeast), recycling endosomes	Autophagosome maturation during antimicrobial autophagy Autophagosome formation during Atg5- and Atg7-independent noncanonical autophagy
Rab11	ER, cis-Golgi	Providing RE-derived membrane source for autophagy Maturation of autophagosomes Regulation of TORC1 activity
Rab24	Biogenesis of lysosome-related organelles, regulation of ER-mitochondria contact	Co-localization with LC3 upon autophagy-induction
Rab32	Biogenesis of lysosome-related organelles, regulation of ER-mitochondria contact	Required for autophagosome formation
Rab33	Medial Golgi	Role in autophagosome formation and maturation

### 1.3 Rab8

Rab8 is a protein with a molecular weight of 24 KDa (Chavrier *et al.*, 1990). In mammals the gene encodes for two isoforms Rab8a and Rab8b, sharing 80% of identity. The two isoforms are ubiquitously expressed throughout the body, and despite some differences in their tissue expression patterns, they have been shown to play similar roles in cells (Armstrong *et al.*, 1996). Contrary to the majority of the Rab GTPase members, which carries two cysteine at their C-ends, Rab8 ends with a *CaaX* motif (where a is any aliphatic aminoacid and x any amino acid), resulting in only one geranylgeranylation (Joberty *et al.*, 1993; Wilson *et al.*, 1998).

As its yeast counterpart Sec4, Rab8 is involved in the post-Golgi trafficking, highlighting the conserved role across species. Early ICC studies have confined Rab8 localisation at the cell periphery, specifically in the Golgi region and in cytoplasmic vesicles (Chen *et al.*, 1993; Huber *et al.*, 1993b; Huber *et al.*, 1993a). Subsequent ICC studies combined with electron microscopy

micrographs have extended Rab8 localisation to the recycling endosome (Ang *et al.*, 2003; Peränen *et al.*, 1996; Hattula *et al.*, 2006).

Functionally, Rab8 is a major regulator of the vesicle trafficking to the basolateral membrane, in polarized epithelial cells (Huber *et al.*, 1993b; Peränen *et al.*, 1996; Nachury, 2008), to the dendrites in neurons (Huber *et al.*, 1993a) and in photoreceptor cells (Deretic *et al.*, 1995; Moritz *et al.*, 2001). In particular, Rab8 has been demonstrated to direct vesicle trafficking between the TGN and the recycling endosome (RE), and from the TGN to the plasma membrane (Ang *et al.*, 2003; Henry & Sheff, 2008). Additionally, a great amount of evidence has demonstrated Rab8 involvement in regulating cellular morphogenesis and shape (Armstrong *et al.*, 1996; Chen & Wandinger-Ness, 2001; Hattula & Peränen, 2000; Hattula *et al.*, 2002; Peränen *et al.*, 1996; Peränen & Furuhjelm, 2001). In neurons Rab8 has been implicated in the transport of receptors such as  $\alpha$ -amino-3-hydroxy-5-methyl-4-isoxazolepropionic acid (AMPA) (Brown *et al.*, 2007; Gerges *et al.*, 2004),  $\alpha$ 2B- and  $\beta$ 2-adrenergic receptors (Dong *et al.*, 2010) and the metabotropic glutamate receptor 1 (mGluR1) (Esseltine *et al.*, 2012).

Beside its well-known role in vesicular traffic, Rab8 has been recently implicated in autophagy. Rab8b and its interacting partner, TANK-binding kinase 1 (TBK-1), are required for the maturation of the autophagosome into autophagolysome (Ao *et al.*, 2014; Bento *et al.*, 2013; Pilli *et al.*, 2012). Moreover, Rab8a is involved in the regulation of the so-called unconventional autophagy-based secretion (Dupont *et al.*, 2011; Jiang *et al.*, 2013). This pathway enables the extracellular delivery of proteins without entering the conventional ER-to Golgi secretory pathway, and it is dependent upon some components of canonical core autophagic machinery, such as Atg5 and LC3 (Light Chain 3; Dupont *et al.*, 2011; Jiang *et al.*, 2013). A schematic representation of the diverse pathways in which Rab8 is involved is shown in Figure 1-9.

### 1.3.1 Rab8 and HTT

The first evidence of a connection between HTT and Rab8 was provided by Hattula and Peränen (2000), who demonstrated the binding of both proteins to Optineurin (OPTN). Subsequently, it was shown that Rab8 co-localises with the motor protein Myosin VI at the perinuclear region of the Golgi (Au *et al.*, 2007; Sahlender *et al.*, 2005).

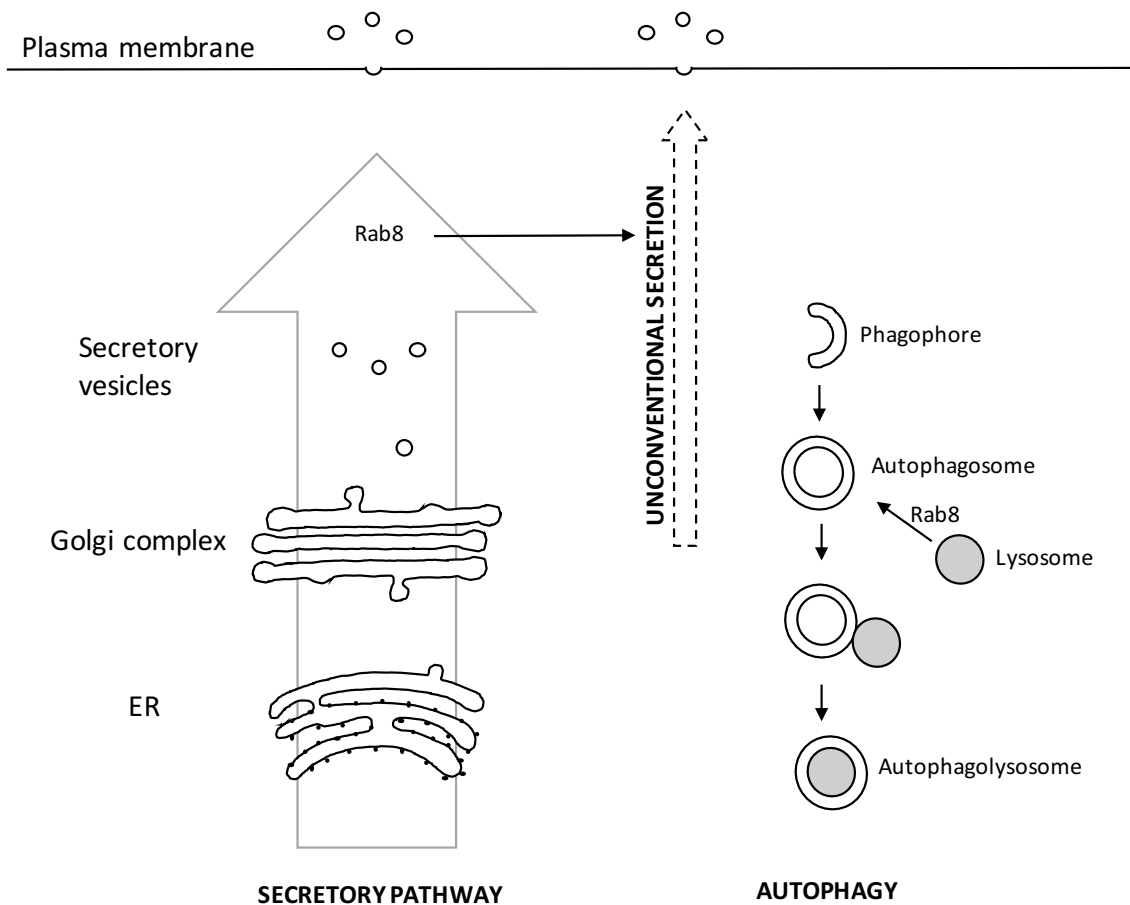


Figure 1-9 Schematic overview of Rab8 cellular pathways.

Rab8 is involved in the canonical vesicle secretory pathway via the ER and Golgi (left). It is also required for conventional autophagy, where it mediates lysosomal trafficking and fusion of lysosomes with autophagosomes (right). Lastly, Rab8 mediates the extracellular delivery of proteins via the unconventional autophagy-based secretion (middle). Vesicles directed both to the autophagy degradation route and to the unconventional-based autophagy are immunopositive for LC3-II/Atg8-II. Redrawn from Bento *et al.*, 2013.

Sahlender and colleagues proposed a model which explains how OPTN connects Rab8 to Myosin VI and to the HTT/HAP1/Dynein complex, mediating vesicle membrane trafficking from the TGN to the cell surface (Figure 1-10). Del Toro and co-workers (2009) provided the first link between Rab8 and HD. Their study revealed that in cells expressing mHTT vesicular trafficking to lysosomal compartments is impaired due to the de-localisation of Rab8/OPTN/HTT complex from the Golgi (del Toro *et al.*, 2009), linking therefore Rab8 to HD neuropathology. Together these evidences suggest that depletion/mis-localisation of Rab8 might aggravate the progression of the disease, possibly by impairing autophagy-lysosomal pathway.

#### 1.4 Modeling HD in *Drosophila*

Modifiers relevant to HD have been found in several large genetic screens using simple models, *i.e.* yeast or cell culture. Many of these genes have been tested in animal models to validate their function *in vivo* (Gusella & MacDonald, 2009; Mason & Giorgini, 2011). The mouse is one of the most useful models in science, especially for human related research. However, its long generation time and the associated costs, makes it very challenging, if not impossible, to test a large numbers of candidate genes in a reasonable amount of time. These challenges can be overcome by reducing the number of candidate genes to a smaller proportion. This screening process can be achieved by using invertebrate models (Green & Giorgini, 2012; Mason & Giorgini, 2011).

*D. melanogaster* has proven to be an excellent model organism in many research fields. This small insect can be conveniently manipulated in the laboratory, allowing the application of many molecular, genetic and behavioral approaches. Its powerful and relatively easy genetics coupled with a short generational time and its unsurpassed molecular toolkit (see below), renders *Drosophila* suitable for dissecting the basis of complex processes, such as neurodegeneration, both at the molecular and at the behavioural levels (O’Kane, 2003). Importantly, comparative genetic analyses have shown a high degree of conservation between the human and the insect genomes: 50% of the fruit fly genes have a human ortholog and almost 80% of the genes are implicated in human diseases are conserved in flies, hence sharing the same cellular and molecular pathways (Bonini & Fortini, 2003). One of the main advantages in using *Drosophila* resides in its nervous system, which allows the animal to perform complex behaviours, such as memory and learning, courtship, aggression and locomotor activity, some of which can be conveniently used as outputs for monitoring neurological damages (Neckameyer & Bhatt, 2016).

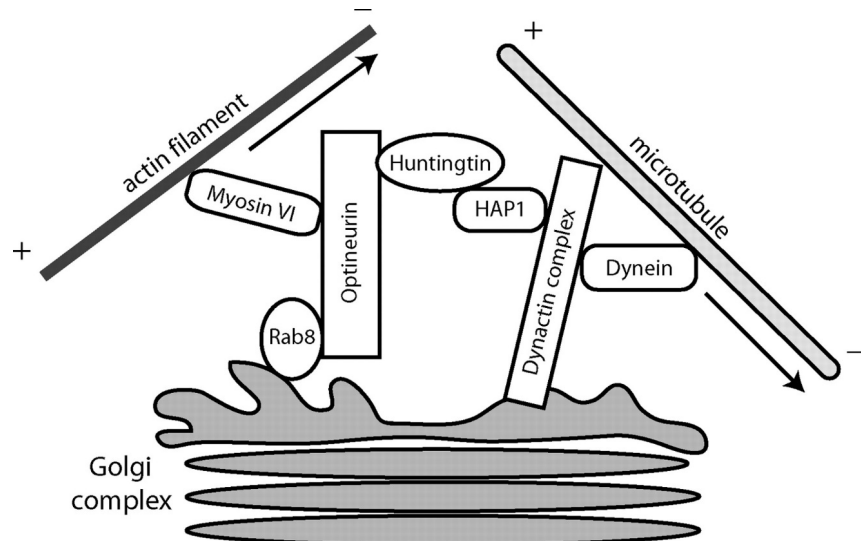


Figure 1-10 Carton showing the relationship between Rab8 and HTT at the TGN as proposed by Sahlender *et al.* (2005).

Motility along actin filaments is the result of the interplay between the Rab8/HTT/OPT complex and myosin VI. Image taken from Sahlender *et al.*, 2005.

In *Drosophila* genetic manipulation is usually achieved *via* the GAL4/UAS system (Brand & Perrimon, 1993). Briefly, a fly promoter with a convenient pattern of expression is cloned upstream of the coding sequence of the yeast transcription factor GAL4; this constitutes the “driver line”. The “reporter” line is generated by cloning the cDNA of the gene of interest downstream of the yeast regulatory sequence UAS. The expression of the cDNA is achieved in the progeny of the cross of driver and reporter lines. In those flies the UAS sequence is recognised by GAL4, driving the overexpression of the gene of interest in the spatial pattern determined by the chosen promoter (Duffy, 2002 and Figure 1-11). Moreover, temporal transgenic expression can be achieved through the TARGET and the gene-switch systems, the first relying on the temperature modulation of the GAL4 (called GAL80) and the latter exploiting drugs to induce transcriptional activation of the UAS (McGuire *et al.*, 2004). Driver and reporter lines are generated using either P element random insertion — the trasposone used to stably incorporate exogenous sequences in *Drosophila*’s genome — or using site-specific chromosomal insertion, the latter mediated by the φC31 integrase system (Bischof *et al.*, 2007; Rubin & Spradling, 1982; Spradling & Rubin, 1982). The recent discovery of the CRISPR/CAS9 system has greatly expanded the possibility of genome editing even further (Gratz *et al.*, 2013). Bloomington, Kyoto, Harvard and Vienna stock centres are the main *Drosophila* strain collections, possessing collectively thousands of fly lines readily available and easily accessible (FlyBase Consortium, 2003).

The degenerative nature of HD pathology can be modelled in flies expressing mHTT, which produces phenotypes that recapitulate the main human pathogenic features. For instance expressing mHTT with the pan-neuronal *elav-GAL4* driver results in neurodegeneration of the photoreceptors present in the eye, progressive impairment of locomotor activity and ultimately in premature death, phenotypes which are all easy to score (Green & Giorgini, 2012; Marsh & Thompson, 2006).

Several models of HD flies are available (Green & Giorgini, 2012), however flies pan neuronally expressing mHTT exon 1 containing 93Q (hereafter simply referred as to HTT93Q) are most commonly utilized to mimic HD pathogenesis and to screen for modifiers, namely genes that intervene to modulate the phenotypic outcome of mHTT overexpression. Indeed, as already discussed, the proteolytic cleavage of full-length mHTT produces N-terminal fragments of the mutant protein (including those comprising the first exon of the protein), which are extremely toxic for cells. These fragments induce two of the most important HD clinical features: formation of IBs and neuronal death, which is a consistent model of the neuropathology (Slepko *et al.*, 2006).

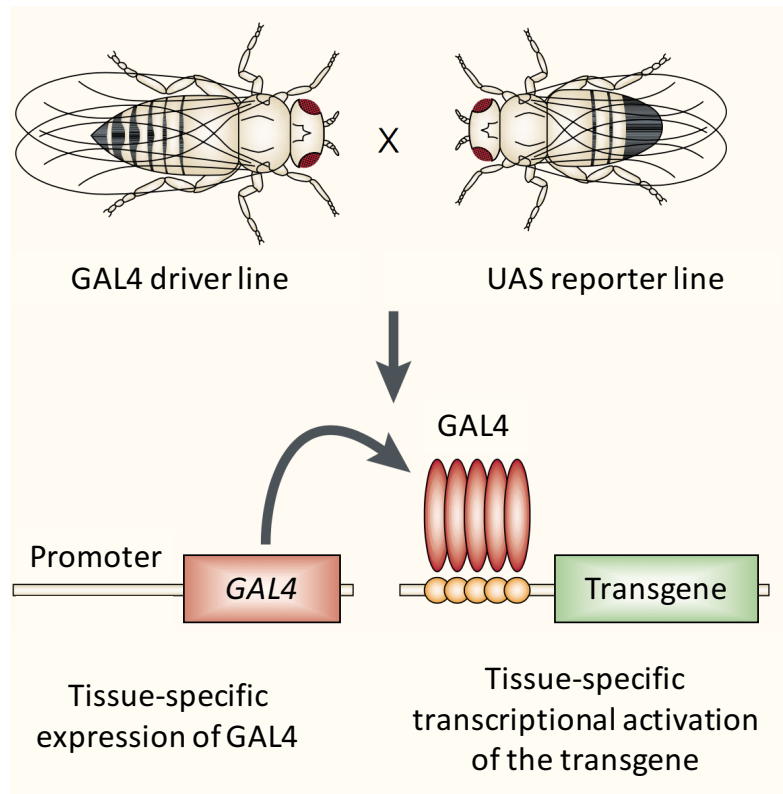


Figure 1-11 GAL4/UAS system.

In the driver line, the yeast GAL4 transcription sequence that is cloned downstream of an endogenous promoter sequence that ensures tissue specific transcription for the transgene of interest carried by the reporter line. Image modified from Muqit & Feany, 2002.

Thanks to the reverse genetics approaches available in *Drosophila*, the HD research community has gained remarkable insights onto the disease. Undoubtedly, one of the major contributions to the field was the implication of metabolites derived from the kynurenine pathway (KP) degradation of tryptophan in HD. An initial screening, performed in yeast (Giorgini *et al.*, 2005), was followed up by study in HD flies, which found that modulation of KP metabolites is protective against HD induced phenotypes (Campesan *et al.*, 2011). These results have been subsequently confirmed in mice (Zwilling *et al.*, 2011), leading to promising results for potential therapeutics. More recently, genome wide screening led to the discovery of overexpression suppressors of mHTT phenotypes in yeast, among which Glutathione Peroxidase (GPx) was identified. Genetic and pharmacological manipulation of the GPx activity in mammal cells and *Drosophila* have confirmed a protective role for the enzyme in the neuropathology (Mason *et al.*, 2013). It is also worth mentioning that two studies have uncovered a protective role of Rab11 in HD cell and *Drosophila* models (Richards *et al.*, 2011; Steinert *et al.*, 2012), confirming the paradigm that the highly conserved nature of molecular processes across models of a diverse complexity can lead to the identification of putative therapeutic targets for HD.

#### 1.4.1 Rab8 as a putative modifier for HD

A recent unpublished screen in mammalian cells in the Giorgini laboratory identified Rab8 as a putative modifier for HD (Mason and Giorgini, unpublished). Specifically, HEK293T cells expressing HTT103Q, which reduced the viability of these cells by ~50%, were co-transfected with individual siRNAs from the Dharmacon siGENOME® siRNA Human Membrane Trafficking Library, enriched to include the vast majority of Rab GTPases (177 genes in total). The WST-1 assay (a colorimetric assay to quantify cell proliferation and cell viability) was used to identify genes that significantly increased or decreased cell viability in the HTT103Q transfected cells. RNAi knock-down of human RAB8 (hRAB8A) significantly aggravated mHTT-induced toxicity. Following this initial finding, this work aims at further characterizing the *in vivo* role of Rab8 in HD model fruit flies. In this work mHTT expression was driven either pan-neuronally, using the *elav-GAL4* driver, to test the ability of Rab8 to ameliorate mHTT-induced phenotypes, or in a specific subset of clock cells, the PDF neurons, where mHTT induces circadian rhythm defects (Mason *et al.*, 2013; Sheeba *et al.*, 2010).

## 1.5 Aims and objectives

In line with a putative role for Rab8 as a modifier of HD, this work aims at developing the following goals:

1. Explore the role of Rab8 in HD pathogenesis using two different models: *Drosophila* and mammalian cells
2. Dissect the nature of the interaction between HTT and Rab8
3. Characterize the relevance of Rab8 in the autophagic clearance of mHTT in *Drosophila*
4. Studying neurodegeneration in the PDF-expressing neurons of *Drosophila*

## Chapter 2

### Materials and methods

#### 2.1 Materials

##### 2.1.1 Oligonucleotides

Table 2-1 Oligonucleotides used in this study.

All DNA oligonucleotides were synthesized and purified in standard desalted quality by Sigma-Aldrich. AT, annealing temperature used in the PCR reaction.

Name	Sequence 5' → 3'	AT
Genotyping		
HTTQs check_F	AGCGCCGGAGTATAAATAGA	60°C
HTTQs check_R	GGCTGAGGAAGCTGAGGAG	60°C
dRab8 check_F	CAAGTGCATTGACCGATA	60°C
dRab8 check_R	CCTGGACAACCAACTGTCT	60°C
DsRed check_F	TGAGCGTTGTATCCTCGTG	60°C
DsRed check_R	CGTCCCTCGTTCTTCATA	60°C
Cloning into pIREShyg3		
GA RatRAB8A_F	ACCGAGCTCGGATCTGTACAGCCACCATTGGCGAACGACC	68°C
GA RatRAB8A_R	GGCGCCTCGAACCGCTAGCTCACAGGAGACTGCACCG	68°C
GA RatRAB8B_F	ACCGAGCTCGGATCTGTACAGCCACCATTGGCGAACGACG	68°C
GA RatRAB8B_R	GGCGCCTCGAACCGCTAGCTAAAGCAGAGAACACCGG	68°C
Cloning into pJet2.1		
dRab8_F	ATGGCCAAACCTACGACTATC	58°C
dRab8_R	CAGACTGCACCTGGACAC	58°C
Cloning into pcDNA3.1		
GA dRab8(dRab8-VC)_F	CTGGCTAGCGTTAACTTAAGGCCACCATTGGCCAAACCTAC	63°C
GA dRab8(dRab8-VC)_R	CCACCAAGCAGACTGCACCTGGACAC	63°C
GA VC(dRab8-VC)_F	GCAGTCTGCTGGTGGCGGTGGATCTGGTG-	65°C
	GAGGCCTGAAGAACGGCATCAAGGCC	
GA VC(dRab8-VC)_R	GGTTAACCGGCCCTAGATTACTGTACAGCTCGTCATG	65°C
GA dRab8(VC-dRab8)_F	TGTACAAGTGGTGGCGGTGGATCTGGTGAGGCGGTATGGCCAAAC-	63°C
	TACGAC	
GA dRab8(VC-dRab8)_R	GGTTAACCGGCCCTAGATTAAAGCAGACTGCACCTGGACAAC	63°C
GA VC(VC-dRab8)_F	CTGGCTAGCGTTAACTTAAGGCCACCATTGAAGAACGGCATCAAGGCC	66°C
GA VC(VC-dRab8)_R	CCGCCACCACTTGTACAGCTCGTCATG	66°C
Sequencing		
pJET1.2_F	CGACTCACTATAGGGAGAGCGGC	64°C
pJET1.2_R	AAGAACATCGATTTCCATGGCAG	64°C
T7_F	TAATACGACTCACTATAGGG	45°C
BGH_R	TAGAAGGCACAGTCGAGG	53°C

## 2.1.2 Plasmids

Table 2-2 Plasmids used in this study.

VC, C-terminus of Venus; VN, N-terminus of Venus.

Construct	Vector	Description	Source
		Expression in HEK293T cells	
<b>DJ-1-GN</b>	pcDNA3.1	BiFC construct expressing the first exon of human <i>DJ-1</i> C-terminal tagged with residues 1 to 172 of GFP (GN)	M Repici University of Leicester
<b>HTT19Q-VN</b>	pcDNA3.1	BiFC construct expressing the first exon of human <i>HTT</i> containing 19Q, N-terminal tagged with residues 1 to 158 of Venus (VN)	F Herrera ITQB, Lisboa
<b>HTT97Q-VN</b>	pcDNA3.1	BiFC construct expressing the first exon of human <i>HTT</i> containing 97Q, N-terminal tagged with residues 1 to 158 of Venus (VN)	F Herrera Universidade de Lisboa
<b>HTT25Q-VC</b>	pcDNA3.1	BiFC construct expressing the first exon of human <i>HTT</i> containing 25Q, N-terminal tagged with residues 159 to 238 of Venus (VN)	F Herrera ITQB, Lisboa
<b>HTT97Q-VC</b>	pcDNA3.1	BiFC construct expressing the first exon of human <i>HTT</i> containing 97Q, N-terminal tagged with residues 159 to 238 of Venus (VN)	F Herrera Universidade de Lisboa
<b>VC-dRAB8</b>	pcDNA3.1	BiFC construct expressing <i>D. melanogaster</i> RAB8 N-terminal tagged with residues 159 to 238 of Venus (VC)	This work
<b>VN</b>	pcDNA3.1	BiFC construct expressing the residues 159 to 238 of Venus (VN)	F Herrera Universidade de Lisboa
<b>mRFP</b>	pcDNA3.1	Construct expressing mRFP used as transfection control for BiFC	R Mason University of Leicester
		Stable transfection of HTT14A2.5 cells	
<b>rRAB8A</b>	pIREShyg3	Rat RAB8 isoform A	This work
<b>rRAB8B</b>	pIREShyg3	Rat RAB8 isoform B	This work

### 2.1.3 Antibodies

Table 2-3 Antibodies used in this study.

IB, immunoblot; ICC, immunocytochemistry.

Name	Species	Application	Dilution	Source
$\alpha$ -Atg8	Rabbit	IB	1:3000	K Koehle ETH Zurich
$\alpha$ -GFP A111222	Rabbit	IB ICC	1:2500 1:200	Invitrogen
$\alpha$ -HTT MAB5374	Mouse	IB ICC	1:2000 1:500	Millipore
$\alpha$ -Rab8 610844	Mouse	IB ICC	1:2500 1:200	BD Bioscience
$\alpha$ -PDF	Rabbit	ICC	1:100	Dr Wilcockson Aberystwyth University
$\alpha$ -PDF C7	Mouse	ICC	1:50	DSHB
$\alpha$ -Tubulin sc-8035	Mouse	IB	1:1000	Santa-Cruz
$\alpha$ -Tubulin T6199	Mouse	IB	1:5000	Sigma
$\alpha$ -mouse HRP PI-2000	Horse	IB	1:10000	Vector
$\alpha$ -rabbit HRP PI-1000	Goat	IB	1:10000	Vector
Alexa Fluor® 488 $\alpha$ -mouse A11059	Rabbit	ICC	1:200	ThermoFisher Scientific
Alexa Fluor® 647 $\alpha$ -mouse A21235	Goat	ICC	1:500	ThermoFisher Scientific
Alexa Fluor® 488 $\alpha$ -rabbit A11034	Goat	ICC	1:500	ThermoFisher Scientific
Cy2 $\alpha$ -mouse ab6944	Goat	ICC	1:200	AbCam
Cy5 $\alpha$ -rabbit ab97077	Goat	ICC	1:200	AbCam

## 2.1.4 Fly stocks

Table 2-4: List of lines used in this study.

Genotype	Hereinafter	Description	Source
w[1118]	w <sup>1118</sup>	Carries a mutation in the <i>white</i> genes that confers white eyes. Used as background control	Laboratory strain
y1 w*	yw	Carries a mutation in the <i>white</i> and <i>yellow</i> genes that confer white eyes and yellow body. Used as background control	Laboratory strain
y1 w*, FM7	FM7	Balancer for the first chromosome	Laboratory strain
w*; CyO/Sco; TM6B/MKRS	CyO/Sco;TM6b/MKRS	Balancer and markers for the second and third chromosome	Laboratory strain
P[GawB] <i>elav</i> <sup>C15S</sup>	<i>elav-GAL4</i>	GAL4 is expressed in all tissues of the embryonic nervous system beginning at stage 12	Bloomington stock centre Indiana University
Stock number: 458		GAL4 is expressed in ventrolateral neurons of the brain and a small number of cells in the CNS	Bloomington Stock centre Indiana University
y1 w*; P{Pdf-GAL4.P2.4}2	<i>Pdf-GAL4</i>	Expresses the 1 <sup>st</sup> exon of human HTT containing 93Q under UAS control	J L Marsh and L Thompson University of California
Stock number: 6900		Expresses a YFP-tagged, <i>Drosophila melanogaster</i> wild type Rab8 (dRAB8) protein under UAS control	Bloomington Stock centre Indiana University
w*; pUAST-HTT93Qex1	<i>UAS-HTT93Q</i>	Expresses a constitutively active, YFP-tagged dRab8 protein under UAS control	Bloomington Stock centre Indiana University
y1 w*; P{UASp-YFP.Rab8}45	<i>yw UAS-dRab8</i>	Expresses a dominant negative, YFP-tagged dRAB8 protein under UAS control	Bloomington Stock centre Indiana University
Stock number: 9782		Expresses a nuclear DsRed protein under UAS control	Bloomington Stock centre Indiana University
y1 w*; P{UASp-YFP.Rab8.Q67L}05	<i>yw UAS-dRab8CA</i>		
Stock number: 9681			
y1 w*; P{UASp-YFP.Rab8.T22N}12	<i>yw UAS-dRab8DN</i>		
Stock number: 9780			
w*; P{UAS-AUG-DsRed}A	<i>UAS-DsRed</i>		
Stock number: 6282			

Table 2-5 List of lines generated in this study.

Following conventional crossing schemes, *FM7* was used to remove *yw* mutation from *yw UAS-Rab8*, *yw UAS-Rab8CA* and *yw UAS-Rab8DN* (Table 2-4), whereas *Cyo/Sco*; *TM6B/MKRS* (Table 2-4) were used to produce the double UAS lines.

Genotype	Hereinafter
w*; P{UASp-YFP.Rab8}45	<i>UAS-dRab8</i>
w*; P{UASp-YFP.Rab8.Q67L}05	<i>UAS-dRab8CA</i>
w*; P{UASp-YFP.Rab8.T22N}12	<i>UAS-dRab8DN</i>
w*; P{UASp-YFP.Rab8}45; pUAST-HTT93Qex1	<i>UAS-HTT93Q,UAS-dRab8</i>
w*; P{UASp-YFP.Rab8.Q67L}05; pUAST-HTT93Qex1	<i>UAS-HTT93Q,UAS-dRab8CA</i>
w*; P{UASp-YFP.Rab8.T22N}12; pUAST-HTT93Qex1	<i>UAS-HTT93Q,UAS-dRab8DN</i>
w*; pUAST-HTT93Qex1, P{UAS-AUG-DsRed}A	<i>UAS-HTT93Q,UAS-DsRed</i>

### 2.1.5 Cell lines

Table 2-6 List of cell lines used in this study.

Cell name	Hereinafter	Description	Source
HTT14A2.5	HTT103Q	Adherent cells derived from a pheochromocytoma of the rat adrenal medulla (PC12 line), which upon Ponasterone A (PA) induction expresses the 1 <sup>st</sup> exon of human HTT containing 103Q fused to EGFP (Apostol et al. 2003)	L Thompson University of California
HTT14A2.5 RAB8A.1	HTT103Q rRAB8A.1	HTT14A2.5 stable transfected with rat RAB8A (pool number 1)	This study
HTT14A2.5 RAB8A.2	HTT103Q rRAB8A.2	HTT14A2.5 stable transfected with rat RAB8A (pool number 2)	This study
HTT14A2.5 RAB8B.1	HTT103Q rRAB8B.1	HTT14A2.5 stable transfected with rat RAB8B (pool number 1)	This study
HTT14A2.5 RAB8B.2	HTT103Q rRAB8B.2	HTT14A2.5 stable transfected with rat RAB8B (pool number 2)	This study
HEK293T	HEK293T	Adherent cells derived from human embryonic kidneys	M Repici University of Leicester

## 2.2 Methods

The following protocols describe the general methodologies employed throughout the thesis work, with a list of chapter-specific techniques provided in the respective individual chapters.

### 2.2.1 *Drosophila* husbandry

*Drosophila* stocks were raised on maize meal food (72gr/l maize meal, 80gr/l glucose, 50gr/l brewer's yeast, 8.5gr/l agar, 2gr/l nipagin) in a 12 hours light-dark regime (LD 12:12) at 25°C.

### 2.2.2 Cell culture

Cell lines were routinely cultured at 37°C, 5% CO<sub>2</sub> in a high glucose Dulbecco modified Eagle's medium (DMEM) (Thermo Fisher Scientific) supplemented with 10% heat inactivated fetal bovine serum (FBS), 100 U/ml penicillin/streptomycin and 2 mM-L-glutamine.

### 2.2.3 Molecular methods

#### 2.2.3.1 Diagnostic genotyping

Diagnostic genotyping was performed on fly genomic DNA, which was extracted as described by Gloor and Engels (1992). Briefly one CO<sub>2</sub> anaesthetized fly was transferred in a 0.2 ml PCR tube containing 50 µl of squishing buffer (10 mM tris-HCl pH 8.2, 1 mM EDTA, 25 mM NaCl, 200 µg/µl Protease K) and mashed using a pipette's tip. The sample was incubated at 37°C for 30 min and then at 95°C for 2 min. PCR reactions were performed with KAPA Taq and buffer A (Kapa Biosystems) according to manufacturer's instructions. Primers (Table 2-1) were designed with Primer3 (Koressaar and Remm 2007, Untergasser *et al.* 2012). Amplifications were carried out on G-Storm GS4 thermal cycler (Agilegene Technologies) using the annealing temperatures reported in Table 2-1. PCRs were run in 0.8-2% agarose gels, prepared by dissolving the appropriate amount of agarose in Tris-Borate-EDTA (TBE) (89 mM tris-base, 89 mM boric acid, 2 mM EDTA), supplemented with 0.004% ethidium bromide (EtBr). DNA loading dye (5% glycerol, 0.04% bromophenol blue) was added to the DNA samples, which were subsequently loaded onto the gel along with the HyperLadder™ (Bioline). Gels were run in 1x TBE, with running voltage and times being tailored to the gel concentration. Visualisation of amplicons was achieved using the Gene Genius apparatus (Synoptics).

#### 2.2.3.2 Cloning

Cloning PCRs were performed using Phusion® High-Fidelity DNA Polymerase and buffer B (New England Biolabs) according to the manufacturers' instruction. Inserts were amplified with cloning primers sharing 15-18 bp with the respective vector (Table 2-1) which were designed

with the NEBuilder® HiFi DNA Assembly Tool (New England Biolabs). At this stage the Kozak consensus sequence – CACC –, the start and the stop codons were incorporated. PCRs were carried out on G-Storm GS4 thermal cycler, using the annealing temperatures reported in Table 2-1.

Backbones (Table 2-2) were linearized using the appropriate restriction enzymes (New England Biolabs) as recommended by the supplier. Following the cloning PCR and the vector linearization, inserts and the backbones were run and extracted from the agarose gel using the E.Z.N.A.® Gel Extraction Spin (Omega Biotech) according to manufacturer instructions. Ligation was performed with Gibson Assembly® Cloning Kit (New England Biolabs) as instructed by manufacturer. 2 µl of a 1:3 diluted ligation product was transformed in 40 µl of XL1-MRF' blue *E. coli* cells (Stratagene), which were made chemically competent and transformed by using the method described in (Mandel and Higa 1970). 100 µl of cells were spread on a LB plate (10 g/l tryptone, 10 g/l NaCl, 5 g/l yeast extract, 15 g/l agar) supplemented 100 µg/ml of ampicillin and incubated overnight at 37°C. Single colonies were inoculated in 5 ml of LB medium (10 g/l tryptone, 10 g/l NaCl, 5 g/l yeast extract) and let grow overnight at 37°C. Plasmid DNA was purified using the E.Z.N.A. Plasmid Miniprep Kit I (Omega Biotech) following the manufacturer's guidelines. Positive constructs, identified via restriction analysis, were sent for Sanger sequencing analysis at GATC (GATC Biotech AG), with sequencing primers listed in Table 2-1.

## 2.2.4 Biochemical methods

### 2.2.4.1 Protein extraction from *Drosophila* heads

50-100 flies per genotype were collected in 15 ml tubes and immediately frozen in liquid nitrogen. Heads were separated from the bodies by alternating 3 times 10 sec of vigorously vortexing with flash freezing in liquid nitrogen. Heads were then sieved and collected on a dry-iced metal plate and moved into fresh 1.5 ml tubes.

For both immunoblots and co-immunoprecipitation, 50 heads were homogenized with an electric pestle in 30 µl of extraction buffer (10 mM tris-HCl pH 7.5, 150 mM NaCl, 0.1% NP-40) supplied with protease inhibitor cocktail (Roche) and centrifuged at 12,100 x g for 10 min at 4°C. Surnatant was moved into a new 1.5 ml tube.

For mHTT aggregate extraction, 100 heads were extracted in 100 µl of PBS supplied with protease inhibitor cocktail and then were sonicated in 5 cycles of 30 sec ON/30 sec OFF as indicated with Bioruptor® (Diagenode). Samples were centrifuged at 200 x g for 5 min at 4°C and the surnatant was carefully moved into a new 1.5 ml tube.

Protein quantification was carried out by diluting the protein extracts 1:1000 in the Bradford reagent (Sigma-Aldrich) allowing the mixture to settle for 15 min at RT. Protein concentration was estimated by measuring the optical density (OD) at 595 nm (OD<sub>595</sub>).

#### **2.2.4.2 Protein extraction from cells**

HEK293T cells were seeded at a density of  $1.5 \times 10^5$  cells/well in a 6-well plate pre-coated with 0.01% poly-L-Lysine and incubated O/N at 37°C, 5% CO<sub>2</sub>. The following day, cells were washed twice with PBS and then incubated for 10 min on ice with 100 µl of lysis buffer (20 mM trizma acetate pH 7.0, 270 mM sucrose, 1 mM EDTA, 1 mM EGTA, 50 mM NaF, 5 mM sodium pyrophosphate decahydrate, 200 mM Na-orthovanadate pH 10, 10 mM β-glycerophosphatase, 1 mM DTT, 1% tritonX-100) supplemented with protease inhibitor cocktail. Cells were then scraped from each well, collected in a new 1.5 ml tube and then centrifuged at 12,100 x g for 10 min at 4°C. Surnatant was carefully moved in a new 1.5 ml tube.

PC12 cells were maintained in T-25 culture flask. Once reaching the confluence, cells were washed twice in PBS, treated with 3 ml of trypsin, incubated at 37°C for 3 min and then resuspended in 12 ml of DMEM. Cells were collected in a 15 ml tube and then were centrifuged at 700 x g for 4 min at 4°C. Pellets were resuspended in 120 µl of CelLytic M (Sigma-Aldrich) and incubated for 10 min on ice. Lysates were moved in a new 1.5 ml tube and then centrifuged at 12,100 x g for 10 min at 4°C. Surnatant was carefully moved in a new 1.5 ml tube.

Protein concentration was quantified with NanoDrop 2000 (Thermo Fisher Scientific).

#### **2.2.4.3 SDS-Polyacrylamide gel electrophoresis (SDS-PAGE) and transfer**

25 µg of cell lysates or 20 µl of 0.25 OD<sub>595</sub> fly extracts were mixed with 5X Laemmli protein loading buffer (62.5 mM tris-HCl pH 6.8, 5% β-mercaptoethanol, 50% glycerol, 2% SDS, 0.1% bromophenol blue) and boiled for 5 min at 95°C. Following denaturation, proteins were separated by SDS-PAGE consisting of 12-15% resolving gels (12-15% bis-acrylamide, 375 mM tris-HCl pH 8.8, 0.1% SDS, 0.1% APS, 0.06% TEMED) and of 4% stacking gel (4% bis-acrylamide, 125 mM tris-HCl pH 6.8, 0.1% SDS, 0.05% APS, 0.1% TEMED). Broad Range (7-175 kDa) (New England Biolabs) was the primary ladder chosen as weight size markers. Gels were run in SDS-PAGE running buffer (25 mM tris, 192 mM glycine, 0.1% SDS), with running voltage and times being tailored to gel size and concentration.

Following SDS-PAGE separation, proteins were electro-transferred on a nitrocellulose membrane with a pore size of 0.2 µm (Amersham). Gels were transferred in transfer buffer (25 mM tris, 192 mM glycine and 20% methanol), with amperage and times being tailored to the gel concentration and size. Transfer of proteins onto membrane was confirmed by ponceau S staining (2% ponceau S dye, 5% acetic acid).

#### **2.2.4.4 Immunoblotting**

Membranes were washed once in TBST buffer (20 mM tris, 150 mM NaCl, 0.1% tween-20) and subsequently blocked in blocking buffer (5% non-fat milk, 20 mM tris, 150 mM NaCl, 0.1%

tween-20). Membranes were incubated overnight at 4°C with the primary antibody dissolved in blocking buffer according to the concentrations listed in Table 2-3. The following day, membranes were washed 3 times with TBST buffer for 15 min at RT, incubated for 2 h at RT with the secondary antibody dissolved in blocking buffer according to the concentrations listed in Table 2-3, and washed 3 times with TBST buffer for 15 min at RT.

Proteins were detected with ECL Primer Western blotting detection reagent (Amersham) according to manufacturer's instruction and then exposed to radiographic film (Fuji) for the appropriate lengths of time. Films were developed in developer agent (RG Universal) until bands became visible, immersed in stop solution (ThermoFisher Scientific), and finally fixed in the fixation fluid (RG Universal). After scanning the films, quantification of the band intensity was measured and analysed with ImageJ (Schneider *et al.*, 2012).

### 2.3 Statistical analyses

Statistical analyses were performed with GraphPad Prism version 6.00 (GraphPad Software, Motulsky 2007). For all the analyses the  $\alpha$  significance level was set as 0.05. The choice between parametric or non-parametric statistics was based on the outcome of the D'Agostino & Pearson normality test. Based on the assumption that the data followed a Gaussian distribution, the one- and the two-way analysis of variance (ANOVA) was used to compare the mean of 3 or more independent variables, the latter being used to account for the interaction between genotypes when considering the time factor. The Newman-Keuls was used as post-hoc test due to its high statistical power. A one-sample t-test was used to compare the means of one variable with a hypothetical value. Details on the choice of the hypothetical values are given in the respective result chapters. Chi square-tests were performed for comparison of categorical variables expressed as percentages. When comparing two groups, the significance level was set as  $\alpha=0.05$ , whereas it was corrected with Bonferroni post-hoc for multiple comparisons. To evaluate a correlation between 2 factors, a linear regression test was used. The Kruskal-Wallis was used as nonparametric statistics for comparing 3 unmatched groups and multiple comparisons were performed with Dunn's post-hoc test. Survival distribution were evaluated by performing a log-rank test and the Bonferroni was used as a post-hoc test.

# Chapter 3

## dRAB8 rescues HD-relevant phenotypes in *Drosophila melanogaster*

### 3.1 Introduction

As discussed above, Rab8 plays a critical role in trafficking of protein from the Golgi to the plasma membrane (Ang *et al.*, 2003; Huber *et al.*, 1993; Moritz *et al.*, 2001). Indeed, Rab8 is found at the *trans*-Golgi network (TGN) and at the recycling endosome (RE), orchestrating the cargo delivery from the TGN to the plasma membrane (Ang *et al.*, 2004; Hattula *et al.*, 2006; Peränen *et al.*, 1996) and the membrane trafficking at recycling endosomes (RE) (Henry & Sheff, 2008).

Recent evidence showed that, in HeLa cells, Rab8 is involved in the formation of a complex with HTT that is required for the normal vesicular trafficking from the Golgi network to the plasma membrane and lysosomes (del Toro *et al.*, 2009; Ying & Yue, 2016). In the HD context, however, mHTT is not correctly located in the Golgi apparatus, causing misplacement of mHTT that in turns leads to an impaired stabilization of Rab8, which results in the accumulation of cargo vesicles and reduced lysosomal activity (del Toro *et al.*, 2009).

A RNAi screen of Rab GTPases and other vesicle trafficking genes identified a number of candidate genes which modulated mHTT toxicity in HEK293T cells (Mason and Giorgini, unpublished). The Dharmacon siGENOME® siRNA Human Membrane Trafficking Library was used to identify genes able to modify toxicity in HEK293T HTT103Q-expressing cells. Among these, Rab8, significantly decreased cell viability suggesting that knockdown of this GTPase aggravates mHTT induced toxicity (Mason and Giorgini, unpublished, see Section 1.5.2). How Rab8 is involved in this process is not yet clear and there are several studies demonstrating that overexpression of Rab8 modifies different neuropathologies. In fact, Rab8 has been shown to provide substantial rescue against Parkinson's disease-induced degeneration of dopaminergic neurons in *C. elegans* (Gitler *et al.*, 2008), and to ameliorate behavioural defects in *Drosophila* models of Parkinson's disease and frontotemporal dementia (Yin *et al.*, 2014; West *et al.*, 2015), although the mechanism remains elusive.

To validate the positive effect of Rab8 on HD pathogenesis *in vivo*, a *Drosophila* model of HD (Steffan *et al.*, 2001) was used to drive mHTT expression in the central nervous system to mimic HD-like phenotypes (Marsh & Thompson, 2006). The aim of this chapter is to evaluate the protection of *Drosophila* Rab8 (dRAB8) overexpression, exploiting three well-established assays

collectively referred to as “standard assays” (Green & Giorgini, 2012): the eclosion assay, the pseudopupil analysis and longevity analysis. The eclosion assay scores the emergence of adult flies from the pupal case. Several previous studies have shown that only a fraction of flies pan-neuronally overexpressing mHTT reaches adulthood and that modifier genes are able to ameliorate this phenotype (Campesan *et al.*, 2011; Richards *et al.*, 2010; Vittori *et al.*, 2014; Wolfgang *et al.*, 2005). The pseudopupil analysis evaluates the neurodegenerative progression in photoreceptor cells of the fly eye. The *Drosophila* compound eye is a highly sophisticated visual structure, which consists of about 800 repetitive units, called ommatidia. Each ommatidium contains 8 microvillar photoreceptor cells (or rhabdomeres) projecting into the central cavity which bundle together in a trapezoidal pattern. Of these only 7 are visible by light microscopy and their presence/absence constitutes the metric for this assay, which has been largely employed for testing modifiers of HD (Mason *et al.*, 2013; Richards *et al.*, 2010; Campesan *et al.*, 2011; dos Santos *et al.*, 2014; Varadarajan *et al.*, 2015; Vittori *et al.*, 2014; Vittori *et al.*, 2013; Sajjad *et al.*, 2014; Ravikumar *et al.*, 2004; Steffan *et al.*, 2001). Finally the longevity analysis measures the total lifespan of a cohort of flies. Indeed, pan-neuronal mHTT expression leads to a dramatic decrease in fly viability, shortening the median survival, namely  $T_{50}$  (time at which the population is halved), and has been previously used to test modifiers of HD (Steffan *et al.*, 2001; Vittori *et al.*, 2014; Richards *et al.*, 2010). Due to their fast and reliable read-out, these assays were used as an initial *in vivo* screen.

To fully explore dRAB8 expression in HD flies in relation to its GDP/GTP exchange cycle, the effects of two dRAB8 mutants – a dominant negative (DN) form and a constitutively active (CA) form – were explored in the context of the standard assays. The dominant negative mutant has a threonine to asparagine substitution at the residue 22 (T22N; Figure 3-1), which results in a lower affinity for GTP than for GDP (Feig & Cooper, 1988). Moreover, as the mutation has been reported to sequester GEFs (Guanine nucleotide exchanging factors), which catalyse the exchange of GDP for GTP, dRAB8DN has a dominant negative effect on the endogenous GTPase. dRAB8CA, on the other hand, has a glutamine to leucine substitution at the residue 67 (Q67L; Figure 3-1), which, by inhibiting the catalysts of GTP hydrolysis, *i.e.* GAPs (GTPase-activating proteins), renders dRAB8 constitutively active (Der *et al.*, 1986).

All in all, my results support the idea of a beneficial role of dRAB8 overexpression in HD model flies and that dRAB8 rescue depends on the nucleotide-binding state of the GTPase.

dRAB8	1	MAKTYDYLFKLLLIGDSGVGKTCILFRFSEDAFNTTFISTIGIDFKIRTI	50
dRAB8DN	1	MAKTYDYLFKLLLIGDSGVGKNCILFRFSEDAFNTTFISTIGIDFKIRTI	50
dRAB8CA	1	MAKTYDYLFKLLLIGDSGVGKTCILFRFSEDAFNTTFISTIGIDFKIRTI	50
<u>Consensus_ss:</u>		eeeeeeeeee hhhhhhhhhh eeeeeeeeeee	
dRAB8	51	ELDNKKIKLQIWDTAGQERFRTITTAYYRGAMGIMLVYDITQEKSFENIK	100
dRAB8DN	51	ELDNKKIKLQIWDAGQERFRTITTAYYRGAMGIMLVYDITQEKSFENIK	100
dRAB8CA	51	ELDNKKIKLQIWDAGLERFRTITTAYYRGAMGIMLVYDITQEKSFENIK	100
<u>Consensus_ss:</u>		ee eeeeeeee hhhhhhhhhh eeeeeee hhhhhhhhhh	
dRAB8	101	NWIRNIEENASADVEKMLLGNKCELTDKRQVSKERGEQLAIEYGIKFMET	150
dRAB8DN	101	NWIRNIEENASADVEKMLLGNKCELTDKRQVSKERGEQLAIEYGIKFMET	150
dRAB8CA	101	NWIRNIEENASADVEKMLLGNKCELTDKRQVSKERGEQLAIEYGIKFMET	150
<u>Consensus_ss:</u>		hhhhhhhhh eeeee hh hhhhhhhhhh eeee	
dRAB8	151	SAKASINVEEAFLTLASDIKAKTEKRMEANNPPKGHQLKPMDSRTKDSW	200
dRAB8DN	151	SAKASINVEEAFLTLASDIKAKTEKRMEANNPPKGHQLKPMDSRTKDSW	200
dRAB8CA	151	SAKASINVEEAFLTLASDIKAKTEKRMEANNPPKGHQLKPMDSRTKDSW	200
<u>Consensus_ss:</u>		hhhhhhhhhhhhhhhhh	
dRAB8	201	LSRC <b>SLL</b> 207	
dRAB8DN	201	LSRC <b>SLL</b> 207	
dRAB8CA	201	LSRC <b>SLL</b> 207	
<u>Consensus_ss:</u>		ee	

Figure 3-1 Secondary structure alignment of dRAB8 with dRAB8DN and dRAB8CA.

Highlighted aminoacids represent the T22L and the Q67L mutations, whereas consensus\_ss indicates  $\alpha$ -helics (h) or  $\beta$ -sheets (e). Alignment and prediction of the secondary structures were performed with MultAlin (Corpet, 1988).

## 3.2 Materials and methods

### 3.2.1 *Drosophila* crosses

Pan-neuronal expression of the genes was achieved by crossing UAS females (Table 2-5) with the X-chromosome driver *elav-GAL4* (Table 2-4), resulting in F1 progeny whereby only the females express the reporters as shown in Table 3-2. UAS and GAL4 control crosses were generated by crossing UAS females (Table 2-5) with  $w^{1118}$  males or  $w^{1118}$  females with *elav-GAL4* males (Table 2-4) respectively as shown in Table 3-1. Crosses were set up on maize food and kept at 25°C for 10 days.

Table 3-1 Parental crosses and their F1 progeny genotypes of experimental lines.

DN, dominant negative; CA, constitutive active.

Parental crosses	F1 progeny
<i>elav&gt;UAS</i>	
♀ <i>UAS-HTT93Q</i> x ♂ <i>elav-GAL4</i>	♀ <i>elav&gt;HTT93Q</i> ♂ HTT93Q UAS ctrl
♀ <i>UAS-HTT93Q, UAS-DsRed</i> x ♂ <i>elav-GAL4</i>	♀ <i>elav&gt;HTT93Q, DsRed</i> ♂ HTT93Q, DsRed UAS ctrl
♀ <i>UAS-HTT93Q, UAS-dRab8</i> x ♂ <i>elav-GAL4</i>	♀ <i>elav&gt;HTT93Q, dRab8</i> ♂ HTT93Q, dRab8 UAS ctrl
♀ <i>UAS-HTT93Q, UAS-dRab8CA</i> x ♂ <i>elav-GAL4</i>	♀ <i>elav&gt;HTT93Q, dRab8CA</i> ♂ HTT93Q, dRab8CA UAS ctrl
♀ <i>UAS-HTT93Q, UAS-dRab8DN</i> x ♂ <i>elav-GAL4</i>	♀ <i>elav&gt;HTT93Q, dRab8DN</i> ♂ HTT93Q, dRab8DN UAS ctrl
UAS ctrl	
♀ <i>UAS-HTT93Q</i> x ♂ $w^{1118}$	♀ HTT93Q UAS ctrl ♂ HTT93Q UAS ctrl
♀ <i>UAS-HTT93Q, UAS-DsRed</i> x ♂ $w^{1118}$	♀ HTT93Q, DsRed UAS ctrl ♂ HTT93Q, DsRed UAS ctrl
♀ <i>UAS-HTT93Q, UAS-dRab8</i> x ♂ $w^{1118}$	♀ HTT93Q, dRab8 UAS ctrl ♂ HTT93Q, dRab8 UAS ctrl
♀ <i>UAS-HTT93Q, UAS-dRab8CA</i> x ♂ $w^{1118}$	♀ HTT93Q, dRab8CA UAS ctrl ♂ HTT93Q, dRab8CA UAS ctrl
♀ <i>UAS-HTT93Q, UAS-dRab8DN</i> x ♂ $w^{1118}$	♀ HTT93Q, dRab8DN UAS ctrl ♂ HTT93Q, dRab8DN UAS ctrl
GAL4 ctrl	
♀ $w^{1118}$ x ♂ <i>elav-GAL4</i>	♀ GAL4 ctrl ♂ GAL4 ctrl

### 3.2.2 Diagnostic genotyping

Diagnostic PCR was performed as described in Section 2.2.3 with primers (HTT93Qs check F and R, dRab8 check F and R, DsRed check F and R) listed in Table 2-1.

### 3.2.3 Eclosion assay

10 parallel vials containing 5 females and 5 males each were set up as reported in Table 3-1. Parents were removed after 5 days and the number of females and males hatching from

each tube was recorded, until all the viable F1 had eclosed. The percentage of eclosion was calculated as the ratio between females and total number of eclosed flies for each vial. One-way ANOVA followed by Newman-Keuls multiple comparisons test was performed using GraphPad Prism.

### 3.2.4 Pseudopupil analysis

Females expressing the transgenes, *i.e.* *elav>HTT93Q*, *elav>HTT93Q,DsRed*, *elav>HTT93Q,dRab8*, *elav>HTT93Q,dRab8CA* and *elav>HTT93Q,dRab8DN* (Table 3-1) and UAS control males from the same parents, *i.e.* HTT93Q UAS ctrl, HTT93Q,DsRed UAS ctrl, HTT93Q,dRab8 UAS ctrl, HTT93Q,dRab8CA UAS ctrl, HTT93Q,dRab8DN UAS ctrl (Table 3-1) were collected at day 1 and day 7 post-eclosion, with day 0 indicating the day of eclosion. 15 to 40 heads per genotype were glued on a slide for analysis by light microscopy, and the number of rhabdomeres for 30 to 90 ommatidia was scored for each head. Eyes were analysed at on a Nikon Optiphot-2 microscope (Nikon), using an immersion-oil Plan Apo 40x/1.0NA objective. Two-way ANOVA followed by Newman-Keuls multiple comparisons test was performed using GraphPad Prism.

### 3.2.5 Longevity assay

For each genotype (*elav>HTT93Q*, *elav>HTT93Q,DsRed*, *elav>HTT93Q,dRab8*, *elav>HTT93Q,dRab8CA* and *elav>HTT93Q,dRab8DN*, Table 3-1), 100 females were collected within 6 h of emergence, equally allocated into 10 vials, and kept at 25°C. The number of surviving flies was recorded daily and fresh food was provided to the animals every other day. Lifespan and survival curves were plotted following Kaplan-Meier survival analysis, and statistical significance of curves was assessed using the log-rank (Mantel-Cox) test using GraphPad Prism. After comparing the 5 test groups, genotypes were compared two at a time, with the significance being adjusted with Bonferroni, to account for multiple comparisons.

## 3.3 Results

### 3.3.1 Overexpression of dRAB8 ameliorates impaired eclosion in HD *Drosophila* model

To test whether dRAB8 improves failure of emergence from the pupal case, flies carrying HTT93Q and dRAB8 were mated to *elav-GAL4* males (Table 3-1) and the F1 progeny hatching from this cross – where only the females express the transgenes – were scored as described in the previous Section (3.2.3).

As expected, a one-way ANOVA ( $F_{(11,108)}=18.92$ ,  $p<0.0001$ , Figure 3-2) showed that the *elav>HTT93Q* sex ratio significantly deviated from the ~50% exhibited by control strains (post-hoc Newman-Keuls, *elav>HTT93Q* vs HTT93Q UAS ctrl,  $p<0.0001$ ; *elav>HTT93Q* vs GAL4 ctrl,

$p < 0.0001$ , Figure 3-2). The overexpression of dRAB8 ameliorated this phenotype, showing a  $\sim 1.4$  fold increase in eclosion levels (post-hoc Newman-Keuls, *elav>HTT93Q* vs *elav>HTT93Q,dRab8*,  $p < 0.05$ , Figure 3-2).

To determine whether the ability of dRAB8 to switch between its GDP/GTP state was required for the observed rescue, I also assayed flies expressing either the dominant negative (dRAB8DN, Table 2-5), or the constitutive active (dRAB8CA, Table 2-5) forms (Zhang *et al.*, 2007), *elav>HTT93Q,dRab8DN* and *elav>HTT93Q,dRab8CA* respectively. I found comparable sex ratio values between *elav>HTT93Q,dRab8DN* and *elav>HTT93Q* (*elav>HTT93Q,dRab8DN* vs *elav>HTT93Q*,  $p > 0.05$ , Figure 3-2), suggesting that the dominant negative mutant does neither improve nor worsen the emergence of flies from their pupal case. I also found comparable values between *elav>HTT93Q,dRab8CA* and *elav>HTT93Q,dRab8* (post-hoc Newman-Keuls, *elav>HTT93Q,dRab8CA* vs *elav>HTT93Q,dRab8*,  $p > 0.05$ , Figure 3-2), suggesting that the constitutively active form of dRAB8 increases the eclosion levels similarly to the wild type form.

In order to exclude potential GAL4 titration from the *UAS-HTT93Q* site as the reason for dRAB8 rescue, I adopted the strategy of Steinert *et al.* (2012), who co-expressed HTT93Q with DsRed.

In line with my expectations, the number of *elav>HTT93Q* females was comparable to its titration control counterpart (post-hoc Newman-Keuls, *elav>HTT93Q* vs *elav>HTT93Q,DsRed*,  $p > 0.05$ , Figure 3-2), suggesting that dRAB8 ameliorates the eclosion phenotype.

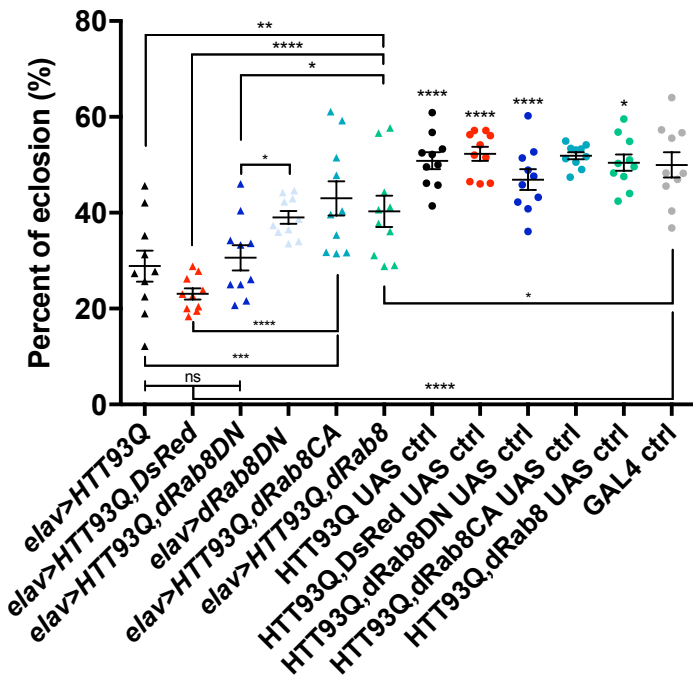


Figure 3-2 Overexpression of dRAB8 partially rescues adult emergencies failure of HD flies.

Sex ratios of eclosing flies calculated as % of females/total number of flies over 9 days. Triangles represent tests flies (*elav>HTT93Q*, *elav>HTT93Q, DsRed*, *elav>HTT93Q, dRab8*, *elav>HTT93Q, dRab8DN*, *elav>dRab8DN*, *elav>HTT93Q, dRab8CA*,) whereas circles represent UAS and the GAL4 controls. For graphic simplicity, asterisks above UAS ctrl indicate a statistical difference with their *elav-GAL4* counterpart. Data are mean  $\pm$  SEM. One-way ANOVA,  $F_{(11,108)}=18.92$ ,  $p<0.0001$ . Post-hoc Newman-Keuls: *elav>HTT93Q* vs *HTT93Q* UAS ctrl,  $p<0.0001$ , *elav>HTT93Q* vs *GAL4* ctrl,  $p<0.0001$ , *elav>HTT93Q* vs *elav>HTT93Q, dRab8*,  $p<0.01$ , *elav>HTT93Q* vs *elav>HTT93Q, DsRed*,  $p>0.05$ , *elav>HTT93Q, DsRed* vs *HTT93Q, DsRed* UAS ctrl,  $p<0.0001$ , *elav>HTT93Q, DsRed* vs *GAL4* ctrl,  $p<0.0001$ , *elav>HTT93Q, DsRed* vs *elav>HTT93Q, dRab8*,  $p<0.001$ , *elav>HTT93Q, dRab8DN* vs *HTT93Q, dRab8DN* UAS ctrl,  $p<0.001$ , *elav>HTT93Q, dRab8DN* vs *GAL4* ctrl,  $p<0.0001$ , *elav>HTT93Q, dRab8DN* vs *elav>HTT93Q, dRab8*,  $p<0.05$ , *elav>HTT93Q, dRab8DN* vs *elav>HTT93Q, dRab8CA*,  $p<0.05$ , *elav>HTT93Q, dRab8* vs *UAS HTT93Q, dRab8*,  $p<0.05$ , *elav>HTT93Q, dRab8* vs *GAL4* ctrl,  $p<0.05$ . N=10 for each genotype, based on the following number of total eclosed flies: *elav>HTT93Q* N=896, *HTT93Q* UAS ctrl N=1006, *elav>HTT93Q, DsRed* N=940, *HTT93Q, DsRed* UAS ctrl N=1118, *elav>HTT93Q, dRab8* N=851, *elav>HTT93Q, dRab8DN* N=908, *HTT93Q, dRab8DN* UAS ctrl N=1282, *elav>dRab8DN* N=1282, *elav>HTT93Q, dRab8CA* N=730, *HTT93Q, dRab8CA* UAS ctrl N=817, *HTT93Q, dRab8* UAS ctrl N=943, *GAL4* ctrl N=1091.

### 3.3.2 dRAB8 overexpression ameliorates neurodegeneration in the eyes

To further evaluate dRAB8 rescue, I scored neurodegeneration of the photoreceptor neurons of *Drosophila*'s eyes at day 1 and day 7 post-eclosion. Controls flies (HTT93Q UAS ctrl, HTT93Q,DsRed UAS ctrl, HTT93Q,dRab8CA UAS ctrl, HTT93Q,dRab8DN UAS ctrl and GAL4 ctrl, Table 3.1) displayed 7 rhabdomeres at both time points (Figure 3-3). A two-way ANOVA showed a significant effect of age ( $F_{(1,233)}=192.3$ ,  $p<0.0001$ , Figure 3-3.C), genotype ( $F_{(4,233)}=80.47$ ,  $p<0.0001$ , Figure 3-3.C) and a significant interaction age x genotype ( $F_{(4,233)}=26.24$ ,  $p<0.0001$ , Figure 3-3.C). The Newman-Keuls post-hoc, revealed an age-dependent loss of photoreceptor cells in *elav>HTT93Q* flies (day1 vs day7,  $p<0.0001$ , Figure 3-3.C). dRAB8 overexpression significantly ameliorated degeneration by reducing the loss of rhabdomeres at both day 1 (post-hoc Newman-Keuls, *elav>HTT93Q* vs *elav>HTT93Q,dRab8*,  $p<0.0001$ , Figure 3-3.C) and at day 7 (post-hoc Newman-Keuls, *elav>HTT93Q* vs *elav>HTT93Q,dRab8*,  $p<0.0001$ , Figure 3-3.C).

Interestingly, co-expression of mHTT with dRAB8DN (*elav>HTT93Q,dRab8DN*) was not significantly different from flies expressing mHTT solely at day 1 (post-hoc Newman-Keuls, *elav>HTT93Q* vs *elav>HTT93Q,dRab8DN*,  $p>0.05$ , Figure 3-3.C), however, it aggravated the the loss of photoreceptor cells at day 7 (post-hoc Newman-Keuls, *elav>HTT93Q* vs *elav>HTT93Q,dRab8DN*,  $p>0.0001$ , Figure 3-3.C). As dRAB8DN *per se* (*elav>dRab8DN*) did not show a decreased number of rhabdomeres neither at day 1 nor at day 7 (Figure 3-3.C), these results might suggest a synergistic interaction of the inactive GTPase with the toxic polyQ protein.

Also *elav>dRab8CA* flies showed a wild type-like phenotype (*i.e.* 7 rhabdomeres at both times points, Figure 3-3.C), whereas co-expression of dRAB8CA with mHTT provided a modest but significant rescue at day 7 (post-hoc Newman-Keuls, *elav>HTT93Q* vs *elav>HTT93Q,dRab8CA*,  $p<0.05$ , Figure 3-3.C), but not at day 1 (post-hoc Newman-Keuls, *elav>HTT93Q* vs *elav>HTT93Q,dRab8CA*,  $p>0.05$ , Figure 3-3.C). No GAL4 titration effect was observed at day 1, as no difference was observed between *elav>HTT93Q* and *elav>HTT93Q,DsRed* flies (post-hoc Newman-Keuls,  $p>0.05$ , Figure 3-3.C). However, a minor rescue was observed at day 7, with *elav>HTT93Q,DsRed* flies displaying a significant higher number of rhabdomeres compared to mHTT flies (post-hoc Newman-Keuls, *elav>HTT93Q* vs *elav>HTT93Q,DsRed*,  $p<0.05$ , Figure 3-3.C), which could underlie a slight titration effect. However, the fact that *elav>HTT93Q,dRab8* flies displayed significantly more rhabdomeres than *elav>HTT93Q,DsRed* flies at day 7 (post-hoc Newman Keuls,  $p<0.0001$ , Figure 3-3.C) further supports the beneficial role of dRAB8 in ameliorating neurodegeneration in the eyes and highlights that the wild-type, fully functional protein is required to provide protection.

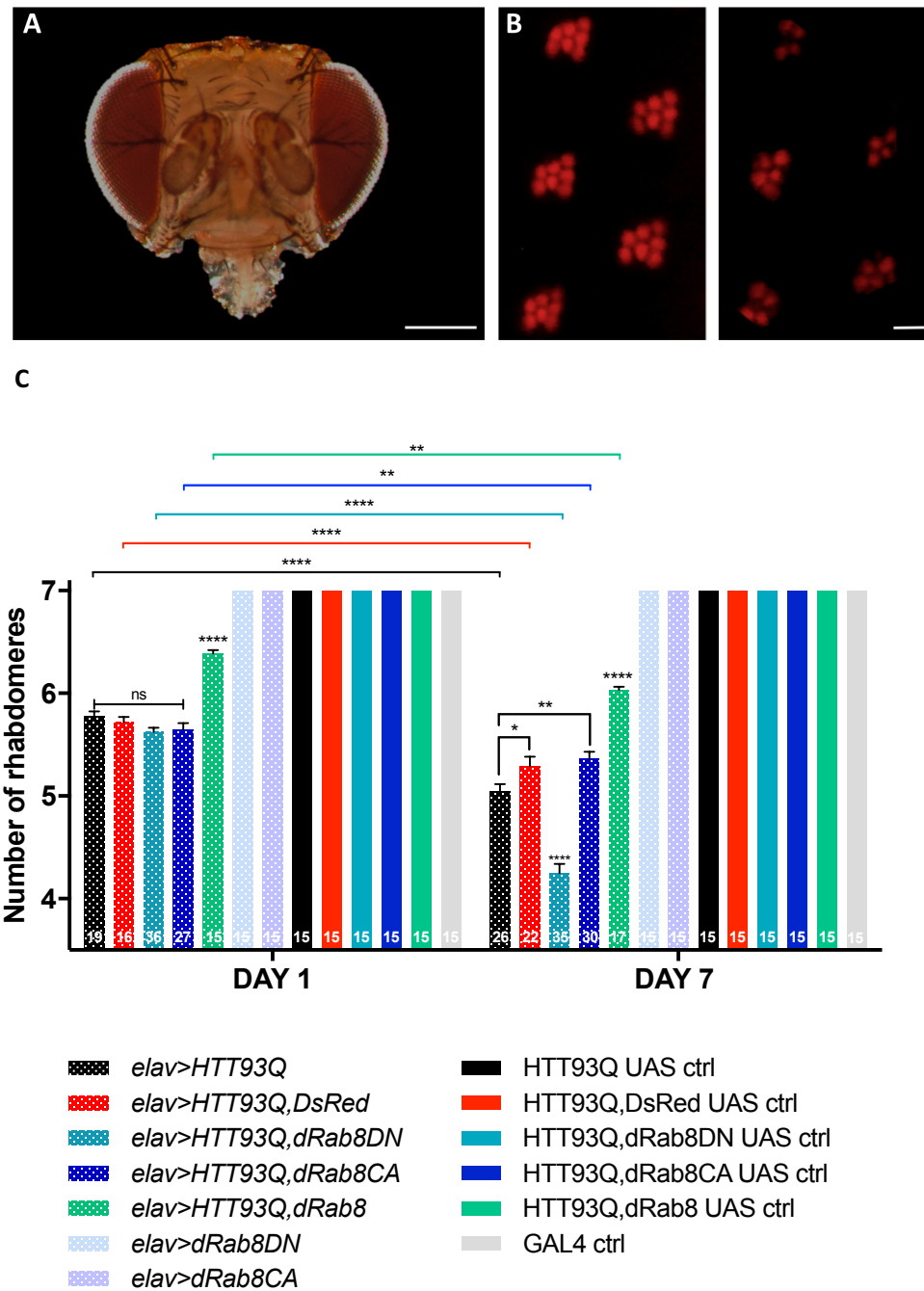


Figure 3-3 Overexpression of dRAB8 slows down HD neurodegeneration in the rhabdomeres.

**A** *Drosophila*'s head showing composite eyes, scale bar=250  $\mu$ m. **B** Representative pseudopupil images at day 7 of WT flies and *elav>HTT93Q*. In control flies 7 rhabdomeres are visible (left panel), whereas overexpression of HTT93Q induced loss of neuronal photoreceptor cells (right panel). Scale bar=10  $\mu$ m. **C** Quantification of average rhabdomeres per ommatidium calculated for at least 30 ommatidia per fly head at day 1 and day 7 in *elav>HTT93Q*, *elav>HTT93Q,DsRed*, *elav>HTT93Q,dRab8*, *elav>HTT93Q,dRab8CA* and *elav>HTT93Q,dRab8DN* flies. Data are mean  $\pm$ SEM. Two-way ANOVA, Interaction Age x Genotype  $F_{(4,233)}=26.24$ ,  $p<0.0001$ , Age  $F_{(1,233)}=192.3$ ,  $p<0.0001$ , Genotype  $F_{(4,233)}=80.47$ ,  $p<0.0001$ . Post-hoc Newman-Keuls, Genotypes comparison: DAY1: *elav>HTT93Q* vs *elav>HTT93Q,dRab8*,  $p<0.0001$ , *elav>HTT93Q* vs *elav>HTT93Q,DsRed*,  $p>0.05$ , *elav>HTT93Q* vs *elav>HTT93Q,dRab8DN*,  $p>0.05$ , *elav>HTT93Q* vs *elav>HTT93Q,dRab8CA*,  $p>0.05$ , *elav>HTT93Q,DsRed* vs *elav>HTT93Q,dRab8*,  $p<0.0001$ , *elav>HTT93Q,dRab8DN* vs *elav>HTT93Q,dRab8*,  $p<0.0001$ , *elav>HTT93Q,dRab8CA* vs *elav>HTT93Q,dRab8*,  $p<0.0001$ ; DAY 7: *elav>HTT93Q* vs *elav>HTT93Q,dRab8*,  $p<0.0001$ , *elav>HTT93Q* vs *elav>HTT93Q,DsRed*,  $p>0.05$ , *elav>HTT93Q* vs *elav>HTT93Q,dRab8DN*,  $p<0.0001$ , *elav>HTT93Q* vs *elav>HTT93Q,dRab8CA*,  $p<0.01$ , *elav>HTT93Q,DsRed* vs *elav>HTT93Q,dRab8*,  $p<0.0001$ , *elav>HTT93Q,dRab8DN* vs *elav>HTT93Q,dRab8*,  $p<0.0001$ , *elav>HTT93Q,dRab8CA* vs *elav>HTT93Q,dRab8*,  $p<0.0001$ . Post-hoc Newman Keuls, Ages comparison: *elav>HTT93Q* DAY1 vs DAY7,  $p<0.0001$ , *elav>HTT93Q,DsRed*, DAY1 vs DAY7,  $p<0.0001$ , *elav>HTT93Q,dRab8*, DAY1 vs DAY7,  $p<0.01$ , *elav>HTT93Q,dRab8CA* DAY1 vs DAY7,  $p<0.01$ , *elav>HTT93Q,dRab8DN*, DAY1 vs DAY7,  $p<0.0001$ . Numbers within columns represent N values (number of heads analysed).

### 3.3.3 dRAB8 overexpression improves shortened lifespan in HD flies

To further examine the protective role of dRAB8, I investigated the effects of the overexpression of this small GTPase on a cohort's viability.

The log-rank analysis (Mantel-Cox  $\chi^2_{(4)}=115.8$ ,  $p<0.0001$ ) showed that early lethality was moderately rescued by dRAB8 overexpression (post-hoc Bonferroni, *elav>HTT93Q* vs *elav>HTT93Q,dRab8*,  $p>0.001$ , Figure 3-4 and Table 3-3). In addition I found that while the survival curve of *elav>HTT93Q* was not significantly different compared to *elav>HTT93Q,dRab8DN* (*elav>HTT93Q* vs *elav>HTT93Q,dRab8DN*,  $p>0.05$ , Figure 3-4 and Table 3-3), *elav>HTT93Q,dRab8CA* showed an increased lifespan compared to HD flies (*elav>HTT93Q* vs *elav>HTT93Q,dRab8CA*,  $p<0.01$ , Figure 3-4 and Table 3-3), yet significantly shorter than the lifespan of *elav>HTT93Q,dRab8* flies (*elav>HTT93Q,dRab8* vs *elav>HTT93Q,dRab8CA*,  $p<0.01$ , Figure 3-4 and Table 3-3), suggesting once again a beneficial effect of wild-type dRAB8 versus the constitutively active form.

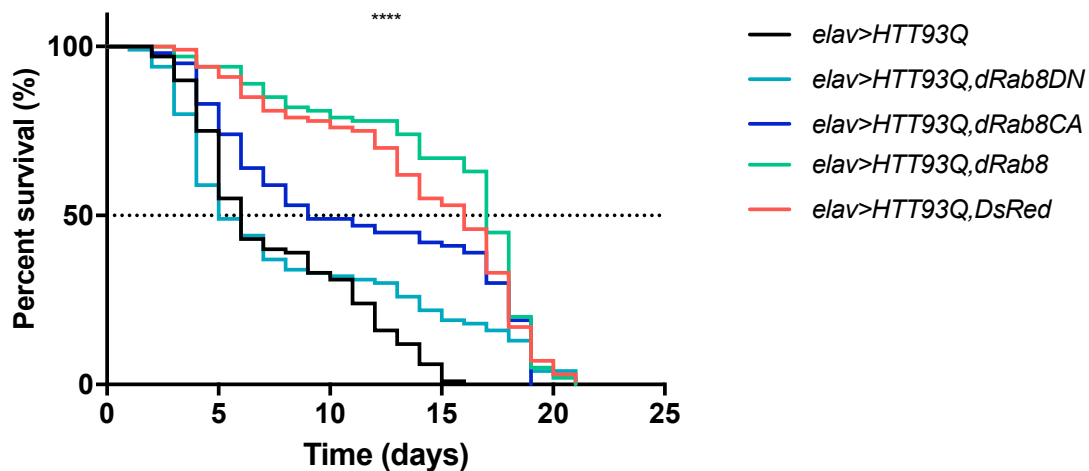


Figure 3-4 Overexpression of dRAB8 extends the lifespan of HD flies.

Female longevity data plotting survival percentages versus time of *elav>HTT93Q*, *elav>HTT93Q,DsRed*, *elav>HTT93Q,dRab8*, *elav>HTT93Q,dRab8CA* and *elav>HTT93Q,dRab8DN* flies. Flies were kept at 25°C. Log-rank (Mantel-Cox test), df=4, p<0.0001. Median lifespan ( $T_{50}$ ): *elav>HTT93Q*=6 days, *elav>HTT93Q,DsRed*=16 days, *elav>HTT93Q,dRab8*=17 days, *elav>HTT93Q,dRab8CA*=9 days and *elav>HTT93Q,dRab8DN*=5 days. Pairwise comparison corrected with Bonferroni for multiple comparison test: *elav>HTT93Q* vs *elav>HTT93Q,DsRed*, p<0.001, *elav>HTT93Q* vs *elav>HTT93Q,dRab8DN*, p>0.05, *elav>HTT93Q* vs *elav>HTT93Q,dRab8CA*, p<0.001, *elav>HTT93Q* vs *elav>HTT93Q,dRab8*, p<0.001, *elav>HTT93Q,DsRed* vs *elav>HTT93Q,dRab8*, p>0.05, *elav>HTT93Q,dRab8DN* vs *elav>HTT93Q,dRab8*, p<0.001, *elav>HTT93Q,dRab8CA* vs *elav>HTT93Q,dRab8*, p<0.01. N=100 flies per genotype.

Table 3-3 Log-rank (Mantel-Cox) analysis for pairwise comparison of survival curves.

Survival curves are compared and significance was adjusted with Bonferroni post-hoc. \* p<0.05, \*\* p<0.01, \*\*\* p<0.001, n.s. p>0.05.

Genotypes	<i>elav&gt;HTT93Q</i>	<i>elav&gt;HTT93Q,DsRed</i>	<i>elav&gt;HTT93Q,dRab8</i>
<i>elav&gt;HTT93Q</i>	-		
<i>elav&gt;HTT93Q,DsRed</i>	***	-	
<i>elav&gt;HTT93Q,dRab8</i>	***	n.s.	-
<i>elav&gt;HTT93Q,dRab8CA</i>	**		**
<i>elav&gt;HTT93Q,dRab8DN</i>	n.s.		***

Interestingly, since no statistical difference between *elav>HTT93Q,DsRed* and *elav>HTT93Q,dRab8* was observed (*elav>HTT93Q,DsRed* vs *elav>HTT93Q,dRab8*,  $p>0.05$ , Figure 3-4 and Table 3-3) a series of analyses were carried out to validate these results.

Firstly, to exclude the possibility of contamination between the fly lines, the assay was replicated and death flies were genotyped by PCR. This confirmed that the survival curves already obtained (Appendix, Figure 8-1 and Table 8-1) as derived from correct genotypes (Figure 3-5).

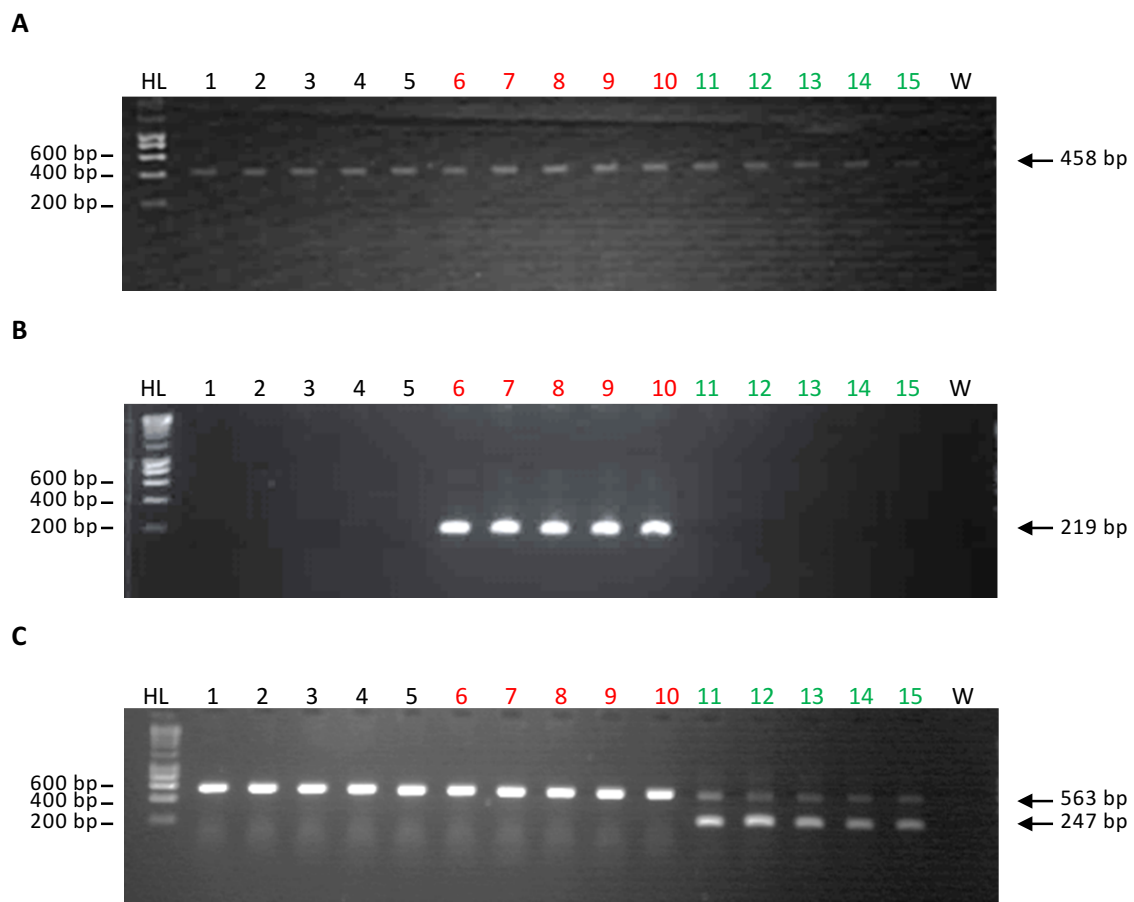


Figure 3-5 PCR results confirming the genotype of flies tested.

Representative PCR genotyping for *elav>HTT93Q* (1-5), *elav>HTT93Q,DsRed* (6-10) and *elav>HTT93Q,dRab8* (11-15) flies used in the longevity assay. **A** Reaction including primers to amplify *HTT93Q* from *UAS-HTT93Q* (458 bp). **B** Reaction including primers to amplify *DsRed* from *UAS-DsRed* (219 bp). **C** Reaction including primers to amplify *dRab8* from genomic *UAS-dRab8* DNA (563 bp and 247 bp respectively). HL, Hyperladder molecular weight marker; W, water (negative control). Arrows indicate the molecular weights of the bands of interest.

If the observed prolonged *elav>HTT93Q,DsRed* flies lifespan was a result of the GAL4 being titrated from the *UAS-HTT93Q* site, then one should expect a significantly lower mHTT expression in *elav>HTT93Q,DsRed* flies compared to *elav>HTT93Q* flies. However, immunoblot analysis revealed comparable HTT93Q expression levels in the three fly lines (one-way ANOVA,  $p=0.0473$ , post-hoc Newman-Keuls,  $p>0.05$ , Figure 3-6), thereby arguing against a titration effect, both for DsRed and for dRAB8. A remote possibility was represented by the *w;UAS-HTT93Q,UAS-DsRed* line having accumulated modifiers over time that might have contributed to the phenotype observed. However, replicates of pseudopupil analysis and eclosion assay (Appendix, Figure 8-2) indicated that this was not the case or at least that the accumulated modifiers influenced the longevity solely.

Finally, a plausible explanation could rely on DsRed's ability to provide rescue, acting as a non-inert protein (see discussion for more details).

As the spectrum of possibilities was vast to explore and the answer of this question was beyond the scope of this work, I have concluded that *elav>HTT93Q,DsRed* is not a good titration control and given the immunoblot results, I have decided to remove it from further analyses in subsequent chapters.

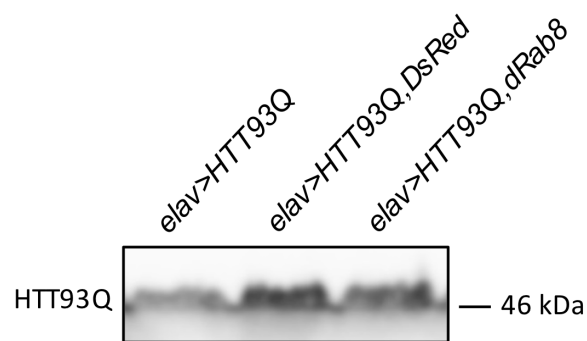
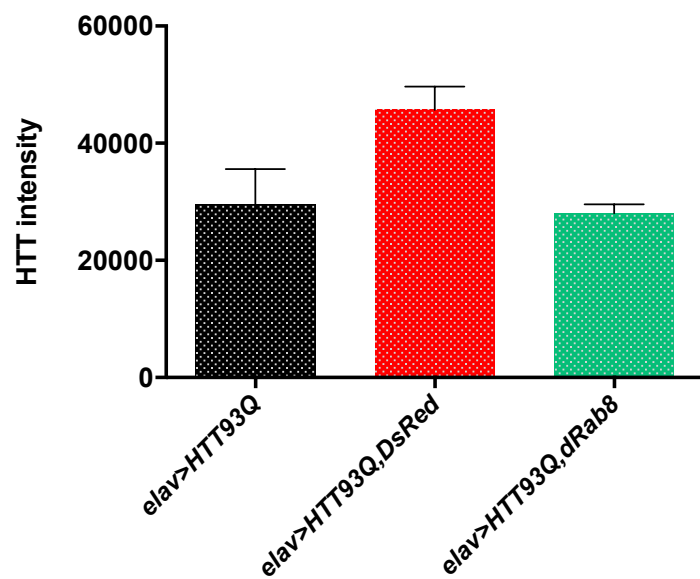
**A****B**

Figure 3-6 HTT expression is not titrated by the presence of a second *UAS-transgene*.

**A** Representative immunoblot showing HTT93Q expression in *elav>HTT93Q*, *elav>HTT93Q,DsRed* and *elav>HTT93Q,dRab8* flies at day 1. **B** Protein quantification revealed comparable HTT relative abundance in all three fly lines. Data are mean  $\pm$ SEM. One-way ANOVA,  $F_{(2,6)}=5.297$ ,  $p=0.0473$ . Post-hoc Newman-Keuls, n.s. N=3.

### 3.4 Discussion

Following an initial screen performed in mammalian cells (Mason and Giorgini, unpublished), I sought to determine whether dRAB8 overexpression improved mHTT-induced neurodegeneration in a *Drosophila* model of HD. This aim was approached by performing three well-established neurodegenerative assays: assessing eclosion, pseudopupil analysis and lifespan analysis.

Failure of eclosion was partially rescued by dRAB8 overexpression, implicating a beneficial role of this modifier in HD pathogenesis from early developmental stages. It is worth noting that the constitutive active form of dRAB8 (dRAB8CA), but not the dominant negative one (dRAB8DN), provided a rescue comparable to the wild type protein, thus highlighting the importance of the activated state of the GTPase.

Neurodegeneration in the eyes was also partially rescued by dRAB8 overexpression, with a trend that over time suggested a slowing down of the neurodegeneration process. Interestingly mHTT loss of rhabdomeres at day 7 was enhanced when HTT93Q was co-expressed with dRAB8DN, suggesting a synergistic effect between the two proteins. Remarkably, in the frog *Rana berlandieri*, Rab8 has been proposed to play a role in the post-Golgi transport of rhodopsin (Deretic *et al.*, 1995), which plays a structural role also in *Drosophila* photoreceptor development (Kumar & Ready, 1995). Later studies have shown that a Rab8 inactive mutant caused retinal degeneration in the toad *Xenopus laevis* (Moritz *et al.*, 2001), therefore it is tempting to link dRAB8DN overexpression also to abnormalities in rhodopsin transport in *Drosophila*. If that was case, the lack of rhabdomere loss in *elav>dRab8DN* flies could be explained by testing too early of a time point (day 7), and would therefore be interesting to score rhabdomere number at later stages. dRAB8CA (*elav>HTT93Q,dRab8CA*) provided no (day 1) or little (day 7) rescue, suggesting that the cycling of dRAB8 between GTP- and GDP-bound forms is crucial for conferring protection.

dRAB8 overexpression extended the median lifespan of HD flies by about one week. Similarly, *elav>HTT93Q,dRab8CA* flies showed a prolonged lifespan, whereas no difference was observed in *elav>HTT93Q,dRab8DN* flies. These data suggest once again that a functional dRAB8 protein is required for the observed beneficial effects. Indeed the mechanism of action of the GTPases is superimposed onto their GTP/GDP exchange cycle, which is responsible for the association/disassociation from the subcellular membranes. In their inactive form, GDP-bound Rabs are found in the cytoplasm, where they interact with GDI (GDP Dissociation Inhibitor) proteins, forming cytosolic Rab-GDI complexes that are targeted to specific membrane compartments. Once in the membrane, Rabs are activated by GEFs (guanine nucleotide exchange factors) which

catalyse the exchange of GDP to GTP. In their active GTP-bound form, Rabs recruit their effectors thus driving downstream functions, *i.e.* migration, docking and fusion of vesicles to the acceptor membrane. Rabs are recycled back to the donor membrane when GAPs (GTPase-Activating Proteins) hydrolyse GTP to GDP (Zhen & Stenmark, 2015). Therefore the Rab dominant negative mutant – whose inability to switch to its active form, constrains the Rab to a permanent “off” state – and the Rab constitutively active mutant – whose recycle is abolished due to its inability to switch to an “off” state – function as negative regulators in protein transport, suggesting how the impairment of “fine-tuning” dRAB8 function could compromise cellular trafficking which produces detrimental consequences in the HD context (Peränen *et al.*, 1996).

To ensure that the rescue observed by dRAB8 co-expression with HTT93Q was genuine and not a titration effect, I generated a reporter line carrying two UAS, *i.e.* *UAS-HTT93Q,UAS-DsRed* (Table 2-5). The advantage of having the two UAS inserts of interest already in the same fly line compared to having the driver and the reporter in the same line, is that it eliminates the need of generating multiple stocks for different drivers. Moreover, a *GAL4>UAS* stock that constantly expresses the reporter gene, could potentially accumulate background modulators and distort the phenotypical analysis. In my hands, the titration control *elav>HTT93Q,DsRed* showed a modest rescue of rhabdomeres at day 7 (although not as marked as in *elav>HTT93Q,dRab8* flies) and a survival curve comparable to *elav>HTT93Q,dRab8*, raising uncertainty about dRAB8 protection and about the titration control’s legitimacy. Although a clear explanation for the DsRed rescue is not currently available, this could reflect a line-specific position effect deriving from the random P element. Indeed genomic insertions of *UAS-dRab8* and *UAS-DsRed* might disrupt different genes having pleiotropic effects on both phenotypes. This hypothesis could be tested by using a different *UAS-HTT93Q,UAS-DsRed* fly line.

Another possibility is that the DsRed rescue could reflect a protective action exerted by the fluorophore itself, perhaps acting as a scavenger of reactive oxygen species (ROS). There is much evidence for a role of oxidative stress in HD pathogenesis (Ross & Tabrizi, 2011; Bates *et al.*, 2014) and of the positive effects of antioxidants slowing down disease progression in model systems (Gil-Mohapel *et al.*, 2014). The *Discosoma sp.* fluorescent protein, might affect the REDOX state of the cells *via* light induced electron transfer in a GFP-like manner (Bogdanov *et al.*, 2009). Although purely speculative, it is plausible that in flies the overexpression of DsRed may constitutively activate the anti-ageing/anti-ROS cellular response, thus behaving as an antioxidant protein (Funahashi *et al.*, 2016; Palmer *et al.*, 2009). This would provide protection against oxidative stress derived from the expression of mHTT and ultimately improve lifespan (Besson *et al.*, 2010; Sun & Tower, 1999). Measuring ROS production in flies expressing mHTT, would provide a direct test to this hypothesis.

Given all this, a titration effect is unlikely to underlie the rescue observed by dRAB8 over-expression, as its mutants, dRAB8DN and dRAB88CA, showed consistently a predictable phenotype in all the assays when co-expressed with HTT93Q. In the pseudopupil assay, moreover, dRAB8DN expression on its own did not lead to evident phenotypic changes, thus arguing against any titration artefacts. Indeed, if co-expression of dRAB8DN and HTT93Q titrates the GAL4 from the UAS sites of both *HTT93Q* and *dRAB8DN*, then one would expect to find more rhabdomeres in *elav>HTT93Q,dRab8DN* flies compared to *elav>HTT93Q* flies at day 7 and not *viceversa* as observed. Most importantly the immunoblot analysis confirmed similar HTT93Q expression levels in all the experimental fly lines, *de facto* eliminating the need of a titration control line.

In conclusion, these assays provided an initial, yet robust and reproducible, support for dRAB8 as modifier of polyglutamine toxicity in *Drosophila melanogaster*. While, the actual mechanism of neuroprotection against HD-relevant phenotypes is far from clear, it is plausible that overexpression of dRAB8 could rescue the lysosomal pathway that has been shown to be disrupted in a HD cell model (del Toro *et al.*, 2009). In the following chapters, I sought to investigate a putative interaction between dRAB8 and mHTT – as well as other parameters – to provide a mechanistic understanding on how this GTPase exerts its protective action against mutant HTT toxicity.

## Chapter 4

### Exploring Rab8-HTT interaction dynamics

#### 4.1 Introduction

The work presented in this chapter extends the findings of the previous chapter by exploring the role of Rab8 as a modifier for HD in a well-characterized mammalian neuronal cell model. Here I exploited a mHTT inducible cell line derived from a pheochromocytoma of rat adrenal medulla (PC12 cells), which was developed by Apostol and colleagues (2003). This inducible gene switch system consists of a clonal PC12 cell line constitutively expressing an ecdysteroid hybrid receptor (No *et al.*, 1996). The two required ecdysone receptor proteins, the ecdysone receptor (VgEcR) and the retinoid X receptor (RXR), are transcribed from a bicistronic cytomegalovirus (CMV) expression cassette (Wyborski *et al.*, 2001; Galimi *et al.*, 2005). Once translated, the two proteins form a dimer that, in the presence of the ecdysone analogue Ponasterone A (PA), binds to a hybrid ecdysone/glucocorticoid responsive element (GRE) of a second integrated vector, activating the transcription of a truncated form of mHTT exon1 (HTT103Q; Galimi *et al.*, 2005 and Figure 4-1).

Following mHTT expression by PA induction, these cells exhibit visible aggregates and increase of caspase-3 and -7 activity, both key features of early events in HD progression (Apostol *et al.*, 2006; Li *et al.*, 2000; Sanchez Mejia & Friedlander, 2001). Different caspases are implicated in apoptotic-mediated cell death; however, caspase-3/7 activities are of particular interest, because they are downstream effector caspases, implicated in the cascade of events leading to cellular apoptosis (Budihardjo *et al.*, 1999). Caspases belong to a family of cysteine proteases (Cysteinyl Aspartate-Specific Proteases) that cleave their substrates through recognition of a specific cleavage site. They are expressed as zymogenes (inactive enzyme precursors) and biochemical changes, such as proteolytic processing, are required for their activation. Caspases are broadly divided in two functional groups: the initiators of apoptosis (caspase-1, -2, -4, -5, -8 and -9, -10, -11 and -12) and the executioners of apoptosis (caspase-3, -6 and -7). Activation of initiators of caspases results in the cleavage of the activation sequence of the executioner caspases, which process the subsequent cleavage of cellular key targets, resulting in programmed cell death.

How mHTT triggers apoptosis has not yet been elucidated, however, there is growing evidence that different initiators of apoptosis caspases - such as caspase-1, -2, -6, -8 and -9 - play

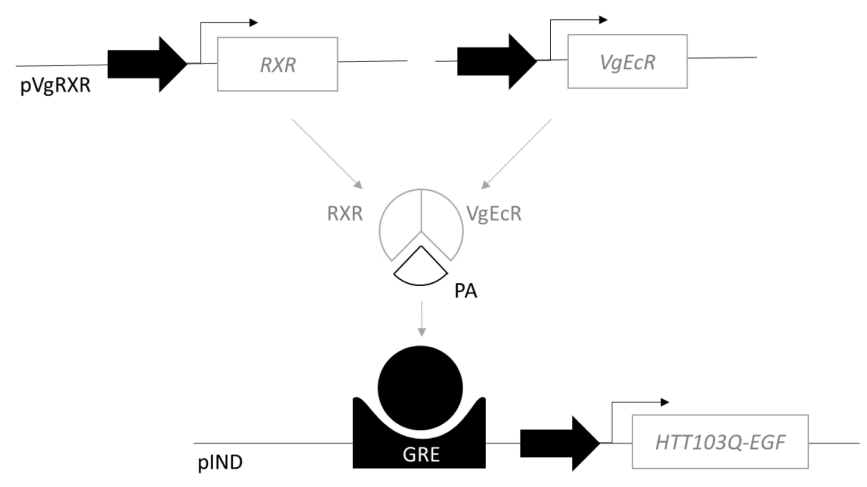


Figure 4-1 Schematic representation of mHTT induction process in PC12 cells.

RXR and VgEcR are transcribed from the integrated vector pVgRXR and once translated they dimerise forming an ecdysteroid hybrid receptor. A second vector, pIND, contains a truncated form of HTT103Q (including the first 17 AA of the exon 1 containing 103Q) fused at the C-terminus to an enhanced GFP (EGFP). This is cloned downstream the ecdysone/glucocorticoid responsive element (GRE). The ecdysteroid hybrid receptor in presence of Ponasterone (PA) form a complex that binds to GRE, promoting HTT103Q-EGFP transcription. Adapted from Galimi *et al.* (2005).

a role in HD neurodegeneration (Chen *et al.*, 2000; Graham *et al.*, 2011; Hermel *et al.*, 2004; Kiechle *et al.*, 2002; Li *et al.*, 2000; Majumder *et al.*, 2007; Ona *et al.*, 1999; Sanchez Mejia & Friedlander, 2001; Sawa, 2001; Wang *et al.*, 2015; Warby *et al.*, 2008; Zhang *et al.*, 2003). All the different apoptotic signaling pathways converge upon caspase-3/7 activation, two executioner caspases, which therefore can be used as a read out of cellular dysfunction. As such, the measure of caspase-3/7 activation allows the study of mechanistic aspects of HD pathogenesis relevant to neuronal dysfunction, making this assay particularly suitable for determining the effects of candidate HD modulating genes or compounds (Apostol *et al.*, 2003; Mason *et al.*, 2013; Smalley *et al.*, 2016).

For this purpose, an apoptotic assay based on caspase-3/7 activation was performed on HTT103Q model PC12 cells, which were stably transfected with rat Rab8 (rRAB8). Contrary to insects, in mammals Rab8 consists of two closely related isoforms, (Rab8a and Rab8b), encoded by two different genes (Armstrong *et al.*, 1996). The proteins share ~80% of homology (Armstrong *et al.* 1996 and Figure 4-2) and are expressed at similar levels (Sato *et al.*, 2014), making it difficult to distinguish them from each other and thereby understand their individual functions. As the two isoforms could play different roles, HTT103Q model PC12 cells were stably transfected with either rRAB8A or rRAB8B.

In this chapter, I also explored the interaction dynamics between HTT and dRAB8. Several pieces of evidence have linked HTT to Rab8. HTT is primarily a cytoplasmic protein, abundantly found in subcellular membranes, including the trans-Golgi network (DiFiglia *et al.*, 1995; Hoffner *et al.*, 2002; Imarisio *et al.*, 2008). It localizes in vesicles, endosomes and plasma membrane, and interacts indirectly with Rab8 (Hattula & Peränen, 2000). Del Toro and coworkers (2009) have recently shown that Rab8 and its effectors recruit HTT to the Golgi forming a complex. This is essential for maintaining Golgi organization and functional post-Golgi vesicular trafficking (PGT) in healthy neurons (Sahlender *et al.*, 2005). Del Toro and coworkers (2009) transfected M213 primary striatal cultures with full-length HTT75Q (FL-HTT75Q), and observed that mHTT showed reduced localization in the Golgi apparatus. That in turn affected normal PGT by delocalising Rab8 from the Golgi, which resulted in overall altered lysosomal function. The authors also showed reduced binding between FL-HTT75Q and Rab8 (del Toro *et al.*, 2009).

rRAB8A	1 MAKTYDYLFKLLLIGDSGVGKTCVLFRFSEDAFNSTFISTIGIDFKIRTI	50
rRAB8B	1 MAKTYDYLFKLLLIGDSGVGKTCLLFRFSEDAFNTTFISTIGIDFKIRTI	50
rRAB8A	51 ELDGKRIKLQIWDTAGQERFRTITTAYYRGAMGIMLVYDITNEKSFDNIR	100
rRAB8B	51 ELDGKKIKLQIWDTAGQERFRTITTAYYRGAMGIMLVYDITNEKSFDNIK	100
rRAB8A	101 NWIRNIEEHASADVEKAMILGNKCDVNDKRQVSKERGEKLALDYGIKFMET	150
rRAB8B	101 NWIRNIEEHASSDVERMILGNKCDMNDKRQVSKERGEKLAIDYGIKFLET	150
rRAB8A	151 SAKANINVENAFFTLARDIKAKMDKKLEGNSPQGSSHGVKITVEQQKRTS	200
rRAB8B	151 SAKSSTNVEEAAFFTLARDIMTKLNRMNDNSSGAGGPVKITESRSKKTS	200
rRAB8A	201 FFRC SLL 207	
rRAB8B	201 FFRC SLL 207	

Figure 4-2 Sequence alignment between rRAB8A and rRAB8B.

Alignment of the amino acid sequences of rRAB8A and rRAB8B performed with EMBOSS Needle, showing the similarity between the two proteins. Identity = 83.6%, Similarity = 93.2%. NCBI Accession numbers, rRAB8A: AAI05864.1, rRAB8B: AAA99782.1.

In this chapter, I combine immunohistochemistry (ICC) and Bimolecular Fluorescent Complementation (BiFC) to assess whether the dynamic of the interactions between Rab8 and HTT resembles that described by del Toro *et al.* (2009), namely decreased binding of Rab8 to mHTT. The BiFC is an approach that allows visualization of protein interactions in living cells, by exploiting the reconstitution of a fluorophore that is split into two fragments, each fused to a potential interaction partner. When the proteins interact, the two fragments come together reconstituting the fluorophore (Kerppola, 2008 and Figure 4-3). This technique is of interest for two reasons. First, the BiFC allows the study of protein-protein interactions in living cells, allowing direct *in vivo* visualization of the complexes within their natural environment. Second, once formed, the BiFC complexes are irreversible (Shyu & Hu, 2008), giving the significant advantage of detecting weak and transient protein-protein interactions.

Below I provide evidence that mHTT binds to dRAB8 and that their interaction is enhanced by mutant forms of HTT.

## 4.2 Materials and Methods

### 4.2.1 Immunoblotting

Immunoblotting was performed as described in Section 2.2.4.4 with no modifications. Quantification was performed using ImageJ (Rasband, 2008).

### 4.2.2 Generation of constructs

For molecular cloning of rat Rab8a and rat Rab8b (hereafter referred to as rRAB8A and rRAB8B) into pIREShyg3 (Table 2-2), *rRab8A* and *rRab8B* were amplified from a cDNA library generated by Dr Robert Mason (Giorgini group) with the pIREShyg3 primers listed in Table 2-1. Inserts were subsequently cloned in pIREShyg3 using BsrGI/Nhel restriction sites as described in Section 2.2.3.2.

For cloning of *dRab8-VC* and *VC-dRab8* into pcDNA3.1 (Table 2-2), the transgenic coding region of *Drosophila melanogaster Rab8* (*dRab8*) was amplified from genomic DNA of *UAS-dRab8* flies (Table 2-4) using the pJet2.1 primers listed in Table 2-1. The amplicon was inserted into the vector pJet2.1 (Thermo Fisher Scientific) according to the instructions of the manufacturer. Once sequenced, *dRab8* was re-amplified specific pcDNA3.1 primers (Table 2-1), whereas the sequence coding for the C-terminus of Venus (VC) was amplified from HTT19Q-VC – a construct kindly provided by Dr Federico Herrera (Herrera *et al.*, 2011) – using the same flanking pcDNA3.1 primers as above (Table 2-1). pcDNA3.1 was digested with AflIII/XbaI and *dRab8* and VC were cloned into the backbone by three-way ligation (see also Section 2.2.3.2).

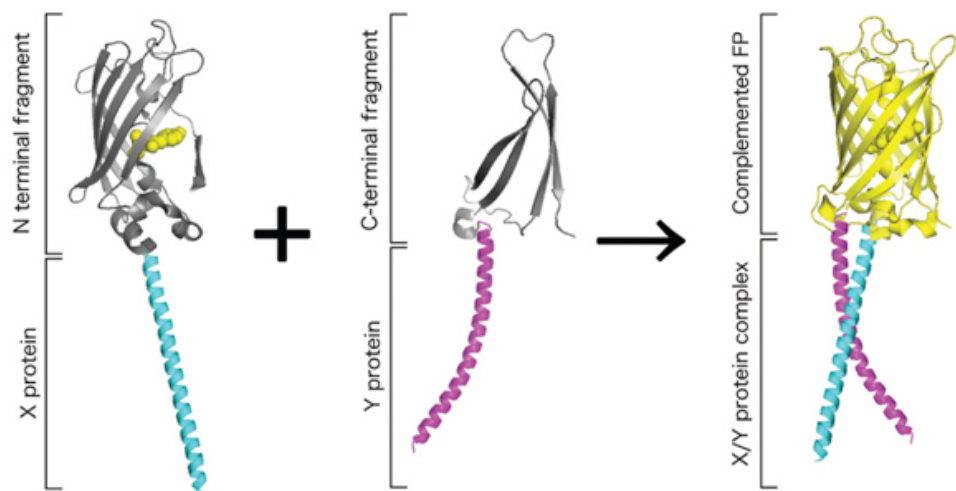


Figure 4-3 Reconstitution of a fluorophore by BiFC.

X and Y proteins are fused respectively to the N- and the C-terminus fragments of a fluorophore (FP). Interaction between X and Y allows reconstitution of the FP (yellow). Image taken from Kodama & Hu (2012).

#### 4.2.3 Stable transfection of HTT103Q model PC12 cells

PC12 cells carrying an inducible HTT103Q construct (line HTT14A2.5, in this study simply referred to as HTT103Q, Table 2-6) were cultured as described in Section 2.2.2. One day before transfection, 4x3 ml of cells in DMEM (Dulbecco modified Eagle's medium) at a density of 1.5 x 10<sup>5</sup> cells/ml were seeded into a 6-wells plate and incubated at 37°C, 5% CO<sub>2</sub>. Each well was then transfected with a reaction mix containing 4 µg of either rRAB8A or rRAB8B and Turbofect™ (Fermentas) following the manufacturer's instructions. 24 h post-transfection, the medium was replaced with serum-free DMEM. Cells were then incubated for further 24 h, after which 300 µg/ml of Hygromycin B (Invitrogen) were added to each well. Cells were maintained for two weeks by replacing the serum-free DMEM medium supplied with 300 µg/ml Hygromycin B, until few dozens of Hygromycin B resistant colonies appeared. All the colonies from a same well were moved to a new T25 flasks and gently resuspended in 5 mL of serum-free DMEM to form a pool. The four pools, hereafter referred as HTT103Q rRAB8A.1, HTT103Q rRAB8A.2, HTT103Q rRAB8B.1, HTT103Q rRAB8B.2 (Table 2-6), were incubated overnight with serum-free DMEM. Then 300 µg/ml of Hygromycin B were added to the medium, which thereafter was maintained with the selection agent. Each pool was assayed by Western immunoblot to confirm the stable expression of rRAB8A/B proteins.

#### 4.2.4 Caspase assay

For each pool described above and for un-transfected HTT103Q (hereafter referred as WT), 2500 cells in 200 µl of DMEM were seeded per well in a 96-wells plate (Greiner). These were incubated at 37°C, 5% CO<sub>2</sub> for 24 h. Then half of the wells – hereafter referred as “induced” – were treated with 1 mM Ponasterone (PA) in DMSO to induce mHTT expression, whereas the other half – hereafter referred as “non-induced” – were treated with DMSO (vehicle) as a control, see Figure 4-4. After 5 days, the cells were incubated 1 h at room temperature (RT) with Caspase-Glo® 3/7 reagent (Promega) following the manufacturer's instructions. This kit is based upon the cleavage of the tetrapeptide sequence DEVD. This is a pro-luminescent caspase-3/7 substrate, which, once cleaved, releases aminoluciferin. The addition of luciferase to the samples produces a “glow-type” luminescent signal that is proportional to the amount of the luciferin in the sample and that therefore correlates with the levels of caspase activity.

Luminescence was measured with a FLUOstar Omega Plate Reader (BMG LABTECH) using the following settings: top optic, emission filter lens, gain 3600, positioning delay 0.2. MARS software (BMG LABTECH) was used for data analysis.

For each induced well (A-E, 1-4, Figure 4-4) readings were corrected using the average of the non-induced wells (A-E, 5-8, Figure 4-4). The relative activation of caspase-3/7 was

calculated by normalizing the corrected luminescence against the average signal of HTT103Q cells (E, Figure 4-4), thus HTT103Q was set as 1. The assay was replicated four times. For each pool, the relative activation of caspase-3/7 was averaged across the four technical replicates and compared to the hypothetical value of 1 using a one sample t-test. One sample t-test and linear regression analysis were performed using GraphPad Prism.

#### 4.2.5 ICC on cells

HEK293T cells were grown on poly-lysine coated coverslips (Sigma-Aldrich), placed at the bottom of wells of a 6 wells-plate. Before seeding the coverslip had been washed in 12.5% HCl, 47% HNO<sub>3</sub> in H<sub>2</sub>O and sterilized in 100% IMS. Cells were transfected as described in Section 4.2.3 with a reaction mix containing 0.4 µg of HTT25Q-VC or HTT97Q-VC (Table 2-2). 48 h post transfection, coverslips were washed once in phosphate buffer solution (PBS) and then fixed in 4% filtered paraformaldehyde-phosphate buffer solution (PFA-PBS) for 20 min at RT. Cells were subsequently washed 3 times with PBS and blocked with blocking solution (PBS with 1% BSA, 0.2% triton X-100) for 30 min at RT. Cells were incubated with the appropriate primary antibody ( $\alpha$ -HTT and  $\alpha$ -Rab8, Table 2-3) diluted in blocking solution overnight (O/N) at 4°C. Afterwards, cells were washed 3 times in PBS, stained with Hoechst 33342 (Invitrogen) for 2 min and washed 3 times in PBS, all at RT. Cells were then incubated with the appropriate secondary antibodies (AlexaFluor®488 and AlexaFluor®647, Table 2-3) for 2 h at RT. Cells were washed again 3 times in PBS and mounted onto a glass slide with a drop of Mowiol which was allowed to settle O/N at RT.

Cells were imaged on an Olympus FV1000 confocal laser scanning microscope. An immersion-oil UPLSAPO 60x/1.35NA objective was used. Green fluorescence was excited using the 488 nm argon laser line, and detected at 500-600 nm. Far red fluorescence was excited using a 635 nm laser line, and detected at 655-755 nm. Hoechst signal was imaged using a laser line excitation of 405 nm and emission at 425-475 nm. Images were taken using the same voxel (volume pixel) resolution (XY dimension 85 nm, Z dimension 250 nm). Co-localisation analyses were carried out with ImarisColoc (Bitplane). ROIs, as well as determination of the intensities to include in the analysis, *i.e.* the threshold selection, were selected manually. To obtain a fair comparison between conditions, the Manders correlation coefficient (MCC) was calculated for each channel (Manders *et al.*, 1993). The MCC measures for each channel the portion of intensity overlapping with the other channel. M1 refers to the proportion of green signal (HTT) overlapping the far-red signal (hRAB8) and M2 refers to the proportion of far-red signal (hRAB8) overlapping the green signal (HTT). The MCC is primarily sensitive to co-occurrence of the two signals, whereas it is not sensitive to intensity variations in the image analysis, as it takes into

	<b>A</b>	<b>B</b>	<b>C</b>	<b>D</b>	<b>E</b>
<b>1</b>	HTT103Q rRAB8A.1	HTT103Q rRAB8A.2	HTT103Q rRAB8B.1	HTT103Q rRAB8B.2	HTT103Q
<b>2</b>	HTT103Q rRAB8A.1	HTT103Q rRAB8A.2	HTT103Q rRAB8B.1	HTT103Q rRAB8B.2	HTT103Q
<b>3</b>	HTT103Q rRAB8A.1	HTT103Q rRAB8A.2	HTT103Q rRAB8B.1	HTT103Q rRAB8B.2	HTT103Q
<b>4</b>	HTT103Q rRAB8A.1	HTT103Q rRAB8A.2	HTT103Q rRAB8B.1	HTT103Q rRAB8B.2	HTT103Q
<b>5</b>	rRAB8A.1	rRAB8A.2	rRAB8B.1	rRAB8B.2	WT
<b>6</b>	rRAB8A.1	rRAB8A.2	rRAB8B.1	rRAB8B.2	WT
<b>7</b>	rRAB8A.1	rRAB8A.2	rRAB8B.1	rRAB8B.2	WT
<b>8</b>	rRAB8A.1	rRAB8A.2	rRAB8B.1	rRAB8B.2	WT

Figure 4-4 Schematic representation of the caspase assay layout.

Grey shades indicate mHTT induced wells, white shades indicate non-induced wells that express only rRAB8. WT refers as to the non-induced HTT103Q cell line.

account the fraction of voxel with positive values for both channels, regardless of signal intensities. This coefficient allows therefore the ability to measure the overlap between two probes, regardless of the signal intensity. The MCC varies from 1 to 0, where 1 is perfect overlap and 0 is complete non-overlap. A MCC of 0.4, for example, indicates that 40% of the probes in the sample overlap. The Manders coefficient used for correlation analysis was calculated with ImarisColoc.

#### 4.2.6 BiFC assay

HEK293T cells were cultured as described in Section 4.2.3. One day before transfection,  $1.5 \times 10^5$  cells in 2 ml of DMEM were seeded per well in a 6-well plate pre-coated with 0.01% poly-L-Lysine and incubated at 37°C, 5% CO<sub>2</sub>. Cells were transfected with Effectene® (Qiagen) following the manufacturer's instructions. The transfection mix contained 0.16 µg each of the BiFC constructs (Table 2-2) and 0.08 µg of a mRFP construct (Table 2-2) used as transfection control. The transfection medium was removed after 24 h and replaced with 2 ml DMEM, supplemented with 10% FBS and 2 mM L-glutamine. 48 h post-transfection, cells were washed once in PBS, and covered with 2 ml of phenol red-free DMEM supplemented with 10% FBS, 2 mM L-glutamine, 1000 U/ml penicillin and 100 µg/ml streptomycin. BiFC and the mRFP signals were detected on live cells with an Olympus ScanR microscope system, keeping the settings constant across the whole experiment. While imaging, cells were kept at 37°C, 5% CO<sub>2</sub>. BiFC signal was detected with FITC 492/18 nm excitation filter and hqFITC (Dichroic 505LP) 535/50 nm emission filter. mRFP was detected with an mRFP excitation filter at 556/20 nm and an emission triple bandpass filter (DAPI/FITC/TRITC). The experiment was conducted as optimized by Repici *et al.* (2013). Briefly, 100 images/well were acquired and analysed using ScanR software (Olympus), using an Olympus 20X/0.45NA LUCPlanFLN objective. The intensity of the BiFC signal was calculated only on cells expressing mRFP. Red cells were identified by the software using intensity detection; neighbouring cells with similar intensity were considered as a single unit (Figure 4-5). The intensity of mRFP and BiFC signals were adjusted for background using settings suggested by the software (Olympus). Overexposed cells were automatically excluded from the analysis. The ratio between BiFC and RFP intensity was calculated for each single unit and then averaged for each well.

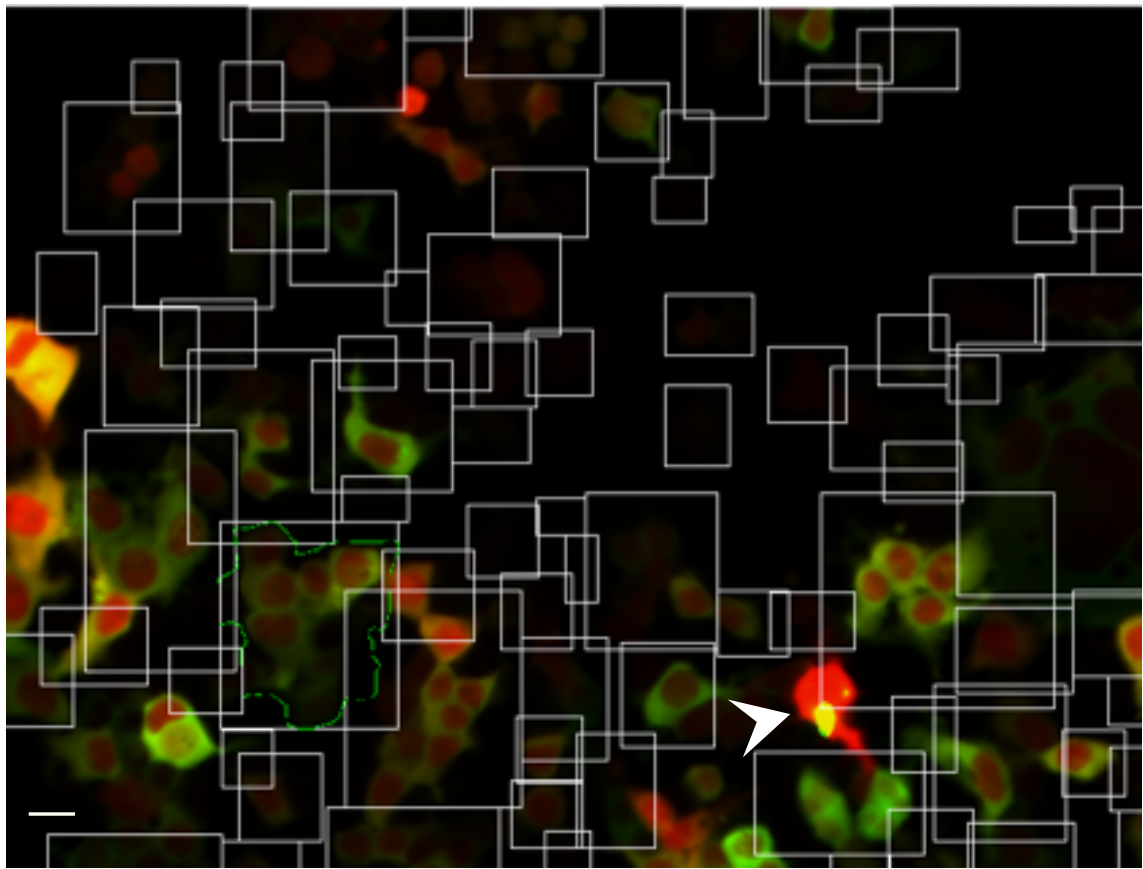


Figure 4-5 Example of ScanR software cell recognition output.

White rectangles identify single units of neighbouring cells emitting similar RFP intensity. The green selected area inside one of the white rectangles represents the edges of a single unit used in the quantification of the red and green signals. The white arrow shows an overexposed red cell excluded from the analysis. Scale bar=10  $\mu$ m.

## 4.3 Results

### 4.3.1 mHTT induced cellular toxicity is affected by rRAB8 expression levels

To validate rRAB8 as a modifier for HD in a mammalian system I exploited PC12 cells, a well-characterized neuron-like HD model derived from rat pheochromocytoma. These cells express a truncated form of the first exon of HTT103Q upon Ponasterone A (PA) induction (Apostol *et al.*, 2003, Table 2-6 and Figure 4-1). Initially I cloned the rat orthologous of *Drosophila dRab8*, *rRab8A* and *rRab8B*, in pIREShyg3, a vector utilised for stable transfection of HTT103Q cells. This approach was favoured due to the poor transient transfection efficiency of PC12 cells. After plasmid integration and selection of stable clones, I combined clones expressing either rRAB8A or rRAB8B into pools, namely rRAB8A.1, rRAB8A.2, rRAB8B.1, rRAB8B.2, respectively. This approach reduces variability by preventing the accidental selection of high or low rRAB8A/B expressing clones, which would bias the results. The expression of rRAB8A/B was confirmed by immunoblot analysis (Figure 4-6).

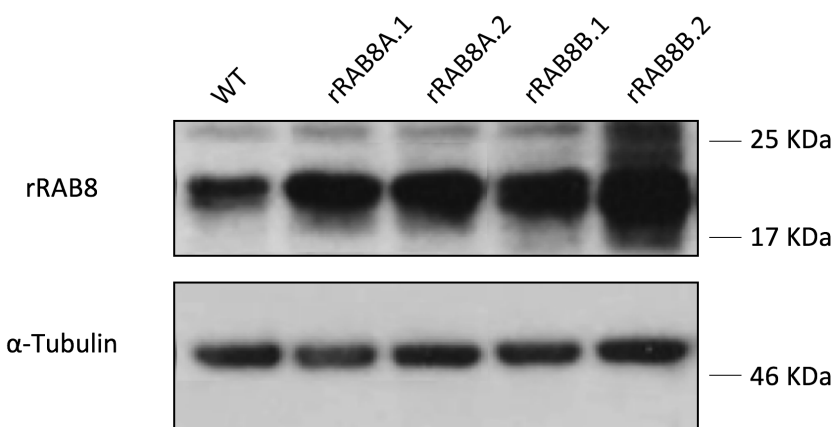


Figure 4-6 Expression of rRAB8A and rRAB8B in PC12 cells.

PC12 cells (HTT103Q line) constitutively over-expressing rRAB8A (rRAB8A.1 and rRAB8A.2) and rRAB8B (rRAB8B.1 and rRAB8B.2) show a larger band compared to the non-induced HTT103Q line (WT) expressing only endogenous RAB8A/B. This confirms the success of the stable transfection of the rRABA/B pools. Tubulin was assayed as a loading control. Primary antibodies:  $\alpha$ -Rab8 1:2500 (BD Bioscience, Table 2-3),  $\alpha$ -Tubulin 1:5000 (Sigma, Table 2-3). Secondary antibody:  $\alpha$ -mouse HRP (Vector, Table 2-3).

A first hypothesis to explain the protective role of Rab8 is that its overexpression (*i.e.*, either rRAB8A or rRAB8B) could interfere with the induction of programmed cell death by mHTT; thus, I measured the amount of caspase-3/7 in the cells. This is a well-characterized and reliable apoptotic assay that has been widely employed for the screening of modifier genes and of compounds with anti-HD activity (Apostol *et al.*, 2003; Apostol *et al.*, 2006; Apostol *et al.*, 2008; Mason *et al.*, 2013; Smalley *et al.*, 2016).

The experiment was performed four times and a certain degree of variability was observed among the biological replicates. Thus, each biological experiment was analyzed independently and the readings of each technical replicate were considered as a single data point to compare to the other three. Each data point was normalized to the average (from four measures) obtained for HTT103Q, which therefore was set to 1. Surprisingly, a one-sample t-test revealed that none of the HTT103Q rRAB8A/B transfectant pools conferred protection towards HTT103Q induced-apoptosis, while in some cases the apoptotic response was enhanced. Compared to HTT103Q, HTT103Q rRAB8A.2 and HTT103Q rRAB8B.1 induced higher apoptotic responses two times out of four. HTT103Q rRAB8A.1 was less variable, driving higher apoptosis in three biological replicates out of four. Finally, HTT103Q rRAB8B.2 was always significantly more apoptotic than HTT103Q (Table 4-1).

To provide a broader overview of the pools the data for the technical replicates of each biological experiment were averaged, and the analyses were repeated. A one-sample t-test confirmed that toxicity levels of cells overexpressing HTT103Q rRAB8A.2 and HTT103Q rRAB8B.1, were comparable to HTT103Q cells (HTT103Q rRAB8A.2 vs HTT103Q  $p=0.1526$  and HTT103Q rRAB8B.1 vs HTT103Q  $p=0.8232$ , Figure 4-7), whereas HTT103Q rRAB8A.1 and HTT103Q rRAB8B.2 displayed higher toxicity compared to HTT103Q cells (HTT103Q rRAB8A.1 vs HTT103Q  $p<0.05$  and HTT103Q rRAB8B.2 vs HTT103Q  $p<0.05$ , Figure 4-7), therefore indicating that rRAB8 might increase cellular toxicity, regardless of which isoform is overexpressed.

Table 4-1 Biological variation in the caspase assay.

The table indicates the biological variability of rRAB8 transfectant pools (columns) in the caspase assay. Levels of caspase-3/7 activation were measured in four independent experiments. Each biological replicate was analysed independently. The values of the caspase-3/7 activation of HTT103Q rRAB8 pools were compared to those of HTT103Q cells. Based on the results of a one sample t-test, each biological replicate was assigned to one of the following category: "significantly protective", "neither protective nor toxic", "significantly toxic". Finally, results were combined in this table, which indicates the total number of biological replicates falling in each category. One sample t-test: HTT103Q rRAB8A.1:  $b_1 t=2.370$ ,  $p=0.0985$ ,  $b_2 t=5.684$ ,  $p=0.0108$ ,  $b_3 t=26.51$ ,  $p=0.0001$ ,  $b_4 t=14.89$ ,  $p=0.0007$ ; HTT103Q rRAB8A.2:  $b_1 t=16.05$ ,  $p=0.0005$ ,  $b_2 t=0.8912$ ,  $p=0.4385$ ,  $b_3 t=0.2707$ ,  $p=0.8042$ ,  $b_4 t=4.982$ ,  $p=0.0155$ ; HTT103Q rRAB8B.1,  $b_1 t=2.833$ ,  $p=0.0660$ ,  $b_2 t=6.346$ ,  $p=0.0079$ ,  $b_3 t=6.949$ ,  $p=0.0061$ ,  $b_4 t=0.1587$ ,  $p=0.8840$ ; HTT103Q rRAB8A.2,  $b_1 t=18.91$ ,  $p=0.0003$ ,  $b_2 t=5.782$ ,  $p=0.0103$ ,  $b_3 t=6.621$ ,  $p=0.0070$ ,  $b_4 t=17.38$ ,  $p=0.0004$ . ( $b_1$ ,  $b_2$ ,  $b_3$  and  $b_4$  are the different biological replicates). N=4 for each biological replicate.

	HTT103Q rRAB8A.1	HTT103Q rRAB8A.2	HTT103Q rRAB8B.1	HTT103Q rRAB8B.2
Significantly Protective	0	0	0	0
Neither protective not toxic	1	2	2	0
Significantly Toxic	3	2	2	4

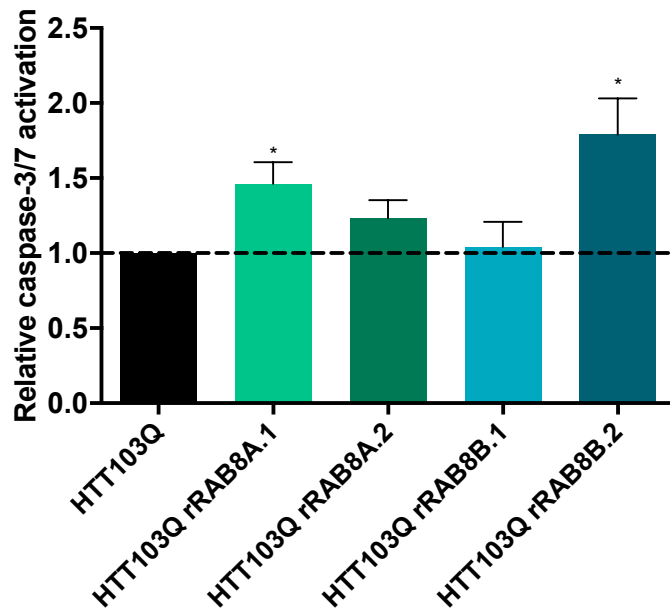


Figure 4-7 rRAB8 overexpression does not confer protection against mHTT induced toxicity in PC12 cells.

Relative caspase-3/7 activation levels in HTT103Q rRAB8A.1, HTT103Q rRAB8A.2, HTT103Q rRAB8B1 and HTT103Q rRAB8B.2 cells compared to HTT103Q cells. The data shown are ratio of the mean values between caspase-3/7 activation of rRAB8 pools and caspase-3/7 activation of HTT103Q. One sample t-test with the hypothetical value=1. HTT103Q rRAB8A.1,  $t=3.185$ ,  $p=0.0499$ , HTT103Q rRAB8A.2  $t=1.907$ ,  $p=0.1526$ , HTT103Q rRAB8B.1  $t=0.2437$ ,  $p=0.8232$ , HTT103Q rRAB8B.2,  $t=3.274$ ,  $p=0.0466$ , N=4. Data are mean  $\pm$ SEM.

Finally, I examined whether rRABA/B expression was toxic in cells not induced with PA, *i.e.* in pools expressing rRABA/B but not HTT103Q. Non-induced HTT103Q cells (WT) were included as a control. A one-way ANOVA revealed no significant differences among samples (ANOVA  $F_{(4,15)}=0.3715$ ,  $p=0.825$ , Figure 4-8), suggesting that the levels of caspase-3/7 activation were similar among non-induced cells and supporting the idea that rRAB8 is toxic only in an HD context.

While the reasons for the increased toxicity in presence of mHTT is unclear, one possible scenario is that expressing rRAB8A/B at high concentrations might have an impact on cellular homeostasis, exacerbating mHTT toxicity (see discussion for more details). I tested this possibility by quantifying the rRAB8A/B proteins extracted from the four pools by immunoblot. The results indicated a positive correlation between the levels of rRAB8A/B expression and the relative activation of caspase-3/7 (linear regression,  $R^2=0.4437$ ,  $F_{(1,14)}= 11.17$ ,  $p<0.01$ , Figure 4-9).

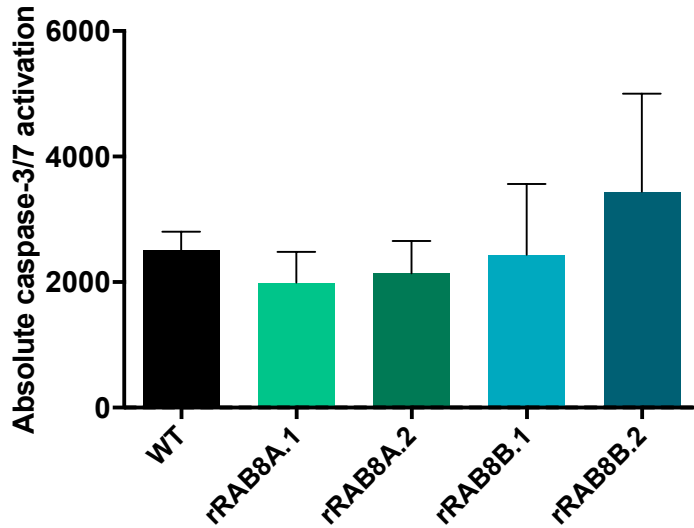


Figure 4-8 Absolute caspase-3/7 activation levels of non-induced cells are not toxic.

Comparison of absolute caspase-3/7 activation levels in non-induced HTT103Q model PC12 cells (WT) and in PC12 cell pools expressing rRAB8A.1, rRAB8A.2, rRAB8B.1 and rRAB8B.2. The data shown represent the mean  $\pm$ SEM of the mean values obtained from four technical replicates. One-way ANOVA  $F_{(4,15)}=0.3715$ ,  $p=0.825$ , ns,  $N=4$ .

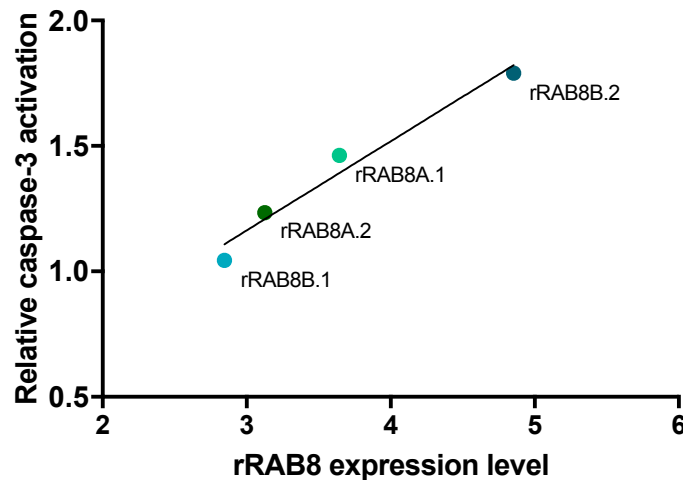
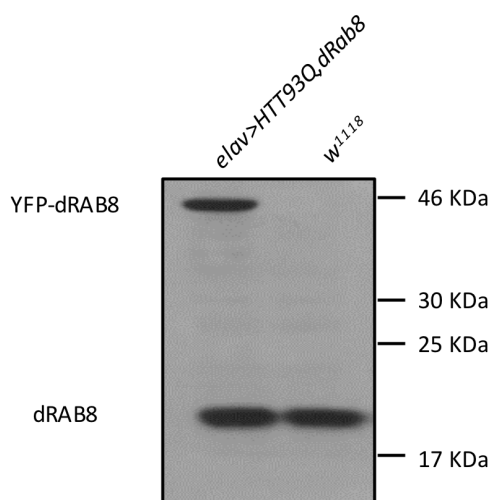


Figure 4-9 Caspase-3/7 activation correlates with rRAB8 expression levels.

Linear regression based on the relative caspase-3/7 activation of HTT103Q rRAB8A.1, HTT103Q rRAB8A.2, HTT103Q rRAB8B.1 and HTT103Q rRAB8B.2 cells reported in Figure 4-8, plotted against the relative expression of rRAB8. rRAB8 expression was normalized against Tubulin and then corrected for WT endogenous rRAB8 expression. Relative rRAB8 expression is presented as ratio of the mean value obtained from WT cells.  $R^2=0.4437$ ,  $F_{(1,14)}= 11.17$ ,  $p=0.0048$ . Caspase assay  $N=4$ , Western blot  $N=3$ .

In the four rRAB8A/B pools examined, toxicity was associated with a 3- to 5-fold increase in rRAB8 expression compared to endogenous levels. Inference from the linear regression ( $Y=0.3552*X + 0.09786$ , Figure 4-9) might suggest that a 2-fold increased rRAB8 expression could be less detrimental, or even protective and that overexpression levels could be critical with regards to conferring protection. Due to time constraints, new pools expressing rRAB8A/B at lower levels were not generated and this hypothesis was not tested. However, I checked the level of overexpression in dRAB8 flies (*i.e. elav>HTT93Q,dRab8*) to provide a parallel between the two systems. Immunoblot analysis on head protein extracts revealed that exogenous dRAB8 was expressed at lower levels than the endogenous protein (mean  $0.7\pm0.13$ , Figure 4-10). Though, these results should be interpreted with caution. In flies, overexpression of dRAB8 was driven by *elav*, which is present at high levels in neurons and eyes. However, proteins were extracted from the whole head, which comprises neuronal and non-neuronal tissues, *de facto* averaging dRAB8 expression across the whole fly head.

**A**



**B**

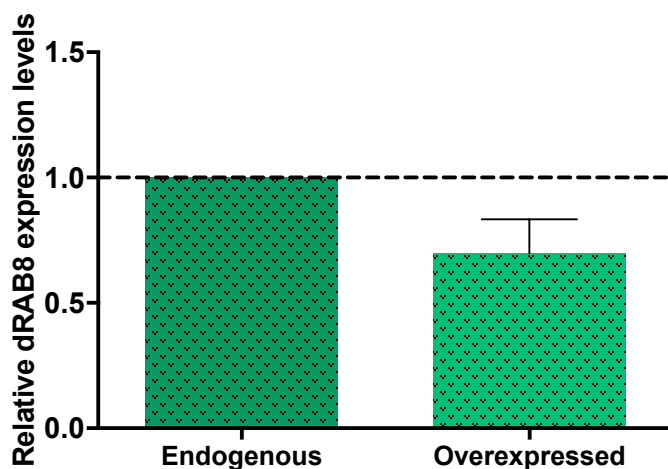


Figure 4-10 dRAB8 in flies is not expressed at higher levels compared to the endogenous dRAB8.

**A** Representative immunoblot of *elav>HTT93Q,dRab8* head extracts, showing the endogenous (23 KDa) and the overexpressed YFP tagged-dRAB8 (46 KDa). dRAB8 endogenous levels are comparable to *w<sup>1118</sup>* fly extracts. Primary antibody:  $\alpha$ -Rab8 1:2500 (BD Bioscience, Table 2-3). Secondary antibody:  $\alpha$ -mouse HRP 1:10000 (Vector, Table 2-3). **B** Quantification of exogenous dRAB8 overexpression. The data shown are ratio of the mean value obtained from endogenous dRAB8 and are presented as mean  $\pm$ SEM of three experiments.

#### 4.3.2 ICC on HEK293T cells suggests co-localisation between hRAB8 and mHTT aggregates

Next, I investigated how the distribution of endogenous Rab8 was affected in the presence of wild type HTT (HTT25Q) or mutant HTT (HTT97Q). Due to the experimental difficulties encountered with PC12 cells stably expressing rRAB8, and because the rate of transient transfection of PC12 is poor, I used HEK293T cells as an alternative cell model.

First, I tested whether the  $\alpha$ -Rab8 antibody (raised against dRAB8, Table 2-3) could recognize the native conformation of human Rab8 (hRAB8). Immunolabelling of hRAB8 (Figure 4-11) revealed cytoplasmic and perinuclear distribution, in accordance with published literature (Chen *et al.*, 1993; Hattula *et al.*, 2006; Just & Peränen, 2016; Rowe *et al.*, 2008).

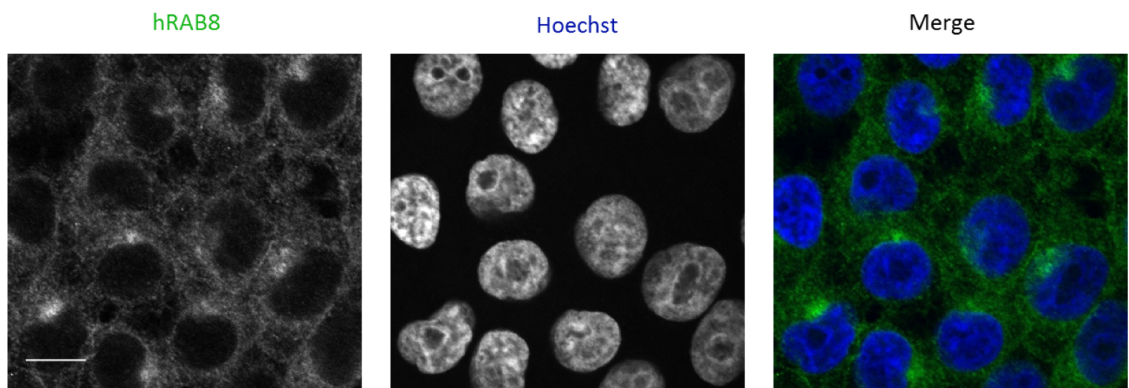


Figure 4-11 Endogenous distribution of hRAB8.

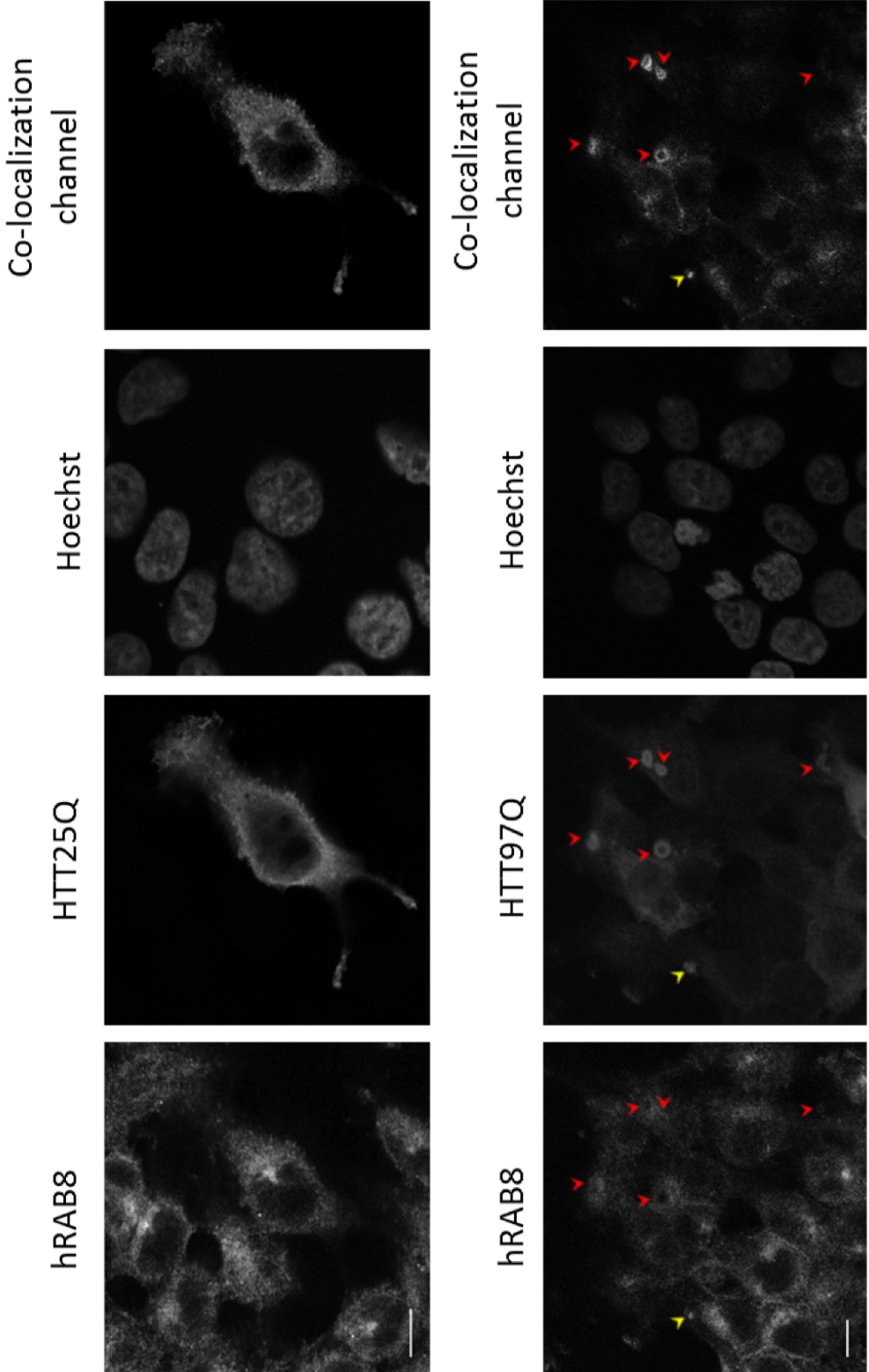
HEK293T cells showing the distribution of endogenous hRAB8. In green hRAB8, in blue nuclei (Hoechst). Primary antibody:  $\alpha$ -Rab8 1:200 (BD Bioscience, Table 2-3). Secondary antibody: AlexaFluor<sup>®</sup>488 1:500 (ThermoFisher Scientific, Table 2-3). Single optical confocal section. Scale bar=10  $\mu$ m.

Next, I transfected HEK293T cells with a plasmid encoding either wild-type or mutant HTT. Because HEK293T cells express endogenous HTT, I used tagged constructs, namely HTT25Q-VC and HTT97Q-VC (Table 2-3 and Figure 4-14). VC represent amino acid 159-238 of Venus – a YFP derived fluorophore – which is recognised by any  $\alpha$ -GFP polyclonal antibody (Repici, personal communication), therefore limiting detection to exogenous HTT.

As expected, the distribution of hRAB8 was comparable to that of non-transfected cells, (cfr. Figure 4-11 and Figure 4-12) and overlapped extensively with HTT25Q, which was limited to the cytoplasm (Herrera *et al.*, 2011 and Figure 4-12).

Interestingly, cells transfected with HTT97Q exhibited small and large aggregates. In single optical sections, small aggregates appeared as foci of  $\sim 1 \mu\text{m}$  diameter. However, the vast majority were large aggregates appearing as rings of diameter  $>3.5 \mu\text{m}$  (Figure 4-12).

Figure 4-12 Distribution of hRAB8 is affected in presence of HTT97Q.



The overlap between hRAB8 and HTT97Q appeared reduced compared to hRAB8 and HTT25Q. To support this, I quantified the correlation between hRAB8 and HTT. Cells were imaged using *ad hoc* settings for each image and the Manders correlation coefficient (MCC) was calculated for each channel.

An unpaired t-test revealed that the proportion of signal from HTT correlating with the signal from hRAB8 (M1) was significantly lower in cells transfected with HTT97Q compared to cells transfected with HTT25Q ( $t=2.814$ ,  $df=18$ ,  $p=0.0115$ , Figure 4-13.A). Likewise, the proportion of signal from hRAB8 correlating with signal from HTT (M2) was lower in cells transfected with HTT97Q than with HTT25Q ( $t=3.919$ ,  $df=18$ ,  $p=0.001$ , Figure 4-13.B). This suggests that in cells transfected with mutant HTT, the overall correlation with hRAB8 is reduced, supporting previous co-localisation analyses (Figure 4-12).

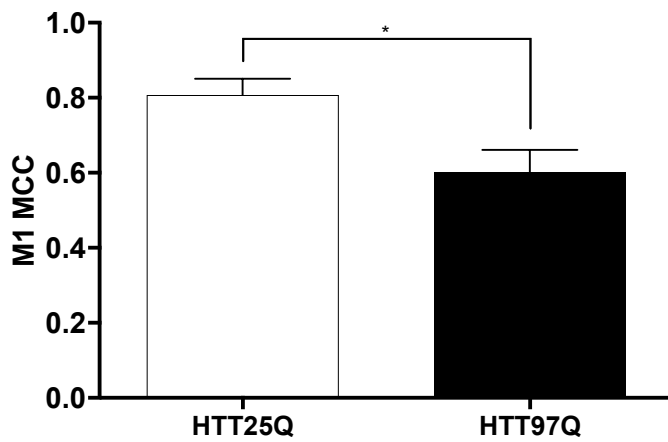
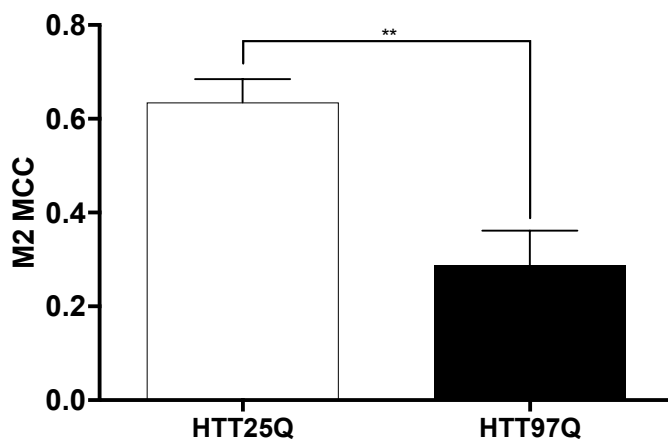
**A****B**

Figure 4-13 Correlation between hRAB8 and HTT is polyQ dependent.

Comparison of correlation (measured as Manders coefficient) between overexpressed HTT and endogenous hRAB8. HEK293T cells were transfected with either HTT25Q-VC (HTT25Q) or HTT97Q-VC (HTT97Q). **A** MCC indicating the proportion of HTT signal correlating with hRAB8 signal (M1). Unpaired two-tailed t-test  $t=2.814$  df=18,  $p=0.0115$ . N=10. Data are mean  $\pm$ SEM. **B** MCC indicating the proportion of hRAB8 signal correlating with HTT signal (M2). Unpaired two-tailed t-test  $t=3.919$  df=18,  $p=0.001$ . N=10. Data are mean  $\pm$ SEM.

Although the correlation between HTT97Q and hRAB8 was reduced, overall, the co-localisation channel revealed a perfect overlap between the hRAB8 speckles and small aggregate foci of mutant HTT (Figure 4-12, yellow arrow). Conversely, the cytoplasmic distribution of hRAB8 was interrupted by black circular patches, which overlapped the immunonegative structure at the centre of large mutant HTT aggregates (Figure 4-12, red arrows). This could be either a result of hRAB8 being at the centre of the inclusion, yet unable to be detected by the antibody – similarly to HTT – or it could be that hRAB8 is not a constituent of the aggregates. Interestingly, however, the co-localisation channel revealed a positive signal between hRAB8 and mHTT at the periphery of the aggregates.

#### 4.3.3 BiFC assay reveals interaction between mHTT and dRAB8 in HEK293T cells

I next investigated a potential interaction between dRAB8 and mHTT by Bimolecular Fluorescent complementation assay (BiFC), a technique employed for the visualisation of protein interaction in living cells (Kerppola, 2008; Kodama & Hu, 2012).

If HTT (either the wild type or the mutant form) interacts with Rab8, the two non-fluorescent fragments would associate, forming a fluorescent protein that is detectable *in vivo*, without the use of antibodies. Since BiFC required the overexpression of the two interacting partners, and since the ultimate goal of this study was to study the role of Rab8 in a *Drosophila* model of HD, I investigated the interaction between HTT and dRAB8.

The coding sequence of *Drosophila melanogaster Rab8* was amplified from *UAS-dRab8* flies (Table 2-4) and fused with the C-terminus (159-240 AA) of Venus (VC), a variant of yellow fluorescent protein (YFP), as described in Section 2.2.3. Venus was chosen because of its strong fluorescence intensity (Shyu *et al.*, 2006). To minimize potential steric constraints that might prevent BiFC formation due to the two non-fluorescent fragments facing opposite sides of the complex, VC was cloned either at the C- or at the N-terminus of dRAB8 (Table 2-2 and Figure 4-14). Moreover, to reduce steric constraints further, a GGGGSGGGG flexible linker was cloned between dRAB8 and VC (Figure 4-14).

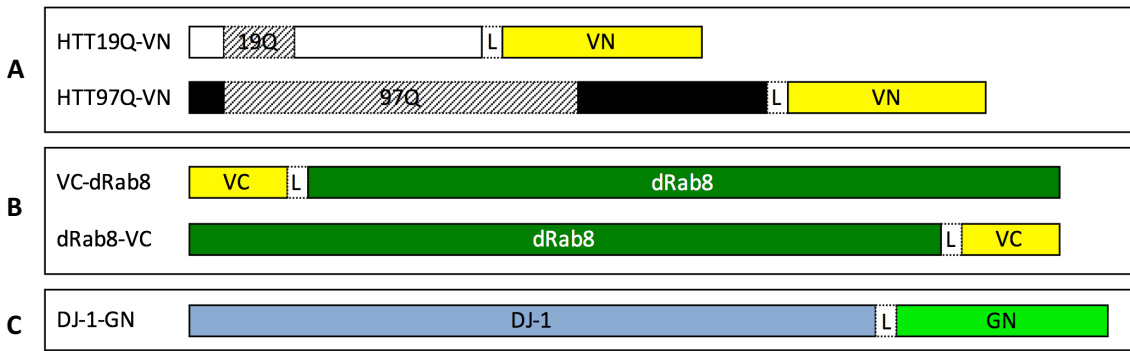
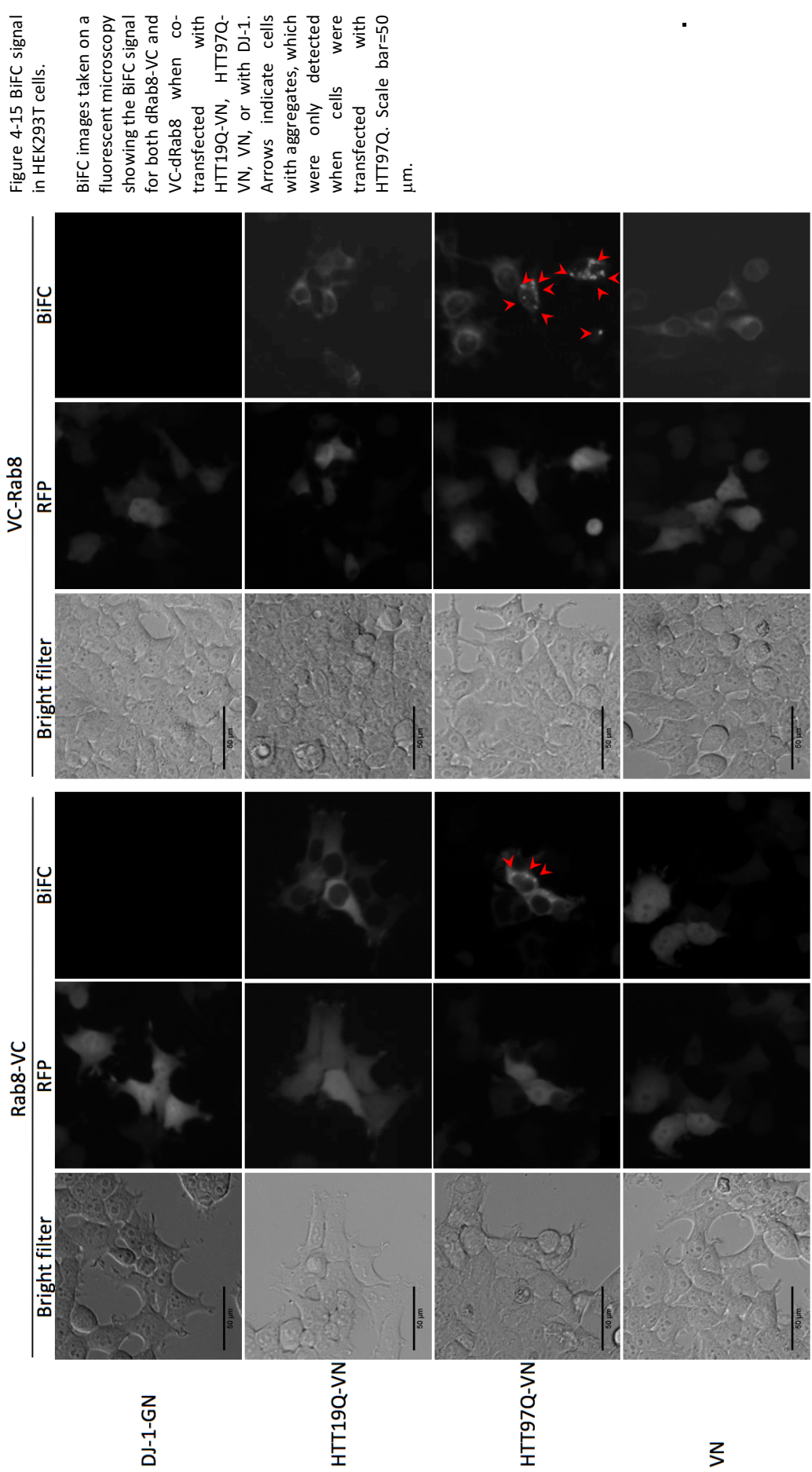


Figure 4-14 BiFC constructs used in this study.

Representation of BiFC constructs used in this study. **A** HTT19Q and HTT97Q are fused to the N-terminus fragment of Venus (1-158 AA). **B** dRAB8 is fused to the C-terminus of Venus (159-240 AA) either at its N-terminus (top construct) or at its C-terminus (bottom construct). **C** DJ-1 is fused to the N-terminus of GFP (1-172). L=linker, VN=Venus 1-158 AA, VC=Venus 159-240 AA, GN=GFP 1-172 AA.

Each construct was co-transfected either with wild-type HTT (HTT19Q-VN) or with mutant HTT (HTT97Q-VN). Moreover, to check whether the tag itself could influence dRAB8 localisation, the dRab8 BiFC constructs were co-transfected with VN alone. In this condition, the reconstitution of Venus depends on the random collision between VC (fused to dRAB8) and VN, which diffuses in every compartment of cells, including the nucleus. Even though the resulting signal intensity is not informative *per se* and cannot be used as background control (Kodama & Hu, 2012), the fluorescence allows the visualization of dRAB8 distribution – which would be otherwise only possible by ICC – fulfilling the purpose of localisation control. Furthermore, as a background control, I co-transfected dRAB8 with a construct encoding a protein expressed in the same cellular compartment as dRAB8, but not known to interact with dRAB8. Based on the BiFC constructs already validated in our laboratory, I chose DJ-1-GN (Repici *et al.*, 2013) (Table 2-2 and Figure 4-14), whose localization is predominantly cytoplasmic (Nagakubo *et al.*, 1997). DJ-1-GN was fused to the N-terminus (1-172 AA) of GFP (Figure 4-14), a non-fluorescent fragment that could complement VC (Shyu *et al.*, 2006). Moreover, RFP (table 2-2) was co-transfected in each condition as transfection control. As expected, cells transfected with dRAB8 + DJ-1 exhibited no detectable fluorescence (Figure 4-15), whereas a BiFC signal was detected when dRab8 constructs where co-transfected with VN (Figure 4-15) and when co-transfected with either HTT19Q-VN or with HTT97Q-VN (Figure 4-15).

Figure 4-15 BiFC signal in HEK293T cells.



Interestingly, the distribution of the BiFC signal showed a different pattern depending on which side VC was fused to dRAB8 (N-terminus or C-terminus). In fact, the dRab8-VC + VN combination showed a diffuse cytoplasmic and nuclear BiFC signal, whereas the BiFC signal of VC-dRab8 + VN was cytoplasmic with the typical perinuclear distribution (Figure 4-15), resembling the endogenous one (Figure 4-11). This observation led me to conclude that the VC tag at dRAB8 C-terminus side had a mis-localization effect, and therefore these data were excluded from further analysis.

Despite this, when dRab8-VC or VC-dRab8 were co-transfected with HTT97Q-VN, which leads to the formation of aggregates (Herrera *et al.*, 2011 and Figure 4-12) inclusion bodies were detected for both dRab8-VC and VC-dRab8 (Figure 4-15), suggesting an interaction between dRAB8 and mutant HTT aggregates.

To determine whether those interactions were polyQ-dependent, the BiFC signal was quantified and normalised to the RFP signal. A Kruskal-Wallis test performed on the BiFC/RFP ratio intensities followed by a Dunn's multi comparison test revealed a significantly increased signal for the HTT97Q-VN/VC-dRab8 pair compared to the HTT19Q-VN/VC-dRab8 pair (ANOVA  $H_{(2,12392)}=5928$ ,  $p<0.0001$ , VC-dRab8 + HTT19Q-VN vs VC-dRab8 + HTT97Q-VN,  $p<0.0001$ , Figure 4-16).

Note that to allow comparisons among different conditions all the images were taken with the same settings. In the presence of large mutant HTT aggregates, the intensity of the BiFC signal was extremely bright (this was observed in about 9.5% of the single units of neighbouring cells – see Figure 4-5 –, Table 4-2). Cells with bright aggregates resulted in overexposure and were automatically excluded from the analysis. Adjusting the settings to best detect the bright aggregates resulted in underexposure of the majority of the cells. Therefore, in the analysis above the interaction between mutant HTT aggregates and dRAB8 has been underrepresented, making this interaction even more striking.

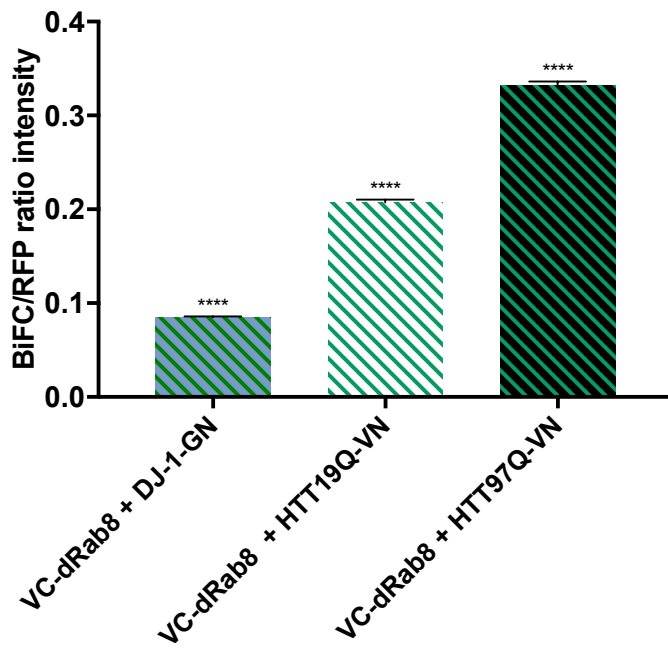


Figure 4-16 BiFC/RFP ratio intensity.

Average ratio intensity (green/red) per well for dRab8-VC or VC-dRab8 co-transfected alone or with DJ-1-GN, HTT19Q, HTT97Q or VN in HEK293T cells. Kruskal-Wallis test,  $H_{(2,12392)}=5928$ ,  $p<0.0001$ . Post-hoc Dunn, VC-dRab8 + HTT19Q-VN vs VC-dRab8 + HTT97Q-VN,  $p<0.0001$ , VC-dRab8 + HTT19Q-VN vs VC-dRab8 + DJ-1-GN,  $p<0.0001$ , VC-dRab8 + HTT97Q-VN vs VC-dRab8 + DJ-1-GN,  $p<0.0001$ . VC-dRab8 + DJ-1-VN N=4466; VC-dRab8 + HTT19Q-VN N=3946; VC-dRab8 + HTT97Q-VN N=3980. Data are expressed as mean  $\pm$  SEM.

Table 4-2 Percentages of overexposed cells co-transfected with VC-dRab8 in the BiFC experiment.

Condition	Number of selected cells	Number of overexposed cells	% of overexposed cells
VC-dRab8	2993	0	0
VC-dRab8 + DJ-1-GN	4466	0	0
VC-dRab8 + HTT19Q-VN	3946	45	1.14
VC-dRab8 + HTT97Q-VN	3980	377	9.47
VC-dRab8 + VN	4299	51	1.19

#### 4.4 Discussion

To validate the ability of dRAB8 to rescue mutant HTT dependent phenotypes in *Drosophila*, I sought to investigate the effects of rRAB8 overexpression in a HD mammalian system. Results from apoptotic assays on stably transfected cells overexpressing rRAB8A or rRAB8B revealed that rRAB8A/B did not suppress, and in some cases even increased, the level of caspase-3/7 activation induced by HTT103Q. However, rRAB8 expression was not toxic *per se*, as increased caspase-3/7 activation was only observed upon HTT103Q expression. Protein toxicity is not unusual in overexpression studies and is often caused by overwhelmingly high protein levels (Moriya, 2015). Highly expressed genes titrate cellular components required by transcription and translation machineries, creating a metabolic burden for the cell (Moriya, 2015). Moreover, protein expression, whose regulation is fundamental for cellular homeostasis, relies on a fine balance of space, time and level. Disruption of this physiological equilibrium impacts on cell proliferation and differentiation and might trigger enhanced apoptotic responses. In addition, the relative amounts of proteins participating in complexes play a pivotal role. In fact, according to the balance hypothesis context (Sopko *et al.*, 2006), the relative level of proteins participating in stoichiometric complexes is more important than their absolute amount, as changes in expression can affect the stoichiometry of physically interacting proteins. Thus, overexpression of proteins could be harmful due to an imbalance in the concentrations of interacting subunits (Veitia, 2005) and this effect could be enhanced in a disease context (Sopko *et al.*, 2006).

While the mechanism by which rRAB8 overexpression exacerbated apoptotic levels is not clear, toxicity induced by the overexpression of Rab proteins is hinted at by several high-throughput studies in yeast. Overexpression of *Saccharomyces cerevisiae* Rab orthologues such as Ypt1 (Rab1), Ypt6 (Rab6), Ypt10 (Rab5), Ypt11 (Rab11), Ypt31 (Rab11), Ypt52 (Rab5) and Sec4 (Rab8) decreased cell growth (Makanae *et al.*, 2013; Sopko *et al.*, 2006; Yoshikawa *et al.*, 2011), whereas other defects such as abnormal distribution of the proteins and decreased autophagy have been described for Ypt7 (Rab7) and Ypt31 (Rab11) (Kim *et al.*, 2016; Lachmann *et al.*, 2012) and for Sec4 (Rab8) overexpression (Geng *et al.*, 2010), respectively.

Parallel studies in our laboratory have also shown that large changes in rRAB expression (*i.e.* when exogenous rRAB expression is on average >50% higher than the endogenous level) are deleterious for mammalian cells (Mason & Giorgini, unpublished). In these studies, HTT103Q model PC12 cells stably overexpressing rRABs were generated in the same fashion as described in the Materials and Methods of this chapter (Section 4.2.3), to obtain pools overexpressing rRAB1A, rRAB2A, rRAB5A, rRAB8A, rRAB11A and rRAB27A. Decreased cell proliferation and

activation of caspase-3/7 were observed for all rRAB transfectant pools where HTT103Q was induced by PA (namely HTT103Q rRAB1A, HTT103Q rRAB2A, HTT103Q rRAB5A, HTT103Q rRAB8A, HTT103Q rRAB11B and HTT103Q rRAB27A) and in some cases even in pools where HTT103Q expression was not induced (namely rRAB1A, rRAB5A) (Mason & Giorgini unpublished).

Interestingly, I found that the average expression levels from pooled rRAB8 stable transfectants was 3- to 5-fold higher than rRAB8 endogenous levels and strikingly, a positive correlation was found between rRAB8 expression levels and caspase-3/7 activation. Given this technical caveat and the time constraints, the characterization of rRAB8 in PC12 cells was not explored further during the course of this project.

In line with my observations however, extensive work in our laboratory showed that by changing the optimal Kozak (CCACC) to a weaker one (CCGCC) - known to significantly reduce the translation efficiency (Kozak, 1986) - in HTT103Q model PC12 cells overexpressing RAB1A, RAB2A, RAB5A, RAB11B and RAB27A, reduced exogenous rRAB expression was observed, with average levels <50% relative to the endogenous proteins (Mason & Giorgini, unpublished). Modulation of rRAB expression, by mean of a reduction of exogenous rRAB expression levels, led to the rescue of HTT103Q induced toxicity in PC12 cells and to the loss of deleterious phenotypes in PC12 non-induced cells (Mason & Giorgini, unpublished).

Taken together, these observations suggest that the “window” of overexpression for rRAB8 protection might be rather modest. Though the molecular and the physiological reasons why high levels of rRAB8 expression being detrimental were not explored in detail, overall these results strongly link rRAB8 expression levels with toxic or protective phenotypes.

HTT plays a pivotal role in the localization of Rab8 at the Golgi apparatus (del Toro *et al.*, 2009). Consistent with the study of del Toro *et al.* (2009), ICC performed on HEK293T cells showed that, while the distribution of hRAB8 in un-transfected cells or in cells transfected with HTT25Q was cytoplasmic with perinuclear staining, the distribution of endogenous hRAB8 was perturbed in the presence of HTT97Q. Although no Golgi marker was used, I have noticed loss or reduction of perinuclear hRAB8 staining in cell transfected with HTT97Q, consistent with mutant HTT delocalising Rab8 from the Golgi (del Toro *et al.*, 2009). Del Toro and co-workers (2009) also reported a decreased interaction with Rab8 of mutant HTT (FL-HTT75Q) compared to wild type HTT (FL-HTT17Q). I therefore quantified the correlation between hRAB8 and HTT. The most common way to calculate correlation is the Pearson correlation coefficient (PCC); however, as a fundamental requirement, the images must be acquired with identical settings including the gain. In other words, to compare the correlation of two signals in two conditions (*e.g.* condition A and condition B), the gain used for channel 1 in condition A must be identical

to the gain used for channel 1 in condition B and the same applies for channel 2. While this requirement was fulfilled when imaging hRAB8, bright aggregates in HTT97Q samples precluded the possibility to use the same setting for cells transfected with HTT25Q. In fact, keeping the same settings resulted in overexposure of HTT97Q cells, or loss of HTT25Q signal. Moreover, not every cell transfected with HTT97Q exhibited the same number of aggregates, which also differed in signal intensity. With these premises, the overlap between hRAB8 and HTT signals was lower in HEK293T cells transfected with HTT97Q compared to cells transfected with HTT25Q, in line with what observed by del Toro *et al.* (2009).

Moreover, analysis of the MCC revealed a reduced correlation coefficient for hRAB8 and HTT97Q, suggesting a reduced interaction between the two proteins.

A pathological hallmark of HD is the presence of intracellular aggregates (DiFiglia *et al.*, 1997; Davies *et al.*, 1997; Muchowski, 2002; Sherman & Goldberg, 2001). ICC performed on HEK293T cells transfected with HTT97Q exhibited aggregates varying in sizes and immunostaining intensity. In confocal optical sections, small aggregates were detected as cytoplasmic punctae, whereas large aggregates appeared as empty spheres, where only the external surface was immunolabelled, possibly because the spatial organization of mHTT in the aggregate masked the epitope (Chun *et al.*, 2001), or because of the inability of the antibody to penetrate in the inclusion bodies. Interestingly, while in the presence of small aggregates hRAB8 formed cytoplasmic speckles perfectly overlapping mutant HTT punctae, in the presence of large aggregates the distribution of hRAB8 resembled that of mutant HTT, *i.e.* staining at the periphery but not at the center of the aggregate. As HTT signal was expected to be found in the aggregates, this result raises the question of what is the meaning of Rab8 lack of signal at the center of the aggregates. One possible interpretation is that hRAB8 interacts with insoluble mHTT, however, as the aggregates become larger, for unknown reasons, immunolabelling of hRAB8 (and HTT93Q) cannot be detected and hence the lack of hRAB8 signal would reflect a technical artefact. A second possibility is that hRAB8 interacts only with small mHTT aggregates, and when the aggregates become larger, the interaction persists at the aggregate's periphery. Either way, the ICC has proven to be an approach with some technical limits, deriving from the need to label proteins with antibodies.

These limitations have however been overcome by using the BiFC assay, which unveiled a significant polyQ-dependent interaction dynamics of dRAB8 with HTT. When VC-dRab8 was co-expressed with HTT97Q-VN, the BiFC signal was about 1.7-fold higher than the signal produced by the co-expression of VC-dRab8 + HTT19Q-VN. However, only results relative to one orientation (VC-dRab8) have been analysed as the BiFC experiments showed that the tag at the C-terminus (*i.e.* dRab8-VC), but not at the N-terminus (*i.e.* VC-dRab8), suffered a localization

problem. Indeed, when cells were co-transfected with dRab8-VC + VN, the BiFC signal exhibited an evenly diffused cytoplasmic and nuclear distribution. Moreover, no BiFC perinuclear signal was detected, indicating that dRAB8 was mis-localized. Conversely, when cells were transfected with VC-dRab8 + VN the BiFC signal was not detected in the nucleus, and resembled those already described for the GTPase. How the Rab proteins localize to their target membranes has not been clarified yet. However, the COOH-terminal hypervariable region has been reported to be important for the correct targeting of Rab proteins to their final compartments (Chavrier *et al.*, 1991) and therefore it is plausible that the VC tag the C-terminus of dRAB8 might interfere with it, preventing dRAB8 correct localization.

Interestingly, imaging of native fluorescence revealed BiFC inclusion bodies of various sizes without “zones of exclusion”, indicating extensive interaction between dRAB8 and mHTT aggregates. These results moreover, suggest that the ICC images likely suffered from a technical artefact, where the lack of the  $\alpha$ -Rab8 signal was a false negative, and hence that immunolabelling of hRAB8 at the aggregate could not be detected *via* ICC, rendering the study of endogenous hRAB8 interaction dynamics challenging.

Del Toro and co-workers (2009) were the first to explore the changes of Rab8 dynamic interactions with HTT. Their study showed a reduced interaction between mutant HTT and Rab8. The authors however, limited their investigation to soluble mutant HTT and did not explore the interaction dynamics at the aggregates. The lack of evidence in the literature, of a relationship between Rab8 and mutant HTT aggregates, raises the question of why this increased interaction occurs.

Albeit very speculative, a possible explanation could be based on a scenario where, in the aggregation process driven by mutant HTT, Rab8, as other essential proteins involved in vesicle trafficking, might be sequestered and removed from its cytoplasmic location (Qin *et al.*, 2004). The decreased interaction with soluble mutant HTT observed in the ICC and the interaction with mutant HTT aggregates observed in the BiFC assay could reflect a situation where dRAB8 is sequestered by the aggregates. In this scenario, the protection conferred by dRAB8 overexpression observed in flies could derive from restoring cytoplasmic dRAB8 levels, which could compensate for the sequestered dRAB8 and recover those pathways that have been impaired, such as the lysosomal trafficking from the TGN (del Toro *et al.*, 2009). Indeed, this study found that the presence of a functional Rab8 is necessary for the TGN trafficking to the lysosome (del Toro *et al.*, 2009). Also, Rab8 has been recently identified as one of the key Rabs participating in autophagosome maturation into the autolysosome, therefore playing an essential role in autophagy (Ao *et al.*, 2014). The autophagy-lysosome pathway is crucial for degradation of pathogenic proteins and has been shown to have a therapeutic effect on HD

(Ravikumar *et al.*, 2002; Ravikumar *et al.*, 2004; Sarkar & Rubinsztein, 2008; Shibata *et al.*, 2006). Given the intimate link between Rab8 and the autophagy-lysosome pathway, in the next chapter I will investigate this in detail using a fruit fly model of HD.

# Chapter 5

## Investigating dRAB8 rescue mechanism in a fly model of HD

### 5.1 Introduction

In this chapter, I address the possible mechanisms by which dRAB8 rescues phenotypes caused by the expression of mutant HTT in *Drosophila* with a focus on autophagy. Autophagy is a catabolic process that is of fundamental importance in the homeostatic balance between synthesis, degradation and recycling of cellular components. Autophagy is free from the steric constraints that limits UPS in the degradation of unfolded proteins. Thus, autophagy constitutes a response mechanism that allows the cell to survive critical stress conditions (Klionsky & Emr, 2000). During autophagy, targeted cellular components, such as organelles, proteins and aggregates can all be isolated in double membrane vesicles (autophagosomes), and delivered to lysosomes for degradation (Kroemer *et al.*, 2010). Therefore, autophagy is a key degradative pathway for toxic mHTT species due to failure of the UPS to efficiently degrade mHTT (Hara *et al.*, 2006; Komatsu *et al.*, 2006). Pioneering studies carried out in yeast led to the discovery of the Autophagy-related (Atg) proteins, the group of proteins directing autophagy (Klionsky, 2007). So far more than 30 Atg proteins have been found to constitute the canonical molecular core of the autophagic pathway, which is highly conserved in all eukaryotes. Autophagy is a tightly regulated process, which consists of 4 major steps (summarized in Figure 5-1): induction of autophagy, autophagosome formation, cargo degradation and amino acid recycling (Xie & Klionsky, 2007):

- **Induction of autophagy:** in normal conditions, the class-I phosphatidylinositol-3-kinase (PI3K) signalling pathway activates the target of rapamycin (Tor), which functions as a negative regulator of autophagy. By phosphorylating Atg1, Tor inhibits autophagy induction and maintains it at basal activity levels. However, stress conditions such a nutrient starvation or rapamycin treatment, repress Tor activity. It follows the dephosphorylation and activation of Atg1, which associates with Atg13 consequently inducing autophagy.
- **Autophagosome formation:** once autophagy is induced, cellular components are sequestered by the phagophore, which in its matured form resembles a monolayer cisterna. Although the precise mechanism and source of membranes forming the phagophore is still unclear, Atg9 seems to be pivotal in delivering membranes to form the phagophore. The formation of the phagophore requires the class III phosphatidylinositol 3-kinase (PtdIns3K) complex — which is constituted by Atg6, Vps34, Vsp15 and Atg14 — to convert phosphati-

dylinositol (PtdIns) into phosphatidylinositol 3-phosphate (PtdIns3P). PtdIns3P is a signal molecule that functions in the recruitment of many other Atg proteins to the phagophore membrane. The phagophore elongates to sequester the cytoplasmic components, quickly maturing into a double membrane vesicle, the autophagosome. The phagophore elongation requires a series of reactions catalysed by 8 different Atg proteins (Atg3, Atg4, Atg5, Atg7, Atg8, Atg10, Atg12 and Atg16), which engage two-ubiquitin-like conjugation reactions. In the first reaction, the ubiquitin-like molecule Atg12 is conjugated to Atg5. This complex then interacts with Atg16, to form the Atg12-Atg5-Atg16 complex, which binds to the outer membrane of the phagosome. In the second reaction, the ubiquitin-like molecule Atg8 is cleaved by Atg4, and then is lipidated by Atg7 via conjugation to phosphatidylethanolamine (PE). Atg8 is integrated in the autophagosome double phospholipidic layer. Because Atg8 is synthesised as a precursor and then it is cleaved and lipidated, the free cytosolic (precursor) form is referred to as Atg8-I, whereas its mature, autophagosome-associated form is referred to as Atg8-II. The mammalian ortholog of Atg8 is called LC3 (Light Chain 3). Atg8-II/LC3-II are considered the most reliable marker of autophagy as once incorporated into the membrane, Atg8-II/LC3-II is stably associated with the autophagosome until the cargo degradation (Klionsky *et al.*, 2016). At this stage, the autophagosome can fuse with multi-vesicular bodies (MVBs) or with a late endosome, forming an amphisome.

- **Autolysosome formation:** in the final stage of its maturation, the autophagosome (or the amphisome) fuses with a lysosome, producing an autolysosome. Although largely unknown, this process is directed by a number of proteins among which class C vacuolar protein sorting (Vps), endosomal sorting complex required for transport (ESCRTs) and soluble NSF attachment protein receptors (SNAREs).
- **Cargo degradation:** lysosomal hydrolases degrade the content of the autolysosome and the inner membrane of the autolysosome itself to macromolecules and aminoacids, which are released into the cytoplasm. At this stage, the intraluminal Atg8-II is degraded, whereas Atg8-II integrated in the outer autolysosome membrane undergoes an Atg4-mediated de-lipidation. Atg8 and other macromolecules and amino acids are released into the cytoplasm for recycle *via* permeases found at the autolysosome membrane.

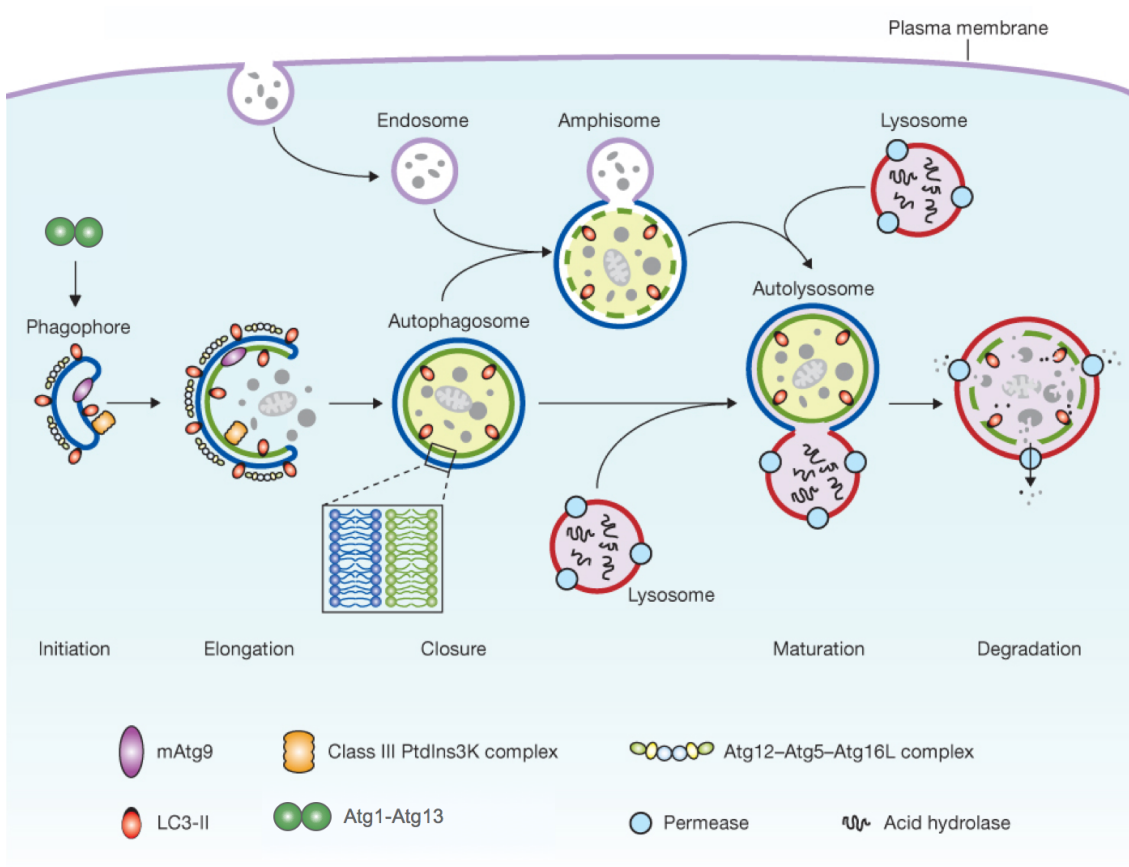


Figure 5-1 Overview of autophagy and the canonical autophagic core machinery.

Autophagy is induced by the Atg1 complex (Atg1-Atg13) that triggers the formation of a phagophore. The phagophore membrane contains Atg9 (which is essential in providing membranes for phagophore formation), Atg8-I, and two conjugation systems: class III PtdIns3K complex and Atg12-Atg5-Atg16 complex (which are involved in the phagophore maturation into autophagosome). The autophagosome or the amphisome (the latter resulting by the fusion of the autophagosome with an endosome) finally fuses with the lysosome, to produce an autolysosome, where, through the action of acid hydrolases, the engulfed cytoplasmic material is degraded and reintroduced in the cytoplasm *via* permeases as amino acids or macromolecules. Adapted from Yang & Klionsky, 2010.

Numerous studies have shown that at least 10 Rabs — Rab1, Rab4, Rab5, Rab7, Rab8, Rab9, Rab11, Rab24, Rab32 and Rab33 — are involved in different steps of autophagy (Ao *et al.*, 2014; Jain & Ganesh, 2016, and Table 1-1). Interestingly, there is growing evidence that over-expressing Rabs to upregulate autophagy might have therapeutic potential for several neuro-degenerative disorders. For instance, Ravikumar and colleagues (2008) showed that Rab5 conferred protection in COS-7 cells and fly models of HD by regulating the autophagy-dependent clearance of toxic mHTT. Studies in our laboratory have confirmed the protective role of Rab5 (more precisely rRAB5A) in the HTT103Q PC12 cell model. Furthermore, they have suggested an autophagy-related role in the rescue of HD phenotypes mediated by the overexpression of rRAB2A, rRAB11B and rRAB27A in the same cell system (Mason & Giorgini, unpublished).

Besides its well-characterized role in vesicle delivery from the Golgi to the plasma membrane, Rab8 is also involved in autophagy, being involved in the fusion of the autophagosome with the lysosome (Figure 1-10), thus, providing a rationale for investigating the role of Rab8 in the modulation of autophagy and cellular mHTT cellular clearance.

Moreover, the observation of del Toro and co-workers (2009) that mHTT expression leads to Rab8 de-localization from the Golgi and subsequent impairment of lysosomal trafficking provides a further rationale for linking Rab8 with autophagy. If overexpression of dRAB8 to functional cytoplasmic levels restores the normal lysosomal trafficking, autophagy might be consequently upregulated. On the other hand, dRAB8 overexpression could promote the unconventional based-autophagy, a pathway where proteins are cleared from the cytosol *via* autophagosomal sequestration and extracellular secretion (Lim & Yue, 2015). Either routes are hence expected to provide cellular clearance of toxic mHTT species: the autophagic route *via* mHTT degradation, the unconventional autophagy-based secretion *via* extracellular delivery of mHTT.

Based on these observations, it is possible to imagine that a similar scenario might also occur in *Drosophila*, owing to the high degree of conservation between fly and mammalian Rab8 (West *et al.*, 2015). I therefore assessed whether autophagy is abnormal in flies expressing mHTT by measuring the levels of processed ATG8 (the homolog of LC3), a key autophagic core-machinery component. Upon proteolysis by ATG4, the precursor of ATG8 is converted into the cytosolic form ATG8-I. Once autophagy is activated, ATG8-I is phosphatidylethanolamine (PE)-lipidated, becoming ATG8-II, which binds to the membrane of the elongating phagophore, helping to recruit the cargo. ATG8-II remains associated with the phagophore until its maturation into autophagolysosome and until complete degradation of the cargo. Thus, ATG8 is the most reliable marker to monitor changes in the basal level of autophagy (Klionsky *et al.*, 2016).

Moreover, to further assess whether dRAB8 contributes to the autophagic degradation of mHTT, I used two biochemical techniques, the filter retardation assay and AGERA (agarose gel electrophoresis for resolving aggregates). Both methods allow to quantify cellular aggregated mHTT and hence to assess dRAB8 influence on mHTT clearance.

Overall, my results do not support upregulation of autophagy nor mHTT clearance upon dRAB8 overexpression in HD flies. On the contrary, dRAB8 overexpression seems to promote aggregation of mHTT, suggesting a novel mechanism for the Rab GTPase family.

## 5.2 Materials and Methods

### 5.2.1 Autophagy assay

The autophagy assay measured the amount of ATG8-I vs ATG8-II via Western immunoblot. Female flies expressing HTT93Q or HTT93Q and dRAB8 were generated by crossing females *UAS-HTT93Q* (Table 2-4) and *UAS-HTT93Q,dRab8* (Table 2-5) to *elav-GAL4* males (Table 2-5). UAS-only and GAL4-only control females were generated by crossing *UAS-HTT93Q* (Table 2-4) and *UAS-HTT93Q,dRab8* (Table 2-5) to *w<sup>1118</sup>* or to *elav-GAL4* males (Table 2-5) respectively (see Table 3-1). Protein extraction was performed as described in Section 2.2.4 with no modification to the protocol. Membranes were incubated with primary and secondary antibodies ( $\alpha$ -Atg8 and  $\alpha$ -rabbit HRP, Table 2-3) as described in Section 2.2.4. Immunoblot analysis was performed as described in section 2.2.4.4 with ImageJ. Autophagy was monitored measured as ATG8-II/ATG8-I. The means of three independent experiments were used in a one-way ANOVA, followed by a Newman-Keuls post-hoc using GraphPad Prism.

### 5.2.2 Filter retardation assay

Proteins were extracted from fly heads as described in Section 2.2.4.1, using females expressing HTT93Q or HTT93Q and dRAB8 as test flies and male flies as UAS controls (see Table 3-1). Total protein concentration was determined with the Bradford assay relative to a bovine serum albumin (BSA) standard. 300  $\mu$ l of Bradford reagent were mixed with 10  $\mu$ l of protein extract and incubated in the dark for 15 min before reading the absorbance at 595 nm with a plate reader. Then 100  $\mu$ g of proteins per sample were resuspended in 150  $\mu$ l of 2% SDS in PBS. A cellulose acetate membrane (0.45  $\mu$ m, Whatman) was equilibrated in 2% SDS in PBS before loading the samples. These were then blotted onto the membrane by vacuum using a HybriSlot 24 slot blotting apparatus (Core Life Science) according to the manufacturer's instructions. Each spot was washed 3 times with 150  $\mu$ l of 2% SDS in PBS and the membrane was subsequently air-dried prior to standard blocking and incubation with antibodies ( $\alpha$ -HTT and  $\alpha$ -mouse HRP, Table 2-3). Immunoblot analysis was performed as described in section 2.2.4.4

with ImageJ. The relative abundance of  $\alpha$ -HTT signal in *elav>HTT93Q,dRab8* flies was normalized to the abundance of the  $\alpha$ -HTT signal of *elav>HTT93Q* samples, the latter thus set as 1. The means of three independent experiments were used in a one-sample t-test, performed with Graphpad Prism.

### 5.2.3 AGERA

The AGERA protocol was adapted for fly samples from Weiss *et al.* (2008). Proteins were extracted from 100 fly heads and samples were quantified as described in Section 2.2.4.1. Females overexpressing HTT93Q or HTT93Q and dRAB8 were used as test flies and males were used as UAS controls (see Table 3-1). Protein extracts were normalised to OD<sub>595</sub>=0.5. For each sample 30  $\mu$ l were diluted 1:1 with a non-reducing Laemmli buffer (50 mM tris-HCl pH 6.8, 33% glycerol, 1.2% SDS, 0.001% bromophenol blue) before incubating at 95°C for 5 min. Then the samples were loaded on an agarose gel (1.5% agarose, 375 mM tris-HCl, pH8.8, 0.1% SDS) and run in Gly-Tris buffer (192 mM glycine, 25 mM tris-base, 0.1% SDS) at 20 V O/N. Gels were blotted onto a nitrocellulose membrane using a semi-dry blotter (BioRad) following the manufacturer's instructions, the transfer buffer consisted of 25 mM tris, 192 mM glycine, 0.1% SDS, 15% methanol. Membranes were incubated with primary and secondary antibodies ( $\alpha$ -HTT and  $\alpha$ -mouse HRP, Table 2-3) as described in Section 2.2.4.4. Immunoblot analysis, relative abundance of the  $\alpha$ -HTT signal and statistical analysis were performed as described in the previous section.

### 5.2.4 Fly co-Immunoprecipitation (Co-IP)

Co-immunoprecipitation was performed with GFP-Trap®\_A (Chronotek) with slight modifications to the manufacturer's protocol for fly extracts optimization. Proteins were extracted from 400 heads as described in Section 2.2.4.1. 100  $\mu$ l of proteins were then diluted in 400  $\mu$ l of dilution buffer (10 mM tris-HCl pH7.5, 150 mM NaCl) and incubated 2 h at 4°C with 60  $\mu$ l of equilibrated GFP-Trap®\_A beads (Chronotek). 50  $\mu$ l of diluted proteins were mixed with 50  $\mu$ l of 4x Laemmli buffer (240 mM tris-HCl pH6.8, 5% -mercaptoethanol, 40% glycerol, 8% SDS, 0.04% bromophenol blue) and used as input fraction. The rest of the lysate was subsequently washed 3 times with dilution buffer. 50  $\mu$ l of the last discarded wash was diluted in 50  $\mu$ l of 4x Laemmli buffer and used as non-bound fraction (flow through). Washed proteins were diluted in 100  $\mu$ l of 2x Laemmli buffer (120 mM tris-HCl pH6.8, 2.5%  $\beta$ -mercaptoethanol, 20% glycerol, 4% SDS, 0.04% bromophenol blue). Samples were heated 10 min at 95°C and then centrifuged 2 min at 2,500 x g at RT for beads removal. Each sample was equally split and loaded onto two 12.5% SDS-PAGE gels, which were transferred onto a nitrocellulose membrane (see Section 1.3.4.3). Membranes were incubated with primary ( $\alpha$ -HTT and  $\alpha$ -Rab8, Table 2-3) and second-

ary ( $\alpha$ -mouse HRP, Table 2-3) antibodies as described in Section 2.2.4.

## 5.3 Results

### 5.3.1 dRAB8 overexpression does not up-regulate basal autophagy

To examine the contribution of dRAB8 overexpression to the autophagy-lysosome pathway, the autophagy marker ATG8 was quantified *via* immunoblot using and  $\alpha$ -Atg8 antibody on *elav>HTT93Q*, *elav>HTT93Q,dRab8* flies and controls (HTT93Q UAS ctrl, HTT93Q,dRab8 UAS ctrl and GAL4 ctrl). Autophagy and autophagic flux can be monitor in several ways (reviewed in Klionsky *et al.*, 2016), however, protein extraction and immunoblot detection of the autophagic marker ATG8 is certainly the cheapest and quickest way for a preliminary analysis. Indeed, as the cytosolic and the PE-lipidated vacuoles-associated forms (ATG8-I and ATG8-II respectively) differ by  $\sim$ 3 kDa, these can be easily discriminated and quantified *via* immunoblotting.

The amount of ATG8-II was normalized to the amount of its cytoplasmic form, ATG8-I. This quantification should provide a more sensitive readout compared to the normalization of ATG8-II with a housekeeping protein (*e.g.* Actin). If in *elav>HTT93Q,dRab8* flies the ATG8 turnover is more rapid than in *elav>HTT93Q* flies, then one should expect not only an increase of ATG8-II, but also a decrease of ATG8-I, and this difference will be emphasised by a higher ratio.

A one-way ANOVA of the average signal intensities of ATG8-II/ATG8-I revealed no significant difference for any of the samples analysed (one-way ANOVA,  $F_{(4,10)}=0.4555$ ,  $p=0.7667$ , Figure 5-2). These data seem to suggest that the autophagic activity is not enhanced in HD flies overexpressing dRAB8, or at least, that this assay is not suitable for detecting changes in the autophagic levels.

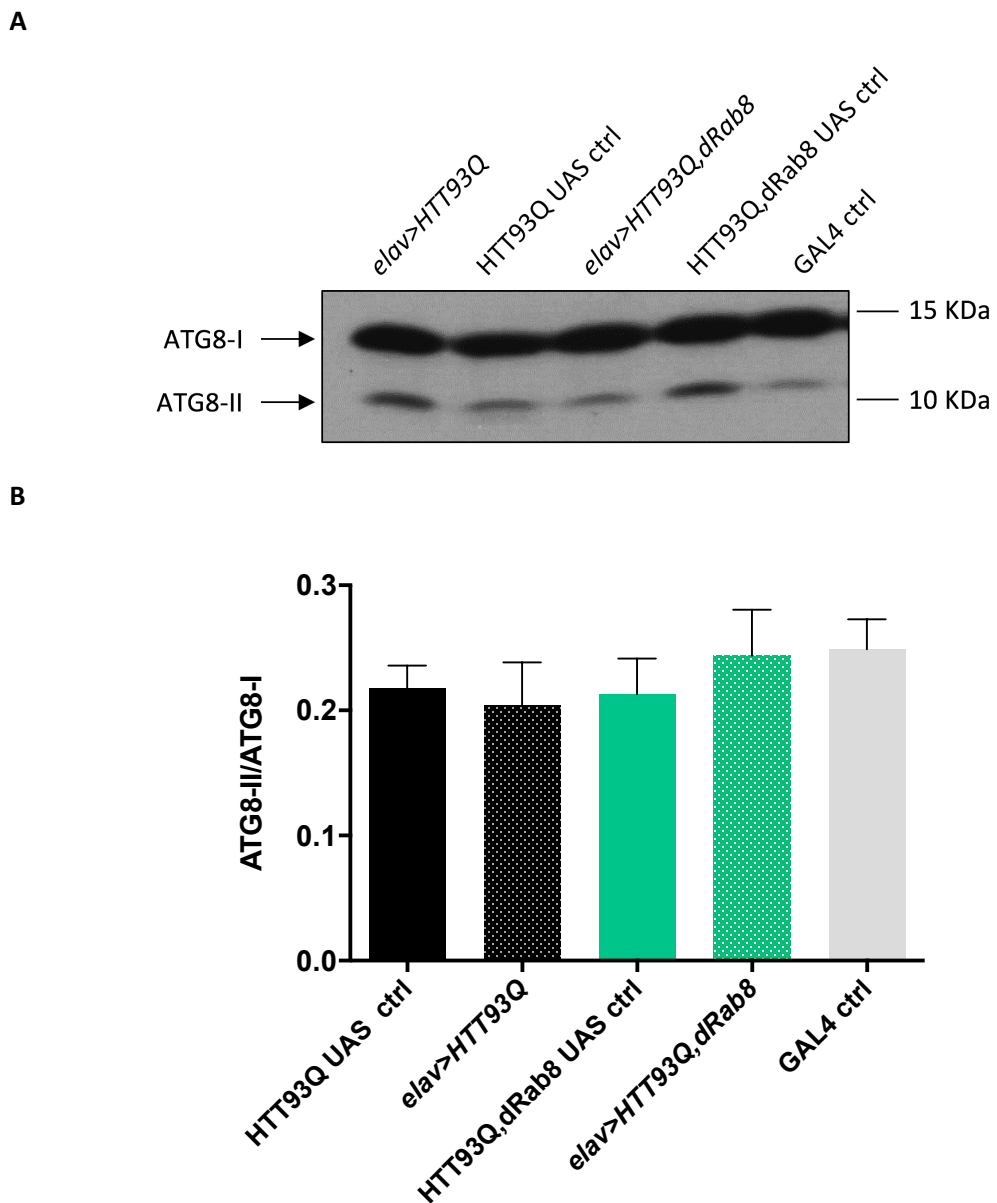


Figure 5-2 Autophagic levels of ATG8-II in HD flies are not enhanced by dRAB8 overexpression.

**A** Representative immunoblot of head fly extracts from *elav>HTT93Q*, *elav>HTT93Q,dRab8* and their controls (HTT93Q UAS ctrl, HTT93Q,dRab8 UAS ctrl and GAL4 ctrl), showing the two forms of endogenous ATG8: the cytosolic form, *i.e.* ATG8-I (15 KDa) and its cleaved, PE-lipidated and autophagosome associated form, *i.e.* ATG8-II (12 KDa). Primary antibody:  $\alpha$ -ATG8 1:3000 (Dr Koehle, Table 3). Secondary antibody:  $\alpha$ -rabbit HRP 1:10000 (Vector, Table 3). **B** Quantification of ATG8 expression levels. The data shown are the ratio between ATG8-II and ATG8-I, and are presented as mean  $\pm$ SEM of three experiments. One-way ANOVA,  $F_{(4,10)}=0.4555$ ,  $p=0.7667$ , ns.

### 5.3.2 dRAB8 likely promotes mHTT aggregation

To further clarify the mechanism(s) of dRAB8 rescue of HD phenotypes in flies, filter retardation assays were employed. Protein extracts from *elav>HTT93Q* flies, *elav>HTT93Q,dRab8* flies and their UAS controls (HTT93Q UAS ctrl and HTT93Q,dRab8 UAS ctrl respectively) were vacuum blotted on a cellulose acetate membrane of pore size 0.45 µm, which was subsequently probed with an  $\alpha$ -HTT antibody (Table 2-3). While all proteins, including soluble mHTT, pass through the pores of the membrane, large aggregates are retained on the membrane due to their insolubility in SDS and large size. With this assay, it is possible to evaluate the relative degradation of mHTT aggregates; if dRAB8 overexpression causes more efficient cellular degradation of mHTT aggregates, the amount of aggregated mHTT bound to the membrane should decrease. Conversely, if, as suggested in the previous section, basal autophagy is not upregulated by dRAB8 overexpression, then one should expect a comparable signal between *elav>HTT93Q* and *elav>HTT93Q,dRab8* flies.

Figure 5-3 shows that the average levels of mHTT aggregates were enhanced in flies overexpressing dRAB8. A weak but discernible background signal was observed also in the negative controls (HTT93Q UAS ctrl and HTT93Q,dRab8 UAS ctrl, Figure 5-3.A). The  $\alpha$ -HTT positive spots were quantified and normalized to levels detected for *elav>HTT93Q*. The levels of aggregated mHTT were on average ~1.5 fold higher in flies overexpressing dRAB8 (Figure 5-3.B). A one sample t-test on the relative abundance of  $\alpha$ -HTT signal revealed a significant difference between the two genotypes (one sample t-test  $t=6.907$ ,  $df=2$ ,  $p=0.0203$ , Figure 5-3.B), confirming that dRAB8 rescue is autophagy-independent and also suggesting that dRAB8 may actually promote mHTT aggregation.

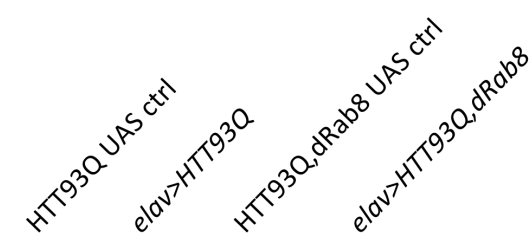
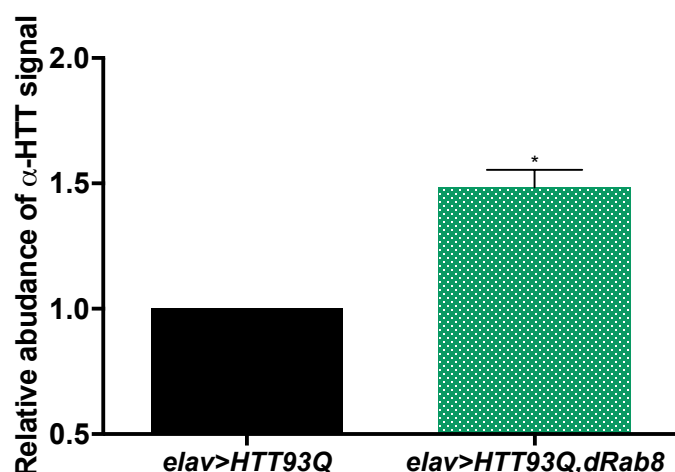
**A****B**

Figure 5-3 Filter-blot reveals that overexpression of dRAB8 enhances levels of aggregate form of mHTT.

**A** Representative cellulose acetate blot of head fly extracts from *elav>HTT93Q*, *elav>HTT93Q,dRab8* and controls (HTT93Q UAS ctrl and HTT93Q,dRab8 UAS ctrl). Primary antibody:  $\alpha$ -HTT 1:2000 (Millipore, Table 2-3). Secondary antibody:  $\alpha$ -mouse HRP 1:10000 (Vector, Table 2-3). **B** Quantification of aggregate mHTT expression levels. The data shows mHTT levels normalized to those of *elav>HTT93Q* flies, and are presented as mean  $\pm$ SEM of three experiments. One-sample t-test,  $t=6.907$ ,  $df=2$ ,  $p=0.0203$ .

### 5.3.3 dRAB8 likely promotes the formation of larger mHTT aggregates

To further validate dRAB8 aggregation data, I have optimized the AGERA technique for fly extracts. Protein extracts from *elav>HTT93Q*, *elav>HTT93Q,dRab8* and respective UAS controls (HTT93Q UAS ctrl and HTT93Q,dRab8 UAS ctrl) were run in agarose gel using non-reducing conditions and the proteins were then transferred onto a nitrocellulose membrane. Due to the nature of AGERA, mHTT aggregates are separated according to their size, allowing the detection of heterogeneous mHTT aggregate species (Figure 5-4.A).

Consistent with the filter retardation assay, quantification of the  $\alpha$ -HTT signal revealed a ~1.5 fold-increase of mHTT aggregates in flies overexpressing dRAB8 (Figure 5-4.B) and a one-sample t-test confirmed that this difference was significant (one sample t-test,  $t=4.395$ ,  $df=2$ ,  $p=0.0481$ , Figure 5-4.B).

Comparison of the  $\alpha$ -HTT signal smears, revealed mHTT species of higher sizes in *elav>HTT93Q,dRab8* (Figure 5-4.A, red arrows), which were not present in *elav>HTT93Q* flies. All together, these observations strongly suggest that dRAB8 is able to modulate mHTT aggregation, not only by increasing the levels, but also by increasing the size of mHTT aggregates.

**A**

HTT93Q UAS ctrl  
*elav>HTT93Q*  
HTT93Q,*dRab8* UAS ctrl  
*elav>HTT93Q,dRab8*

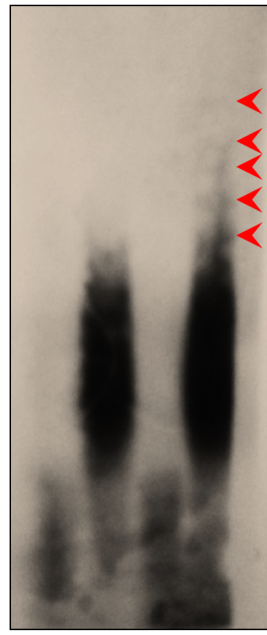
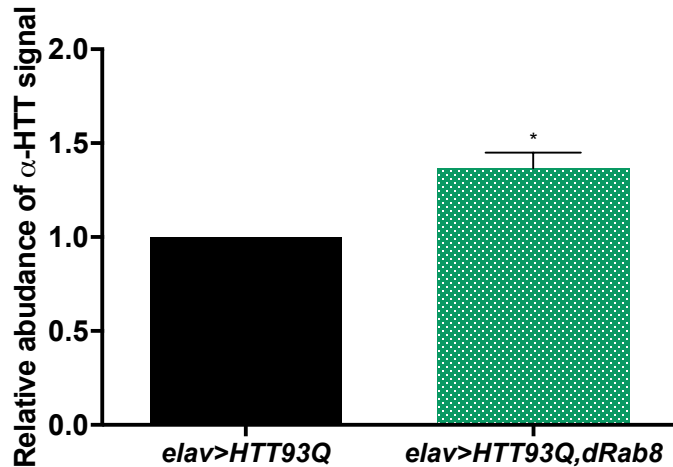
**B**

Figure 5-4 AGERA reveals that overexpression of dRAB8 enhances levels of aggregate form of mHTT .

**A** Representative cellulose acetate blot of head fly extracts from *elav>HTT93Q*, *elav>HTT93Q,dRab8* and controls (HTT93Q UAS ctrl and HTT93Q,dRab8 UAS ctrl). Red arrows in *elav>HTT93Q,dRab8* sample indicate the presence of bigger mHTT species, that were not found in the *elav>HTT93Q* sample. Primary antibody: α-HTT 1:2000 (Millipore, Table 2-3). Secondary antibody: α-mouse HRP 1:10000 (Vector, Table 2-3). **B** Quantification of aggregate mHTT expression levels. The data shows mHTT levels normalized to those of *elav>HTT93Q* flies, and are presented as mean of three experiments. One-sample t-test,  $t=4.395$ ,  $df=2$ ,  $p=0.0481$ .

### 5.3.4 Co-Immunoprecipitation in flies revealed no interaction between soluble mHTT and RAB8

Could it be that the dRAB8/mHTT interaction observed in cells (Chapter 4) underlies the mechanism by which dRAB8 increases the number of mHTT aggregates observed *via* filter retardation assay and AGERA? I explored this possibility by investigating a putative interaction between dRAB8 and soluble mHTT by co-immunoprecipitation (Co-IP) in flies.

Proteins were extracted from *elav>HTT93Q,dRab8* flies and YFP-tagged dRAB8 was pulled down with GFP-trap®, as described in Section 5.2.4. The HTT93Q,dRab8 UAS ctrl was used as a negative control, whereas flies expressing HTT93Q but not dRAB8 (*elav>HTT93Q*) were used to assess dRAB8 beads specificity.

Immunoblots of the total protein fraction (input) revealed a band at 46 KDa in *elav> HTT93Q,dRab8* flies, corresponding to the overexpressed YFP-dRAB8 (Figure 5-5). A very low α-Rab8 signal was detected in the flow-through fraction (FT), however the majority of dRAB8 signal was revealed in the immunoprecipitated fraction (IP), confirming the success of dRAB8 pull-down. HTT93Q was present only in the input fraction of *elav>HTT93Q,dRab8* and of *elav>HTT93Q* flies, but not in the IP fraction (Figure 5-5). These results suggest no interaction between the two proteins, or at least under these experimental conditions, which analyses proteins either that are in the soluble fraction or that are easily removed from the membrane.

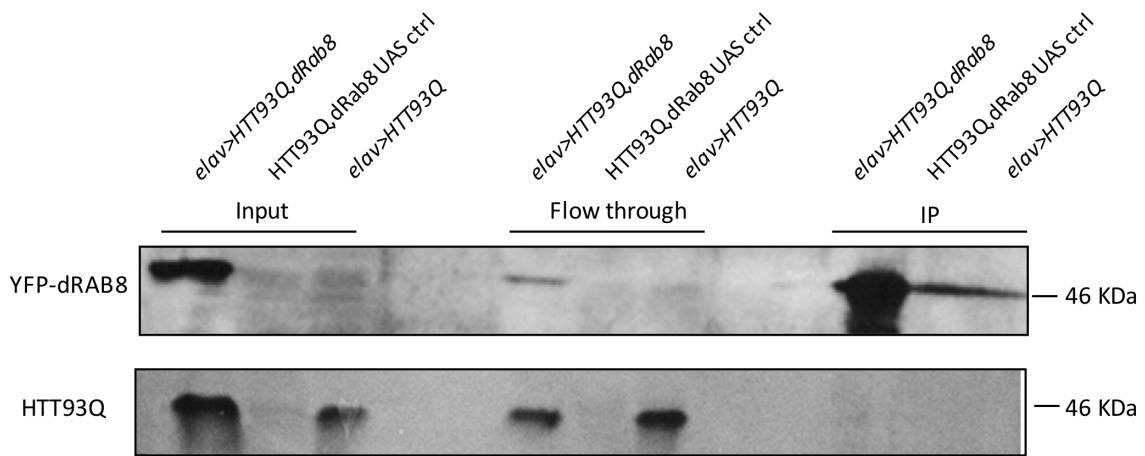


Figure 5-5 Co-IP in flies reveals no direct interaction between soluble HTT93Q and dRAB8.

Representative Co-IP immuno-blot. Total extracts from fly heads of *elav>HTT93Q,dRab8*, HTT93Q,dRab8 UAS ctrl, and *elav>HTT93Q*, which were immuno-precipitated using an  $\alpha$ -GFP antibody (GFP-trap $\circledast$ ). YFP-dRAB8 was revealed with  $\alpha$ -Rab8 antibody in the input fraction (top panel, input), in a small amount in the flow-through fraction (top panel, flow-through) and in the IP fraction (top panel, IP).  $\alpha$ -HTT antibody revealed successful expression of HTT93Q in *elav>HTT93Q,dRab8* (bottom panel, input), however it also revealed no interaction between dRAB8 and HTT93Q, as HTT93Q was found in the flow-through fraction (bottom panel, flow-through) but not in the IP fraction (bottom panel, IP). Total extracts from fly heads of HTT93Q,dRab8 UAS ctrl were used as UAS negative control.  $\alpha$ -Rab8 and  $\alpha$ -HTT antibodies confirmed neither YFP-dRAB8 nor HTT93 expression (top panel, input and bottom panel, input). Total extracts from fly heads of *elav>HTT93Q* confirmed beads specificity for dRAB8 as HTT93Q was revealed in the input fraction (bottom panel, input), in the flow-through fraction (bottom panel, flow-through), but not in the IP fraction (bottom panel, IP). This experiment was replicated 3 times. Primary antibodies:  $\alpha$ -Rab8 1:2500 (BD Bioscience, 1:2500, Table 2-3),  $\alpha$ -HTT 1:2000 (Millipore, Table 2-3). Secondary antibody:  $\alpha$ -mouse HRP 1:10000 (Vector, Table 2-3).

## 5.4 Discussion

Autophagy is the main cellular clearance pathway that protects the cells from misfolded proteins, aggregates and damaged organelles. Its contribution in HD has been highlighted by numerous studies, which have shown that higher levels of autophagy protect the cell from HD induced toxicity by reducing the amount of toxic aggregated mHTT (Martin *et al.*, 2015; Mizushima *et al.*, 2008; Ravikumar & Rubinsztein, 2004; Rubinsztein *et al.*, 2007). A great deal of evidence has highlighted a role for the involvement of Rab GTPases in the autophagic clearance of mHTT. Rab5 was the first GTPase discovered to mediate degradation of mHTT via autophagy-upregulation (Ravikumar *et al.*, 2008). The effects of Rab5 overexpression have been found to be protective in cells and flies HD models. Studies in our laboratories, moreover, have demonstrated that also rRAB2A, rRAB11B and rRAB27A have the ability to upregulate autophagy, ameliorating mHTT induced toxicity in cells (Mason & Giorgini, unpublished). In this chapter, I sought to investigate whether overexpression of dRAB8 triggers a similar protective mechanism that could explain the rescue observed in the flies (Chapter 3). Rab8 has been indeed implicated in two key steps of the autophagic pathway: Rab8b mediates the fusion of autophagosomes with lysosomes, thus forming autophagolysosomes; whereas Rab8a promotes the unconventional autophagy-based pathway, called also secretory way or exocytosis (Ao *et al.*, 2014; Bento *et al.*, 2013; Dupont *et al.*, 2011; Jiang *et al.*, 2013; Pilli *et al.*, 2012).

The data gathered so far suggest that overexpression of dRAB8 promotes the formation of mHTT aggregates and not their clearance *via* a mechanism involving upregulation of autophagy. The autophagosome marker ATG8-II was indeed not enhanced in flies overexpressing dRAB8, suggesting that, contrary to expectations, autophagy was not upregulated by dRAB8 overexpression.

This has been further confirmed by two independent biochemical assays, the filter retardation assay and the AGERA, whereby overexpression of dRAB8, consistently corresponded to a 1.5-fold increase in the amount of aggregated mHTT. Notably, while the filter-retardation assay allows a quantitative measure of the aggregates, it precludes any qualitative analysis as the threshold for detection is imposed by the membrane pore-size (0.45 µm). Conversely, because mHTT aggregates are electrophoretically resolved on an agarose gel and subsequently transferred onto a nitrocellulose membrane, the AGERA technique allows a quantitative and qualitative analysis of mHTT aggregates (Weiss *et al.*, 2008). The AGERA results indicated that *elav>HTT93Q,dRab8* flies displayed larger aggregates compared to *elav>HTT93Q* flies, indicating the ability of dRAB8 to promote mHTT aggregation, a mechanism that could underlie its ability to rescue HD phenotypes.

In the aggregation process, mHTT undergoes conformational changes producing different species of mHTT: monomer, soluble oligomers and insoluble inclusion bodies (IBs) (Cattaneo *et al.*, 2005 and see Section 1.1.5.1). To date it is not clear what species of mHTT are toxic, however protein aggregation leading to IBs formation has been suggested as a mechanism to detoxify the cytotoxic intermediate mHTT species (Arrasate & Finkbeiner, 2012). Contrary to initial models, numerous studies have found no correlation between IBs and cellular death (Arrasate *et al.*, 2004; Arrasate & Finkbeiner, 2012), whereas strategies promoting the formation of IBs have shown potential benefit in HD models. One example is B2, a drug, which, by boosting the formation of large IBs has been found to have beneficial properties against HD and PD (Parkinson's disease) phenotypes in PC12 model cells (Bodner *et al.*, 2006).

How dRAB8 promotes aggregation is yet to be determined, however, I speculate it could be *via* a positive feedback mechanism following the first interaction with the aggregates. The BiFC data in Chapter 4 do not contradict this view: dRAB8 interacted more strongly with mHTT rather than wtHTT, and the brightest signal was associated with IBs (Figure 4-16). This increased interaction could reflect a protective cellular mechanism to cope with polyQ toxicity (induction of aggregates) rather than sequestration into IBs as discussed in the previous chapter.

The aggregation process could be triggered by dRAB8 interacting with soluble, yet not aggregated mHTT. Alternatively, dRAB8 could interact with mHTT aggregates promoting their aggregation even further. To distinguish between these two possibilities, I performed a Co-IP on flies overexpressing dRAB8. Large mHTT aggregates are insoluble in SDS, and do not enter the SDS-PAGE stacking gel. This allows one to investigate specifically the interaction between dRAB8 and soluble mHTT. Co-IP analysis revealed that dRAB8 does not interact with soluble mHTT, suggesting that the dRAB8/mHTT interaction involves exclusively with aggregates. To conclude this set of experiments, it would have been interesting to probe the filter-retardation membranes with an  $\alpha$ -Rab8 antibody, unfortunately I encountered technical difficulties that prevented me from addressing this question.

In the literature, there are additional examples of proteins with higher affinity for mHTT aggregates than wtHTT (Davranche *et al.*, 2011). Once bound to the aggregates, these proteins can promote post-translational modifications interfering with the formation of aggregates. For example, in a study published by Subramaniam *et al.* (2009), the small guanine nucleotide-binding protein Rhes has been reported to have a higher affinity for mHTT compared to wtHTT, in conditionally immortalized mHTT knock-in striatal neuronal cells ( $STHdh^{Q111/Q111}$ ), in HD transgenic mice and *in vitro*. Contrary to what I observed for dRAB8, Rhes has an anti-aggregation effect, which, increased neurotoxicity in several cell lines, including HD model

HEK293 cells, mHTT knock-in striatal cells ( $STHdh^{Q111/Q111}$ ), and HD model PC12 cells. Rab8, which is also a G protein, could have a similar propensity for binding to aggregates, but causing aggregation of mHTT instead (Seredenina *et al.*, 2011; Subramaniam *et al.*, 2009). Rab8 could act like GAPDH (glyceraldehyde-3-phosphate dehydrogenase) which has been shown to have increased affinity for mHTT aggregates, promoting aggregation even further (Lazarev *et al.*, 2015). If that was true, GCK (Germinal Center Kinase), also known as MAP4K2 (Mitogen-activated protein kinase kinase kinase 2), is an attractive candidate to bridge the gap between dRAB8 overexpression and IBs formation. Rab8 interacts with and might regulate activation of GCK, a serine/threonine-protein kinase that acts as an essential component of the MAP (Mitogen-activated protein) signal transduction pathway (Chuang *et al.*, 2016; Kyriakis, 1999; Ren *et al.*, 1996). GCK is an upstream regulator of MEKK1 (MAP/extracellular signal-regulated protein kinase (ERK) kinase kinase 1), a kinase that has been shown to stimulate the formation of IBs in HD models of HeLa, HEK293 and rat hippocampal neuronal cells (Meriin *et al.*, 2001). Interestingly, the authors have demonstrated that MEKK1 co-localises with IBs, but it is not associated with soluble mHTT, this is similar to what I found for dRAB8 (Meriin *et al.*, 2001). More importantly, the authors have shown that MEKK1 promotes an early nucleation step that triggers the formation of IBs (Meriin *et al.*, 2001).

Given this, I believe that is possible that overexpression of dRAB8 could activate GCK leading to a cascade of events that involves activation of MEKK1, ultimately triggering nucleation of mHTT aggregates and IBs formation. The novel possibility that dRAB8 could enhance mHTT aggregation by modulating MEKK1 activity and the downstream MAPK signalling pathway that catalyses nucleation of polyQ aggregates, would be in line with the BiFC and Co-IP results, as well as with the filter-retardation assay and the AGERA data. In addition, as IBs have been found to be protective in HD, this hypothesis could explain the rescue of the relevant HD phenotypes observed in Chapter 3. Unfortunately, due to time constraints, I was not able to pursue this hypothesis further.

In conclusion, these results seem to provide evidences for dRAB8 stimulating induction of mHTT aggregation that could underlie a novel mechanism of HD protection within the Rab GTPase family.

# Chapter 6

## Investigating neuronal dysfunction in PDF-expressing cells of *Drosophila melanogaster*

### 6.1 Introduction

Following the initial characterization of dRAB8 using a pan-neuronal driver (*elav-GAL4*), the data presented in this chapter sought to explore dRAB8 function in a subset of clock cells: the PDF<sup>+</sup> neurons, *i.e.* s-LNvs (small-lateral ventral neurons) and l-LNvs (large-lateral ventral neurons). The s-LNvs are considered key pacemaker neurons controlling self-sustained rhythms – rhythms that are sustained even in the absence of external stimuli – whereas the l-LNvs are involved in sleep and arousals (Sheeba *et al.*, 2008; Nitabach *et al.*, 2006; Grima *et al.*, 2004). Manifestation of circadian rhythms requires precise coordination of molecular components within cells and synchronisation among cells, hence it provides an exquisite and sensitive model to look at the relationship between neuronal dysfunction and behaviour. Thus, expression of mHTT leading to deterioration of neuronal function, should impact on the daily cycle of locomotor activity, for instance on the ability of self-sustain rhythmicity.

#### 6.1.1 *Drosophila* circadian rhythms

Daily rhythms of physiology and behaviour are controlled by an endogenous circadian oscillator (pacemaker). This system likely evolved as an adaptation to the daily environmental cycles driven by the 24 hours rotation of the Earth around its axis. The clock is able to perceive and to anticipate environmental changes and to act accordingly as the organism's timekeeper. Circadian clocks of different organisms share similar properties. For instance, they are entrained by external cycling stimuli (*Zeitgebers*, or time givers) such as light, which is undoubtedly the most relevant environmental cue. Moreover, they are self-sustained, meaning they are able to maintain rhythmicity even in the absence of external cues (free-running conditions), and are temperature-compensated, as their period is independent from the temperature at which they operate (within physiological limits) (Aschoff & Pohl, 1978).

During the last 40 years the mechanisms that regulate cycling behaviours have been intensely investigated and the molecular basis of the circadian rhythms have found wide acceptance in the so-called Transcriptional Translational feedback Loop (TTL) model (Figure 6-1), which is based upon two negative interlocked transcription/translation feedback loops (reviewed in Ozkaya & Rosato, 2012). According to the model, the heterodimer CLOCK (CLK)-CYCLE (CYC) activates the transcription of several clock genes: *period* (*per*) and *timeless* (*tim*),

which constitute the first loop, and *vri* (vri) and *Par domain Protein 1ε* (*Pdp1ε*), which form the second one. *per* and *tim* are rhythmically expressed, peaking in the evening, between *Zeitgeber* times (ZT) 13-16 (being ZT 0 the time when lights are on, e.g. 8 am). Transcripts are translocated to the cytoplasm, where their translation takes place. Here, different post-transcriptional modifications, mediated by several kinases such as DOUBLETIME (DBT), SHAGGY (SGG), and CASEIN KINASE II (CKII), and phosphatases such as Protein Phosphatase 1 (PP1) and Protein Phosphatase 2A (PP2A), affect TIM and PER stability inhibiting their accumulation for about 6 hours. It is only in the middle of the night that PER and TIM enter the nucleus where they repress the CLK-CYC complex thereby inhibiting their own transcription. A second loop ensures the rhythmic expression of *Clk* and *cry* (*cryptochrome*), a flavo-protein that is the main circadian photoreceptor. Early in the evening, *vri* and *Pdp1ε* are expressed by CLK-CYC. VRI quickly accumulates, dimerises and binds to the promoter sequences of *Clk* and *cry*, thereafter inhibiting their transcription. Late at night PDP1ε accumulates and out-competes VRI and promotes the transcription of *Clk* and *cry*, which peak at ZT 1-7. At the beginning of the day, light activates CRY that in turn binds to TIM. The interaction between the two proteins induces post-transcriptional modifications that ultimately lead to TIM (and consequently PER) degradation, resetting the clock (Figure 6-1).

These TTL generate and sustain the rhythmicity of the clock. Many cells express clock genes in the body and the head. However, only ~150 neurons within the brain are crucial determinants for circadian rhythmicity. They are classified in six main clusters reflecting their anatomical position in the brain (Figure 6-1). There are three groups of dorsal neurons (DNs) and three groups of lateral neurons (LNs). The former is further subdivided in DN1s (16 cells), DN2s (2 cells) and DN3s (40 cells). The lateral neurons are separated in posterior (LPN, 3 cells), dorsal (LNdS, 6 cells) and ventral (LNvs), which in turn differentiate into large (l-LNvs, 4-6 cells), small (s-LNvs, 4 cells) and the 5<sup>th</sup> small (Sandrelli *et al.*, 2008; Helfrich-Förster *et al.*, 1998 and Figure 6-2).

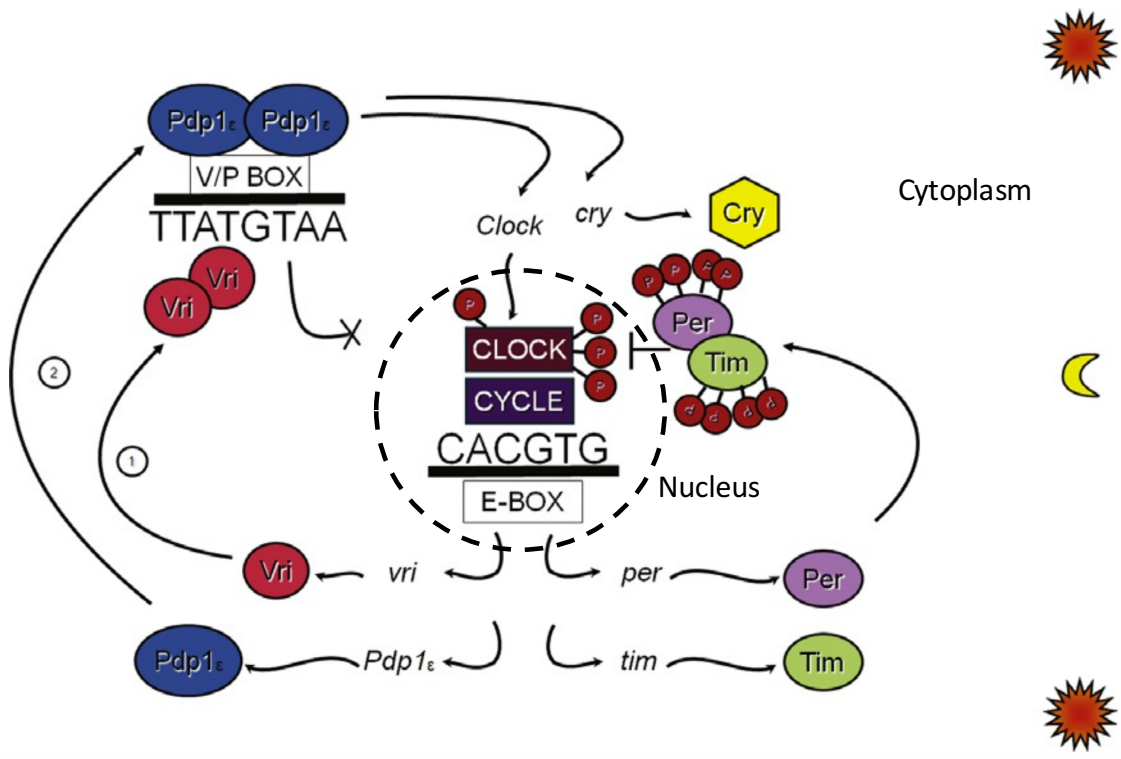


Figure 6-1 Transcriptional/Translational feedback Loops.

Schematic representation of the two interlocked negative feedback loops that regulate the molecular circadian clock in *Drosophila*. On the right the “classical” negative feedback loop is depicted. *per* and *tim* transcription is promoted by the CLK/CYC heterodimer binding to the E-BOX promoter sequence (CACGTG, enhancer box). PER and TIM proteins accumulate in the cytoplasm later during the night where they undergo posttranslational modifications, such as phosphorylation. Phosphorylated PER/TIM dimers, can therefore re-enter the nucleus, where they inhibit their own transcription. During the day, light activated CRY promotes TIM degradation. On the left the second loop is shown. CLK-CYC heterodimers trigger the transcription of VRI and PDP1 $\epsilon$ . During the day, VRI accumulates more quickly than PDP1 $\epsilon$  and it can therefore inhibit CLK and CRY transcription (1), by binding to the V/P BOX promoter sequence (TTATGTAA). 4 h later, PDP1 $\epsilon$  accumulates in the cytoplasm and by inhibiting VRI activity, it promotes CLK and CRY transcription (2). The whole cycle takes roughly 24 h. Image taken modified Ozkaya & Rosato (2012).

### 6.1.2 Pigment dispersing factors (PDF) neurons and their properties

Pigment dispersing factors (PDFs) are neuropeptides named for their ability to cause retinal screening pigment dispersion, when assayed on the optic stalk of *Uca pugilator* (Rao & Riehm, 1989). This resembles the function of the crustacean's Pigment dispersing hormones (PDHs) family (Rao & Riehm, 1989). Staining against  $\beta$ -PDH in *Drosophila* identified different PDH-immunoreactive neuron clusters in the brain and in the body, observed in larval, prepupal, pupal and adult stages and this allowed the determination of the distribution of *Drosophila*'s PDF expressing neurons (Helfrich-Förster, 1998; Renn *et al.*, 1999).

The first cluster of PDF expressing neurons is represented by four s-LNvs. These neurons develop in the medulla region, close to larval optic neuropil of the first instar larva, and persist in the pupal and adult stages in the lateral protocerebrum close to the accessory medulla. Throughout pupal development two other clusters of PDF expressing neurons mature: four to five l-LNvs in the lateral protocerebrum, which maintain their structural characteristics also in adults, and two to four PDFTri (tritocerebrum) neurons, in the anterior-ventral tritocerebrum, which undergo apoptosis within four days after eclosion.

While the function of PDFTri neurons is poorly understood, LNvs are important mediators of complex behaviours such as the circadian locomotor activity rhythm. As shown by Renn and co-workers (1999), *Pdf* null mutants (*Pdf*<sup>01</sup>) become rapidly arrhythmic in free-running conditions, with the few rhythmic flies displaying a shorter period compared to controls, while in LD conditions mutant flies lose the morning peak and show earlier anticipation of the lights off event. Interestingly, a similar result was observed by the genetic ablation of the LNvs (Renn *et al.*, 1999) and by electrically silencing the LNvs (Nitabach *et al.*, 2002). Subsequent analyses on PER localisation showed that the arrhythmic behaviour of *Pdf*<sup>01</sup> flies was not due to a lack of molecular oscillations within individual clock neurons but rather to an internal desynchronization among oscillators. This confirmed a role for PDF as a main circadian neurotransmitter required to coordinate and maintain synchronization among different oscillators (Lin *et al.*, 2004). Moreover, electrical hyperexcitation of the LNvs following the expression of NaChBac, a voltage-gated sodium channel, resulted in complex free-running rhythms showing multiple components (Nitabach *et al.*, 2006) and a phase shift in the oscillation of clock proteins in the DN1 and DN2 clusters. These results support the idea that a normal electrical activity of the PDF cells is required for achieving synchronization of multiple oscillators within the clock. Taken together these observations reveal a hierarchical structure for the circadian clock. The LNvs (the s-LNvs in particular) act as the main pacemaker that resets the dorsal oscillators daily *via*

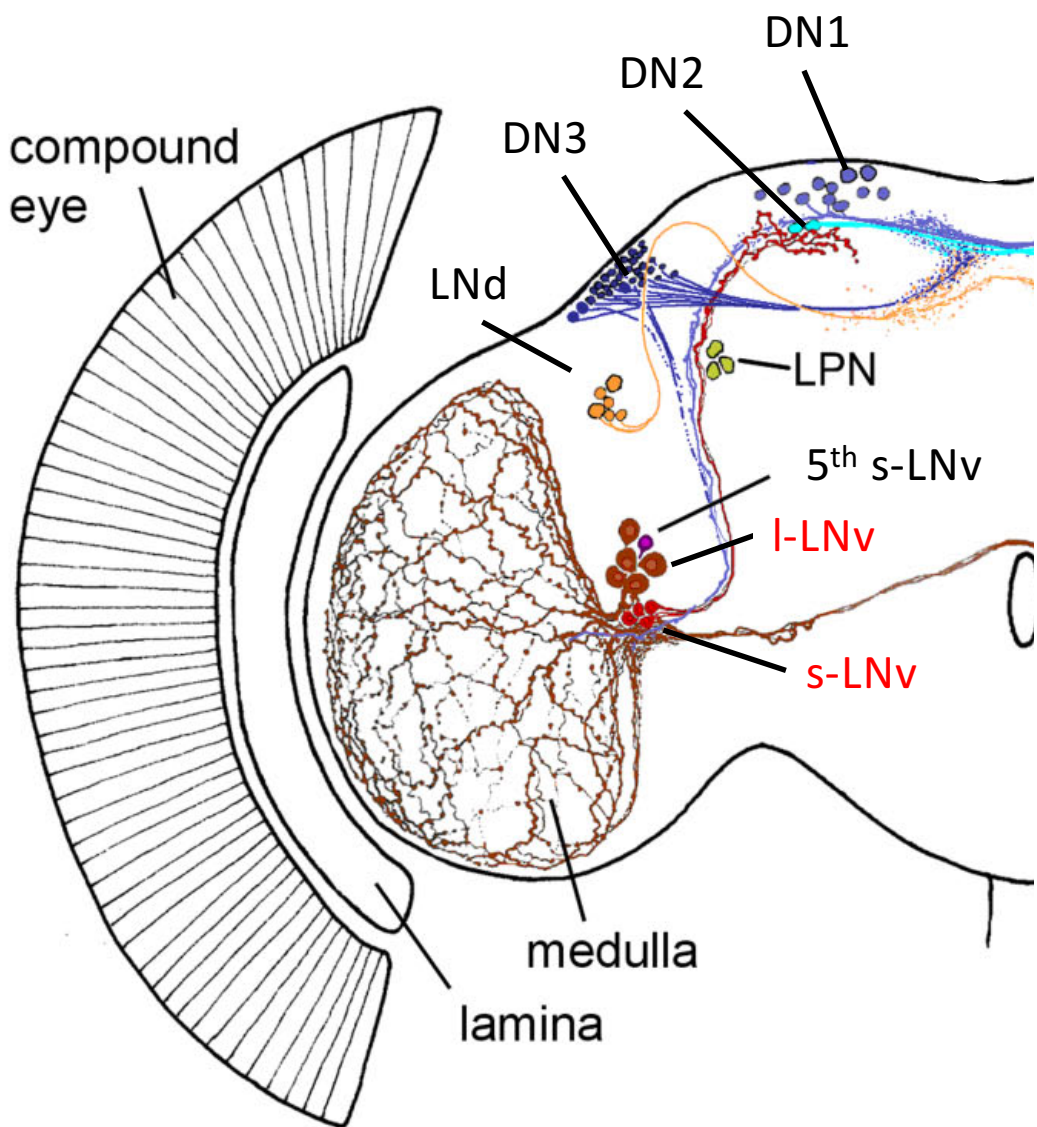


Figure 6-2 Schematic representation of *Drosophila*'s neuronal pacemaker.

Schematic representation of the left hemisphere of *Drosophila*'s brain with the main circadian clock neuronal clusters and their projection depicted. PDF neurons (s- and I-LNvs) are annotated in red. The compound eye, the lamina (peripheral optic neuropil) and the medulla (second optic neuropil) are shown. Image modified from Helfrich-Förster *et al.* (2007).

PDF expression, even in the absence of external stimuli, therefore acting as a cellular *Zeitgeber* (Stoleru *et al.*, 2005) in accordance to the dual oscillator model proposed by (Pittendrigh & Daan, 1976).

#### 6.1.3 Dual oscillator model and clock cells communication

The “classical dual oscillator model” proposed by Pittendrigh & Daan in 1976 posits that the clock is hierarchically structured as cell-autonomous neuronal clusters with two main neuronal clusters. More recently, the dual oscillator has been generally accepted by fly chronobiologists (Allada & Chung, 2010), who are investigating whether such dual organisation could be seen also in *Drosophila*. In this view the PDF positive ( $\text{PDF}^+$ ) cells control the morning peak of activity and the remaining more dorsal PDF negative ( $\text{PDF}^-$ ) neurons control the evening peak (evening cells). Based on the current model the  $\text{PDF}^+$  cells (s-LNvs in particular) are the clock’s main pacemaker being able to daily re-set the rhythm of the  $\text{PDF}^-$  neurons *via* PDF expression (Stoleru *et al.*, 2005). This model, however, has been recently challenged by Yao and Shafer (2014) and Dissel and colleagues (2014), who introduced the concept of network plasticity and described the clock as multiple integrated oscillators. Among the  $\text{PDF}^-$  cells only half of them express PDF Receptor (PDFR), suggesting that the activity of the morning cells can only influence a small proportion of evening cells. By altering the period of  $\text{PDF}^+$  cells expressing a variant of the *DBT* gene with reduced kinase activity, *DBT<sup>L</sup>*, and therefore altering PDF expression, Yao and Shafer demonstrated that a cluster of evening cells (5<sup>th</sup> s-LNV and the LNdS) are actually formed by three independent oscillators differently coupled to PDF-expression. Moreover, Dissel and co-workers have showed, by genetically manipulating individual neuronal clusters, that endogenous rhythmicity of wild-type flies is the result of the interplay of all clock neurons and not the dominant effect of a single group (Dissel *et al.*, 2014). Therefore, the circadian clock appears to consist of multiple oscillators coupled together *via* activation/inhibition interactions rather than a single cluster of pacemaker neurons (Dissel *et al.*, 2014).

#### 6.1.4 Locomotor activity in *Drosophila*

There are several approaches for monitoring circadian rhythms in flies. For example, eclosion, courtship, feeding, sleeping and egg deposition are timed by the endogenous clock (Allada & Chung, 2010; Tataroglu & Emery, 2014). However, the monitoring of locomotor activity is probably the most widely used system to examine daily behaviours of fruit flies (Schlichting & Helfrich-Förster, 2015; Allada & Chung, 2010). In standard 12:12 h light:darkness (LD) laboratory conditions, *Drosophila* displays two bouts of activity during the day, the first before the lights are ON and the second in the late afternoon, before the lights are switched OFF (Collins *et al.*, 2005; Vanin *et al.*, 2012; Helfrich-Förster, 2001). These are called morning

and evening peaks respectively (Figure 6-3). However, these peaks are preceded by increased locomotor activity, called morning and evening anticipation, respectively (Helfrich-Förster, 2001; Stoleru *et al.*, 2004; Allada & Chung, 2010). During the day and night, flies tend to reduce their activity and remain in sleep-like states (Tataroglu & Emery, 2014; Allada & Chung, 2010). The activity profile is often represented as an actogram, as shown in Figure 6-3. The highly automated *Drosophila* activity monitor (DAM) system (see below) permits measurement of fly locomotor activity continuously for several days (Schlichting & Helfrich-Förster, 2015; Zordan *et al.*, 2007), a feature particularly convenient when monitoring the effects of neurodegeneration. Here, I monitored adult locomotor activity over a time window of 3 weeks to evaluate neuronal damage triggered by mHTT on the PDF neurons. In particular, I analysed the ability of HD flies to self-sustained rhythmicity in absence of light (DD conditions). I also conducted preliminary immunofluorescence (IF) experiments on brains, to correlate behavioural changes with the physiological state of the neurons.

Results are consistent with the notion that dRAB8 is a modifier for HD-induced phenotypes and provide support to the emerging concept of a non-autonomous clock organization (Dissel *et al.*, 2014). Moreover, the data presented here seem in line with the hypothesis that dRAB8 modulates mHTT aggregation.

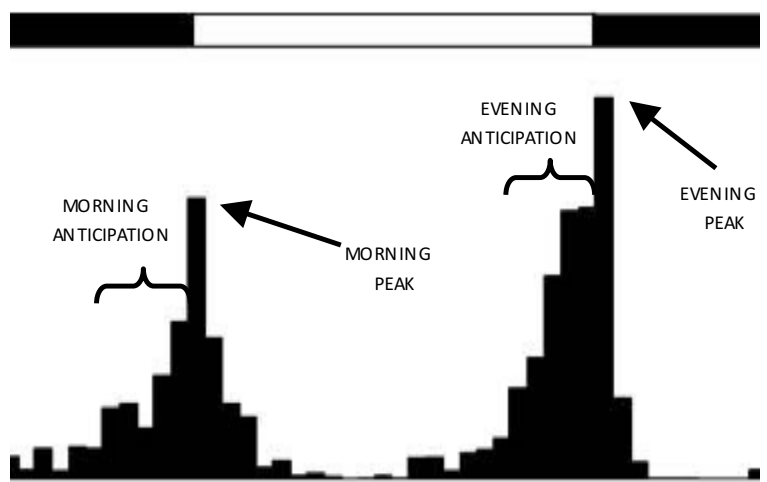


Figure 6-3 Representative actogram of a wild-type fly.

The locomotor activity is presented as actogram, where each histogram shows the average activity collapsed in 30 min bin. Black and white bars on top of each actogram represent the subjective night (black) and the subjective day (white). X axis=time (h), Y axis=activity.

## 6.2 Materials and methods

### 6.2.1 *Drosophila* crosses

Expression of the transgenes in the s- and l-LNvs was achieved by crossing UAS males (Table 2-5) with *Pdf-GAL4* females (Table 2-4), whereas UAS and GAL4 control crosses were generated by crossing UAS males (Table 2-5) with *w<sup>1118</sup>* females or *w<sup>1118</sup>* males with *Pdf-GAL4* females (Table 2-4) respectively as shown in Table 6-1. Crosses were set up on maize food and kept at 25°C.

Table 6-1 Parental crosses and F1 progeny tested.

For the list of parental genotypes, refer to Table 2-4 and Table 2-5.

Parental crosses	F1 progeny tested
	<b><i>Pdf&gt;UAS</i></b>
♀ <i>Pdf-GAL4</i> x ♂ <i>UAS-HTT93Q</i>	♂ <i>Pdf&gt;HTT93Q</i>
♀ <i>Pdf-GAL4</i> x ♂ <i>UAS-HTT93Q, UAS-dRab8</i>	♂ <i>Pdf&gt;HTT93Q, dRab8</i>
♀ <i>Pdf-GAL4</i> x ♂ <i>UAS-dRab8</i>	♂ <i>Pdf&gt;dRab8</i>
	<b>UAS ctrl</b>
♀ <i>w<sup>1118</sup></i> x ♂ <i>UAS-HTT93Q</i>	♂ HTT93Q UAS ctrl
♀ <i>w<sup>1118</sup></i> x ♂ <i>UAS-HTT93Q, UAS-dRab8</i>	♂ HTT93Q, dRab8 UAS ctrl
♀ <i>w<sup>1118</sup></i> x ♂ <i>UAS-dRab8</i>	♂ dRab8 UAS ctrl
	<b>GAL4 ctrl</b>
♀ <i>Pdf-GAL4</i> x ♂ <i>w<sup>1118</sup></i>	♂ GAL4 ctrl

### 6.2.2 Behavioural assays

All the activity experiments were performed at 25°C, using the TriKinetics® *Drosophila* Activity Monitoring System (TriKinetics). Newly eclosed males were individually placed in activity tubes (5 mm x 80 mm Pyrex glass) provided with sugar food (46 gr/L sucrose, 46 gr/L yeast, 10 gr/L agar, 2 gr/L nipagine) at one end (sealed with a plastic cap to avoid desiccation) and cotton bung at the other. Each tube was placed in the monitoring apparatus (32 tubes/monitor), consisting of an infrared emitter and detector able to sense the movement of the fly within a 5 min time bin. Flies were entrained in LD (12 h light:12 h dark) for 3 days and then tested in DD (constant darkness) conditions for 3 weeks.

### 6.2.3 Behavioural analysis

The TriKinetics monitor data were collected using DAM System 2.1.3 software (TriKinetics). For each week, results were analysed by running the autocorrelation and CLEAN spectral analyses, using the MAZ software (Zordan *et al.*, 2007). Flies were considered rhythmic when autocorrelation and spectral analyses were significant; only periods showing a peak above 99% confidence limit in spectral and autocorrelation analyses were considered rhythmic. Flies showing multiple peaks, or none peak above the 99% confidence limit were considered ar-

rhythmic, flies showing exactly 2 rhythms above the 99% confidence limit were considered having complex rhythms. The robustness of the peaks was calculated by mean of the CLEAN spectral analysis. The average raw locomotor was collapsed in 30 min activity bins and displayed as double-plotted actograms (48 h plots).

#### 6.2.4 Immunofluorescence and confocal microscopy

10-15 flies per genotype were fixed for 2 hours at RT (room temperature) in a 4% filtered PFA-PBS (paraformaldehyde-phosphate buffer solution) with 0.1% triton-X100. Flies were subsequently washed 3 times for 15 min in PBST (PBS with 0.1% triton-X100) and the brain dissection was performed in ice cold PBS. Brains were washed 3 times for 15 min in PBST prior to blocking in blocking solution (PBS with 0.5% triton-X100 and 10% goat serum) O/N at 4°C. Fly brains were then incubated for 3 days at 4°C either with  $\alpha$ -HTT, with  $\alpha$ -PDF or with  $\alpha$ -PDF and  $\alpha$ -HTT primary antibodies (see Table 2-3) diluted in blocking solution, washed 3 times for 15 min in PBST and finally incubated 2 hours at RT with the secondary antibodies (Cy2  $\alpha$ -mouse and Cy5  $\alpha$ -rabbit, Table 2-3) diluted in blocking solution. Brains were washed 3 times for 15 min in PBST, mounted onto glass slides in a solution of 80% glycerol and 3% n-propylgallate in PBS and left O/N at 4°C. Slides were visualised using a laser scanning confocal microscope Olympus FV1000 and images were processed with the FV-10 ASW 2.0 viewer program (Olympus), maintaining the same settings for pictures taken within the same week. The number of  $\alpha$ -PDF positive neurons was counted and averaged considering each hemisphere as an independent sample. Similarly, the number of  $\alpha$ -HTT inclusions in PDF<sup>+</sup> neurons were averaged for all the PDF<sup>+</sup> neurons found in one hemisphere.

### 6.3 Results

#### 6.3.1 Expression of mHTT in LNvs neurons leads to arrhythmia and period shortening in total darkness.

I expressed mHTT in the LNvs (*i.e.* *Pdf>HTT93Q*) and I analysed locomotor activity rhythms in newly eclosed males maintained in darkness (DD) for three weeks, after 3 days of light:dark (LD) entrainment. To further validate the protective role of dRAB8 in a HD context, I also tested flies co-expressing mHTT and dRAB8, *i.e.* *Pdf>HTT93Q,dRab8*. Overall *Pdf>HTT93Q* flies showed higher levels of arrhythmia compared to controls (HTT93Q UAS ctrl and GAL4 ctrl) throughout the 3 weeks of the experiment (Figure 6-4). A two-tailed exact Fisher's test corrected for Bonferroni indicated a significant difference between *Pdf>HTT93Q* and *Pdf>HTT93Q,dRab8* flies during the 1<sup>st</sup> week ( $p<0.001$ , Figure 6-4), suggesting a protective role mediated by the Rab GTPase. No effect of dRAB8 was observed during the 2<sup>nd</sup> and the 3<sup>rd</sup>

weeks (two-tailed exact Fisher's test corrected for Bonferroni,  $Pdf>HTT93Q$  and  $Pdf>HTT93Q, dRab8$ ,  $p>0.05$ , Figure 6-4). Interestingly, mHTT-driven arrhythmicity was reduced over time, *i.e.* I observed ~79% arrhythmic flies during the 1<sup>st</sup> week compared to ~51% of flies during the 2<sup>nd</sup> week and to ~59% of flies during the 3<sup>rd</sup> week (Figure 6-4). A two-tailed exact Fisher's test corrected for Bonferroni indicated a significant effect of time on the arrhythmicity of  $Pdf>HTT93Q$  flies (1<sup>st</sup> week vs 2<sup>nd</sup> week,  $p<0.001$  and 1<sup>st</sup> week vs 3<sup>rd</sup> week,  $p<0.001$ , Figure 6-4). However, between the 2<sup>nd</sup> and 3<sup>rd</sup> week no statistical significance was observed (two-tailed exact Fisher's test corrected for Bonferroni, 2<sup>nd</sup> week vs 3<sup>rd</sup> week,  $p>0.05$ , Figure 6-4).

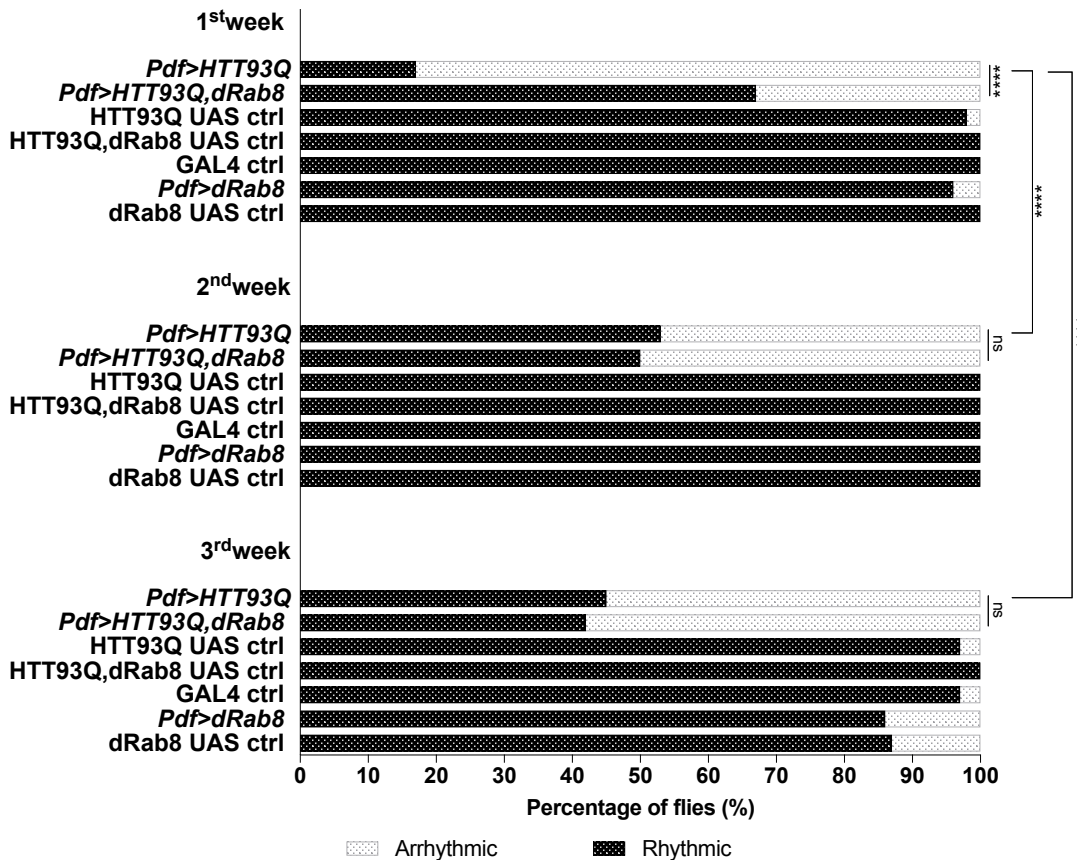


Figure 6-4 Percentage of AR HD flies in DD decreases after the 1<sup>st</sup> week.

Percentages of rhythmic and arrhythmic flies are calculated considering those alive week by week. Two-tailed exact Fisher's test corrected with Bonferroni test for multiple comparison. Comparison among Genotypes, 1<sup>st</sup> week: *Pdf>HTT93Q* vs *Pdf>HTT93Q,dRab8*, p<0.001. Comparison among Weeks: *Pdf>HTT93Q*, 1<sup>st</sup> week vs 2<sup>nd</sup> week, p<0.001; 1<sup>st</sup> week vs 3<sup>rd</sup> week, p<0.01. *Pdf>HTT93Q* 1<sup>st</sup> week N=158, 2<sup>nd</sup> week N=152, 3<sup>rd</sup> week N=98; HTT93Q UAS ctrl 1<sup>st</sup> week N=83, 2<sup>nd</sup> week N=74, 3<sup>rd</sup> week N=61; *Pdf>HTT93Q,dRab8* 1<sup>st</sup> week N=61, 2<sup>nd</sup> week N=60, 3<sup>rd</sup> week N=40; HTT93Q,dRab8 UAS ctrl 1<sup>st</sup> week N=59, 2<sup>nd</sup> week N=54, 3<sup>rd</sup> week N=24; GAL4 ctrl 1<sup>st</sup> week N=96, 2<sup>nd</sup> week N=72, 3<sup>rd</sup> week N=63; *Pdf>dRab8* 1<sup>st</sup> week N=45, 2<sup>nd</sup> week N=41, 3<sup>rd</sup> week N=21; dRab8 UAS ctrl 1<sup>st</sup> week N=32, 2<sup>nd</sup> week N=30, 3<sup>rd</sup> week N=15.

It is worth noting that not only did the percentage of rhythmic *Pdf>HTT93Q* flies increase significantly throughout the course of the experiment, but strikingly, that individual *Pdf>HTT93Q* flies became progressively more rhythmic (Figure 6-5.A). As a measure of the robustness of the rhythm, the power of the spectral peak calculated by CLEAN (hereafter referred simply to as power) was quantified. It corresponds to the ordinate's value at the CLEAN spectral peak, given in arbitrary units (Figure 6-5.A). The power was calculated for 35 flies that were rhythmic during week 2 and 3. Of these only 3 were rhythmic during week 1. A one-way ANOVA revealed a significant difference among the 3 weeks ( $F_{(2,102)}=39.35$ ,  $p<0.0001$ , Figure 6-5.B), with the 2<sup>nd</sup> week also being significant different from the 3<sup>rd</sup> week (post-hoc Newman-Keuls,  $p<0.01$ , Figure 6-5.B).

This recovery from behavioural arrhythmia in constant darkness reinforces the idea of a plastic organization of the circadian network (Dissel *et al.*, 2014).

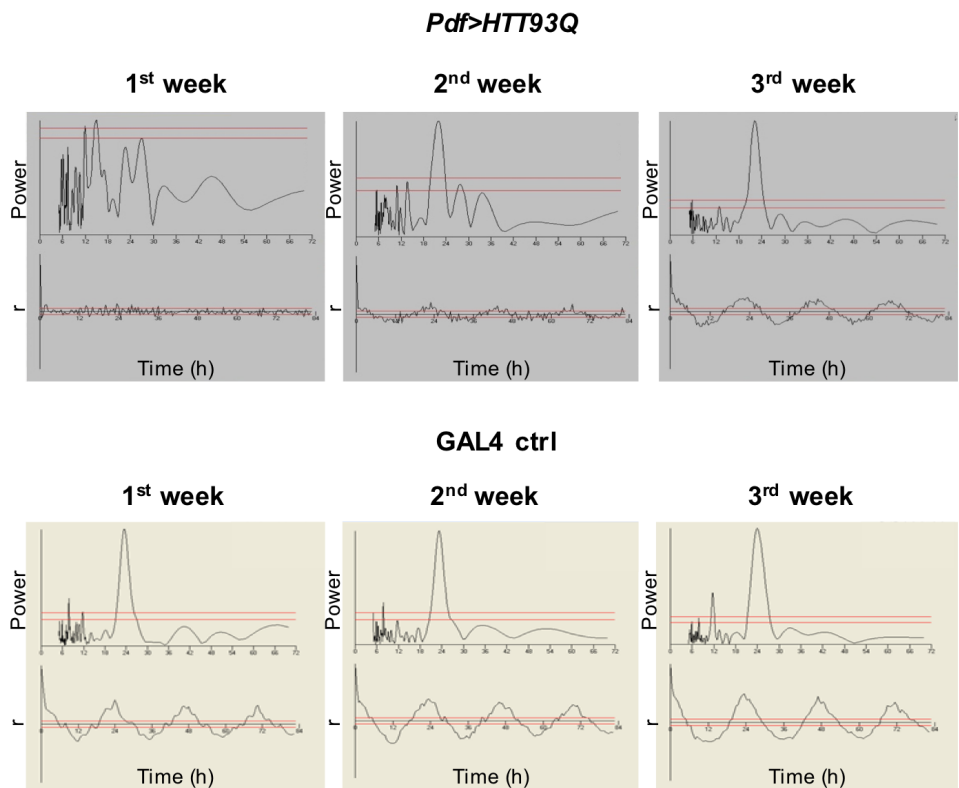
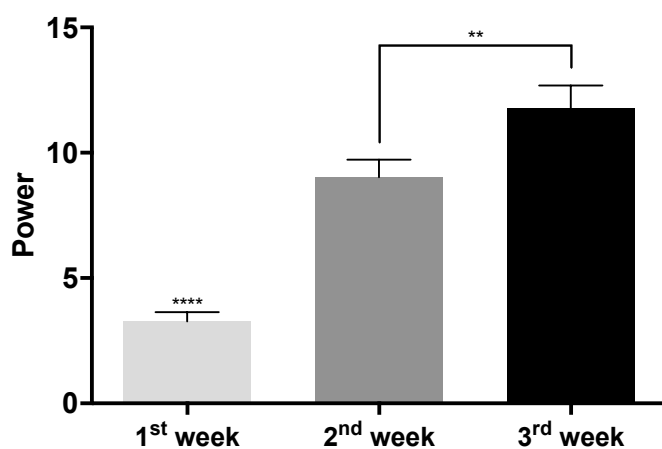
**A****B**

Figure 6-5 *Pdf>HTT93Q* flies recover from behavioural arrhythmia.

**A** Outputs of the CLEAN spectral analysis (top panels) and autocorrelation (bottom panels) of a representative *Pdf>HTT93Q* fly which was arrhythmic during the 1<sup>st</sup> week and rhythmic during the 2<sup>nd</sup> and 3<sup>rd</sup> week, compared to a control fly, *GAL4 ctrl*, which was rhythmic for the whole experiment. **B** Quantification of the power of CLEAN spectral analysis for 35 *Pdf>HTT93Q* flies throughout 3 weeks, chosen because considered rhythmic during the 2<sup>nd</sup> and 3<sup>rd</sup> week. Data are ±SEM. One-way ANOVA,  $F_{(2, 102)}=39.35$ ,  $p<0.0001$ . Post-hoc Newman-Keuls: 1<sup>st</sup> week vs 2<sup>nd</sup> week,  $p<0.0001$ , 1<sup>st</sup> week vs 3<sup>rd</sup> week,  $p<0.0001$ , 2<sup>nd</sup> week vs 3<sup>rd</sup> week,  $p<0.01$ . N=35.

The locomotor activity data were used to build the actograms reported in Figure 6-6.A, which for every genotype display the average activity of all the flies monitored during the experiment, regardless of their rhythmicity. From the actograms, arrhythmicity was identified as the main component of locomotor behaviour of both *Pdf>HTT93Q* and *Pdf>HTT93Q,dRab8* flies, although both short and long rhythms (yellow and white arrows, Figure 6-6.A) were observed over the course of the weeks. In addition the mean periods for rhythmic flies was calculated for individual weeks (Figure 6-6.B). To investigate if mHTT overexpression has an effect on the period of the flies, a two-way ANOVA with repeated measures would be the appropriate statistical analysis, as those are not in fact independent observations. However, given the small proportion of *Pdf>HTT93Q* flies rhythmic during the 1<sup>st</sup> week and retaining rhythmicity for the following two weeks (5 out of 148), this approach, would be misrepresentative of the sample. Given these thoughts, I found it preferable to consider the data as multiple observations. A two-way ANOVA analysis showed significant genotype x week interaction ( $F_{(8,603)}=1.87$ ,  $p=0.061$ , Figure 6-6.B) suggesting that the flies were not responding similarly throughout the course of the entire experiment, although a significant difference among genotypes ( $F_{(4,603)}=18.62$ ,  $p<0.0001$ , Figure 6-6.B) and weeks ( $F_{(2,603)}=9.26$ ,  $p=0.0001$ , Figure 6-6.B) was observed.

Interestingly, while mHTT expressing flies overall showed a short period over the weeks (1<sup>st</sup> week,  $22.63 \text{ h} \pm 0.39$ ; 2<sup>nd</sup> week,  $22.64 \text{ h} \pm 0.07$ ; 3<sup>rd</sup> week= $23.26 \text{ h} \pm 0.25$ , Figure 6-6.B), co-expression of HTT and dRAB8 generated longer periods during the 1<sup>st</sup> ( $24.7 \text{ h} \pm 0.22$ , Figure 6-6.B), that progressively shortened to almost wild type levels during the 2<sup>nd</sup> ( $23.49 \text{ h} \pm 0.29$ , Figure 6-6.B) and 3<sup>rd</sup> week ( $23.3 \text{ h} \pm 0.53$ , Figure 6-6.B). The Newman Keuls post-hoc revealed that the two genotypes were significantly different only during the first weeks (1<sup>st</sup> week,  $p<0.001$ , 2<sup>nd</sup> week,  $p<0.001$ ). Remarkably, while the period of *Pdf>HTT93Q,dRab8* flies was consistently long during the 1<sup>st</sup> week, during the 2<sup>nd</sup> week a shorter component appeared, which took over during the 3<sup>rd</sup> week (Figure 6-6.A).

To interpret those data further, the behaviour of individual *Pdf>HTT93Q* and *Pdf>HTT93Q,dRab8* flies was examined. Flies were assigned to 6 categories: arrhythmic, complex rhythms, long rhythms, circadian rhythms, short rhythms or dead (Figure 6-7). This approach suggests that the effects described above are not due to a mere statistical artefact. In addition this kind of data visualization revealed that during the 2<sup>nd</sup> week, rhythmic *Pdf>HTT93Q* had predominantly short rhythms whereas during the last week they clustered in mainly two groups: half retaining a short period (<24 h) and the other half displaying a circadian period (~24 h; Figure 6-7). Conversely, *Pdf>HTT93Q,dRab8* flies exhibited long periods during the 1<sup>st</sup> week, but they appeared desynchronized during the 2<sup>nd</sup> week and 3<sup>rd</sup> week.

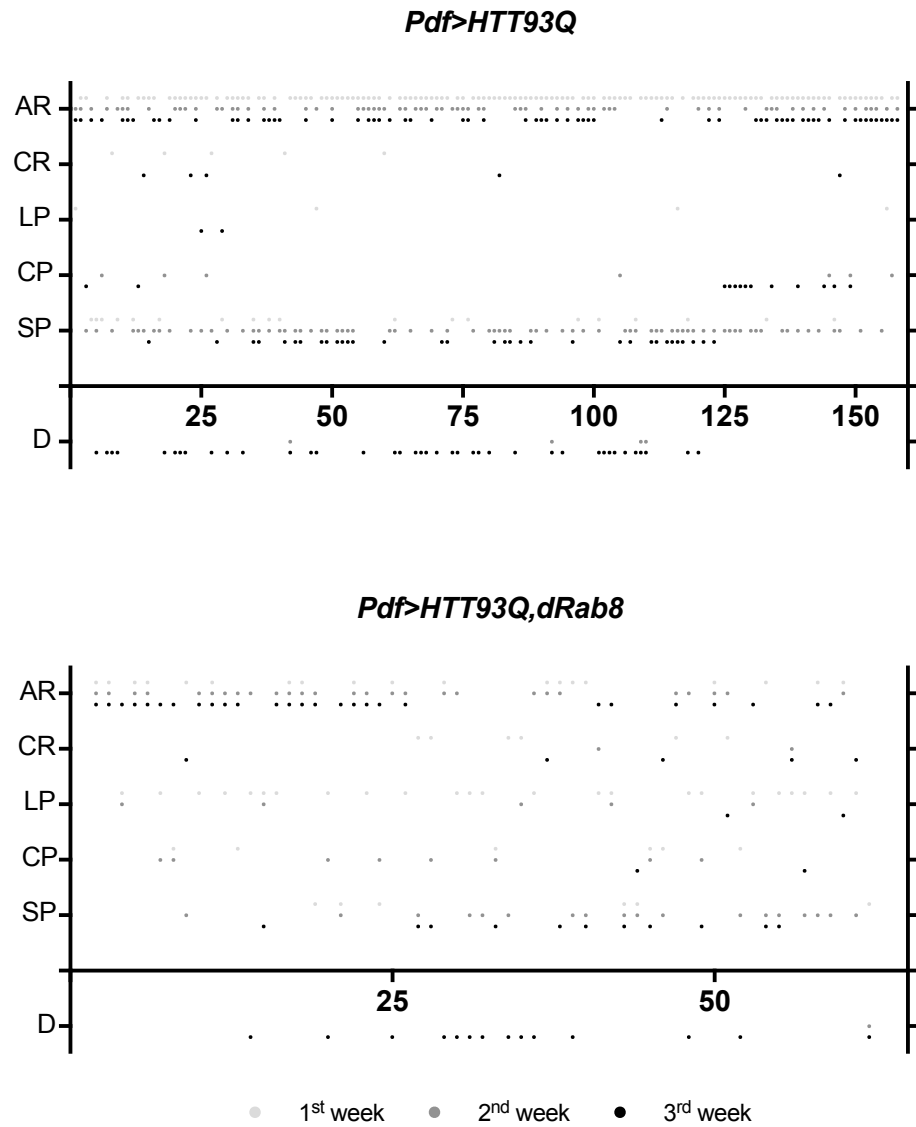


Figure 6-7 Visual summary of the behavioural pattern of *Pdf>HTT93Q* and *Pdf>HTT93Q, dRab8* flies throughout three weeks of DD.

Each point correspond to one fly, whereas the three different shades of grey, indicate the three different time points. Hence three aligned points in the same column represent the same fly over time. X axis=flies tested, hence major ticks represents the n<sup>th</sup> flies tested. AR, arrhythmic; CR, complex rhythm; CP, circadian rhythm (period included between 23.5 h and 24.5 h); D, dead; LP, long period (> 24.5 h); SP, short period (< 23.5 h). *Pdf>HTT93Q* 1<sup>st</sup> week N=158, 2<sup>nd</sup> week N=152, 3<sup>rd</sup> week N=98; *Pdf>HTT93Q, dRab8* 1<sup>st</sup> week N=61, 2<sup>nd</sup> week N=60, 3<sup>rd</sup> week N=40.

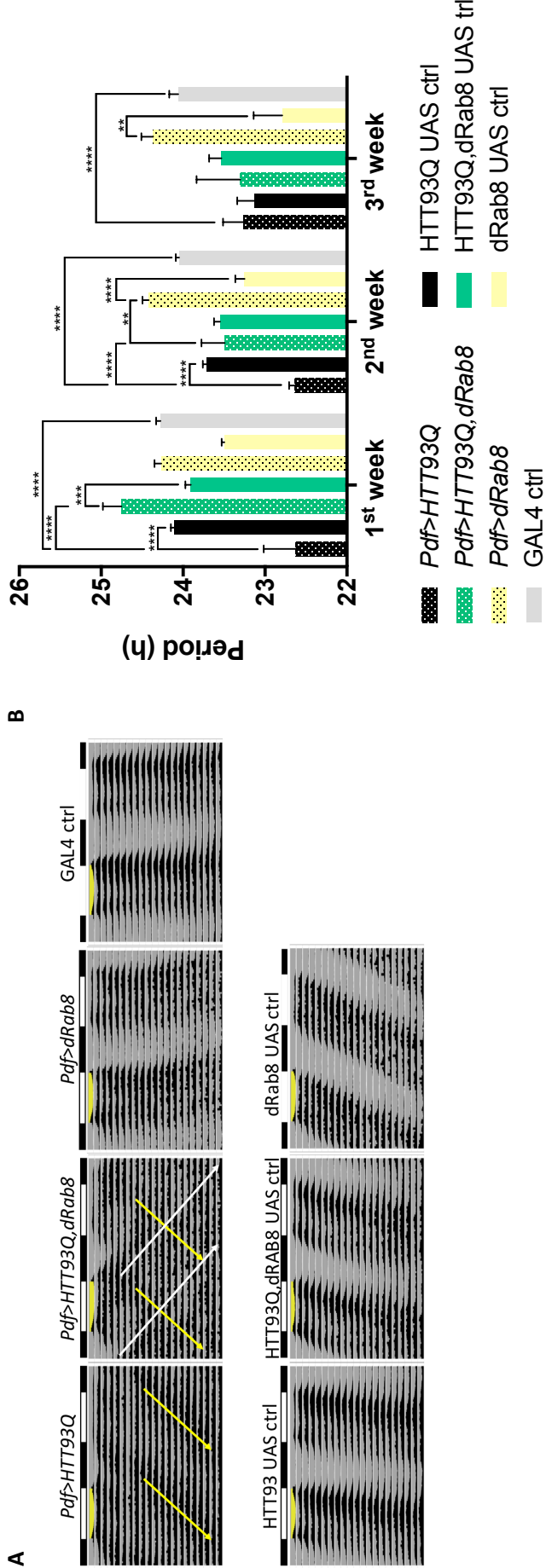


Figure 6-6 *Pdf>HTT93Q* flies shorten their period over time.

### 6.3.1 mHTT-expressing flies exhibit loss of s-LNvs and accumulation of $\alpha$ -HTT signal in IB-like structures

To correlate locomotor activity data with measures of molecular dysfunction, preliminary IF experiments were conducted at day 1, 7 and 14 on brains probed with  $\alpha$ -PDF (Figure 6-8.A). These time points corresponded to the beginning of the 1<sup>st</sup>, 2<sup>nd</sup> and 3<sup>rd</sup> weeks previously analysed. In agreement with what had been previously reported (Sheeba *et al.*, 2010; Mason *et al.*, 2013), I did not observe loss of immunoreactivity in the I-LNvs, neither in *Pdf>HTT93Q* nor in *Pdf>HTT93Q,dRab8* samples. The s-LNvs were counted in all brains. Loss of s-LNvs was found in *Pdf>HTT93Q* at day 7 (mean 3.5±0.2, Figure 6-8.B) and at day 14 (mean 3.5±0.2, Figure 6-8.B) whereas *Pdf>HTT93Q,dRab8* always displayed 4 s-LNvs (Figure 6-8.B). A one sample t-test against the hypothetical value of 4 indicated a significant loss of s-LNvs only at day 14.

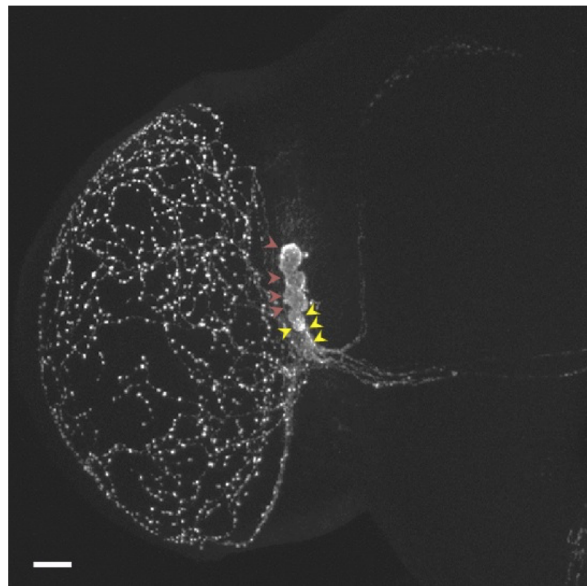
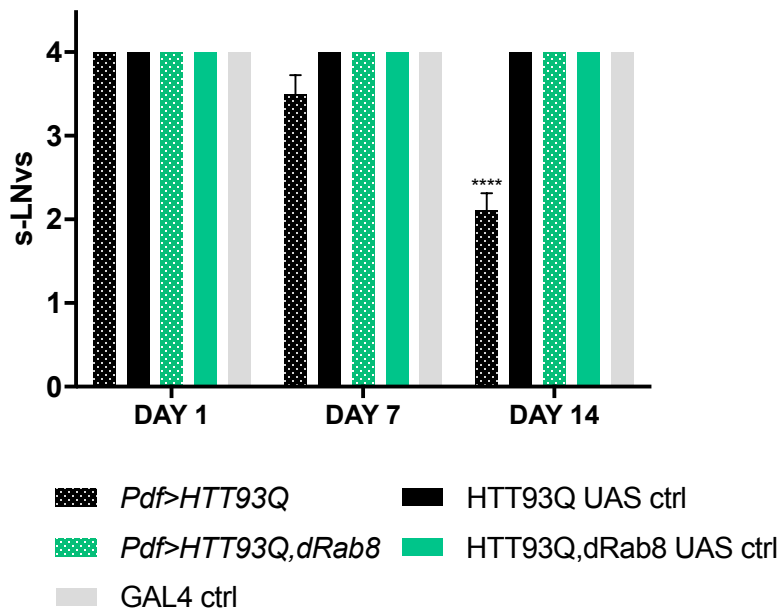
**A****B**

Figure 6-8 The number of s-LN<sub>v</sub>s is significantly decreases in mHTT expressing flies at day 14.

**A** Representative confocal maximum projection of a control hemisphere brain (GAL4 ctrl) treated with α-PDF. The staining shows 4 I-LNvs (red arrows), 4 s-LNvs (yellow arrows), PDF arborisation in the medulla and the dorsal and lateral PDF projections. Primary antibody: α-PDF 1:50 (DSHB, Table 2-3). Secondary antibody: Cy2 α-mouse 1:200 (AbCam, Table 2-3). Scale bar=10 μm. **B** Following 3 day entrainment in LD, flies were aged 1 day in DD. The number of s-LNvs was quantified for *Pdf>HTT93Q*, *Pdf>HTT93Q,dRab8*, HTT93Q UAS ctrl, HTT93Q,dRab8 UAS ctrl and GAL4 ctrl. Data are presented as the average number of s-LNvs per hemisphere ±SEM, based on the following numbers of hemispheres: *Pdf>HTT93Q* day 1 N=6, day 7 N=6, day 14 N=9; HTT93Q UAS ctrl day 1 N=6, day 7 N=5, day 14 N=6; *Pdf>HTT93Q,dRab8* day 1 N=7, day 7 N=5, day 14 N=6; HTT93Q,dRab8 UAS ctrl day 1 N=6, day 7 N=5, day 14 N=6; GAL4 ctrl day 1 N=4, day 7 N=5, day 14 N=6. One-sample t-test for *Pdf>HTT93Q* flies: day 7, hypothetical value=4, t=2.236, sf=5, p=0.0756, ns. One sample t-test for *Pdf>HTT93Q* flies: day 14, hypothetical value=4, t=9.3430, df=8, p<0.0001.

Next, I examined the expression of mHTT in the s-LNvs neurons. Immunostainings with  $\alpha$ -HTT and  $\alpha$ -PDF antibodies were performed in flies either expressing HTT93Q alone or with dRAB8 in the PDF<sup>+</sup> neurons. Flies were aged 1 day, after which brains were dissected and stained as described in Section 6.2.4. Confocal analyses of *Pdf>HTT93Q* and *Pdf>HTT93Q,dRab8* flies revealed that for both genotypes the  $\alpha$ -HTT signal was not ubiquitously distributed in the s-LNvs neurons, rather it formed punctate structures resembling IBs (Figure 6-9.A). I also noticed that the s-LNvs of *Pdf>HTT93Q,dRab8* flies had a greater number of these  $\alpha$ -HTT positive structures. Hence, the number of punctae in each neuron was counted and averaged for the total number of neurons per brain hemisphere. A two-tailed exact Fisher's test did not reveal a significant increase in the number of punctae in *Pdf>HTT93Q,dRab8* (Two-tailed exact Fisher test,  $t=1.364$   $df=16$ ,  $p=0.1913$ , Figure 6-9.B), although the proportion of  $\alpha$ -HTT positive structures in this genotype was 1.5 higher than in *Pdf>HTT93Q* flies.

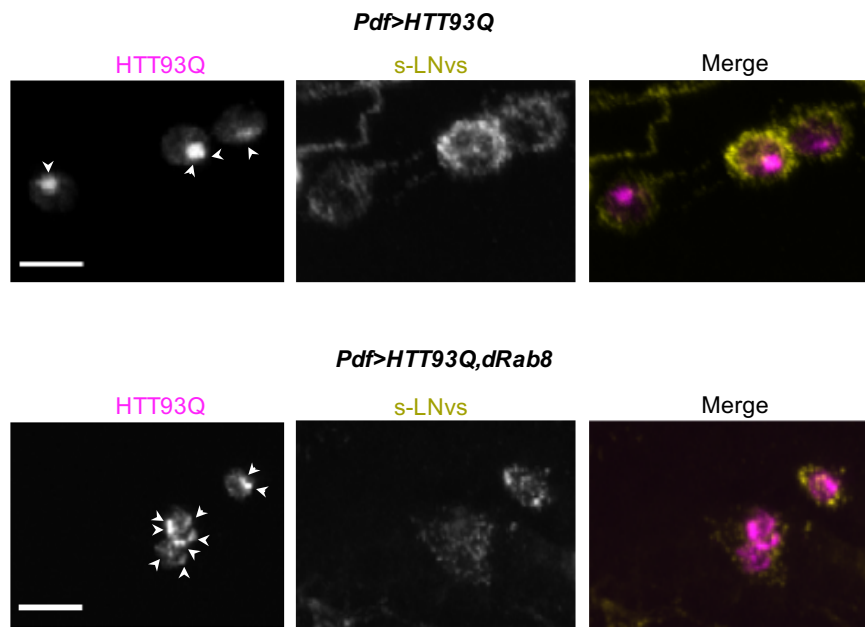
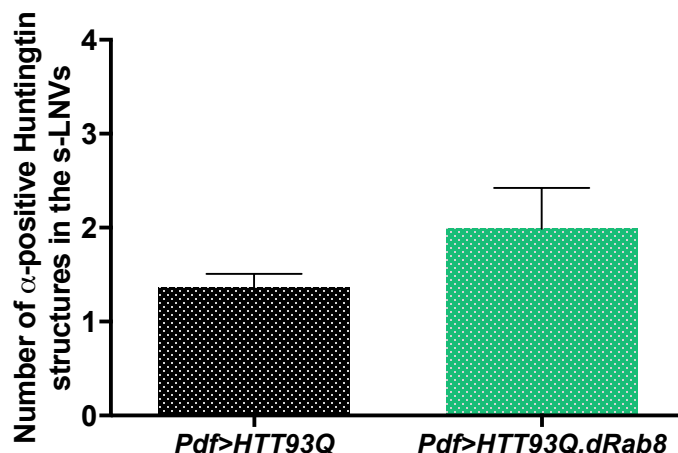
**A****B**

Figure 6-9 dRAB8 overexpression induces the formation of  $\alpha$ -HTT positive punctae in the s-LNvs of mHTT flies.

**A** Representative confocal maximum projections of 3 s-LNvs of *Pdf>HTT93Q* and *Pdf>HTT93Q, dRab8* stained with  $\alpha$ -PDF and  $\alpha$ -HTT at day 1 post eclosion. White arrows indicate  $\alpha$ -HTT positive punctae. Primary antibodies:  $\alpha$ -HTT 1:2000 (Millipore, Table 2-3),  $\alpha$ -PDF 1:100 (Dr Wilcockson, Table 2-3). Secondary antibodies: Cy2  $\alpha$ -mouse 1:200 (AbCam, Table 2-3), Cy5  $\alpha$ -rabbit 1:200 (AbCam, Table 2-3). Scale bar=10  $\mu$ m. **B** Mean of  $\alpha$ -HTT positive punctae found in the s-LNvs, averaged for the number of s-LNvs per hemisphere. Two-tailed exact Fisher test,  $t=1.364$   $df=16$ ,  $p=0.1913$ , ns. *Pdf>HTT93Q*,  $N=9$ ; *Pdf>HTT93Q, dRab8*  $N=9$ .

## 6.4 Discussion

The expression of mHTT in PDF<sup>+</sup> cells, *i.e.* s- and l-LNvs, led to behavioural arrhythmia in constant darkness and dRAB8 overexpression was able to alleviate those phenotypes, further validating the Rab GTPase as modifier for HD in *D. melanogaster*. Flies were monitored for three weeks, and their behaviour was analysed week by week. The majority of mHTT expressing flies was arrhythmic during the first week. Overexpression of dRAB8 significantly increased the percentage of rhythmic flies during the first week. During the 2<sup>nd</sup> and 3<sup>rd</sup> week, there was actually no difference between the percentages of *Pdf>HTT93Q* and *Pdf>HTT93Q,dRab8* rhythmic flies. Indeed, *Pdf>HTT93Q* flies became progressively more rhythmic as a function of time. Although a circadian interpretation of these data is beyond the scope of this thesis, re-emergence of rhythmicity might reflect a reconfiguration or adaptation of the circadian network after the s-LNvs – an important group of clock neurons – become dysfunctional by the expression of mHTT. If we assume that dRAB8 delays the weakening of the s-LNvs, we can understand why initially the *Pdf>HTT93Q,dRab8* flies are more rhythmic but then they show less rhythmicity (their activity profile displays a mix of long and short rhythmic components) that results from the interference of the s-LNvs and the delay in the reconfiguration of the network (Dissel *et al.*, 2014).

Preliminary confocal analyses may support this view. Immunostaining on brains revealed that while the l-LNvs seemed to be unaffected by mHTT expression, a progressive loss of s-LNvs, was observed, in accordance to previous studies (Sheeba *et al.*, 2010). However, it is important to remember that although a reduction in PDF immunoreactivity may provide a measure of neuronal dysfunction, it does not necessarily measure neuronal death. To answer this question and to determine when the death of s-LNvs death occurs, it would be necessary to use apoptotic markers such as TUNEL analysis.

In the previous chapter I proposed a role of dRAB8 in promoting aggregation that might explain the rescue observed so far. The increased in number of α-HTT positive structures observed in the s-LNvs upon dRAB8 overexpression is reminiscent of IBs formation observed previously (Chapter 5), and could support the idea that dRAB8 has a direct effect on the aggregation state of mHTT. Taken together these data suggest a role for dRAB8 as a neuroprotective agent against HD phenotypes even when its overexpression is limited to a small number of cells. Moreover these results highlight the ability of the circadian neuronal network to reconfigure.

## Chapter 7

### Discussion

HD is a fatal neurodegenerative disorder caused by loss of regions of the brains such as the striatum and cortex, which manifests with physical, psychological and psychiatric symptoms. At the molecular level HD is triggered by an abnormal *CAG* repeat length in the first exon of the *HTT* gene, encoding for a polyQ expansion in the translated protein. When the polyQ tract exceeds the critical threshold of 40 repeats, the mutation causes the protein to misfold and aggregate, leading to cellular dysfunction, such as transcriptional dysregulation, mitochondrial and axonal transport defects, progressively leading to neuronal death (Bates *et al.*, 2014). Notwithstanding the inverse correlation existing between the number of repeats and the age of onset, patients carrying the same expansion length can manifest differences in the clinical onset of the disease (Wexler *et al.*, 2004). While the *CAG* repeat length is the primary determinant for the pathogenic process, 38% of the onset variability depends on genetic factors (Gusella & MacDonald, 2009). The search of genetic modifiers, *i.e.* genetic variants in the human genome that can alter the disease progression, is the focus of intense research, as their identification might lead to new therapeutic targets for HD. Genetic screens carried in yeast or in cell culture have been used to identify modifiers of mHTT-induced toxicity, uncovering cellular pathways involved in the pathogenic process and identifying novel therapeutic targets (Giorgini *et al.*, 2005; Mason *et al.*, 2013; Smalley *et al.*, 2016). One pathway impaired in HD is the vesicular trafficking, including those directed by the Rab GTPases. Several lines of evidence have reported defects of Rabs function and localization upon mHTT expression (del Toro *et al.*, 2009; Li *et al.*, 2009a; Li *et al.*, 2009b; Li *et al.*, 2010; Ravikumar *et al.*, 2008), and overexpression of several Rabs has shown to be protective in *Drosophila* and mammalian cell HD models (Li *et al.*, 2009a; Ravikumar *et al.*, 2008; Richards *et al.*, 2011; Steinert *et al.*, 2012). A siRNA screen targeting the majority of Rabs has identified candidate genes able to modulate mHTT-induced toxicity in HEK293T cells (Mason & Giorgini, unpublished). Among these, Rab8 – which coordinates the secretory pathway from the TGN – was identified as a putative modifier of HD, in fact human Rab8a (hRAB8A) down-regulation increased mHTT-induced toxicity (Mason & Giorgini, unpublished). This important finding has set the scene for the research undertaken during my PhD. The work presented in this thesis had the primary aim of validating and characterizing dRAB8 as a biological modifier of HD phenotypes *in vivo*, using *Drosophila* as model system.

## 7.1 dRAB8 delays the onset of HD-phenotypes in *Drosophila*

HD pathology was modelled in *Drosophila* by expressing the first exon of mHTT carrying 93Q (Steffan *et al.*, 2001). This mHTT-truncated form is often used to model HD, as its pan-neuronal expression, achieved using the CNS driver *elav-GAL4* (Table 2-4), recapitulates many aspects of the pathology, such as neurodegeneration in the eyes, impaired emergence from the pupal case and shortened life-span (Green & Giorgini, 2012). Neurodegeneration in these flies can be easily scored by performing the so-called “standard assays” (Green & Giorgini, 2012). In the pseudopupil analysis the progressive neurodegeneration of the photoreceptor cells is evaluated by scoring for presence of the 7 light-microscopy visible rhabdomers, which progressively decrease in function of time (Mason *et al.*, 2013; Richards *et al.*, 2010; Campesan *et al.*, 2011; dos Santos *et al.*, 2014; Varadarajan *et al.*, 2015; Vittori *et al.*, 2014; Vittori *et al.*, 2013; Sajjad *et al.*, 2014; Ravikumar *et al.*, 2004; Steffan *et al.*, 2001). The eclosion assay measures the emergence of the flies from the pupal case, which is reduced in HD flies (Campesan *et al.*, 2011; Richards *et al.*, 2010; Vittori *et al.*, 2014; Wolfgang *et al.*, 2005). Finally, as the life-span is reduced upon mHTT expression, the median survival, can be used as a metric assess to neurodegeneration (Richards *et al.*, 2011; Steffan *et al.*, 2004).

Pan-neuronal expression of the polyQ-expanded HTT fragment driven by the *elav-GAL4* driver (*i.e.* *elav>HTT93Q*) caused a 1.6-fold decrease in the rate of pupal emergence (Figure 3-2). Moreover, *elav>HTT93Q* flies showed an age dependent loss of photoreceptor cells (roughly a 15% decrease between day 1 and day 7, Figure 3-3.C), and exhibited a reduced life-span, displaying a median survival of 7 days (Figure 3-4 and Table 3-2), which is very short compared to the about 1.5 months of a wild type fly. These findings are in agreement with earlier reports, underlying the high reproducibility of these assays. (Mason *et al.*, 2013; Richards *et al.*, 2010; Campesan *et al.*, 2011; dos Santos *et al.*, 2014; Varadarajan *et al.*, 2015; Vittori *et al.*, 2014; Vittori *et al.*, 2013; Sajjad *et al.*, 2014; Ravikumar *et al.*, 2004; Steffan *et al.*, 2001). All these HD-relevant phenotypes were ameliorated by overexpression of dRAB8. Eclosion rates of flies *elav>HTT93Q,dRab8* were increased to levels comparable to controls (Figure 3-2). dRAB8 overexpression resulted in 10% and 15% neuroprotection in the photoreceptor cells at day 1 and day 7 respectively (Figure 3-3.C). Notably, the number of rhabdomers at day 7 displayed by *elav>HTT93Q,dRab8* flies was comparable to those of *elav>HTT93Q* flies displayed at day 1 (~6, Figure 3-3.C), suggesting that dRAB8 overexpression delays neurodegeneration by 6 days. Also, the lifespan was extended, as the median survival of *elav>HTT93Q,dRab8* flies was more than doubled compared to that of *elav>HTT93Q* flies (Figure 3-4 and Table 3-2). Collectively these results underlie dRAB8 ability to modify the onset of HD-phenotypes by slowing

down the progression of the disease.

It was important at this stage to determine whether the rescue observed was due to the GTP-binding state of dRAB8. Rabs use the molecular cycling between the active, GTP- and the inactive, GDP- bound forms to regulate the different steps of vesicular traffic. Rabs ability to switch between the ON and OFF states ensures their correct localisation of function (Zhen & Stenmark, 2015 and Figure 1-8). Constitutively active and dominant negative forms of dRAB8 (*i.e.* dRAB8CA and dRAB8DN) were tested for their ability to rescue HD-relevant phenotypes. The eclosion rates of *elav>HTT93Q,dRab8DN* and *elav>HTT93Q* flies were not significantly different (Figure 3-2). Similarly, the two genotypes showed comparable median survivals (Figure 3-4 and Table 3-2). Interestingly however, *elav>HTT93Q,dRab8DN* flies aggravated the loss of rhabdomeres loss at day 7 (but not at day 1; Figure 3-3). As expression of dRAB8DN *per se* produced a wild-type phenotype, these results suggest a synergistic effect of mHTT with dRAB8DN. As already discussed in Chapter 3, Rab8 was described as a regulator of the rhodopsin transport in retinal photoreceptor cells in *R. berlandieri* (Moritz *et al.*, 2001). Expression of Rab8DN mutant was shown to cause degeneration of the retina in *X. laevis* (Deretic *et al.*, 1995). If the role of Rab8 is conserved along the evolutionary scale, it might explain why co-expression of dRAB8DN in the HD background aggravated photoreceptor loss. Whether overexpression of dRAB8DN alone is sufficient to trigger loss of rhabdomeres in *Drosophila* could be tested at later time points, *e.g.* day 14 or day 21. Overexpression of dRAB8CA ameliorated the emergence from the pupal case (Figure 3-2), increased the number of rhabdomeres at day 7 (Figure 3-3.C), and extended the life-span (Figure 3-4 and Table 3-2). In particular, while the eclosion rate was completely rescued to wild type levels in *elav>HTT93Q,dRab8CA* flies (Figure 3-2), neuroprotection scored in the pseudopupil analysis and in the longevity assay was lower compared to *elav>HTT93Q,dRab8* flies (Figure 3-3.C, Figure 3-4 and Table 3-2). These results indicate that the rescue provided by dRAB8 overexpression depends upon the binding state of the GTPase, namely, is it essential for the protein to switch between the ON and OFF states.

Neurodegenerative diseases, including HD, affect sleep and circadian rhythms (Morton *et al.*, 2005). These disturbances are linked with the pathological dysfunction of the hypothalamus, and in particular of the superchiasmatic nucleus (Kremer *et al.*, 1990; Petersén & Gabery, 2012). *Drosophila* has been extremely helpful in dissecting the basis of the mechanisms that generate circadian rhythms, making this insect particularly suited for chronobiology studies. *Drosophila* clock consists of only ~150 clock neurons (Figure 6-2). These neurons are clustered in relation to their anatomical position: there are three groups of dorsal neurons (DN1, DN2 and DN3), a group of lateral posterior neurons (LPN) and two groups of lateral neurons (LN), the lateral dorsal neurons (LNdS) and the later ventral neurons (LNvS). The LNvS are an

important group of clock cells, consisting of 16 neurons, 4 small (s-LNvs) and 4 large (l-LNvs) in each hemisphere (Helfrich-Förster *et al.*, 1998). These express PDF, a neuropeptide important for entraining the clock and for sustaining rhythmicity in the absence of external clue (free-running conditions) such as darkness (Renn *et al.*, 1999; Peschel & Helfrich-Förster, 2011). One rhythmic behaviour that is marked by circadian rhythms is locomotor activity. In laboratory conditions, with 12:12 h light:dark settings, flies are active at dawn and dusk, displaying two characteristic bouts of activity, the morning and the evening peaks (Allada & Chung, 2010 and Figure 6-1). Because one characteristic of any endogenous clock is the self-sustainability in free-running conditions, the activity peaks persist also in constant darkness (DD), showing a period slightly shorter than 24 h (Collins *et al.*, 2005; Helfrich-Förster, 2001; Peschel & Helfrich-Förster; 2011; Vanin *et al.*, 2012). As manifestation of circadian rhythms requires precise coordination among cellular components, these are an excellent model to look at the relationship between neuronal dysfunction and behaviour. mHTT expression in the PDF<sup>+</sup> cells has been shown to cause rhythmic defects and to cause the neuronal death of the s-LNvs (Mason *et al.*, 2013; Sheeba *et al.*, 2010). Hence the circadian system of the fly, and in particular the subset of the PDF clock cells, provide a robust model to measure neuronal dysfunction, and test the protective effects of dRAB8. The locomotor activity of flies tested in DD was monitored for 3 weeks. Each week was analysed independently from each other and will be referred to as 1<sup>st</sup>, 2<sup>nd</sup> or 3<sup>rd</sup> week. *Pdf>HTT93Q* flies, namely flies expressing mHTT in PDF<sup>+</sup> neurons, exhibited abnormal locomotor activity behaviours, indeed only ~20% of *Pdf>HTT93Q* flies were rhythmic during the 1<sup>st</sup> week (Figure 6-2). Strikingly, dRAB8 overexpression rescued the behavioural arrhythmia. I observed ~65% of rhythmic *Pdf>HTT93Q,dRab8* flies during the 1<sup>st</sup> week (Figure 6-4), supporting once again the neuroprotective role of this small GTPase. During the following weeks, however, there was no difference between the percentages of rhythmic *Pdf>HTT93Q* and rhythmic *Pdf>HTT93Q,dRab8* flies. While the percentage of rhythmic *Pdf>HTT93Q,dRab8* flies remained constant throughout the 3 weeks, the percentage of rhythmic *Pdf>HTT93Q* increased in function of time. Strikingly, I observed ~50% and ~40% of rhythmic *Pdf>HTT93Q* flies during the 2<sup>nd</sup> and 3<sup>rd</sup> week respectively (Figure 6-4). Moreover, analysis of the periods revealed a predominant short component for *Pdf>HTT93Q* flies, and a mix of a short and long components for *elav>HTT93Q,dRab8* flies. Although counterintuitive, these results can be explained by the weakening of the s-LNvs, which become dysfunctional upon mHTT expression. As these neurons – which are important for sustaining free-running rhythms – progressively die, the circadian network might re-organize its connections, with the consequent re-emergence of behavioural rhythmicity. Assuming that the protection conferred by dRAB8 delays the weakening of the s-LNvs, it is clear why its overexpression increases the percentage of

rhythmic flies at the beginning, and shows desynchronized rhythms later on. This view was supported by preliminary immunofluorescence analyses on HD fly brains, which, consistently with published studies, showed progressive loss of the s-LNvs (Figure 6-8.B; Mason *et al.*, 2013; Sheeba *et al.*, 2010). Although mHTT induced significant loss of the s-LNvs only at day 14, neuronal loss was already observed at day 7 (Figure 6-8.B). Moreover, flies co-expressing mHTT and dRAB8 were not subject to neuronal loss (Figure 6-8.B), again providing evidence for the protective role of dRAB8.

Collectively, dRAB8 overexpression has been shown to be protective against mHTT-induced toxicity both in the CNS and in a subset of clock cells, the PDF neurons.

## 7.2 The molecular mechanisms underlying dRAB8 rescue

One promising therapeutic strategy in HD is up-regulation of autophagy (intended as macroautophagy), for cellular clearance of soluble, toxic mHTT species. Through the formation of an autophagosome, toxic mHTT species are isolated and target to the lysosomes for degradation (Mizushima *et al.*, 2008; Menzies *et al.*, 2006). Up-regulation of autophagy has been shown to reduce the levels of aggregated mHTT and to reduce mHTT-induced toxicity (Ravikumar *et al.*, 2002; Ravikumar *et al.*, 2004; Sarkar *et al.*, 2009). Interestingly, Rab5 has been previously found to modulate aggregation and toxicity of aggregated mHTT *via* up-regulation of autophagy (Ravikumar *et al.*, 2008). Remarkably, Rab8 has been linked to autophagy being involved in the fusion of the autophagosomes with the lysosomes (Ao *et al.*, 2014; Bento *et al.*, 2013; Pilli *et al.*, 2012; Szatmári & Sass, 2014). Moreover, Rab8 was shown to be mis-localized from the Golgi in HD HeLa model cells, consequently impairing the trafficking to lysosomes, a feature that has been suggested to contribute to the pathology (del Toro *et al.*, 2009). Given this, I assessed the autophagic levels of *elav>HTT93Q* vs *elav>HTT93Q,dRab8* flies by measuring the protein levels of ATG8 cleavage by immunoblotting. ATG8 is a key protein involved in autophagy. When autophagy is induced, cytosolic ATG8 (ATG8-I) is cleaved and lipidated. This mature form (ATG8-II) is associated to the autophagosomes until lysosomal degradation, hence it constitutes a reliable marker of autophagy (Klionsky *et al.*, 2016). Immunoblot analyses on head protein extracts revealed that basal autophagy of *elav>HTT93Q,dRab8* flies were unaltered compared to *elav>HTT93Q* flies (Figure 5-1.B). To test this hypothesis further, the levels of aggregated mHTT were measured through two biochemical assays, the dot-blot and the AGERA. In the dot-blot, protein extracts are spotted and vacuumed onto a membrane. Due to the membrane pore size, large aggregates are trapped onto the membrane surface and can therefore be detected by immunoblot. In the AGERA, protein extracts are electrophoretically resolved on an agarose gel, and proteins are subsequently transferred onto a membrane for

immuno detection. Both assays revealed that in *elav>HTT93Q,dRab8* flies the amount of aggregated mHTT was consistently 1.5-fold higher compared to *elav>HTT93Q* flies (Figure 5-2.B and Figure 5-3.B), confirming that dRAB8 does not up-regulate autophagy, but rather it promotes aggregation of mHTT. Although preliminary, immunostainings on the s-LNvs showed that mHTT forms IBs, whose number seems to be increased upon dRAB8 overexpression (Figure 6-7.A and Figure 6-7.B). All together these results are in agreement with a model whereby dRAB8 stimulates mHTT aggregation and IBs formation. Despite the long debate about the role of IBs in HD pathogenesis, it is now widely accepted that they are protective structures confining toxic mHTT into compact structures (Arrasate *et al.*, 2004), hence dRAB8 stimulation of aggregation might be the protective mechanism that underlies the dRAB8 observed rescue.

How dRAB8 promotes mHTT aggregation remains an outstanding question, however it might depend on an interaction between dRAB8 and mHTT. A series of results collectively suggest that dRAB8 preferentially interacts with mHTT rather than with wild type HTT. For instance, Co-IP experiments performed on head extracts of *elav>HTT93Q,dRab8* flies failed to show interaction between soluble mHTT and dRAB8 (Figure 5-4). Further insights were provided by the BiFC assay. The BiFC technique allows visualization of protein-protein interaction in living cells and is based upon the reconstruction of a fluorophore, for instance Venus, which is split in two halves, each fused to either putative interaction partners (Kerppola, 2008; Kodama & Hu, 2012 and Figure 4-13). Reconstitution of the fluorophore is achieved when the two interacting partners are in close proximity. The fluorophore signal (referred to as BiFC signal) can be used as a measure of protein-protein interaction. Following the generation of a construct expressing dRAB8 fused to the C-terminus of Venus (VC-dRab8), HEK293 cells were co-transfected either with VC-dRab8 and HTT19Q-VN (*i.e.* wild type HTT fused to the N-terminus of Venus) or with VC-dRab8 and HTT97Q-VN (*i.e.* mHTT fused to the N-terminus of Venus). The VC-dRab8/HTT97Q-VN combination showed a BiFC signal ~1.7-fold higher than the VC-dRab8/HTT19Q-VN combination. One of the advantages of the BiFC technique is that it allows visualisation of the BiFC complexes within their natural environment. While the VC-dRab8/HTT19Q-VN pair produced a perinuclear, evenly diffused BiFC signal, the BiFC signal produced by the VC-dRab8/HTT97Q-VN pair was confined to aggregates, suggesting a stronger interaction between mHTT and dRAB8 at these sites.

### 7.3 Effects of Rab8 overexpression in HD model PC12 cells

Part of the data presented in this work was undertaken in an inducible HD in a neuron-like rat pheochromocytoma (PC12) cell line. Upon ponasterone (PA) induction, these cells ex-

press a truncated form of HTT103Q (Apostol *et al.*, 2003 and Figure 4-1). This cell model recapitulates many aspects of HD cellular pathology, such as increased levels of the apoptotic marker caspase-3/7 (Apostol *et al.*, 2006; Li *et al.*, 2000; Sanchez Mejia & Friedlander, 2001), which is a convenient measure of toxicity and has been previously used to test putative genes or compounds for HD (Apostol *et al.*, 2006; Mason *et al.*, 2013; Smalley *et al.*, 2016). In mammals there are two Rab8 isoforms, Rab8a and Rab8b (Armstrong *et al.*, 1996; West *et al.*, 2015), hence both were tested for their ability to rescue caspase-3/7 activation in HD model PC12 cells. Four pools (*i.e.* a heterogeneous population of stably transfected cells) expressing rat Rab8a (rRAB8A) and rat Rab8b (rRAB8B) – namely rRAB8A.1, rRAB8A.2, rRAB8B.1, rRAB8B.2 – were generated as described in Section 4.2.2. Following mHTT induction, caspase-3/7 activation was measured. Interestingly, none of the pools showed decreased caspase-3/7 activation levels (Figure 4-7). Conversely, some pools exhibited higher levels of caspase-3/7 activation (Figure 4-7 and Table 4-1). While this seems contradictory to what found so far, there are evidence suggesting that overwhelmingly expression of Rabs disrupts cellular homeostasis (Makanae *et al.*, 2013; Sopko *et al.*, 2006; Yoshikawa *et al.*, 2011). Similarly, studies conducted in our laboratory have shown high expression of Rabs (*i.e.* when levels of overexpressed Rabs are >50% higher than the endogenous ones) are deleterious for mammalian cells (Mason & Giorgini, unpublished). Immunoblot quantification of rRAB8A/B expression levels, revealed a 3- to 5-fold higher compared to endogenous levels. Interestingly, a positive correlation was found between increased caspase-3/7 activation and rRAB8A/B expression levels (Figure 4-8). It would be interesting to test new pools expressing rRAB8A/B at lower levels. This approach has been successfully utilized for other Rabs in our laboratory. Experiments have shown that by changing the Kozak consensus sequence (CCACC) to a weaker one (CCGCC) (Kozak, 1986), Rabs were expressed at lower levels and were able to modify mHTT-induced toxicity in HD model PC12 cells (Mason & Giorgini, unpublished). Similarly, this strategy could be used to validate rRAB8A/B in HD model PC12 cells. New pools could then be tested and assayed for the levels of caspase-3/7 activation. Constitutive active and dominant negative mutants of rRAB8A/B could be also examined for validating the results obtained in flies. HD model PC12 cells would be a convenient system for monitoring mHTT aggregation dynamics. In fact, biochemistry techniques – such as dot-blot and AGERA assays – could be coupled with the monitoring of IBs formation using microscope-based imaging platform, *i.e.* ScanR (Olympus), which allows a fast and automated data collection. This model could serve to quickly test a number of compounds that have been recently identified as Rab GTPase activity modulators (Surviladze *et al.*, 2010). If promising, these could be then validated in *Drosophila* and eventually in mice. A similar strategy for testing compounds has been recently undertaken successful-

ly in Giorgini's lab for the validation of KMO inhibitors and GPx mimetics (Campesan *et al.*, 2011; Mason *et al.*, 2013).

#### 7.4 Future directions

The evidence presented in this thesis suggests a protective role for dRAB8 in HD model flies expressing HTT93Q exon 1, which possibly relies on induction of mHTT aggregation. It is widely accepted that aggregation leading to IBs production may be a cellular neuroprotective mechanism aiming at protecting the cell from toxic mHTT species (Arrasate *et. al.*, 2004). How dRAB8 enhances the production of aggregates has not yet been elucidated, however speculation about the possible pathway that dRAB8 uses to trigger aggregation has been discussed in Chapter 5. There I suggested that there might be a functional link between dRAB8 and proteins known to stimulate formation of IBs, such as MEKK1 (MAP/extracellular signal-regulated protein kinase(ERK) kinase kinase 1) (Meriin *et al.*, 2001), *i.e.* Germinal Center Kinase (GCK). Indeed, Rab8 has been shown to interact and might regulate the activation of GCK, which acts as an upstream regulator of MEKK1 (Meriin *et al.*, 2001; Chuang *et al.*, 2016; Kyriakis, 1999; Ren *et al.*, 1996). Hence, overexpression of dRAB8 might increase the activation of GCK, which could in turn enhance MEKK1. Genetic manipulations coupled with the use of targeted drugs (see below) would be an easy way to test this hypothesis. First, it will be necessary to prove that the increased aggregation has a protective role in dRAB8-mediated rescue. My expectations are that in *elav>HTT93Q,dRab8DN* flies the amount of aggregated mHTT would be similar to that seen in *elav>HTT93Q* flies. Moreover, preventing aggregation of mHTT – which could be performed using an anti-aggregation drug such as the azo-dye congo-red (Apostol 2003; Sanchez *et al.*, 2003) – might reduce the protection conferred by dRAB8 expression, which could be easily monitor exploiting the standard assays described above. Secondly, if my prediction is correct, then the observed dRAB8-mediated IBs formation should occur *via* activation of the GCK/MEKK1 cascade, therefore it would be necessary to show that GCK is more active following overexpression of dRAB8, for example with antibodies specifically targeting phosphorylated GCK. Additionally, I would also expect an increased interaction between GCK and dRAB8 in *elav>HTT93Q,dRab8* flies, which could be demonstrated by Co-IP. Moreover, if mHTT aggregation depends on MEKK1 activity as previously suggested (Meriin *et al.*, 2001), then MEKK1 should be more phosphorylated (*i.e.* more activated) in *elav>HTT93Q,dRab8* flies, whereas MEKK1 down-regulation should prevent aggregate formation, which could both be tested by exploiting the dot-blot and the AGERA assays.

As a conclusive note, it could be limiting to suppose that dRAB8 protection only arises from the enhancement of IBs formation, since other cellular events might occur and contribute

to the rescue observed in flies. If MEKK1 activation is responsible for mHTT aggregation (Merriin *et al.*, 2001), then there is a further link connecting dRAB8 with MEKK1, which might be due to Rab8-mediated glutamatergic signalling (Cowan & Raymond, 2006). One of the primary causes of neuronal death in HD has been attributed to excitotoxicity (over-activation of receptors by excitatory neurotransmitters), which results in excessive calcium influx and formation of ROS, mitochondrial dysfunction, and ultimately cell death (Cowan & Raymond, 2006). Glutamate (Glu) is one of the principal excitatory neurotransmitters both in vertebrates and invertebrates, including *Drosophila* (Heckmann & Dudel, 1997; Cowan & Raymond, 2006). In HD, Glu has been linked to the enhanced excitotoxic neuronal death by over-activating its own receptors, leading to a cascade that increases  $\text{Ca}^{2+}$  in the cell (Ribeiro *et al.*, 2010; Ribeiro *et al.*, 2011). Two different types of glutamatergic receptors have been described: ionotropic and metabotropic. The first ones are ion receptors permeable to cations and have been subdivided into N-methyl-D-aspartate acid receptors (NDMAR),  $\alpha$ -amino-3-hydroxy-5-methyl-4-isoxazolepropionic acid receptors (AMPAR) and kainate receptors (KAR), based on agonist preference (Dhami & Ferguson, 2006). Metabotropic glutamate receptors (mGluRs), on the other hand, are members of the family C of G proteins-coupled receptors (GPCRs), whose activation ultimately leads to the Phospholipase C (PLC)-mediated hydrolysis of phosphatidylinositol-4,5-bisphosphate ( $\text{PIP}_2$ ) in diacylglycerol (DAG) and inositol 1,4,5-trisphosphate ( $\text{IP}_3$ ), via the GTP dependent activation of the G protein  $\text{G}\alpha_{q/11}$  (Dale *et al.*, 2002).  $\text{IP}_3$  binds to the  $\text{IP}_3$  receptors ( $\text{IP}_3\text{R}$ ), resulting in  $\text{Ca}^{2+}$  release from intracellular stores (Dale *et al.*, 2002; Cowan & Raymond, 2006) as well as the activation of PKC, which negatively feeds back phosphorylating the receptors and inactivating them (Dale *et al.*, 2002), and the activation of the extracellular signal-regulated kinase (ERK) pathway, thought to be important for cell survival/proliferation (Ribeiro *et al.*, 2010). In HD, however,  $\text{IP}_3\text{R}$  are sensitized (Esseltine & Ferguson, 2013), hence even sub-threshold amounts of Glu could lead to an enhanced, excitotoxic accumulation of intracellular  $\text{Ca}^{2+}$  (Cowan & Raymond, 2006), as demonstrated in HD mouse model (Ribeiro *et al.*, 2010; Tang *et al.*, 2003). Interestingly, during the asymptomatic stages of the disease, the cells respond to the high levels of  $\text{Ca}^{2+}$  by increasing the PKC-mediated desensitization of mGluRs, thus decoupling the receptors from the G protein, reducing the levels of second messengers  $\text{IP}_3$ , and consequently preventing further release of  $\text{Ca}^{2+}$ , which will eventually lead to excitotoxicity, while over-activating ERK pathway (Ribeiro *et al.*, 2010). Similarly, also mGluR1 antagonists have been shown to be protective against NMDA-triggered excitotoxicity (Battaglia *et al.*, 2001; Bruno *et al.*, 1999). This protective mechanism, however, is lost in mice older than 11 months, and this might be the cause of the progressive neuronal loss (Ribeiro *et al.*, 2010). Interestingly, in HEK293 cells overexpression of Rab8 attenuates mGluR1a – a splicing variant

of mGluR1 – dependent signalling and internalization (Esseltine & Ferguson, 2013). Hence, Rab8 increases the levels of mGluR1a at the synaptic membrane (Esseltine & Ferguson, 2013) and mediates its desensitization through PKC phosphorylation (Ribeiro *et al.*, 2010). The consequence is a reduced IP<sub>3</sub> formation and decreased levels of intracellular Ca<sup>2+</sup> as demonstrated in HEK293 cells and hippocampal primary neurons (Esseltine & Ferguson, 2013). As mentioned above, this pathway also converges in the activation of the MAPK/ERK signalling cascade.

Given this, a bigger picture could therefore involve mGluR metabolism. Rab8 over-expression could counterbalance the sensitization of the mGluRs by promoting their desensitization and activation of MAPK/ERK signalling cascade, thus conferring neuroprotection at least during the early stages of the disease (Figure 7-1).

## 7.5 Concluding remarks

Rab8 is a well-conserved protein that coordinates the vesicular trafficking in the cells of all eukaryotes. In HD Rab8 has been shown to be mis-localized from its compartment, *i.e.* the Golgi (del Toro *et al.*, 2009), a feature that might contribute to the neuropathology observed in the disease. Here, I provided evidence that dRAB8 can delay the appearance of HD phenotypes in flies, both pan-neuronally and in a subset of the PDF<sup>+</sup> neurons. Whether the rescue observed in flies is underlined by the propensity of dRAB8 to stimulate mHTT aggregation needs further clarification, however this study provides support for this hypothesis, possibly highlighting a novel mechanism for neuroprotection amongst the Rab GTPase family members and paving the way for a potential novel therapeutic approach.

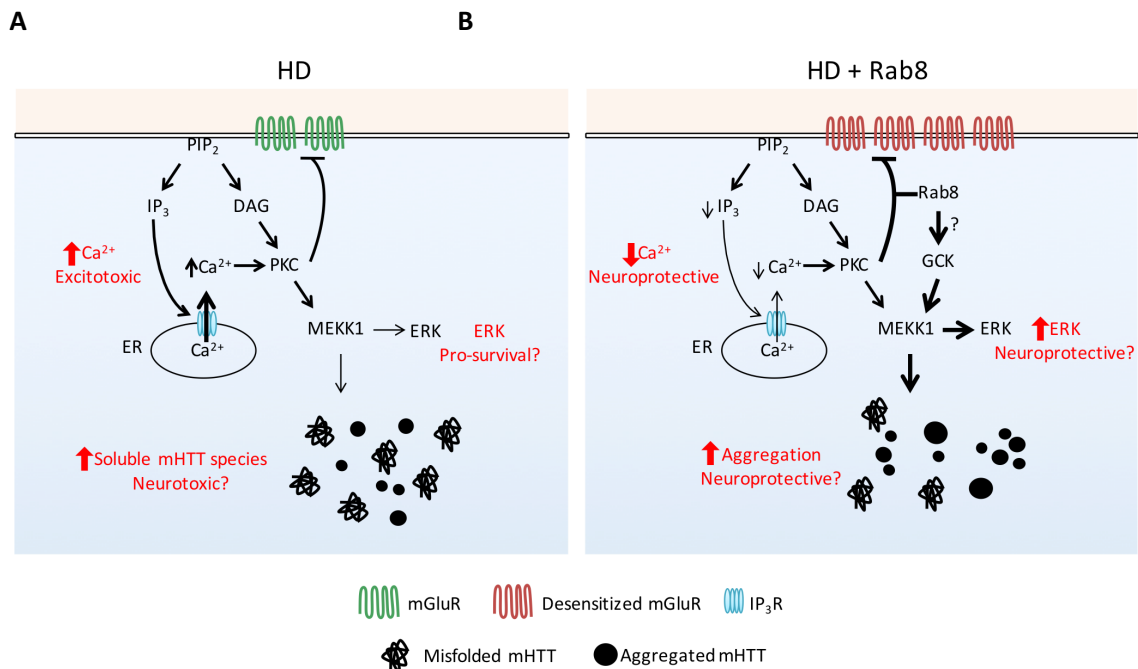


Figure 7-1 Hypothesis on how Rab8 functions in conferring protection against mHTT-induced toxicity.

**A** Upon mHTT expression, IP<sub>3</sub>R are sensitized, causing increasing release of Ca<sup>2+</sup> from the ER stores and hence excitotoxicity. The cell responds to increased Ca<sup>2+</sup> by promoting PKC-dependent desensitization of mGluRs thus reducing IP<sub>3</sub> and promoting PKC-dependent activation of the ERK pathway, which might have a pro-survival role in the asymptomatic stage of the disease. **B** Rab8 attenuates mGluRs internalisation, increasing their levels at the membrane, and attenuates their desensitisation in a PKC-dependent manner. Consequently, IP<sub>3</sub> levels are decreased, causing less Ca<sup>2+</sup> to be released from the ER stores. This could result in overall decreased Ca<sup>2+</sup> levels and reduced excitotoxicity. Rab8 might also activate GCK, leading to activation of MEKK1, which has been previously shown to induce mHTT aggregation. Aggregates are proposed to act a structure that confines toxic species, hence explaining their protective role. Both PKC and GCK pathways converge in ERK activation, which levels might be increased, resulting in neuroprotection. Redrawn from Ribeiro *et al.*, 2010.

## Chapter 8

### Appendix

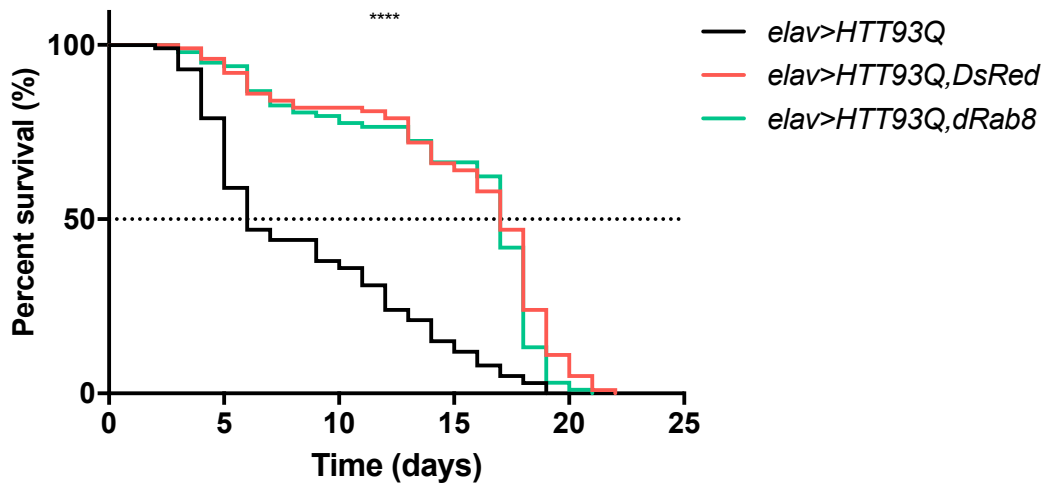


Figure 8-1 Replicate of the life-span assay.

Kaplan-Meier survival (percentages vs time) of *elav>HTT93Q*, *elav>HTT93Q,DsRED* and *elav>HTT93Q,Rab8*. Flies were kept at 25°C. Log-rank (Mantel-Cox), df=2, p<0.0001. Median lifespan ( $T_{50}$ ): *elav>HTT93Q*=6 days, *elav>HTT93Q,DsRED*=17 days, *elav>HTT93Q,Rab8*=17 days.

Table 8-1 Pairwise comparison of survival curves.

Log-rank (Mantel-Cox) analysis for pairwise comparison of survival curves, corrected for Bonferroni. \* p<0.05; \*\* p<0.01; \*\*\* p<0.001; \*\*\*\* p<0.0001; n.s. p>0.05.

Genotype	<i>elav&gt;HTT93Q</i>	<i>elav&gt;HTT93Q,DsRED</i>	<i>elav&gt;HTT93Q,dRab8</i>
<i>elav&gt;HTT93Q</i>	-		
<i>elav&gt;HTT93Q,DsRED</i>	****	-	
<i>elav&gt;HTT93Q,Rab8</i>	****	n.s.	-

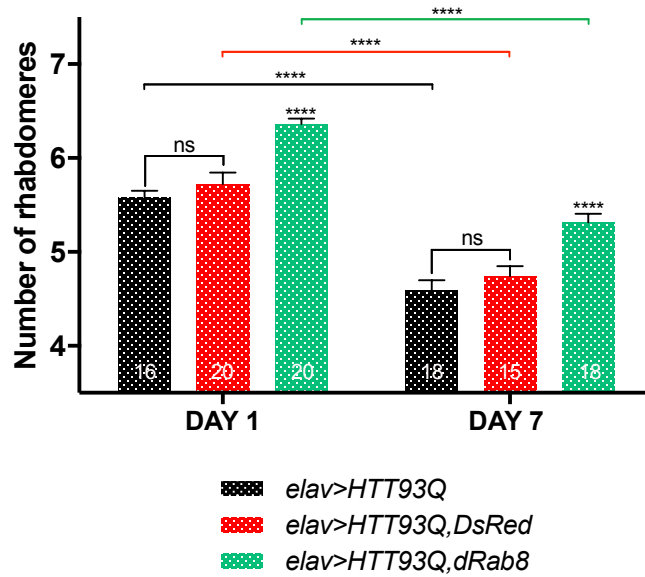


Figure 8-2 Replicate of the pseudopupil analysis.

Two-way ANOVA Interaction Age x Genotype F (2, 101) = 0.08107, p>0.05, Age F (1, 101) = 163.8, p<0.0001, Genotype F (2, 101) = 35.47, p<0.0001. Post-hoc Newman-Keuls, Genotype comparison: DAY1: *elav>HTT93Q* vs *elav>HTT93Q,Rab8*, p<0.0001, *elav>HTT93Q,DsRED* vs *elav>HTT93Q,Rab8*, p<0.0001; DAY 7: *elav>HTT93Q* vs *elav>HTT93Q,Rab8*, p<0.0001, *elav>HTT93Q,DsRED* vs *elav>HTT93Q,Rab8*, p<0.0001, Age comparison: *elav>HTT93Q* DAY1 vs DAY7, p<0.0001, *elav>HTT93Q,DsRED*, DAY1 vs DAY7, p<0.0001, *elav>HTT93Q,Rab8*, DAY1 vs DAY7, p<0.0001. Numbers within columns represent N values (number of heads analysed).

## Chapter 9

### References

Agola, J., Jim, P., Ward, H., Basuray, S., Wandinger-Ness, A., 2011. Rab GTPases as regulators of endocytosis, targets of disease and therapeutic opportunities. *Clinical Genetics*. 80, 305-318.

Aiken, C.T., Steffan, J.S., Guerrero, C.M., Khashwji, H., Lukacsovich, T., Simmons, D., Purcell, J.M., Menhaji, K., Zhu, Y.Z., Green, K., Laferla, F., Huang, L., Thompson, L.M., Marsh, J.L., 2009. Phosphorylation of threonine 3: implications for Huntingtin aggregation and neurotoxicity. *The Journal of Biological Chemistry*. 284, 29427-29436.

Albin, R.L., Reiner, A., Anderson, K.D., Dure, L.S., Handelin, B., Balfour, R., Whetsell, W.O., Penney, J.B., Young, A.B., 1992. Preferential loss of striato-external pallidal projection neurons in presymptomatic Huntington's disease. *Annals of Neurology*. 31, 425-430.

Allada, R. & Chung, B.Y., 2010. Circadian organization of behavior and physiology in *Drosophila*. *Annual Review of Physiology*. 72, 605-624.

Amm, I., Sommer, T., Wolf, D.H., 2014. Protein quality control and elimination of protein waste: The role of the ubiquitin–proteasome system. *Biochimica Et Biophysica Acta (BBA)-Molecular Cell Research*. 1843, 182-196.

Andrade, M.A. & Bork, P., 1995. HEAT repeats in the Huntington's disease protein. *Nature Genetics*. 11, 115-116.

Andrew, S.E., Goldberg, Y.P., Kremer, B., Telenius, H., Theilmann, J., Adam, S., Starr, E., Squitieri, F., Lin, B., Kalchman, M.A., 1993. The relationship between trinucleotide (CAG) repeat length. *Nature Genetics*. 4, 398-403.

Ang, A.L., Folsch, H., Koivisto, U.M., Pypaert, M., Mellman, I., 2003. The Rab8 GTPase selectively regulates AP-1B-dependent basolateral transport in polarized Madin-Darby canine kidney cells. *The Journal of Cell Biology*. 163, 339-350.

Ao, X., Zou, L., Wu, Y., 2014. Regulation of autophagy by the Rab GTPase network. *Cell Death & Differentiation*. 21, 348-358.

Apostol, B.L., Illes, K., Pallos, J., Bodai, L., Wu, J., Strand, A., Schweitzer, E.S., Olson, J.M., Kazantsev, A., Marsh, J.L., Thompson, L.M., 2006. Mutant huntingtin alters MAPK signaling pathways in PC12 and striatal cells: ERK1/2 protects against mutant huntingtin-associated toxicity. *Human Molecular Genetics*. 15, 273-285.

Apostol, B.L., Kazantsev, A., Raffioni, S., Illes, K., Pallos, J., Bodai, L., Slepko, N., Bear, J.E., Gertler, F.B., Hersch, S., Housman, D.E., Marsh, J.L., Thompson, L.M., 2003. A cell-based assay for aggregation inhibitors as therapeutics of polyglutamine-repeat disease and validation in *Drosophila*. *Proceedings of the National Academy of Sciences of the United States of America*. 100, 5950-5955.

Apostol, B.L., Simmons, D.A., Zuccato, C., Illes, K., Pallos, J., Casale, M., Conforti, P., Ramos, C., Roarke, M., Kathuria, S., 2008. CEP-1347 reduces mutant huntingtin-associated neurotoxicity and restores BDNF levels in R6/2 mice. *Molecular and Cellular Neuroscience*. 39, 8-20.

Armstrong, J., Thompson, N., Squire, J.H., Smith, J., Hayes, B., Solari, R., 1996. Identification of a novel member of the Rab8 family from the rat basophilic leukaemia cell line, RBL.2H3. *Journal of Cell Science*. 109(6), 1265-1274.

Arrasate, M. & Finkbeiner, S., 2012. Protein aggregates in Huntington's disease. *Experimental Neurology*. 238, 1-11.

Arrasate, M., Mitra, S., Schweitzer, E.S., Segal, M.R., Finkbeiner, S., 2004. Inclusion body formation reduces levels of mutant huntingtin and the risk of neuronal death. *Nature*. 431, 805-810.

Aschoff, J. & Pohl, H., 1978. Phase relations between a circadian rhythm and its zeitgeber within the range of entrainment. *Naturwissenschaften*. 65, 80-84.

Au, J.S., Puri, C., Ihrke, G., Kendrick-Jones, J., Buss, F., 2007. Myosin VI is required for sorting of AP-1B-dependent cargo to the basolateral domain in polarized MDCK cells. *The Journal of Cell Biology*. 177, 103-114.

Aziz, N.A., Anguelova, G.V., Marinus, J., Lammers, G.J., Roos, R.A., 2010. Sleep and circadian rhythm alterations correlate with depression and cognitive impairment in Huntington's disease. *Parkinsonism & Related Disorders*. 16, 345-350.

Aziz, N.A., van der Burg, J.M., Landwehrmeyer, G.B., Brundin, P., Stijnen, T., EHDI Study Group, Roos, R.A., 2008. Weight loss in Huntington disease increases with higher CAG repeat number. *Neurology*. 71, 1506-1513.

Babcock, D. T., & Ganetzky, B., 2015. Transcellular spreading of huntingtin aggregates in the *Drosophila* brain. *Proceedings of the National Academy of Sciences of the United States of America*, 112(39), E5427-E5433.

Bamford, K.A., Caine, E.D., Kido, D.K., Cox, C., Shoulson, I., 1995. A prospective evaluation of cognitive decline in early Huntington's disease: functional and radiographic correlates. *Neurology*. 45, 1867-1873.

Bates, G., Tabrizi, S. and Jones, L., 2014. *Huntington's disease*. Oxford University Press (UK).

Battaglia, G., Bruno, V., Pisani, A., Centonze, D., Catania, M.V., Calabresi, P., Nicoletti, F., 2001. Selective blockade of type-1 metabotropic glutamate receptors induces neuroprotection by enhancing gabaergic transmission. *Molecular and Cellular Neuroscience*. 17, 1071-1083.

Bence, N.F., Sampat, R.M., Kopito, R.R., 2001. Impairment of the ubiquitin-proteasome system by protein aggregation. *Science (New York, N.Y.)*. 292, 1552-1555.

Bento, C.F., Puri, C., Moreau, K., Rubinsztein, D.C., 2013. The role of membrane-trafficking small GTPases in the regulation of autophagy. *Journal of Cell Science*. 126, 1059-1069.

Bischof, J., Maeda, R.K., Hediger, M., Karch, F., Basler, K., 2007. An optimized transgenesis system for *Drosophila* using germ-line-specific  $\phi$ C31 integrases. *Proceedings of the National Academy of Sciences of the United States of America*. 104, 3312-3317.

Bodner, R.A., Housman, D.E., Kazantsev, A.G., 2006. New directions for neurodegenerative disease therapy: using chemical compounds to boost the formation of mutant protein inclusions. *Cell Cycle*. 5, 1477-1480.

Bonini, N.M. & Fortini, M.E., 2003. Human Neurodegenerative Disease Modeling Using *Drosophila*. *Annual Review of Neuroscience*. 26, 627-656.

Bossy-Wetzel, E., Petrilli, A., Knott, A.B., 2008. Mutant huntingtin and mitochondrial dysfunction. *Trends in Neurosciences*. 31, 609-616.

Brand, A.H. & Perrimon, N., 1993. Targeted gene expression as a means of altering cell fates and generating dominant phenotypes. *Development*. 118, 401-415.

Brinkman, R., Mezei, M., Theilmann, J., Almqvist, E., Hayden, M., 1997. The likelihood of being affected with Huntington disease by a particular age, for a specific CAG size. *American Journal of Human Genetics*. 60, 1202.

Brown, T.C., Correia, S.S., Petrok, C.N., Esteban, J.A., 2007. Functional compartmentalization of endosomal trafficking for the synaptic delivery of AMPA receptors during long-term potentiation. *The Journal of Neuroscience: The Official Journal of the Society for Neuroscience*. 27, 13311-13315.

Bruno, V., Battaglia, G., Kingston, A., O'neill, M.J., Catania, M.V., Di Grezia, R., Nicoletti, F., 1999. Neuroprotective activity of the potent and selective mGlu1a metabotropic glutamate receptor antagonist, (+)-2-methyl-4 carboxyphenylglycine (LY367385): comparison with LY357366, a broader spectrum antagonist with equal affinity for mGlu1a and mGlu5 receptors. *Neuropharmacology*. 38, 199-207.

Budihardjo, I., Oliver, H., Lutter, M., Luo, X., Wang, X., 1999. Biochemical pathways of caspase activation during apoptosis. *Annual Review of Cell and Developmental Biology*. 15, 269-290.

Byers, R.K., Gilles, F.H., Fung, C., 1973. Huntington's disease in children Neuropathologic study of four cases. *Neurology*. 23, 561-561.

Bylsma, F.W., Brandt, J., Strauss, M.E., 1990. Aspects of procedural memory are differentially impaired in Huntington's disease. *Archives of Clinical Neuropsychology*. 5, 287-297.

Campesan, S., Green, E.W., Breda, C., Sathyasaikumar, K.V., Muchowski, P.J., Schwarcz, R., Kyriacou, C.P., Giorgini, F., 2011. The kynurenone pathway modulates neurodegeneration in a *Drosophila* model of Huntington's disease. *Current Biology*. 21, 961-966.

Caron, N.S., Desmond, C.R., Xia, J., Truant, R., 2013. Polyglutamine domain flexibility mediates the proximity between flanking sequences in huntingtin. *Proceedings of the National Academy of Sciences of the United States of America*. 110, 14610-14615.

Cattaneo, E., Zuccato, C., Tartari, M., 2005. Normal huntingtin function: an alternative approach to Huntington's disease. *Nature Reviews Neuroscience*. 6, 919-930.

Cha, J.J., 2000. Transcriptional dysregulation in Huntington's disease. *Trends in Neurosciences*. 23, 387-392.

Chan, C., Scoggin, S., Wang, D., Cherry, S., Dembo, T., Greenberg, B., Jin, E.J., Kuey, C., Lopez, A., Mehta, S.Q., 2011. Systematic discovery of Rab GTPases with synaptic functions in *Drosophila*. *Current Biology*. 21, 1704-1715.

Chavrier, P., Gorvel, J.P., Stelzer, E., Simons, K., Gruenberg, J., Zerial, M., 1991. Hypervariable C-terminal domain of rab proteins acts as a targeting signal. *Nature*. 353, 769-772.

Chavrier, P., Vingron, M., Sander, C., Simons, K., Zerial, M., 1990. Molecular cloning of YPT1/SEC4-related cDNAs from an epithelial cell line. *Molecular and Cellular Biology*. 10, 6578-6585.

Chen, M., Ona, V.O., Li, M., Ferrante, R.J., Fink, K.B., Zhu, S., Bian, J., Guo, L., Farrell, L.A., Hersch, S.M., 2000. Minocycline inhibits caspase-1 and caspase-3 expression and delays mortality in a transgenic mouse model of Huntington disease. *Nature Medicine*. 6, 797-801.

Chen, W. & Wandinger-Ness, A., 2001. Expression and functional analyses of Rab8 and Rab11a in exocytic transport from trans-golgi network. *Methods in Enzymology*. 329, 165-175.

Chen, Y.T., Holcomb, C., Moore, H.P., 1993. Expression and localization of two low molecular weight GTP-binding proteins, Rab8 and Rab10, by epitope tag. *Proceedings of the National Academy of Sciences of the United States of America*. 90, 6508-6512.

Chuang, H., Wang, X., Tan, T., 2016. Chapter Seven-MAP4K Family Kinases in Immunity and Inflammation. *Advances in Immunology*. 129, 277-314.

Chun, W., Lesort, M., Tucholski, J., Ross, C.A., Johnson, G.V., 2001. Tissue transglutaminase does not contribute to the formation of mutant huntingtin aggregates. *The Journal of Cell Biology*. 153, 25-34.

Cicchetti, F., Prensa, L., Wu, Y., Parent, A., 2000. Chemical anatomy of striatal interneurons in normal individuals and in patients with Huntington's disease. *Brain Research Reviews*. 34, 80-101.

Colicelli, J., 2004. Human RAS superfamily proteins and related GTPases. *Science's STKE : Signal Transduction Knowledge Environment*. 2004, RE13.

Colin, E., Zala, D., Liot, G., Rangone, H., Borrell-Pages, M., Li, X.J., Saudou, F., Humbert, S., 2008. Huntingtin phosphorylation acts as a molecular switch for anterograde/retrograde transport in neurons. *The EMBO Journal*. 27, 2124-2134.

Collins, B.H., Dissel, S., Gaten, E., Rosato, E., Kyriacou, C.P., 2005. Disruption of Cryptochrome partially restores circadian rhythmicity to the arrhythmic period mutant of *Drosophila*. *Proceedings of the National Academy of Sciences of the United States of America*. 102, 19021-19026.

Corpet, F., 1988. Multiple sequence alignment with hierarchical clustering. *Nucleic Acids Research*. 16, 10881-10890.

Cowan, C.M. & Raymond, L.A., 2006. Selective neuronal degeneration in Huntington's disease. *Current Topics in Developmental Biology*. 75, 25-71.

Crick, S.L., Jayaraman, M., Frieden, C., Wetzel, R., Pappu, R.V., 2006. Fluorescence correlation spectroscopy shows that monomeric polyglutamine molecules form collapsed structures in aqueous solutions. *Proceedings of the National Academy of Sciences of the United States of America*. 103, 16764-16769.

Cummings, C.J., Reinstein, E., Sun, Y., Antalfy, B., Jiang, Y., Ciechanover, A., Orr, H.T., Beaudet, A.L., Zoghbi, H.Y., 1999. Mutation of the E6-AP ubiquitin ligase reduces nuclear inclusion frequency while accelerating polyglutamine-induced pathology in SCA1 mice. *Neuron*. 24, 879-892.

Dale, L.B., Babwah, A.V., Ferguson, S.S., 2002. Mechanisms of metabotropic glutamate receptor desensitization: role in the patterning of effector enzyme activation. *Neurochemistry International*. 41, 319-326.

Davies, S.W., Turmaine, M., Cozens, B.A., DiFiglia, M., Sharp, A.H., Ross, C.A., Scherzinger, E., Wanker, E.E., Mangiarini, L., Bates, G.P., 1997. Formation of neuronal intranuclear inclusions underlies the neurological dysfunction in mice transgenic for the HD mutation. *Cell*. 90, 537-548.

Davranche, A., Aviolat, H., Zeder-Lutz, G., Busso, D., Altschuh, D., Trottier, Y., Klein, F.A., 2011. Huntingtin affinity for partners is not changed by polyglutamine length: aggregation itself triggers aberrant interactions. *Human Molecular Genetics*. 20, 2795-2806.

de la Monte, S.M., Vonsattel, J.P., Richardson, E.P., 1988. Morphometric demonstration of atrophic changes in the cerebral cortex, white matter, and neostriatum in Huntington's disease. *Journal of Neuropathology and Experimental Neurology*. 47, 516-525.

del Toro, D., Alberch, J., Lazaro-Dieguez, F., Martin-Ibanez, R., Xifro, X., Egea, G., Canals, J.M., 2009. Mutant huntingtin impairs post-Golgi trafficking to lysosomes by delocalizing optineurin/Rab8 complex from the Golgi apparatus. *Molecular Biology of the Cell*. 20, 1478-1492.

Deretic, D., Huber, L.A., Ransom, N., Mancini, M., Simons, K., Papermaster, D.S., 1995. Rab8 in Retinal Photoreceptors may Participate in Rhodopsin Transport and in Rod Outer Segment Disk Morphogenesis. *Journal of Cell Science*. 108(1), 215-224.

Deretic, V., Saitoh, T., Akira, S., 2013. Autophagy in infection, inflammation and immunity. *Nature Reviews Immunology*. 13, 722-737.

Di Maio, L., Squitieri, F., Napolitano, G., Campanella, G., Trofatter, J.A., Conneally, P.M., 1993. Onset symptoms in 510 patients with Huntington's disease. *Journal of Medical Genetics*. 30, 289-292.

DiFiglia, M., Sapp, E., Chase, K., Schwarz, C., Meloni, A., Young, C., Martin, E., Vonsattel, J.P., Carraway, R., Reeves, S.A., 1995. Huntingtin is a cytoplasmic protein associated with vesicles in human and rat brain neurons. *Neuron*. 14, 1075-1081.

Dissel, S., Hansen, C.N., Özkaya, Ö, Hemsley, M., Kyriacou, C.P., Rosato, E., 2014. The logic of circadian organization in *Drosophila*. *Current Biology*. 24, 2257-2266.

Dong, C., Yang, L., Zhang, X., Gu, H., Lam, M.L., Claycomb, W.C., Xia, H., Wu, G., 2010. Rab8 interacts with distinct motifs in alpha2B- and beta2-adrenergic receptors and differentially modulates their transport. *The Journal of Biological Chemistry*. 285, 20369-20380.

dos Santos, J. B., Herrera, F., Giorgini, F., & Outeiro, T. F., 2014. B06 Exploring The Role Of Phosphorylation In Huntingtin Aggregation Dynamics. *Journal of Neurology, Neurosurgery & Psychiatry*, 85(1), A11.

Duffy, J.B., 2002. GAL4 system in *Drosophila*: a fly geneticist's Swiss army knife. *Genesis*. 34, 1-15.

Dupont, N., Jiang, S., Pilli, M., Ornatowski, W., Bhattacharya, D., Deretic, V., 2011. Autophagy-based unconventional secretory pathway for extracellular delivery of IL-1beta. *The EMBO Journal*. 30, 4701-4711.

Duyao, M., Ambrose, C., Myers, R., Novelletto, A., Persichetti, F., Frontali, M., Folstein, S., Ross, C., Franz, M., Abbott, M., 1993. Trinucleotide repeat length instability and age of onset in Huntington's disease. *Nature Genetics*. 4, 387-392.

Duyao, M.P., Auerbach, A.B., Ryan, A., Persichetti, F., Barnes, G.T., McNeil, S.M., Ge, P., Vonsattel, J.P., Gusella, J.F., Joyner, A.L., 1995. Inactivation of the mouse Huntington's disease gene homolog Hdh. *Science*. 269, 407-410.

Esseltine, J.L. & Ferguson, S.S., 2013. Regulation of G protein-coupled receptor trafficking and signaling by Rab GTPases. *Small GTPases*. 4, 132-135.

Esseltine, J.L., Ribeiro, F.M., Ferguson, S.S., 2012. Rab8 modulates metabotropic glutamate receptor subtype 1 intracellular trafficking and signaling in a protein kinase C-dependent manner. *The Journal of Neuroscience: The Official Journal of the Society for Neuroscience*. 32, 16933-16942.

Fan, M.M. & Raymond, L.A., 2007. N-methyl-D-aspartate (NMDA) receptor function and excitotoxicity in Huntington's disease. *Progress in Neurobiology*. 81, 272-293.

Ferrante, R.J., Kowall, N.W., Beal, M.F., Martin, J.B., Bird, E.D., Richardson, E.P., 1987. Morphologic and histochemical characteristics of a spared subset of striatal neurons in Huntington's disease. *Journal of Neuropathology and Experimental Neurology*. 46, 12-27.

FlyBase Consortium, 2003. The FlyBase database of the *Drosophila* genome projects and community literature. *Nucleic Acids Research*. 31, 172-175.

Galimi, F., Saez, E., Gall, J., Hoong, N., Cho, G., Evans, R.M., Verma, I.M., 2005. Development of ecdysone-regulated lentiviral vectors. *Molecular Therapy*. 11, 142-148.

Geng, J., Nair, U., Yasumura-Yorimitsu, K., Klionsky, D.J., 2010. Post-Golgi Sec proteins are required for autophagy in *Saccharomyces cerevisiae*. *Molecular Biology of the Cell*. 21, 2257-2269.

Gerges, N.Z., Backos, D.S., Esteban, J.A., 2004. Local control of AMPA receptor trafficking at the postsynaptic terminal by a small GTPase of the Rab family. *The Journal of Biological Chemistry*. 279, 43870-43878.

Giorgini, F., Guidetti, P., Nguyen, Q., Bennett, S.C., Muchowski, P.J., 2005. A genomic screen in yeast implicates kynurenone 3-monooxygenase as a therapeutic target for Huntington disease. *Nature Genetics*. 37, 526-531.

Gitler, A.D., Bevis, B.J., Shorter, J., Strathearn, K.E., Hamamichi, S., Su, L.J., Caldwell, K.A., Caldwell, G.A., Rochet, J.C., McCaffery, J.M., Barlowe, C., Lindquist, S., 2008. The Parkinson's disease protein alpha-synuclein disrupts cellular Rab homeostasis. *Proceedings of the National Academy of Sciences of the United States of America*. 105, 145-150.

Gloor, G. and Engels, W., Single-fly DNA preps for PCR, *Drosophila Information Service*, 71 148-149, 1992.

Godin, J.D., Colombo, K., Molina-Calavita, M., Keryer, G., Zala, D., Charrin, B.C., Dietrich, P., Volvert, M., Guillemot, F., Dragatsis, I., 2010. Huntingtin is required for mitotic spindle orientation and mammalian neurogenesis. *Neuron*. 67, 392-406.

Graham, R.K., Ehrnhoefer, D.E., Hayden, M.R., 2011. Caspase-6 and neurodegeneration. *Trends in Neurosciences*. 34, 646-656.

Gratz, S.J., Cummings, A.M., Nguyen, J.N., Hamm, D.C., Donohue, L.K., Harrison, M.M., Wildonger, J., O'Connor-Giles, K.M., 2013. Genome engineering of *Drosophila* with the CRISPR RNA-guided Cas9 nuclease. *Genetics*. 194, 1029-1035.

Graybiel, A.M., 2000. The basal ganglia. *Current Biology*. 10, R509-R511.

Green, E.W. & Giorgini, F., 2012. Choosing and using *Drosophila* models to characterize modifiers of Huntington's disease. *Biochemical Society Transactions*. 40, 739.

Grima, B., Chlot, E., Xia, R., Rouyer, F., 2004. Morning and evening peaks of activity rely on different clock neurons of the *Drosophila* brain. *Nature*. 431, 869-873.

Gunawardena, S., Her, L.S., Brusch, R.G., Laymon, R.A., Niesman, I.R., Gordesky-Gold, B., Sintasath, L., Bonini, N.M., Goldstein, L.S., 2003. Disruption of axonal transport by loss of huntingtin or expression of pathogenic polyQ proteins in *Drosophila*. *Neuron*. 40, 25-40.

Gusella, J.F. & MacDonald, M.E., 2000. Molecular genetics: unmasking polyglutamine triggers in neurodegenerative disease. *Nature Reviews Neuroscience*. 1, 109-115.

Halliday, G., McRitchie, D., Macdonald, V., Double, K., Trent, R., McCusker, E., 1998. Regional specificity of brain atrophy in Huntington's disease. *Experimental Neurology*. 154, 663-672.

Hattula, K. & Peränen, J., 2000. FIP-2, a coiled-coil protein, links Huntingtin to Rab8 and modulates cellular morphogenesis. *Current Biology*. 10, 1603-1606.

Hattula, K., Furuhjelm, J., Arffman, A., Peränen, J., 2002. A Rab8-specific GDP/GTP exchange factor is involved in actin remodeling and polarized membrane transport. *Molecular Biology of the Cell*. 13, 3268-3280.

Hattula, K., Furuhjelm, J., Tikkanen, J., Tanhuanpaa, K., Laakkonen, P., Peränen, J., 2006. Characterization of the Rab8-specific membrane traffic route linked to protrusion formation. *Journal of Cell Science*. 119, 4866-4877.

Heckmann, M. & Dudel, J., 1997. Desensitization and resensitization kinetics of glutamate receptor channels from *Drosophila* larval muscle. *Biophysical Journal*. 72, 2160.

Hedreen, J.C., Peyser, C.E., Folstein, S.E., Ross, C.A., 1991. Neuronal loss in layers V and VI of cerebral cortex in Huntington's disease. *Neuroscience Letters*. 133, 257-261.

Heindel, W.C., Butters, N., Salmon, D.P., 1988. Impaired learning of a motor skill in patients with Huntington's disease. *Behavioral Neuroscience*. 102, 141.

Helfrich-Förster, C., 2001. The locomotor activity rhythm of *Drosophila melanogaster* is controlled by a dual oscillator system. *Journal of Insect Physiology*. 47, 877-887.

Helfrich-Förster, C., Stengl, M., Homberg, U., 1998. Organization of the circadian system in insects. *Chronobiology International*. 15, 567-594.

Helfrich-Förster, C., 1998. Development of pigment-dispersing hormone-immunoreactive neurons in the nervous system of *Drosophila melanogaster*. *The Journal of Comparative Neurology*. 380, 335-354.

Helfrich-Förster, C., Shafer, O.T., Wülbeck, C., Grieshaber, E., Rieger, D., Taghert, P., 2007. Development and morphology of the clock-gene-expressing lateral neurons of *Drosophila melanogaster*. *Journal of Comparative Neurology*. 500, 47-70.

Henry, L. & Sheff, D.R., 2008. Rab8 regulates basolateral secretory, but not recycling, traffic at the recycling endosome. *Molecular Biology of the Cell*. 19, 2059-2068.

Henshall, T.L., Tucker, B., Lumsden, A.L., Nornes, S., Lardelli, M.T., Richards, R.I., 2009. Selective neuronal requirement for huntingtin in the developing zebrafish. *Human Molecular Genetics*. 18, 4830-4842.

Hermel, E., Gafni, J., Propp, S., Leavitt, B., Wellington, C., Young, J., Hackam, A., Logvinova, A., Peel, A., Chen, S., 2004. Specific caspase interactions and amplification are involved in selective neuronal vulnerability in Huntington's disease. *Cell Death & Differentiation*. 11, 424-438.

Herrera, F., Tenreiro, S., Miller-Fleming, L., Outeiro, T.F., 2011. Visualization of cell-to-cell transmission of mutant huntingtin oligomers. *PLoS Currents*. 3, RRN1210.

Hipp, M.S., Patel, C.N., Bersuker, K., Riley, B.E., Kaiser, S.E., Shaler, T.A., Brandeis, M., Kopito, R.R., 2012. Indirect inhibition of 26S proteasome activity in a cellular model of Huntington's disease. *The Journal of Cell Biology*. 196, 573-587.

Hodges, A., Strand, A.D., Aragaki, A.K., Kuhn, A., Sengstag, T., Hughes, G., Elliston, L.A., Hartog, C., Goldstein, D.R., Thu, D., Hollingsworth, Z.R., Collin, F., Synek, B., Holmans, P.A., Young, A.B., Wexler, N.S., Delorenzi, M., Kooperberg, C., Augood, S.J., Faull, R.L., Olson, J.M., Jones, L., Luthi-Carter, R., 2006. Regional and cellular gene expression changes in human Huntington's disease brain. *Human Molecular Genetics*. 15, 965-977.

Hoffner, G., Kahlem, P., Djian, P., 2002. Perinuclear localization of huntingtin as a consequence of its binding to microtubules through an interaction with  $\beta$ -tubulin: relevance to Huntington's disease. *Journal of Cell Science*. 115, 941-948.

Huber, L.A., de Hoop, M.J., Dupree, P., Zerial, M., Simons, K., Dotti, C., 1993a. Protein transport to the dendritic plasma membrane of cultured neurons is regulated by rab8p. *The Journal of Cell Biology*. 123, 47-55.

Huber, L.A., Pimplikar, S., Parton, R.G., Virta, H., Zerial, M., Simons, K., 1993b. Rab8, a small GTPase involved in vesicular traffic between the TGN and the basolateral plasma membrane. *The Journal of Cell Biology*. 123, 35-45.

Hughes, A.C., Mort, M., Elliston, L., Thomas, R.M., Brooks, S.P., Dunnett, S.B., Jones, L., 2014. Identification of novel alternative splicing events in the huntingtin gene and assessment of the functional consequences using structural protein homology modelling. *Journal of Molecular Biology*. 426, 1428-1438.

Huntington, G., 2003. On chorea. *The Journal of Neuropsychiatry and Clinical Neurosciences*. 15, 109-112.

Im, S.H. & Taghert, P.H., 2010. PDF receptor expression reveals direct interactions between circadian oscillators in *Drosophila*. *Journal of Comparative Neurology*. 518, 1925-1945.

Imarisio, S., Carmichael, J., Korolchuk, V., Chen, C., Saiki, S., Rose, C., Krishna, G., Davies, J., Ttofi, E., Underwood, B., 2008. Huntington's disease: from pathology and genetics to potential therapies. *Biochem.J.* 412, 191-209.

Jain, N. & Ganesh, S., 2016. Emerging nexus between RAB GTPases, autophagy and neurodegeneration. *Autophagy*. 12, 900-904.

Jeong, H., Then, F., Melia, T.J., Mazzulli, J.R., Cui, L., Savas, J.N., Voisine, C., Paganetti, P., Tanese, N., Hart, A.C., 2009. Acetylation targets mutant huntingtin to autophagosomes for degradation. *Cell*. 137, 60-72.

Jiang, S., Dupont, N., Castillo, E.F., Deretic, V., 2013. Secretory versus degradative autophagy: unconventional secretion of inflammatory mediators. *Journal of Innate Immunity*. 5, 471-479.

Joberty, G., Tavitian, A., Zahraoui, A., 1993. Isoprenylation of Rab proteins possessing a C-terminal Caax Motif. *FEBS Letters*. 330, 323-328.

Jung, C.H., Ro, S., Cao, J., Otto, N.M., Kim, D., 2010. mTOR regulation of autophagy. *FEBS Letters*. 584, 1287-1295.

Just, W.W. & Peränen, J., 2016. Small GTPases in peroxisome dynamics. *Biochimica Et Biophysica Acta (BBA)-Molecular Cell Research*. 1863, 1006-1013.

Kalchman, M.A., Graham, R.K., Xia, G., Koide, H.B., Hodgson, J.G., Graham, K.C., Goldberg, Y.P., Gietz, R.D., Pickart, C.M., Hayden, M.R., 1996. Huntingtin is ubiquitinated and interacts with a specific ubiquitin-conjugating enzyme. *Journal of Biological Chemistry*. 271, 19385-19394.

Kalchman, M.A., Koide, H.B., McCutcheon, K., Graham, R.K., Nichol, K., Nishiyama, K., Kazemi-Esfarjani, P., Lynn, F.C., Wellington, C., Metzler, M., 1997. HIP1, a human homologue of *S. cerevisiae* Sla2p, interacts with membrane-associated huntingtin in the brain. *Nature Genetics*. 16, 44-53.

Kegel, K.B., Kim, M., Sapp, E., McIntyre, C., Castano, J.G., Aronin, N., DiFiglia, M., 2000. Huntington expression stimulates endosomal-lysosomal activity, endosome tubulation, and autophagy. *The Journal of Neuroscience: The Official Journal of the Society for Neuroscience*. 20, 7268-7278.

Kegel, K.B., Meloni, A.R., Yi, Y., Kim, Y.J., Doyle, E., Cuiffo, B.G., Sapp, E., Wang, Y., Qin, Z.H., Chen, J.D., Nevins, J.R., Aronin, N., DiFiglia, M., 2002. Huntingtin is present in the nucleus, interacts with the transcriptional corepressor C-terminal binding protein, and represses transcription. *The Journal of Biological Chemistry*. 277, 7466-7476.

Kerppola, T.K., 2008. Bimolecular fluorescence complementation (BiFC) analysis as a probe of protein interactions in living cells. *Annual Review of Biophysics*. 37, 465-487.

Kiechle, T., Dedeoglu, A., Kubilus, J., Kowall, N.W., Beal, M.F., Friedlander, R.M., Hersch, S.M., Ferrante, R.J., 2002. Cytochrome C and caspase-9 expression in Huntington's disease. *Neuromolecular Medicine*. 1, 183-195.

Kim, J.J., Lipatova, Z., Majumdar, U., Segev, N., 2016. Regulation of golgi cisternal progression by Ypt/RAB GTPases. *Developmental Cell*. 36, 440-452.

Kim, M.W., Chelliah, Y., Kim, S.W., Otwinowski, Z., Bezprozvanny, I., 2009. Secondary structure of Huntingtin amino-terminal region. *Structure*. 17, 1205-1212.

Kirkwood, S.C., Su, J.L., Conneally, P.M., Foroud, T., 2001. Progression of symptoms in the early and middle stages of Huntington disease. *Archives of Neurology*. 58, 273-278.

Klionsky, D.J. & Emr, S.D., 2000. Autophagy as a regulated pathway of cellular degradation. *Science (New York, N.Y.)*. 290, 1717-1721.

Klionsky, D.J., 2007. Autophagy: from phenomenology to molecular understanding in less than a decade. *Nature Reviews Molecular Cell Biology*. 8, 931-937.

Klionsky, D.J., Abdelmohsen, K., Abe, A., Abedin, M.J., Abeliovich, H., Acevedo Arozena, A., Adachi, H., Adams, C.M., Adams, P.D., Adeli, K., 2016. Guidelines for the use and interpretation of assays for monitoring autophagy. *Autophagy*. 12, 1-222.

Kodama, Y. & Hu, C., 2012. "Review". *BioTechniques*. 53, 285-298.

Koressaar, T. and Remm, M., Enhancements and modifications of primer design program Primer3, *Bioinformatics (Oxford, England)*, 23(10), 1289-1291, 2007.

Kozak, M., 1986. Point mutations define a sequence flanking the AUG initiator codon that modulates translation by eukaryotic ribosomes. *Cell*. 44, 283-292.

Kremer, B., Goldberg, P., Andrew, S.E., Theilmann, J., Telenius, H., Zeisler, J., Squitieri, F., Lin, B., Bassett, A., Almqvist, E., 1994. A worldwide study of the Huntington's disease mutation: the sensitivity and specificity of measuring CAG repeats. *New England Journal of Medicine*. 330, 1401-1406.

Kroemer, G., Mariño, G., Levine, B., 2010. Autophagy and the integrated stress response. *Molecular Cell*. 40, 280-293.

Kyriakis, J.M., 1999. Signaling by the germinal center kinase family of protein kinases. *The Journal of Biological Chemistry*. 274, 5259-5262.

Lachmann, J., Barr, F.A., Ungermann, C., 2012. The Msb3/Gyp3 GAP controls the activity of the RAB GTPases Vps21 and Ypt7 at endosomes and vacuoles. *Molecular Biology of the Cell*. 23, 2516-2526.

Landles, C. & Bates, G.P., 2004. Huntingtin and the molecular pathogenesis of Huntington's disease. *EMBO Reports*. 5, 958-963.

Lazarev, V.F., Benken, K.A., Semenyuk, P.I., Sarantseva, S.V., Bolshakova, O.I., Mikhaylova, E.R., Muronetz, V.I., Guzhova, I.V., Margulis, B.A., 2015. GAPDH binders as potential drugs for the therapy of polyglutamine diseases: design of a new screening assay. *FEBS Letters*. 589, 581-587.

Li, S. & Li, X., 2004. Huntingtin–protein interactions and the pathogenesis of Huntington's disease. *TRENDS in Genetics*. 20, 146-154.

Li, S.H., Lam, S., Cheng, A.L., Li, X.J., 2000. Intranuclear huntingtin increases the expression of caspase-1 and induces apoptosis. *Human Molecular Genetics*. 9, 2859-2867.

Li, X., Sapp, E., Chase, K., Comer-Tierney, L.A., Masso, N., Alexander, J., Reeves, P., Kegel, K.B., Valencia, A., Esteves, M., 2009a. Disruption of Rab11 activity in a knock-in mouse model of Huntington's disease. *Neurobiology of Disease*. 36, 374-383.

Li, X., Standley, C., Sapp, E., Valencia, A., Qin, Z.H., Kegel, K.B., Yoder, J., Comer-Tierney, L.A., Esteves, M., Chase, K., Alexander, J., Masso, N., Sabin, L., Bellve, K., Tuft, R., Lifshitz, L., Fogarty, K., Aronin, N., DiFiglia, M., 2009b. Mutant huntingtin impairs vesicle formation from recycling endosomes by interfering with Rab11 activity. *Molecular and Cellular Biology*. 29, 6106-6116.

Li, X., Valencia, A., McClory, H., Sapp, E., Kegel, K.B., DiFiglia, M., 2012. Deficient Rab11 activity underlies glucose hypometabolism in primary neurons of Huntington's disease mice. *Biochemical and Biophysical Research Communications*. 421, 727-730.

Li, X., Valencia, A., Sapp, E., Masso, N., Alexander, J., Reeves, P., Kegel, K.B., Aronin, N., Difiglia, M., 2010. Aberrant Rab11-dependent trafficking of the neuronal glutamate transporter EAAC1 causes oxidative stress and cell death in Huntington's disease. *The Journal of Neuroscience : The Official Journal of the Society for Neuroscience*. 30, 4552-4561.

Lim, J. & Yue, Z., 2015. Neuronal aggregates: formation, clearance, and spreading. *Developmental Cell*. 32, 491-501.

Lin, B., Nasir, J., MacDonald, H., Hutchinson, G., Graham, R.K., Rommens, J.M., Hayden, M.R., 1994. Sequence of the murine Huntington disease gene: evidence for conservation, alternate splicing and polymorphism in a triplet (CCG) repeat [corrected]. *Human Molecular Genetics*. 3, 85-92.

Lin, B., Rommens, J.M., Graham, R.K., Kalchman, M., MacDonald, H., Nasir, J., Delaney, A., Goldberg, Y.P., Hayden, M.R., 1993. Differential 3' polyadenylation of the Huntington disease gene results in two mRNA species with variable tissue expression. *Human Molecular Genetics*. 2, 1541-1545.

Lin, M.T. & Beal, M.F., 2006. Mitochondrial dysfunction and oxidative stress in neurodegenerative diseases. *Nature*. 443, 787-795.

Lin, Y., Stormo, G.D., Taghert, P.H., 2004. The neuropeptide pigment-dispersing factor coordinates pacemaker interactions in the *Drosophila* circadian system. *The Journal of Neuroscience: The Official Journal of the Society for Neuroscience*. 24, 7951-7957.

Lo Sardo, V.L., Zuccato, C., Gaudenzi, G., Vitali, B., Ramos, C., Tartari, M., Myre, M.A., Walker, J.A., Pistocchi, A., Conti, L., 2012. An evolutionary recent neuroepithelial cell adhesion function of huntingtin implicates ADAM10-Ncadherin. *Nature Neuroscience*. 15, 713-721.

Luthi-Carter, R., Strand, A., Peters, N.L., Solano, S.M., Hollingsworth, Z.R., Menon, A.S., Frey, A.S., Spektor, B.S., Penney, E.B., Schilling, G., Ross, C.A., Borchelt, D.R., Tapscott, S.J., Young, A.B., Cha, J.H., Olson, J.M., 2000. Decreased expression of striatal signaling genes in a mouse model of Huntington's disease. *Human Molecular Genetics*. 9, 1259-1271.

MacDonald, M.E., Ambrose, C.M., Duyao, M.P., Myers, R.H., Lin, C., Srinidhi, L., Barnes, G., Taylor, S.A., James, M., Groot, N., 1993. A novel gene containing a trinucleotide repeat that is expanded and unstable on Huntington's disease chromosomes. *Cell*. 72, 971-983.

Majumder, P., Raychaudhuri, S., Chattopadhyay, B., Bhattacharyya, N.P., 2007. Increased caspase-2, calpain activations and decreased mitochondrial complex II activity in cells expressing exogenous huntingtin exon 1 containing CAG repeat in the pathogenic range. *Cellular and Molecular Neurobiology*. 27, 1127-1145.

Makanae, K., Kintaka, R., Makino, T., Kitano, H., Moriya, H., 2013. Identification of dosage-sensitive genes in *Saccharomyces cerevisiae* using the genetic tug-of-war method. *Genome Research*. 23, 300-311.

Mandel, M. and Higa, A., Calcium-dependent bacteriophage DNA infection, *Journal of Molecular Biology*, 53(1), 159-162, 1970.

Manders, E., Verbeek, F., Aten, J., 1993. Measurement of Co-localization of objects in dual-colour confocal images. *Journal of Microscopy*. 169, 375-382.

Mangiarini, L., Sathasivam, K., Seller, M., Cozens, B., Harper, A., Hetherington, C., Lawton, M., Trottier, Y., Lehrach, H., Davies, S.W., 1996. Exon 1 of the HD gene with an expanded CAG repeat is sufficient to cause a progressive neurological phenotype in transgenic mice. *Cell*. 87, 493-506.

Marsh, J.L. & Thompson, L.M., 2006. *Drosophila* in the Study of Neurodegenerative Disease. *Neuron*. 52, 169-178.

Martin, D.D., Ladha, S., Ehrnhoefer, D.E., Hayden, M.R., 2015. Autophagy in Huntington disease and huntingtin in autophagy. *Trends in Neurosciences*. 38, 26-35.

Martinez-Vicente, M., Talloczy, Z., Wong, E., Tang, G., Koga, H., Kaushik, S., De Vries, R., Arias, E., Harris, S., Sulzer, D., 2010. Cargo recognition failure is responsible for inefficient autophagy in Huntington's disease. *Nature Neuroscience*. 13, 567-576.

Mason, R.P. & Giorgini, F., 2011. Modeling Huntington disease in yeast: perspectives and future directions. *Prion*. 5, 269-276.

Mason, R.P., Casu, M., Butler, N., Breda, C., Campesan, S., Clapp, J., Green, E.W., Dhulkhed, D., Kyriacou, C.P., Giorgini, F., 2013. Glutathione peroxidase activity is neuroprotective in models of Huntington's disease. *Nature Genetics*. 45, 1249-1254.

McGuire, S.E., Mao, Z., Davis, R.L., 2004. Spatiotemporal gene expression targeting with the TARGET and gene-switch systems in *Drosophila*. *Science's STKE: Signal Transduction Knowledge Environment*. 2004, pl6.

Menzies, F.M., Ravikumar, B., Rubinsztein, D.C., 2006. Protective roles for induction of autophagy in multiple proteinopathies. *Autophagy*. 2, 224-225.

Meriin, A.B., Mabuchi, K., Gabai, V.L., Yaglom, J.A., Kazantsev, A., Sherman, M.Y., 2001. Intracellular aggregation of polypeptides with expanded polyglutamine domain is stimulated by stress-activated kinase MEKK1. *The Journal of Cell Biology*. 153, 851-864.

Merritt, A., Conneally, P., Rahman, N., Drew, A., 1969. Juvenile Huntington's chorea. *Progress in Neurogenetics*. 1, 645-650.

Mizushima, N., Levine, B., Cuervo, A.M., Klionsky, D.J., 2008. Autophagy fights disease through cellular self-digestion. *Nature*. 451, 1069-1075.

Morimoto, R.I., 2011. The heat shock response: systems biology of proteotoxic stress in aging and disease. *Cold Spring Harbor Symposia on Quantitative Biology*. 76, 91-99.

Moritz, O.L., Tam, B.M., Hurd, L.L., Peränen, J., Deretic, D., Papermaster, D.S., 2001. Mutant rab8 Impairs docking and fusion of rhodopsin-bearing post-Golgi membranes and causes cell death of transgenic *Xenopus* rods. *Molecular Biology of the Cell*. 12, 2341-2351.

Moriya, H., 2015. Quantitative nature of overexpression experiments. *Molecular Biology of the Cell*. 26, 3932-3939.

Mort, M., Carlisle, F.A., Waite, A.J., Elliston, L., Allen, N.D., Jones, L., Hughes, A.C., 2015. Huntington Exists as Multiple Splice Forms in Human Brain. *Journal of Huntington's Disease*. 4, 161-171.

Motulsky, H., 2007. Prism 5 statistics guide, 2007. *GraphPad Software*. 31, 39-42.

Muchowski, P.J., 2002. Protein misfolding, amyloid formation, and neurodegeneration: a critical role for molecular chaperones? *Neuron*. 35, 9-12.

Muqit, M.M. & Feany, M.B., 2002. Modelling neurodegenerative diseases in *Drosophila*: a fruitful approach? *Nature Reviews.Neuroscience*. 3, 237-243.

Nagai, Y., Inui, T., Popiel, H.A., Fujikake, N., Hasegawa, K., Urade, Y., Goto, Y., Naiki, H., Toda, T., 2007. A toxic monomeric conformer of the polyglutamine protein. *Nature Structural & Molecular Biology*. 14, 332-340.

Nagakubo, D., Taira, T., Kitaura, H., Ikeda, M., Tamai, K., Iguchi-Ariga, S.M., Ariga, H., 1997. DJ-1, a novel oncogene which transforms mouse NIH3T3 cells in cooperation withras. *Biochemical and Biophysical Research Communications*. 231, 509-513.

Nasir, J., Floresco, S.B., O'Kusky, J.R., Diewert, V.M., Richman, J.M., Zeisler, J., Borowski, A., Marth, J.D., Phillips, A.G., Hayden, M.R., 1995. Targeted disruption of the Huntington's disease gene results in embryonic lethality and behavioral and morphological changes in heterozygotes. *Cell*. 81, 811-823.

Neckameyer, W.S. & Bhatt, P., 2016. Protocols to Study Behavior in *Drosophila*. *Drosophila: Methods and Protocols*. 303-320.

Ng, E.L. & Tang, B.L., 2008. Rab GTPases and their roles in brain neurons and glia. *Brain Research Reviews*. 58, 236-246.

Niccolini, F. & Politis, M., 2014. Neuroimaging in Huntington's disease. *World Journal of Radiology*. 6, 301-312.

Nitabach, M.N., Blau, J., Holmes, T.C., 2002. Electrical Silencing of *Drosophila* Pacemaker Neurons Stops the Free-Running Circadian Clock. *Cell*. 109, 485-495.

Nitabach, M.N., Wu, Y., Sheeba, V., Lemon, W.C., Strumbos, J., Zelensky, P.K., White, B.H., Holmes, T.C., 2006. Electrical hyperexcitation of lateral ventral pacemaker neurons desynchronizes downstream circadian oscillators in the fly circadian circuit and induces multiple behavioral periods. *The Journal of Neuroscience: The Official Journal of the Society for Neuroscience*. 26, 479-489.

No, D., Yao, T.P., Evans, R.M., 1996. Ecdysone-inducible gene expression in mammalian cells and transgenic mice. *Proceedings of the National Academy of Sciences of the United States of America*. 93, 3346-3351.

O'Kusky, J.R., Nasir, J., Cicchetti, F., Parent, A., Hayden, M.R., 1999. Neuronal degeneration in the basal ganglia and loss of pallido-subthalamic synapses in mice with targeted disruption of the Huntington's disease gene. *Brain Research*. 818, 468-479.

O'Kane, C.J., 2003. Modelling human diseases in *Drosophila* and *Caenorhabditis*, *Seminars in cell & developmental biology*, 2003, Elsevier pp3-10.

Ona, V.O., Li, M., Vonsattel, J.P.G., Andrews, L.J., Khan, S.Q., Chung, W.M., Frey, A.S., Menon, A.S., Li, X., Stieg, P.E., 1999. Inhibition of caspase-1 slows disease progression in a mouse model of Huntington's disease. *Nature*. 399, 263-267.

Ordway, J.M., Tallaksen-Greene, S., Gutekunst, C., Bernstein, E.M., Cearley, J.A., Wiener, H.W., Dure, L.S., Lindsey, R., Hersch, S.M., Jope, R.S., 1997. Ectopically expressed CAG repeats cause intranuclear inclusions and a progressive late onset neurological phenotype in the mouse. *Cell*. 91, 753-763.

Orr, A.L., Li, S., Wang, C.E., Li, H., Wang, J., Rong, J., Xu, X., Mastroberardino, P.G., Greenamyre, J.T., Li, X.J., 2008. N-terminal mutant huntingtin associates with mitochondria and impairs mitochondrial trafficking. *The Journal of Neuroscience: The Official Journal of the Society for Neuroscience*. 28, 2783-2792.

Panov, A.V., Gutekunst, C., Leavitt, B.R., Hayden, M.R., Burke, J.R., Strittmatter, W.J., Greenamyre, J.T., 2002. Early mitochondrial calcium defects in Huntington's disease are a direct effect of polyglutamines. *Nature Neuroscience*. 5, 731-736.

Pecho-Vrieseling, E., Rieker, C., Fuchs, S., Bleckmann, D., Esposito, M. S., Botta, P., Lüthi, A., 2014. Transneuronal propagation of mutant huntingtin contributes to non-cell autonomous pathology in neurons. *Nature neuroscience*, 17(8), 1064-1072.

Peränen, J. & Furuhjelm, J., 2001. [20] Expression, purification, and properties of Rab8 function in actin cortical skeleton organization and polarized transport. *Methods in Enzymology*. 329, 188-196.

Peränen, J., Auvinen, P., Virta, H., Wepf, R., Simons, K., 1996. Rab8 promotes polarized membrane transport through reorganization of actin and microtubules in fibroblasts. *The Journal of Cell Biology*. 135, 153-167.

Pilli, M., Arko-Mensah, J., Ponpuak, M., Roberts, E., Master, S., Mandell, M.A., Dupont, N., Ornatowski, W., Jiang, S., Bradfute, S.B., 2012. TBK-1 promotes autophagy-mediated antimicrobial defense by controlling autophagosome maturation. *Immunity*. 37, 223-234.

Pittendrigh, C.S. & Daan, S., 1976. A functional analysis of circadian pacemakers in nocturnal rodents. *Journal of Comparative Physiology*. 106, 223-252.

Poirier, M.A., Jiang, H., Ross, C.A., 2005. A structure-based analysis of huntingtin mutant polyglutamine aggregation and toxicity: evidence for a compact beta-sheet structure. *Human Molecular Genetics*. 14, 765-774.

Pringsheim, T., Wiltshire, K., Day, L., Dykeman, J., Steeves, T., Jette, N., 2012. The incidence and prevalence of Huntington's disease: A systematic review and meta-analysis. *Movement Disorders*. 27, 1083-1091.

Qin, Z.H., Wang, Y., Sapp, E., Cuiffo, B., Wanker, E., Hayden, M.R., Kegel, K.B., Aronin, N., DiFiglia, M., 2004. Huntington bodies sequester vesicle-associated proteins by a polyproline-dependent interaction. *The Journal of Neuroscience: The Official Journal of the Society for Neuroscience*. 24, 269-281.

Rajkowska, G., Selemion, L.D., Goldman-Rakic, P.S., 1998. Neuronal and glial somal size in the prefrontal cortex: a postmortem morphometric study of schizophrenia and Huntington disease. *Archives of General Psychiatry*. 55, 215-224.

Rao, K.R. & Riehm, J.P., 1989. The pigment-dispersing hormone family: chemistry, structure-activity relations, and distribution. *The Biological Bulletin*. 177, 225-229.

Rasband, W.S., 2008. ImageJ. [Http://Rsbweb.Nih.Gov/Ij/](http://rsbweb.nih.gov/ij/).

Ravikumar, B. & Rubinsztein, D.C., 2004. Can autophagy protect against neurodegeneration caused by aggregate-prone proteins? *Neuroreport*. 15, 2443-2445.

Ravikumar, B., Duden, R., Rubinsztein, D.C., 2002. Aggregate-prone proteins with polyglutamine and polyalanine expansions are degraded by autophagy. *Human Molecular Genetics*. 11, 1107-1117.

Ravikumar, B., Imarisio, S., Sarkar, S., O'Kane, C.J., Rubinsztein, D.C., 2008. Rab5 modulates aggregation and toxicity of mutant huntingtin through macroautophagy in cell and fly models of Huntington disease. *Journal of Cell Science*. 121, 1649-1660.

Ravikumar, B., Vacher, C., Berger, Z., Davies, J.E., Luo, S., Oroz, L.G., Scaravilli, F., Easton, D.F., Duden, R., O'Kane, C.J., 2004. Inhibition of mTOR induces autophagy and reduces toxicity of polyglutamine expansions in fly and mouse models of Huntington disease. *Nature Genetics*. 36, 585-595.

Reilmann, R., Leavitt, B.R., Ross, C.A., 2014. Diagnostic criteria for Huntington's disease based on natural history. *Movement Disorders*. 29, 1335-1341.

Reiner, A., Dragatsis, I., Zeitlin, S., Goldowitz, D., 2003. Wild-type huntingtin plays a role in brain development and neuronal survival. *Molecular Neurobiology*. 28, 259-275.

Ren, M., Zeng, J., De Lemos-Chiarandini, C., Rosenfeld, M., Adesnik, M., Sabatini, D.D., 1996. In its active form, the GTP-binding protein rab8 interacts with a stress-activated protein kinase. *Proceedings of the National Academy of Sciences of the United States of America*. 93, 5151-5155.

Renn, S.C.P., Park, J.H., Rosbash, M., Hall, J.C., Taghert, P.H., 1999. A *pdf* Neuropeptide Gene Mutation and Ablation of PDF Neurons Each Cause Severe Abnormalities of Behavioral Circadian Rhythms in *Drosophila*. *Cell*. 99, 791-802.

Repici, M., Straatman, K.R., Balduccio, N., Enguita, F.J., Outeiro, T.F., Giorgini, F., 2013. Parkinson's disease-associated mutations in DJ-1 modulate its dimerization in living cells. *Journal of Molecular Medicine*. 91, 599-611.

Ribeiro, F. M., Vieira, L. B., Pires, R. G. W., Olmo, R. P., & Ferguson, S. S. G. (2017). Metabotropic glutamate receptors and neurodegenerative diseases. *Pharmacological Research*, 115, 179-191.

Ribeiro, F.M., Paquet, M., Ferreira, L.T., Cregan, T., Swan, P., Cregan, S.P., Ferguson, S.S., 2010. Metabotropic glutamate receptor-mediated cell signaling pathways are altered in a mouse model of Huntington's disease. *The Journal of Neuroscience*. 30, 316-324.

Ribeiro, F.M., Pires, R.G., Ferguson, S.S., 2011. Huntington's disease and Group I metabotropic glutamate receptors. *Molecular Neurobiology*. 43, 1-11.

Richards, P., Didszun, C., Campesan, S., Simpson, A., Horley, B., Young, K.W., Glynn, P., Cain, K., Kyriacou, C.P., Giorgini, F., 2011. Dendritic spine loss and neurodegeneration is rescued by Rab11 in models of Huntington's disease. *Cell Death & Differentiation*. 18, 191-200.

Roos, R.A., 2010. Huntington's disease: a clinical review. *Orphanet Journal of Rare Diseases*. 5, 1.

Rosas, H.D., Liu, A.K., Hersch, S., Glessner, M., Ferrante, R.J., Salat, D.H., van der Kouwe, A., Jenkins, B.G., Dale, A.M., Fischl, B., 2002. Regional and progressive thinning of the cortical ribbon in Huntington's disease. *Neurology*. 58, 695-701.

Rosas, H.D., Salat, D.H., Lee, S.Y., Zaleta, A.K., Pappu, V., Fischl, B., Greve, D., Hevelone, N., Hersch, S.M., 2008. Cerebral cortex and the clinical expression of Huntington's disease: complexity and heterogeneity. *Brain: A Journal of Neurology*. 131, 1057-1068.

Rosenblatt, A., Brinkman, R., Liang, K., Almqvist, E., Margolis, R., Huang, C., Sherr, M., Franz, M., Abbott, M., Hayden, M., 2001. Familial influence on age of onset among siblings with Huntington disease. *American Journal of Medical Genetics*. 105, 399-403.

Rosenblatt, A., Kumar, B.V., Mo, A., Welsh, C.S., Margolis, R.L., Ross, C.A., 2012. Age, CAG repeat length, and clinical progression in Huntington's disease. *Movement Disorders*. 27(2), 272-276.

Ross, C.A. & Tabrizi, S.J., 2011. Huntington's disease: from molecular pathogenesis to clinical treatment. *The Lancet Neurology*. 10, 83-98.

Rowe, R.K., Suszko, J.W., Pekosz, A., 2008. Roles for the recycling endosome, RAB8, and RAB11 in hantavirus release from epithelial cells. *Virology*. 382, 239-249.

Rubin, G.M. & Spradling, A.C., 1982. Genetic transformation of *Drosophila* with transposable element vectors. *Science (New York, N.Y.)*. 218, 348-353.

Rubinsztein, D.C., Barton, D.E., Davison, B.C., Ferguson-Smith, M.A., 1993. Analysis of the huntingtin gene reveals a trinucleotide-length polymorphism in the region of the gene that contains two CCG-rich stretches and a correlation between decreased age of onset of Huntington's disease and CAG repeat number. *Human Molecular Genetics*. 2, 1713-1715.

Rubinsztein, D.C., Gestwicki, J.E., Murphy, L.O., Klionsky, D.J., 2007. Potential therapeutic applications of autophagy. *Nature Reviews Drug Discovery*. 6, 304-312.

Sahl, S.J., Weiss, L.E., Duim, W.C., Frydman, J., Moerner, W., 2012. Cellular inclusion bodies of mutant huntingtin exon 1 obscure small fibrillar aggregate species. *Scientific Reports*. 2, 895.

Sahler, D.A., Roberts, R.C., Arden, S.D., Spudich, G., Taylor, M.J., Luzio, J.P., Kendrick-Jones, J., Buss, F., 2005. Optineurin links myosin VI to the Golgi complex and is involved in Golgi organization and exocytosis. *The Journal of Cell Biology*. 169, 285-295.

Sajjad, M. U., Green, E. W., Miller-Fleming, L., Hands, S., Herrera, F., Campesan, S., & Wyttenbach, A., 2013. DJ-1 modulates aggregation and pathogenesis in models of Huntington's disease. *Human molecular genetics*, ddt466.

Sanchez Mejia, R.O. & Friedlander, R.M., 2001. Caspases in Huntington's disease. *The Neuroscientist: A Review Journal Bringing Neurobiology, Neurology and Psychiatry*. 7, 480-489.

Sanchez, I., Mahlke, C., Yuan, J., 2003. Pivotal role of oligomerization in expanded polyglutamine neurodegenerative disorders. *Nature*. 421, 373-379.

Sanchez, I., Xu, C., Juo, P., Kakizaka, A., Blenis, J., Yuan, J., 1999. Caspase-8 is required for cell death induced by expanded polyglutamine repeats. *Neuron*. 22, 623-633.

Sandrelli, F., Costa, R., Kyriacou, C.P., Rosato, E., 2008. Comparative analysis of circadian clock genes in insects. *Insect Molecular Biology*. 17, 447-463.

Sapp, E., Schwarz, C., Chase, K., Bhide, P., Young, A., Penney, J., Vonsattel, J., Aronin, N., DiFiglia, M., 1997. Huntingtin localization in brains of normal and Huntington's disease patients. *Annals of Neurology*. 42, 604-612.

Sarkar, S. & Rubinsztein, D.C., 2008. Huntington's disease: degradation of mutant huntingtin by autophagy. *FEBS Journal*. 275, 4263-4270.

Sathasivam, K., Neueder, A., Gipson, T.A., Landles, C., Benjamin, A.C., Bondulich, M.K., Smith, D.L., Faull, R.L., Roos, R.A., Howland, D., Detloff, P.J., Housman, D.E., Bates, G.P., 2013. Aberrant splicing of HTT generates the pathogenic exon 1 protein in Huntington disease. *Proceedings of the National Academy of Sciences of the United States of America*. 110, 2366-2370.

Sato, T., Iwano, T., Kunii, M., Matsuda, S., Mizuguchi, R., Jung, Y., Hagiwara, H., Yoshihara, Y., Yuzaki, M., Harada, R., Harada, A., 2014. RAB8a and RAB8b are essential for several apical transport pathways but insufficient for ciliogenesis. *Journal of Cell Science*. 127, 422-431.

Saudou, F. & Humbert, S., 2016. The biology of Huntingtin. *Neuron*. 89, 910-926.

Saudou, F., Finkbeiner, S., Devys, D., Greenberg, M.E., 1998. Huntingtin acts in the nucleus to induce apoptosis but death does not correlate with the formation of intranuclear inclusions. *Cell*. 95, 55-66.

Sawa, A., 2001. Mechanisms for neuronal cell death and dysfunction in Huntington's disease: pathological cross-talk between the nucleus and the mitochondria? *Journal of Molecular Medicine*. 79, 375-381.

Scherzinger, E., Sittler, A., Schweiger, K., Heiser, V., Lurz, R., Hasenbank, R., Bates, G.P., Lehrach, H., Wanker, E.E., 1999. Self-assembly of polyglutamine-containing huntingtin fragments into amyloid-like fibrils: implications for Huntington's disease pathology. *Proceedings of the National Academy of Sciences of the United States of America*. 96, 4604-4609.

Schilling, G., Becher, M.W., Sharp, A.H., Jinnah, H.A., Duan, K., Kotzuk, J.A., Slunt, H.H., Ratovitski, T., Cooper, J.K., Jenkins, N.A., Copeland, N.G., Price, D.L., Ross, C.A., Borchelt, D.R., 1999. Intranuclear inclusions and neuritic aggregates in transgenic mice expressing a mutant N-terminal fragment of huntingtin. *Human Molecular Genetics*. 8, 397-407.

Schlichting, M. & Helfrich-Förster, C., 2015. Chapter Five-Photic Entrainment in *Drosophila* Assessed by Locomotor Activity Recordings. *Methods in Enzymology*. 552, 105-123.

Schneider, C.A., Rasband, W.S., Eliceiri, K.W., 2012. NIH Image to ImageJ: 25 years of image analysis. *Nature Methods*. 9, 671-675.

Sepers, M.D. & Raymond, L.A., 2014. Mechanisms of synaptic dysfunction and excitotoxicity in Huntington's disease. *Drug Discovery Today*. 19, 990-996.

Seredenina, T., Gokce, O., Luthi-Carter, R., 2011. Decreased striatal RGS2 expression is neuroprotective in Huntington's disease (HD) and exemplifies a compensatory aspect of HD-induced gene regulation. *PLoS One*. 6, e22231.

Sheeba, V., Fogle, K.J., Holmes, T.C., 2010. Persistence of morning anticipation behavior and high amplitude morning startle response following functional loss of small ventral lateral neurons in *Drosophila*. *PloS One*. 5, e11628.

Sheeba, V., Fogle, K.J., Kaneko, M., Rashid, S., Chou, Y., Sharma, V.K., Holmes, T.C., 2008. Large ventral lateral neurons modulate arousal and sleep in *Drosophila*. *Current Biology*. 18, 1537-1545.

Shen, F. & Seabra, M.C., 1996. Mechanism of digeranylgeranylation of Rab proteins. Formation of a complex between monogeranylgeranyl-Rab and Rab escort protein. *The Journal of Biological Chemistry*. 271, 3692-3698.

Sherman, M.Y. & Goldberg, A.L., 2001. Cellular defenses against unfolded proteins: a cell biologist thinks about neurodegenerative diseases. *Neuron*. 29, 15-32.

Shibata, M., Lu, T., Furuya, T., Degterev, A., Mizushima, N., Yoshimori, T., MacDonald, M., Yankner, B., Yuan, J., 2006. Regulation of intracellular accumulation of mutant Huntington by Beclin 1. *The Journal of Biological Chemistry*. 281, 14474-14485.

Shyu, Y.J. & Hu, C., 2008. Fluorescence complementation: an emerging tool for biological research. *Trends in Biotechnology*. 26, 622-630.

Shyu, Y.J., Liu, H., Deng, X., Hu, C., 2006. Identification of new fluorescent protein fragments for biomolecular fluorescence complementation analysis under physiological conditions. *BioTechniques*. 40, 61.

Sisodia, S.S., 1998. Nuclear inclusions in glutamine repeat disorders: are they pernicious, coincidental, or beneficial? *Cell*. 95, 1-4.

Slepko, N., Bhattacharyya, A.M., Jackson, G.R., Steffan, J.S., Marsh, J.L., Thompson, L.M., Wetzel, R., 2006. Normal-repeat-length polyglutamine peptides accelerate aggregation nucleation and cytotoxicity of expanded polyglutamine proteins. *Proceedings of the National Academy of Sciences of the United States of America*. 103, 14367-14372.

Smalley, J.L., Breda, C., Mason, R.P., Kooner, G., Luthi-Carter, R., Gant, T.W., Giorgini, F., 2016. Connectivity mapping uncovers small molecules that modulate neurodegeneration in Huntington's disease models. *Journal of Molecular Medicine*. 94, 235-245.

Smith, R., Brundin, P., Li, J., 2005. Synaptic dysfunction in Huntington's disease: a new perspective. *Cellular and Molecular Life Sciences CMLS*. 62, 1901-1912.

Snell, R.G., MacMillan, J.C., Cheadle, J.P., Fenton, I., Lazarou, L.P., Davies, P., MacDonald, M.E., Gusella, J.F., Harper, P.S., Shaw, D.J., 1993. Relationship between trinucleotide repeat expansion and phenotypic variation in Huntington's disease. *Nature Genetics*. 4, 393-397.

Sopko, R., Huang, D., Preston, N., Chua, G., Papp, B., Kafadar, K., Snyder, M., Oliver, S.G., Cyert, M., Hughes, T.R., 2006. Mapping pathways and phenotypes by systematic gene overexpression. *Molecular Cell*. 21, 319-330.

Soto, C., 2003. Unfolding the role of protein misfolding in neurodegenerative diseases. *Nature Reviews Neuroscience*. 4, 49-60.

Spradling, A.C. & Rubin, G.M., 1982. Transposition of cloned P elements into *Drosophila* germ line chromosomes. *Science (New York, N.Y.)*. 218, 341-347.

Sprecher, S.G., Cardona, A., Hartenstein, V., 2011. The *Drosophila* larval visual system: high-resolution analysis of a simple visual neuropil. *Developmental Biology*. 358, 33-43.

Steffan, J.S., Agrawal, N., Pallos, J., Rockabrand, E., Trotman, L.C., Slepko, N., Illes, K., Lukacsovich, T., Zhu, Y.Z., Cattaneo, E., Pandolfi, P.P., Thompson, L.M., Marsh, J.L., 2004. SUMO modification of Huntingtin and Huntington's disease pathology. *Science (New York, N.Y.)*. 304, 100-104.

Steinert, J.R., Campesan, S., Richards, P., Kyriacou, C.P., Forsythe, I.D., Giorgini, F., 2012. Rab11 rescues synaptic dysfunction and behavioural deficits in a *Drosophila* model of Huntington's disease. *Human Molecular Genetics*. 21, 2912-2922.

Stoleru, D., Peng, Y., Agosto, J., Rosbash, M., 2004. Coupled oscillators control morning and evening locomotor behaviour of *Drosophila*. *Nature*. 431, 862-868.

Stoleru, D., Peng, Y., Nawathean, P., Rosbash, M., 2005. A resetting signal between *Drosophila* pacemakers synchronizes morning and evening activity. *Nature*. 438, 238-242.

Subramaniam, S., Sixt, K.M., Barrow, R., Snyder, S.H., 2009. Rhes, a striatal specific protein, mediates mutant-huntingtin cytotoxicity. *Science (New York, N.Y.)*. 324, 1327-1330.

Surviladze, Z., Ursu, O., Miscioscia, F., Curpan, R., Halip, L., Bologa, C., Oprea, T., Waller, A., Strouse, J., Salas, V., Wu, Y., Edwards, B., Wandinger-Ness, A., Sklar, L., 2010. Three small molecule pan activator families of Ras-related GTPases. *Probe Reports from the NIH Molecular Libraries Program*. Bethesda (MD).

Szatmári, Z. & Sass, M., 2014. The autophagic roles of Rab small GTPases and their upstream regulators: a review. *Autophagy*. 10, 1154-1166.

Szebenyi, G., Morfini, G.A., Babcock, A., Gould, M., Selkoe, K., Stenoien, D.L., Young, M., Faber, P.W., MacDonald, M.E., McPhaul, M.J., 2003. Neuropathogenic forms of huntingtin and androgen receptor inhibit fast axonal transport. *Neuron*. 40, 41-52.

Tang, T., Tu, H., Chan, E.Y., Maximov, A., Wang, Z., Wellington, C.L., Hayden, M.R., Bezprozvanny, I., 2003. Huntingtin and huntingtin-associated protein 1 influence neuronal calcium signaling mediated by inositol-(1, 4, 5) triphosphate receptor type 1. *Neuron*. 39, 227-239.

Tartari, M., Gissi, C., Lo Sardo, V., Zuccato, C., Picardi, E., Pesole, G., Cattaneo, E., 2008. Phylogenetic comparison of huntingtin homologues reveals the appearance of a primitive polyQ in sea urchin. *Molecular Biology and Evolution*. 25, 330-338.

Taylor, J.P., Tanaka, F., Robitschek, J., Sandoval, C.M., Taye, A., Markovic-Plese, S., Fischbeck, K.H., 2003. Aggresomes protect cells by enhancing the degradation of toxic polyglutamine-containing protein. *Human Molecular Genetics*. 12, 749-757.

Tong, Y., Ha, T.J., Liu, L., Nishimoto, A., Reiner, A., Goldowitz, D., 2011. Spatial and temporal requirements for huntingtin (Htt) in neuronal migration and survival during brain development. *The Journal of Neuroscience: The Official Journal of the Society for Neuroscience*. 31, 14794-14799.

Touchot, N., Chardin, P., Tavitian, A., 1987. Four additional members of the ras gene superfamily isolated by an oligonucleotide strategy: molecular cloning of YPT-related cDNAs from a rat brain library. *Proceedings of the National Academy of Sciences of the United States of America*. 84, 8210-8214.

Trushina, E., Dyer, R.B., Badger, J.D., Ure, D., Eide, L., Tran, D.D., Vrieze, B.T., Legendre-Guillemain, V., McPherson, P.S., Mandavilli, B.S., Van Houten, B., Zeitlin, S., McNiven, M., Aebersold, R., Hayden, M., Parisi, J.E., Seeberg, E., Dragatsis, I., Doyle, K., Bender, A., Chacko, C., McMurray, C.T., 2004. Mutant huntingtin impairs axonal trafficking in mammalian neurons in vivo and in vitro. *Molecular and Cellular Biology*. 24, 8195-8209.

Untergasser, A., Cutcutache, I., Koressaar, T., Ye, J., Faircloth, B. C., Remm, M., & Rozen, S. G., 2012. Primer3--new capabilities and interfaces, *Nucleic acids research*, 40(15), e115.

Vanin, S., Bhutani, S., Montelli, S., Menegazzi, P., Green, E.W., Pegoraro, M., Sandrelli, F., Costa, R., Kyriacou, C.P., 2012. Unexpected features of *Drosophila* circadian behavioural rhythms under natural conditions. *Nature*. 484, 371-375.

Varadarajan, S., Breda, C., Smalley, J. L., Butterworth, M., Farrow, S. N., Giorgini, F., Cohen, G. M., 2015. The transrepression arm of glucocorticoid receptor signaling is protective in mutant huntingtin-mediated neurodegeneration. *Cell Death & Differentiation*, 22(8), 1388-1396.

Veitia, R.A., 2005. Gene dosage balance: deletions, duplications and dominance. *Trends in Genetics*. 21, 33-35.

Velier, J., Kim, M., Schwarz, C., Kim, T.W., Sapp, E., Chase, K., Aronin, N., DiFiglia, M., 1998. Wild-type and mutant huntingtins function in vesicle trafficking in the secretory and endocytic pathways. *Experimental Neurology*. 152, 34-40.

Vittori, A., Breda, C., Repici, M., Orth, M., Roos, R. A., Outeiro, T. F., REGISTRY investigators of the European Huntington's Disease Network, 2014. Copy-number variation of the neuronal glucose transporter gene SLC2A3 and age of onset in Huntington's disease. *Human molecular genetics*, 23(12), 3129-3137.

Vittori, A., Orth, M., Roos, R. A., Outeiro, T. F., Giorgini, F., Hollox, E. J., 2013.  $\beta$ -Defensin Genomic Copy Number Does Not Influence the Age of Onset in Huntington's Disease. *Journal of Huntington's disease*, 2(1), 107-124.

Waldvogel, H.J., Kim, E.H., Tippett, L.J., Vonsattel, J.G. and Faull, R.L., 2014. The neuropathology of Huntington's disease. *Behavioral Neurobiology of Huntington's Disease and Parkinson's Disease*. Springer. 33-80.

Wang, X., Cao, Q., Zhang, Y., Su, X., 2015. Activation and regulation of caspase-6 and its role in neurodegenerative diseases. *Annual Review of Pharmacology and Toxicology*. 55, 553-572.

Warby, S.C., Doty, C.N., Graham, R.K., Carroll, J.B., Yang, Y.Z., Singaraja, R.R., Overall, C.M., Hayden, M.R., 2008. Activated caspase-6 and caspase-6-cleaved fragments of huntingtin specifically colocalize in the nucleus. *Human Molecular Genetics*. 17, 2390-2404.

Weiss, A., Klein, C., Woodman, B., Sathasivam, K., Bibel, M., Régulier, E., Bates, G.P., Paganetti, P., 2008. Sensitive biochemical aggregate detection reveals aggregation onset before symptom development in cellular and murine models of Huntington's disease. *Journal of Neurochemistry*. 104, 846-858.

West, R.J., Lu, Y., Marie, B., Gao, F.B., Sweeney, S.T., 2015. Rab8, POSH, and TAK1 regulate synaptic growth in a *Drosophila* model of frontotemporal dementia. *The Journal of Cell Biology*. 208, 931-947.

Wexler, N.S., 2004. Venezuelan kindreds reveal that genetic and environmental factors modulate Huntington's disease age of onset. *Proceedings of the National Academy of Sciences of the United States of America*. 101, 3498-3503.

White, J.K., Auerbach, W., Duyao, M.P., Vonsattel, J., Gusella, J.F., Joyner, A.L., MacDonald, M.E., 1997. Huntingtin is required for neurogenesis and is not impaired by the Huntington's disease CAG expansion. *Nature Genetics*. 17, 404-410.

Wilson, A.L., Erdman, R.A., Castellano, F., Maltese, W.A., 1998. Prenylation of Rab8 GTPase by type I and type II geranylgeranyl transferases. *The Biochemical Journal*. 333 (3), 497-504.

Wirawan, E., Walle, L.V., Kersse, K., Cornelis, S., Claerhout, S., Vanoverberghe, I., Roelandt, R., De Rycke, R., Versputen, J., Declercq, W., 2010. Caspase-mediated cleavage of Beclin-1 inactivates Beclin-1-induced autophagy and enhances apoptosis by promoting the release of proapoptotic factors from mitochondria. *Cell Death & Disease*. 1, e18.

Wulff, K., Gatti, S., Wettstein, J.G., Foster, R.G., 2010. Sleep and circadian rhythm disruption in psychiatric and neurodegenerative disease. *Nature Reviews Neuroscience*. 11, 589-599.

Wyborski, D.L., Bauer, J.C., Vaillancourt, P., 2001. Bicistronic expression of ecdysone-inducible receptors in mammalian cells. *BioTechniques*. 31, 618-625.

Xie, Z. & Klionsky, D.J., 2007. Autophagosome formation: core machinery and adaptations. *Nature Cell Biology*. 9, 1102-1109.

Yanai, A., Huang, K., Kang, R., Singaraja, R.R., Arstikaitis, P., Gan, L., Orban, P.C., Mullard, A., Cowan, C.M., Raymond, L.A., 2006. Palmitoylation of huntingtin by HIP14 is essential for its trafficking and function. *Nature Neuroscience*. 9, 824-831.

Yang, Z. & Klionsky, D.J., 2010. Eaten alive: a history of macroautophagy. *Nature Cell Biology*. 12, 814-822.

Yao, Z. & Shafer, O.T., 2014. The *Drosophila* circadian clock is a variably coupled network of multiple peptidergic units. *Science (New York, N.Y.)*. 343, 1516-1520.

Yoshikawa, K., Tanaka, T., Ida, Y., Furusawa, C., Hirasawa, T., Shimizu, H., 2011. Comprehensive phenotypic analysis of single - gene deletion and overexpression strains of *Saccharomyces cerevisiae*. *Yeast*. 28, 349-361.

Zala, D., Colin, E., Rangone, H., Liot, G., Humbert, S., Saudou, F., 2008. Phosphorylation of mutant huntingtin at S421 restores anterograde and retrograde transport in neurons. *Human Molecular Genetics*. 17, 3837-3846.

Zeitlin, S., Liu, J., Chapman, D.L., Papaioannou, V.E., Efstratiadis, A., 1995. Increased apoptosis and early embryonic lethality in mice nullizygous for the Huntington's disease gene homologue. *Nature Genetics*. 11, 155-163.

Zhang, J., Schulze, K.L., Hiesinger, P.R., Suyama, K., Wang, S., Fish, M., Acar, M., Hoskins, R.A., Bellen, H.J., Scott, M.P., 2007. Thirty-one flavors of *Drosophila* rab proteins. *Genetics*. 176, 1307-1322.

Zhang, Y., Ona, V.O., Li, M., Drozda, M., Dubois - Dauphin, M., Przedborski, S., Ferrante, R.J., Friedlander, R.M., 2003. Sequential activation of individual caspases, and of alterations in Bcl-2 proapoptotic signals in a mouse model of Huntington's disease. *Journal of Neurochemistry*. 87, 1184-1192.

Zhen, Y. & Stenmark, H., 2015. Cellular functions of Rab GTPases at a glance. *Journal of Cell Science*. 128, 3171-3176.

Zhong, J. & Kyriakis, J.M., 2004. Germinal center kinase is required for optimal Jun N-terminal kinase activation by Toll-like receptor agonists and is regulated by the ubiquitin proteasome system and agonist-induced, TRAF6-dependent stabilization. *Molecular and Cellular Biology*. 24, 9165-9175.

Zordan, M.A., Benna, C., Mazzotta, G., 2007. Monitoring and analyzing *Drosophila* circadian locomotor activity. *Methods in Molecular Biology (Clifton, N.J.)*. 362, 67-81.

Zuccato, C. & Cattaneo, E., 2007. Role of brain-derived neurotrophic factor in Huntington's disease. *Progress in Neurobiology*. 81, 294-330.

Zuccato, C., Ciarmmola, A., Rigamonti, D., Leavitt, B.R., Goffredo, D., Conti, L., MacDonald, M.E., Friedlander, R.M., Silani, V., Hayden, M.R., Timmus, T., Sipione, S., Cattaneo, E., 2001. Loss of huntingtin-mediated BDNF gene transcription in Huntington's disease. *Science (New York, N.Y.)*. 293, 493-498.

Zuccato, C., Marullo, M., Conforti, P., MacDonald, M.E., Tartari, M., Cattaneo, E., 2008. Systematic assessment of BDNF and its receptor levels in human cortices affected by Huntington's disease. *Brain Pathology*. 18, 225-238.

Zuccato, C., Tartari, M., Crotti, A., Goffredo, D., Valenza, M., Conti, L., Cataudella, T., Leavitt, B.R., Hayden, M.R., Timmusk, T., 2003. Huntingtin interacts with REST/NRSF to modulate the transcription of NRSE-controlled neuronal genes. *Nature Genetics*. 35, 76-83.

Zuccato, C., Valenza, M., Cattaneo, E., 2010. Molecular mechanisms and potential therapeutical targets in Huntington's disease. *Physiological Reviews*. 90, 905-981.

Zwilling, D., Huang, S., Sathyasaikumar, K.V., Notarangelo, F.M., Guidetti, P., Wu, H., Lee, J., Truong, J., Andrews-Zwilling, Y., Hsieh, E.W., 2011. Kynurenone 3-monooxygenase inhibition in blood ameliorates neurodegeneration. *Cell*. 145, 863-874.